Electric Technology U.S.S.R.

ЭЛЕКТРИЧЕСТВО

Volume 4, December, 1958

Selected papers from *Elektrichestvo* Nos. 1 and 2, 1958

COLLEGE OF ENG
LIBRARY
16 JAN 1960

Published by
PERGAMON PRESS *NEW YORK LONDON PARIS LOS ANGELES*
for Pergamon Institute, New York and London, a non-profit-making foundation

ELECTRIC TECHNOLOGY, U.S.S.R.

EDITORIAL BOARD

H. M. BARLOW, *London*; F. W. BOWDEN, *San Luis Obispo*; F. BRAILSFORD, *London*; G. S. BROWN, *Cambridge, Mass.*; F. M. BRUCE, *Glasgow*; C. C. CARR, *Brooklyn*; G. W. CARTER, *Leeds*; A. G. CONRAD, *New Haven, Conn.*; G. F. CORCORAN, *College Park, Md.*; J. D. CRAGGS, *Liverpool*; A. L. CULLEN, *Sheffield*; G. E. DREIFKE, *St. Louis*; V. EASTON, *Birmingham*; A. R. ECKELS, *Vermont*; W. FISHWICK, *Swansea*; C. FROEHLICH, *New York*; C. G. GARTON, *Leatherhead*; J. GREIG, *London*; L. D. HARRIS, *Salt Lake City*; J. D. HORGAN, *Milwaukee*; E. C. JONES, *Morgantown*; E. C. JORDAN, *Urbana*; I. H. LOVETT, *Rolla, Missouri*; J. M. MEEK, *Liverpool*; J. H. MULLIGAN JNR., *N.Y.*; W. A. MURRAY, *Blacksburg, Virginia*; J. E. PARTON, *Nottingham*; H. A. PETERSON, *Madison*; A. PORTER, *London*; J. C. READ, *Rugby*; W. G. SHEPHERD, *Minneapolis*; W. P. SMITH, *Lawrence, Kansas*; PHILIP SPORN (Chairman), *New York*; J. A. STRELZOFF, *East Lansing*; F. W. TATUM, *Dallas, Texas*; C. V. O. TERWILLIGER, *Monterey*; D. H. TOMPSETT, *Stafford*; A. TUSTIN, *London*; S. REID WARREN JNR., *Philadelphia*; A. R. VAN C. WARRINGTON, *Stafford*; A. H. WAYNICK, *Pa.*; E. M. WILLIAMS, *Pittsburgh*; F. C. WILLIAMS, *Manchester*; H. I. WOOD, *Manchester*; C. M. ZIEMAN, *Ohio*.

Translation Editor: O. M. BLUNN, B.Sc.

PERGAMON INSTITUTE

A NON-PROFIT FOUNDATION FOR THE FURTHERANCE
AND DISSEMINATION OF SCIENTIFIC KNOWLEDGE

Joint Presidents of the Board of Governors:
Dr. Detlev W. Bronk
Sir Robert Robinson, O.M., F.R.S.
Executive Director: Captain I. R. Maxwell
4 & 5 Fitzroy Square, London W.1
122 East 55th Street, New York 22, N.Y.

Pergamon Institute can occasionally use additional translators for science and engineering material to assist with this programme of translation from Russian and other Slavonic languages.

Scientists and engineers who have a knowledge of Russian, and who are willing to assist with this work, should apply to the Administrative Secretary of the Institute. They should write to either New York or London for rates of payment and other details.

Financial assistance has also been received from A.S.E.A., Sweden

Four volumes per annum. Approximately 700 pages per annum.
Annual Subscription Rate £20 ($56).
Single volumes may be purchased for £6 ($14).

Orders should be sent to the distributors at either of the following addresses
4 & 5 Fitzroy Square, London W.1
122 East 55th Street, New York 22, N.Y.

PUBLISHED BY
PERGAMON PRESS LTD.
LONDON · NEW YORK · PARIS · LOS ANGELES

s.318 = 15 for [illegible] Journals.
55.60.
B.No.324/D; 16/1/60.
E.M.D.

COLLEGE OF ENGINEERING
No. P45E/M3
GUINDY

TWO-COMMUTATOR ROTARY AMPLIFIER*

I.N. CHUPIATOV and V.F. BAIKO

Obraztsov Institute of Railway Transport
Engineers, Leningrad

(Received 4 March 1957)

Rotary amplifiers are used in various cases of electro-drive in order to improve the quality of regulation.

At present there are a few types of rotary amplifiers differing in their mode of operation and in their working characteristics. Of these, rotary amplifiers with a cross-field are most frequently used in industry and transport. Nevertheless, in certain cases, these amplifiers do not satisfy requirements and cannot be used in automatic control systems.

Therefore, the study of the properties of other amplifier systems is of considerable interest.

In the present article, we consider the mode of operation and the fundamental working characteristics of a two-commutator rotary amplifier which in foreign literature is called "magnavolt". The two-commutator rotary amplifier of this type has not yet found application in our national automatic control systems. Its physico-technical and working characteristics are not elucidated in our technical and scientific literature.

Mode of operation of the amplifier

The two-commutator rotary amplifier differs essentially in principle from amplifiers with an axial field and from those with cross-field as well.

The rotary amplifier in question has, like any ordinary d.c. machine, a yoke on which are fixed main poles and interpoles. But the armature of this amplifier, unlike those of ordinary machines, has two windings, calculated for different numbers of poles. The armature windings are connected to separate commutators, thus they form two independent electrical circuits. In the slots of the armature, the windings are placed in four layers, since every winding has two layers. The characteristic property of the amplifier is its method of excitation. The magnetic circuit of the amplifier consists of the superimposed magnetic circuits of two machines, designed

---

* *Elektrichestvo* No. 1, 1 – 5, 1958 [Reprint Order No. EL. 40].

COLLEGE OF ENGINEERING
LIBRARY BOOK
6 JAN 1960
GUINDY

or different numbers of poles, the ratio of the number of poles of the two combined machines being always equal to two.

The windings of the armature are calculated according to the number of poles of the combined machines.

We consider the principle of action of an amplifier with the number of poles of the combined magnetic circuit equal to $2p = 2$ and $2p = 4$, respectively. On the yoke of such an amplifier, there are four cores of the main poles, on which two excitation windings are placed, forming a two-pole and a four-pole magnetic circuit.

The winding producing a two-pole m.m.f. (two-pole magnetization) is placed on all four cores of the yoke poles and is fed from an independent source. The current in this excitation winding produces the polarity of the poles according to the sequence N-N-S-S., i.e. a two-pole magnetic system is formed. This excitation winding is called a control winding of the amplifier. There may be two or more such windings on the cores of the stator, according to the use of the amplifier and according to the requirements of the system in which it works.

The second excitation winding is placed on the same four cores and is fed from the two-pole armature winding. This excitation winding produces a four-pole m.m.f. (four-pole magnetization) with the polarity sequence N-S-N-S.

Four-pole armature winding of the amplifier ensures the required voltage at the output, U_{out}, and is designed in accordance with the load parameters.

The electric circuit of the amplifier may be represented by the equivalent circuit of two machines (Fig. 1). The first, a two-pole machine, is separately excited and ensures the amplification of the first stage. The four-pole excitation winding acts as a load for the first machine and ensures the second stage of amplification. Thus, the amplifier in question is a two-stage amplifier. The total amplification factor of the amplifier is equal to the product of the amplification factors of its two stages.

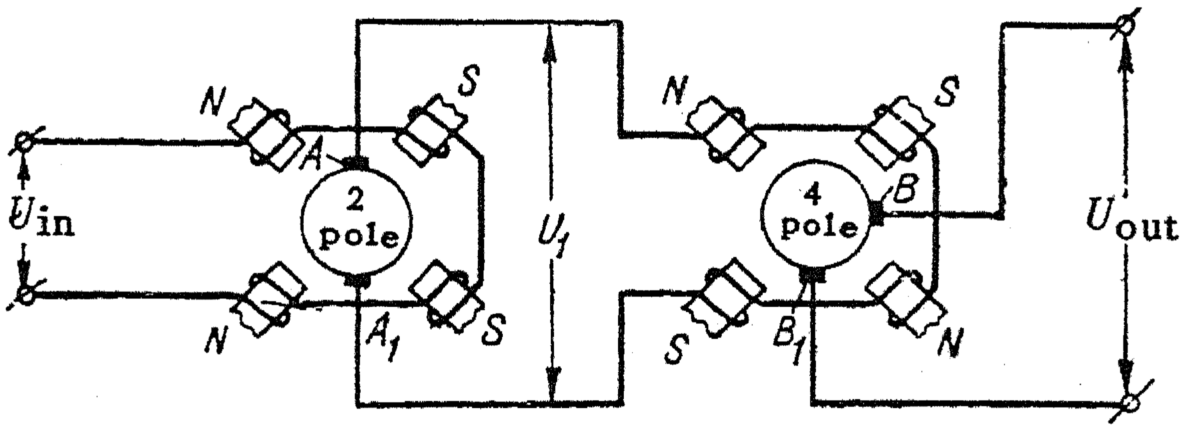

FIG. 1. The equivalent circuit of a two-stage amplifier.

Besides the above-mentioned windings, the amplifier may also have two or four-pole windings for self-excitation. The presence of this winding increases the total amplification factor.

The complete diagram of the electric and magnetic circuit of a two-commutator rotary amplifier is shown in Fig. 2.

For a better understanding of the principle of a two-stage amplifier and its properties, it is necessary to consider the mutual influence of a two-pole and four-pole m.m.f., acting in a single magnetic circuit.

A four-pole excitation system has no influence on the e.m.f. of the two-pole armature winding, since the sides of the sections of this winding are situated by poles of the same polarity.

The two-pole m.m.f. produces a distortion in the distribution of the four-pole m.m.f. The degree of distortion depends on the magnitude of the two-pole m.m.f. and on the degree of saturation of the magnetic circuit of the amplifier. Since, in a two-stage amplifier, the m.m.f. of the control winding (two-pole m.m.f.) is usually very small in comparison with the four-pole m.m.f., its influence is insignificant.

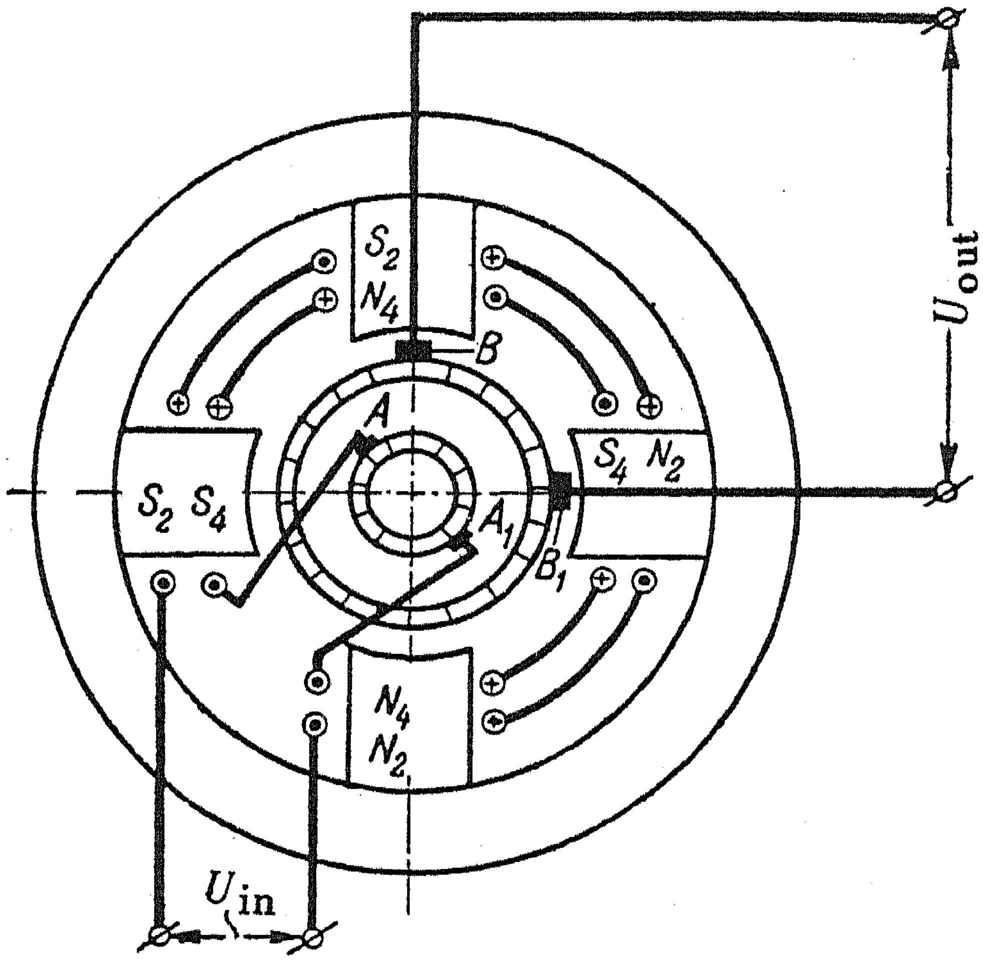

FIG. 2. Electric and magnetic networks of a two-stage amplifier.

But even insignificant distortion of the four-pole m.m.f. under the influence of two-pole excitation necessitates the use of the wave-winding of the armature for a four-pole system, and this excludes the formation of equalizing currents.

In the case of saturation of the magnetic circuit of the machine, the influence of the two-pole magnetic system on the e.m.f. of the four-pole armature winding is practically removed.

Commutation

The presence of two commutators in a two-stage amplifier should be considered as a disadvantage in comparison with other types of rotary amplifiers. Nevertheless, the conditions of current commutation of the armature windings of the amplifier may be quite satisfactory. The current commutation of the two-pole armature winding is practically independent of the load, and usually does not require the addition of interpoles in a two-pole magnetic system.

Since the power of the two-pole armature winding is comparatively small, "commutation by resistance" is quite satisfactory. For a four-pole armature winding only two interpoles can be provided, just as for an ordinary four-pole small-power machine. In this machine two interpoles of the four-pole magnetic system are placed on the line n - n' (Fig. 3), perpendicular to the two-pole magnetic neutral axis m - m''. If an interpole mechanism is required in the two-pole magnetic system, then these two poles are established on the two-pole magnetic neutral m - m'.

In this case the excitation of the interpoles along the axis m - m' should be from a common source; i.e., their excitation windings should be fed by the current of the four-pole armature winding.

The calculation of the m.m.f. of the amplifier interpoles does not differ from analogous calculations of the ordinary d.c. machines. It is necessary to point out that the presence in a two-stage amplifier of a separate armature winding for each amplification stage simplifies the commutation problem, since there is the possibility of the choice of the voltage of the two-pole armature winding, and consequently of the winding parameters.

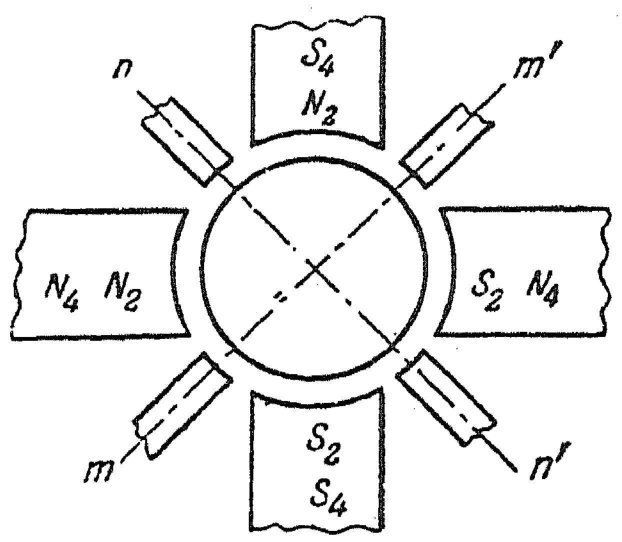

FIG. 3. Magnetic network of a two-stage amplifier with interpoles.

The three-stage amplifier

The two-commutator rotary amplifier may be made as a three-stage amplifier, as diagramatically shown in Fig. 4.

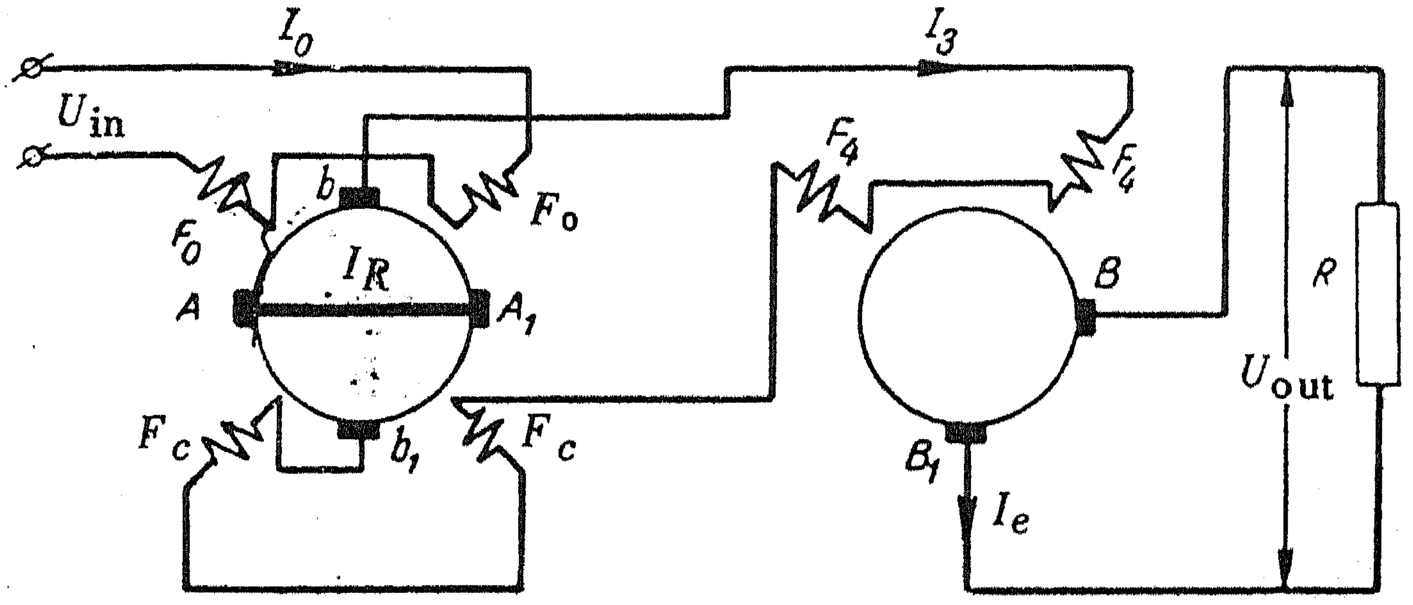

FIG. 4. The equivalent circuit of a three-stage amplifier.

The three-stage amplifier differs in construction from the two-stage machine in that an additional pair of brushes, $b - b_1$, is fixed on the commutator of the two-pole armature winding, these brushes being placed perpendicular to the line of the brushes $A - A_1$. Brushes $A - A_1$ are placed, as stated above, on the two-pole magnetic neutral axis (m.n.a.). Brushes $A - A_1$ are short-circuited. Two windings are connected to the brushes $b - b_1$, the winding of the four-pole excitation system F_4 and the compensation winding F_C, which is fixed on the same cores as the control winding F_0. The role of the four-pole excitation winding F_4 of the amplifier has already been discussed; the action of the compensation winding is to compensate for the armature reaction, occuring along the longitudinal axis of the two-pole system. From the circuit of a three-stage amplifier, shown in Fig. 4, it is clear that the properties of a two-stage amplifier with a cross-field are used for the first two stages of amplification. The flux of the control winding F_0, produced by the current I_0, induces an e.m.f. in the two-pole armature winding, which induces a current I_2 in the network of the short-circuited brushes $A - A_1$. The current of the two-pole armature winding induces a flux in the direction of the cross-axis of the two-pole magnetic system, which in its turn induces an e.m.f. in the same armature winding.

Hence, a current I_3 is produced in the network of brushes b - b_1. The current I_3 induces m.m.f. F_4 which determines the output voltage U_{out} and the load current I_e.

The total power amplification factor of a three-stage amplifier is:

$$K_p = \frac{U_{out} \cdot I_e}{U_{in} \cdot I_o}$$

In a three-stage amplifier, the addition of two brushes on the commutator, and of the compensation winding F_C on the poles, does not increase the size of the machine in comparison with a two-stage amplifier. This also permits a considerable increase of the power amplification factor.

The work of a two-stage two-commutator rotary amplifier in transient conditions

The analysis of transient conditions in a two-stage amplifier of the type in question is carried out, certain assumptions being made. These are usually accepted for the analysis of transient conditions in multi-stage amplifiers.

The initial equations for a two-stage amplifier, when a constant voltage U_{in} is applied to one of its control windings, are:

(a) equations for the balance of e.m.f.'s:

$$U_{in} = i_1 r_1 + w_1 p \Phi_1;$$
$$c_1 n \Phi_1 = r_2 i_2 + w_2 p \Phi_2;$$
$$E_{out} = c_2 n \Phi_2;$$

OF ENGINEERING
LIBRARY BOOK
No.

(b) conditions for the balance of m.m.f.'s:

$$a_1 \Phi_1 = i_1 w_1;$$
$$a_2 \Phi_2 = i_2 w_2,$$

where i_1 – the current in the control winding, i_2 – the current in the four-pole field winding, w_1 and w_2 – the number of turns in the two- and four-pole field windings, r_1 and r_2 – resistances of the two- and four-pole field windings; c_1 and c_2 – constants of the amplifier, a_1 and a_2 – factors of proportionality between m.m.f. and the magnetic flux, Φ_1 and Φ_2 – two- and four-pole magnetic fluxes, E_{out} – e.m.f. at the output of the amplifier.

The solution of this equation gives:

$$E_{out}(p) = U_{in} \frac{k_1 k_2}{(1 + pT_1)(1 + pT_2)},$$

where $k_1 = \frac{w_1 c_1 n}{r_1 a_1}$ – amplification factor of the first stage;

$k_2 = \frac{w_2 c_2 n}{r_2 a_2}$ – amplification factor of the second stage;

$T_1 = \frac{w_1^2}{a_1 r_1}$ – time constant of the two-stage field network;

$T_2 = \dfrac{w_2^2}{a_2 r_2}$ — time constant of the four-pole field network.

Thus, a two-stage amplifier behaves as an inertial amplifying link of the second order and is characterized by the equation analogous to the equation of a rotary cross-field amplifier with a full compensation of the axial armature reaction.

Tests of an experimental model of an amplifier

For the experimental investigation of fundamental working chacteristics of a two-stage amplifier a special experimental model of such an amplifier was made in the electric machines laboratory of the Leningrad Institute of Railway Transport Engineers.

The amplifier has the following nominal chacteristic: $P = 2$ kW; $U = 50$ V; current $I = 40$ A; $n = 2850$ r.p.m. The amplifier was made on the base of a PN-17.5 d.c. machine. On the armature, on its two sides, are fixed two commutators, one of which is connected to the two-pole and the other to the four-pole winding. The fundamental data of the amplifier are given in the appendix.

The static and dynamic characteristics were recorded during the test.

Fig. 5 shows the characteristics of the no-load running of the first stage (curve 1), and of the second stage (curve 2). From these characteristics, the saturation of the magnetic system of the amplifier and its zone of insensitivity can be deduced.

In Fig. 6 a characteristic of the amplifier on load is shown, recorded at a constant resistance of the load $R_l = 1.6\,\Omega$. From these characteristics the dependence of the poweraamplification factor on R_{out} is obtained (Fig. 7). It is necessary to point out that the power amplification factor of this experimental model of a two stage amplifier is comparatively small, owing to defects in the manufacture of the experimental model.

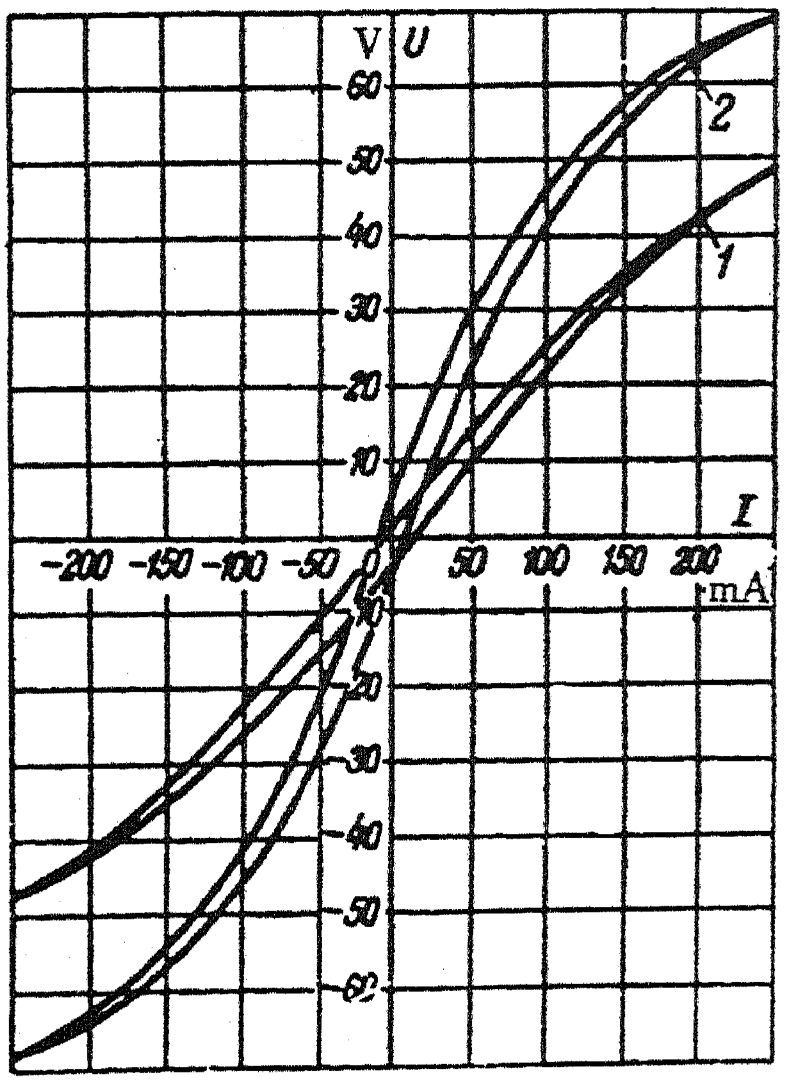

FIG.5. Characteristics of no-load running of the first (1) and second (2) stages of the test-model of the amplifier.

Preliminary tests of a three-stage amplifier have shown that its power amplification factor, in comparison with a two-stage amplifier, is increased considerably more than 20 times.

The dynamic characteristics were determined by measuring the rate of increase of the voltage at the output of the amplifier, after connecting one of its control windings to a source of constant voltage.

Fig. 8 shows the oscillograms of the voltage variation at the output of the amplifier, in no-load conditions, and during its work on load. Control power was equal to 2 W. The rate of voltage-increase per second was more than five times the nominal value of the voltage. This figure is quite permissible for many systems of automatic control, in which similar amplifiers can be used.

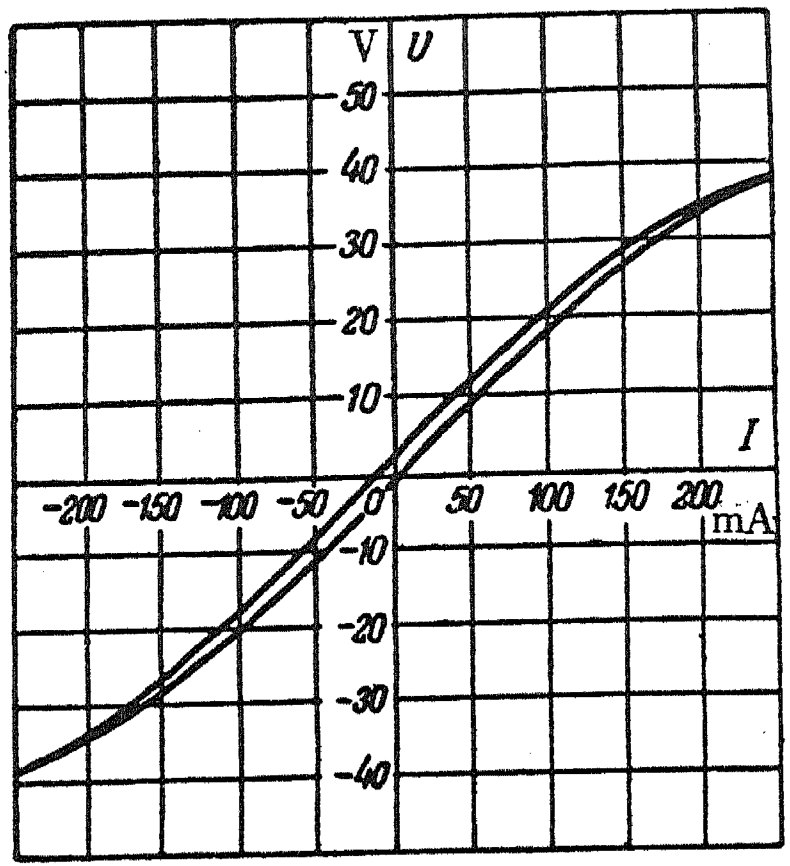

FIG. 6. The load characteristics of the test-model of the amplifier taken at a constant resistance $R_l = 1.6\ \Omega$

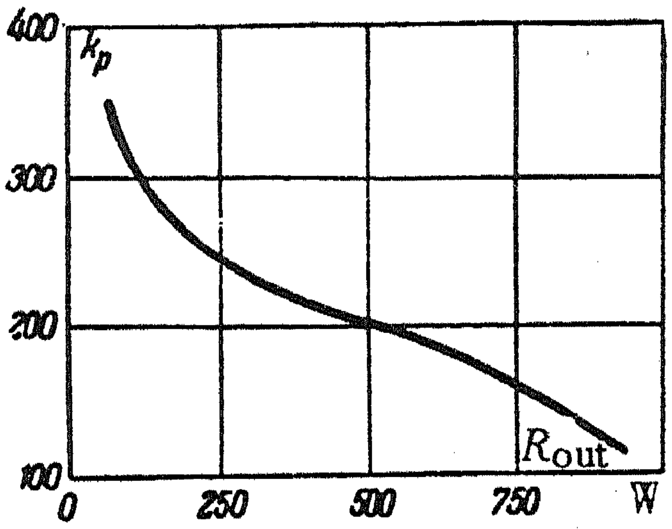

FIG. 7. Power amplification factor K_p as a function of the power at the output of the amplifier.

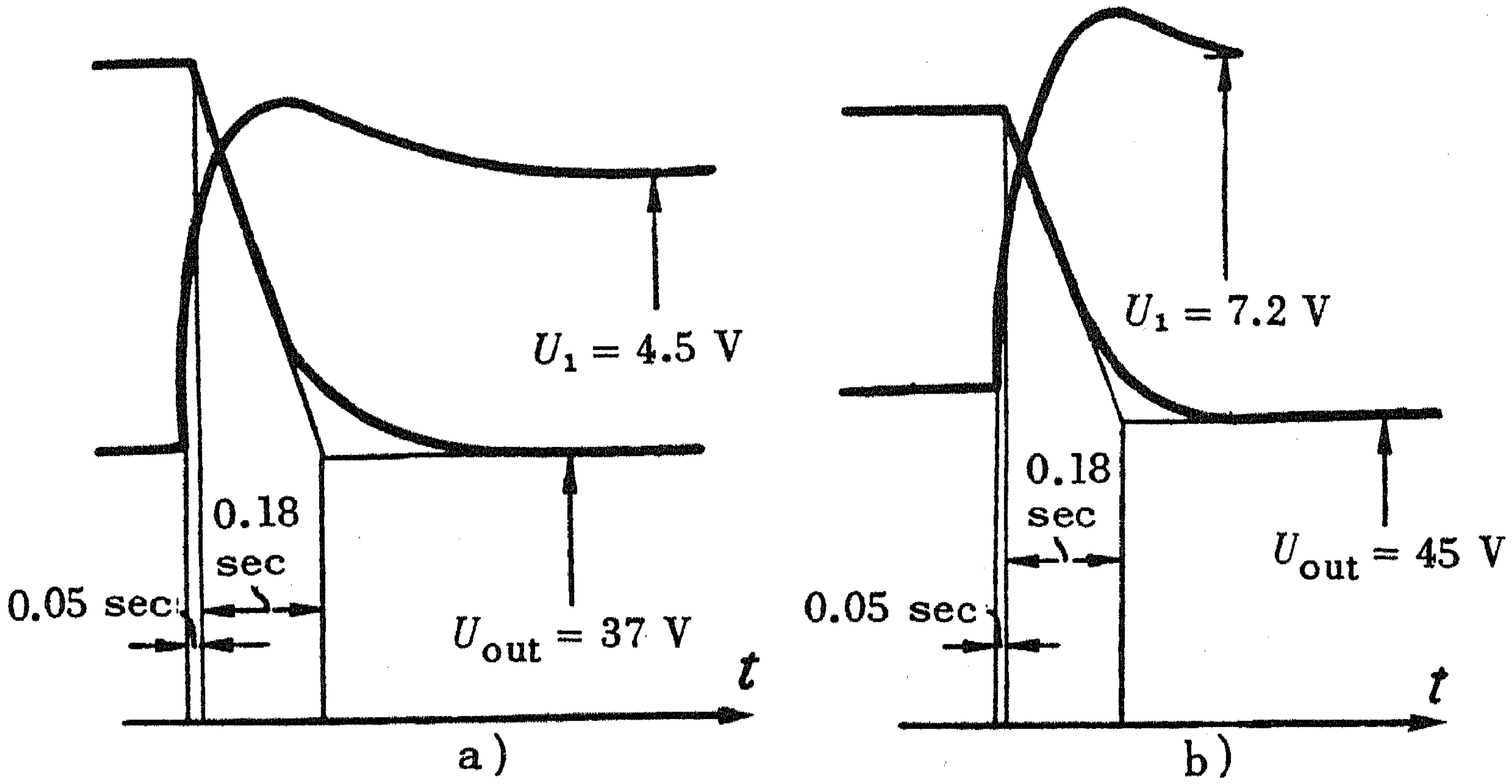

FIG. 8. Oscillograms of the amplifier voltage in no-load conditions (a), and under load (b).

(a) $$\left(\frac{dU_1}{dt}\right)_{\max} = 90\ \text{V/sec.};\quad \left(\frac{dU_{out}}{dt}\right) = 250\ \text{V/sec.}$$

(b) $$\left(\frac{dU_1}{dt}\right)_{\max.} = 144\ \text{V/sec.};\quad \left(\frac{dU_{out}}{dt}\right) = 205\ \text{V/sec.}$$

U_1 – voltage at the output of the first stage; U_{out} – voltage at the output of the second stage.

Conclusions

(1) The power obtained from such a machine equals up to 50 – 55 per cent of that of a machine of the normal type and of the same size.

(2) The specific features and the most important problems in the design of an

amplifier are:

(a) determination of the optimum ratio of the volumes of the armature slot, occupied by the first and the second stage windings;

(b) the determination of the optimum ratio of the areas of the slot opening occupied by the field windings of the corresponding stages of an amplifier. Obviously, the static and dynamic properties of an amplifier will depend on these ratios and on the degree of utilization of its size for the power supplied.

For better determination of the qualitative induces of the amplifiers of the type in question, in comparison with the figures for other types, a more detailed analysis and comparative tests of different amplifiers are needed.

Such investigations will enable classification of the different types of amplifiers according to the requirements imposed upon them in different systems of automatic control. A very important advantage of the amplifiers in question, in comparison with amplifiers with an axial field, is the possibility of their use in conditions of variable load resistance, without any additional mechanisms.

Appendix

Fundamental numerical data

Armature diameter $D_a = 135$ mm; the length of the armature $l_a = 135$ mm; the number of slots $Z = 20$; the number of commutator segments for a four-pole system ($2p = 4$) $K_1 = 59$; for a two-pole system ($2p = 2$), $K_2 = 60$. Air gap under the main poles $\delta = 1.5$ mm.

The data of the two-pole armature winding

Two-pole armature winding is laid in the lower part of the slot and occupies 38 per cent of its volume. Number of conductors in a slot – 24; the number of windings in a section $w_s = 4$; area of the cross-section of the winding $q = 1.21$ mm^2; slot pitch – $y_s = 10$; armature winding resistance – $R_a = 0.90\ \Omega$.

Four-pole field winding of the amplifier

Number of turns per pole $w_4 = 72$; area of copper cross-section of the winding $q_4 = 2.99$ mm^2; winding resistance $R_4 = 0.93\ \Omega$; time constant $T_4 = 0.112$ sec.

First control winding

Number of turns per pole $w_{01} = 485$; area of the copper cross-section of the winding $q_{01} = 0.152$ mm^2; winding resistance $R_{02} = 100\ \Omega$, time constant $T_{01} = 0.069$ sec..

Second control winding

Number of turns per pole $w_{02} = 485$; area of the copper cross-section $q_{02} = 0.152$ mm^2, winding resistance $R_{02} = 100\ \Omega$, time constant $T_{02} = 0.069$ sec.

Translated by S. Szymanski, Dipl. Ing.

REFERENCES

1. A. Vallini; Rotary amplifiers, *L'Energia, Elettrica* (1953).
2. M.G. Say (Editor); *Rotary amplifiers* (1954).

COLLEGE OF ENGINEERING GUINDY
LIBRARY BOOK

THE THEORY OF THE ELECTRICAL CIRCUIT FOR THE THREE-PHASE ORE-REDUCTION FURNACE*

N.A. MARKOV

Kuibyshev Industrial Institute

(Received 4 February 1957)

In the ore-reduction arc furnace the arcs burn under a layer of hard charge substances. The conducting charge produces a charge current circuit in the furnace, parallel to the arc. In addition, the ore-reduction furnace has a layer of slag and melt separating the arc from the pool of metal, and which is connected in series with the arc [1].

Fig. 1 is a representative diagram for the electrical circuit of an installation with a three-phase ore-reduction furnace. In this diagram the resistance of the arc, the charge and the layer are replaced by resistances, and the resistances of the supply circuit by resistances and inductive reactances. The resistances of the arcs and charge for the separate circuit phases are connected to two parallel star connexions. The furnace may also contain charge resistances connected in mesh between the electrodes of the separate furnace phases. This impedance mesh may be replaced by an equivalent star connexion, which is also connected in parallel with the arc resistance star connexions.

Both the arc resistances and those of the charge and the layer of melt alter during operation of the furnace.

When all the furnace phases are loaded equally and the circuit is symmetrical, the values characterizing the electrical working conditions of the furnace are linked by the following equations:

$$V = ir + L.di/dt + i_d R_s + u_d; \tag{1}$$

$$V = ir + L.\ di/dt + i_{sh} R_{sh}; \tag{2}$$

where V is the phase voltage of the circuit, i is the total electrode current, r is the supply circuit resistance, L is the supply circuit inductance, R_s is the layer resistance, R_{sh} is the charge resistance and u_d is the arc voltage; in the conditions in an ore-reduction furnace, this may be assumed not to depend on the current and to be linearly dependent on arc length.

---

* *Elektrichestvo* No. 1, 10 – 13, 1958 [Reprint Order No. EL 41].

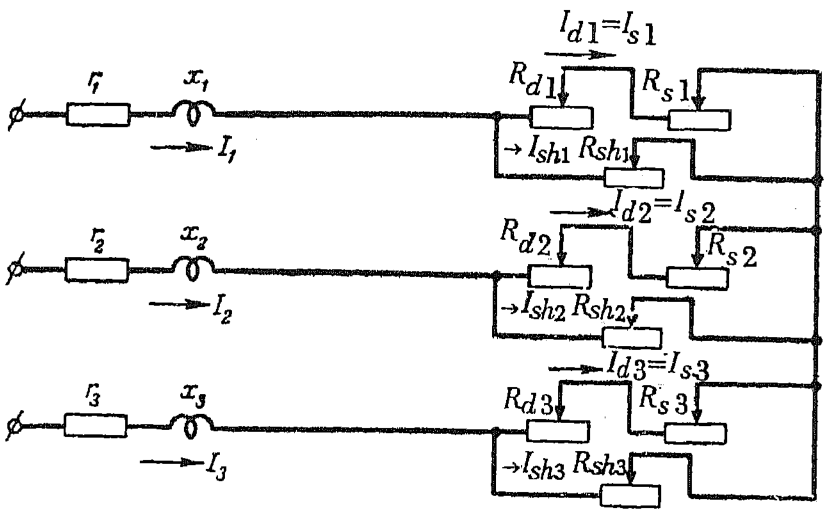

FIG. 1. Equivalent for a three-phase ore-reduction furnace electrical unit.

If there is no layer of melt ($R_c = 0$), the voltages between the ends of the arc and the charge are identical and remain unchanged in magnitude if the arc length is constant. Therefore, when the charge resistance alters and the arc length is constant, the total electrode current remains unchanged and all that occurs is redistribution of the current between the arc and the charge [1].

If there is no layer of melt ($R_c = 0$), the voltages between the ends of the arc and the charge are identical and remain unchanged in magnitude if the arc length is constant. Therefore, when the charge resistance alters and the arc length is constant, the total electrode current remains unchanged and all that occurs is redistribution of the current between the arc and the charge [1].

For the total electrode current, we have

$$i = i_d + i_{sh} = i_d + \frac{u_d}{R_{sh}}, \tag{3}$$

and for the melt layer current:

$$i_s = i_d. \tag{4}$$

The curve for the voltage across the ends of the charge and of the arc, approximately equal to the furnace voltage, will, depending on time, in a given case be sinusoidal with a truncated top and small excitation and extinction spikes (Fig. 2).

The size of the angle $\alpha = \omega t_1$, which defines the moments of arc excitation and extinction, depends on the charge resistance and the charge current. The lower the resistance of the charge and the higher the current in it, the larger the angle α and also the interval of time between arc extinction and excitation.

It follows from the curves in Fig. 2, that the relationship between the currents in the charge for different charge resistances and constant arc voltage is determined by the equation:

$$\frac{I_{sh1}}{I_{sh2}} = \frac{\sin \omega t_1}{\sin \omega t_2}. \tag{5}$$

If the arc voltage is of square form, the arc current will be:

$$i=\frac{V}{z}\sin(\omega t+\varphi-\psi)+\frac{u_d}{r}\left(\frac{2e^{-\frac{r}{L}t}}{1+e^{-\frac{r\pi}{\omega L}}}-1\right).\qquad(6$$

The arc current curve is practically sinusoidal, particularly in the three-phase circuits of an ore-reduction furnace with no neutral conductor, since there are no third and multiples-of-three harmonic components in the current curve for a symmetrical circuit.

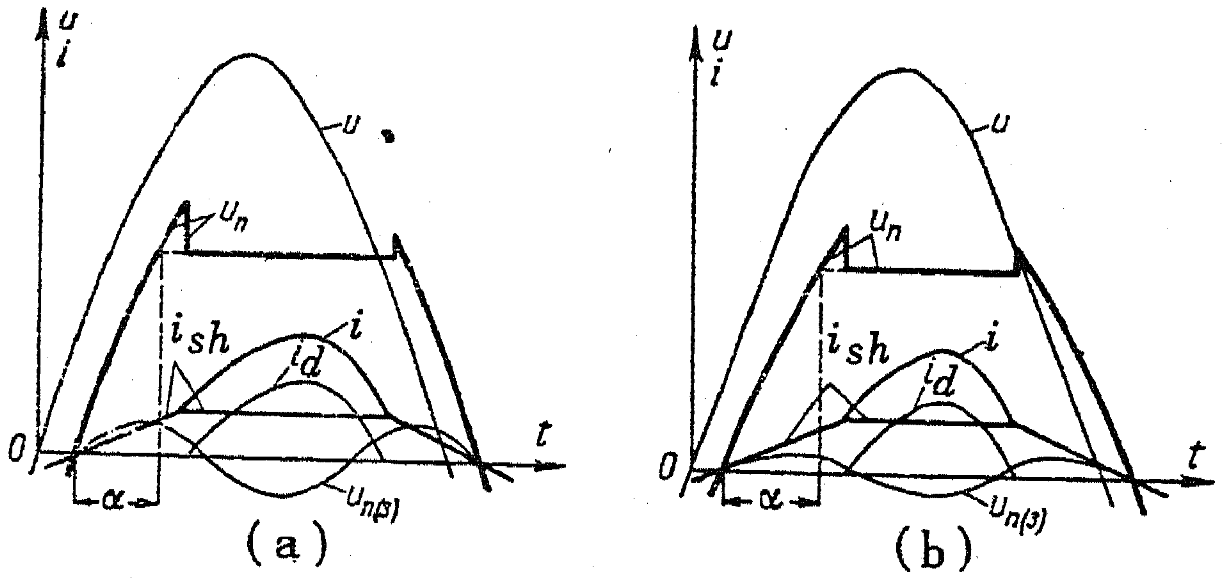

(a) (b)

FIG. 2. Curves for furnace voltages and currents for different charge resistances. (a) for $R_{sh}1$; (b) for $R_{sh}2 < R_{sh}1$.

The curve for the current i the charge during arc burning is of square form, similar to the arc potential curve; when the arc is extinguished, the curve for the current in the charge is of sinusoidal form [2]. The curve for the total current may be obtained as the sum of the arc and charge current curves (Fig. 2).

Let us resolve the curve for the voltage across the ends of the arc and charge into Fourier series.

Between 0 and a the change in this curve is expressed by the equation

$$y_1 = mA\sin x$$

and between a and $\frac{\pi}{2}$ by the equation

$$y_2 = A,$$

where A is the height of the square part of the curve and mA is the sine curve amplitude of the sinusoidal part of the curve; it follows that the amplitudes of the harmoni components are determined from the equation

$$A_k=\frac{4}{\pi}\left(\int_0^{\alpha} mA\sin x\sin kx\,dx+\int_{\alpha}^{\pi/2}A\sin kx\,dx\right)=$$

$$=\frac{4A}{\pi}\left[\frac{m}{2(1-k)}\sin(1-k)\alpha-\frac{m}{2(1+k)}\sin(1+k)\alpha+\frac{1}{k}\cos k\alpha\right]$$

and that the voltage across the ends of the charge and the arc may be represented as follows:

$$u_n=\frac{4A}{\pi}\left[\left(-\frac{m}{4}\sin 2\alpha+\cos\alpha\right)\sin x+\left(\frac{m}{4}\sin 2\alpha-\right.\right.$$
$$\left.-\frac{m}{8}\sin 4\alpha+\frac{1}{3}\cos 3\alpha\right)\sin 3x+\left(\frac{m}{8}\sin 4\alpha-\right.\qquad(7)$$
$$\left.\left.-\frac{m}{12}\sin 6\alpha+\frac{1}{5}\cos 5\alpha\right)\sin 5x+\ldots\right].$$

The presence of a layer of melt alters the correlation between the electrical values of the circuit, and changes the aspect of the curve for the voltage across the charge.

In this case the voltage across the charge (the furnace voltage) will be:

$$u_n = u_d + i_d R_s \tag{8}$$

and the current in the charge will be:

$$i_{sh} = u_n / R_{sh} = (u_d + i_d R_s) / R_{sh} \tag{9}$$

If the resistance of the charge alters at the same time as the currents in the charge and in the arc are redistributed, the furnace voltage also will change, and so in consequence will the total current.

The presence of a layer of melt can therefore be gauged from the changes in furnace voltage where there are changes in the charge resistance, for example when charging the furnace. If, for example, the resistance of the charge is increased for fixed electrode positions, this will reduce the current in the charge and increase the current in the arc, and will in consequence raise the furnace voltage, according to equation (8), from u_{n1} to u_{n2}. At the same time, with circuit voltages and supply circuit resistances unchanged, the total current will drop from I_1 to I_2 according to the equation

$$u_n = -Ir + \sqrt{(V^2 - I^2 x^2)} \tag{10}$$

The difference between these furnace potentials is:

$$u_{n1} - u_{n2} = (I_{d1} - I_{d2})\, R_s = (I_1 - I_2 - I_{sh1} + I_{sh2})\, R_s,$$

and in consequence

$$R_s = (u_{n1} - u_{n2}) / (I_1 - I_2 - I_{sh1} + I_{sh2}) \tag{11}$$

Since the curve for arc current is almost sinusoidal for a symmetrical circuit, the curve for voltage drop in the layer will also be almost sinusoidal. Therefore the curve for furnace voltage against time will, disregarding the arc excitation and extinction spikes, be depicted by two sine curves of different amplitudes and periods: the sine curve for voltage drop in the charge and that for voltage drop in the layer (Fig. 3).

Let us resolve this curve into Fourier series. Since the alteration in this curve between 0 and a is expressed by the equation:

$$y_1 = mA \sin x$$

and between a and $\pi/2$ by the equation:

$$y_2 = A + nA \sin lx,$$

where nA is the amplitude of the sine curve for voltage drop in the layer, and since $l = (\pi - 2a)/\pi$, the relationship of the arc burning time interval to a half-cycle, therefore the amplitudes of the harmonic components are determined by the equation:

COLLEGE OF ENGINEERING SURREY
LIBRARY BOOK
No.

$$A_k = \frac{4}{\pi}\left[\int_0^{\alpha} mA\sin x\sin kx\,dx + \int_{\alpha}^{/2}(A + nA\sin lx)\sin kx\,dx\right] =$$

$$= \frac{4A}{\pi}\left\{\frac{m}{2(1-k)}\sin(1-k)\alpha - \frac{m}{2(1+k)}\sin(1+k)\alpha + \frac{1}{k}\cos\alpha + \right.$$

$$+ \frac{n}{2(l-k)}\left[\sin(l-k)\frac{\pi}{2} - \sin(l-k)\alpha\right] -$$

$$\left. - \frac{n}{2(l+k)}\left[\sin(l+k)\frac{\pi}{2} - \sin(l+k)\alpha\right]\right\}.$$

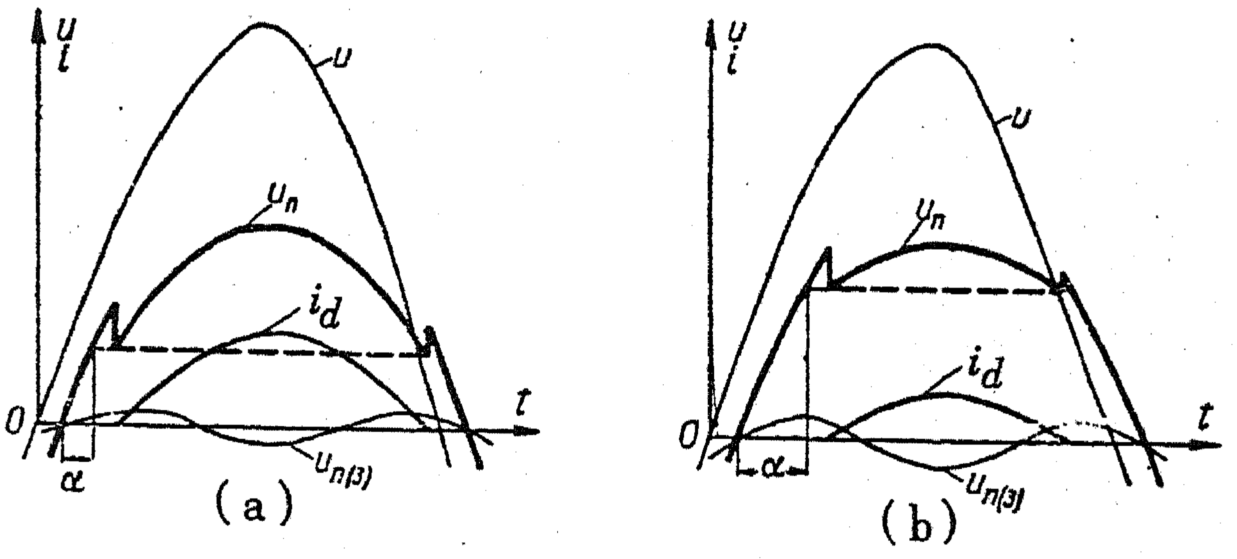

FIG. 3. Curves for furnace voltages for different layer and charge resistances. (a) for R_{s1}; (b) $R_{s2} < R_{s1}$.

Therefore the furnace voltage may be represented as follows:

$$u_n = \frac{4A}{\pi}\left\{\left\{\left[-\frac{m}{4}\sin 2\alpha + \cos\alpha + \frac{n}{2(l-1)}\left(\sin\alpha + \sin\frac{2\alpha^2}{\pi}\right) - \right.\right.\right.$$

$$\left.\left. - \frac{n}{l+1}\left[\sin\alpha - \sin 2\alpha\left(1 - \frac{\alpha}{\pi}\right)\right]\right\}\sin x + \left\{\left[\frac{m}{4}\sin 2\alpha - \frac{m}{8}\sin 4\alpha + \frac{1}{3}\cos 3\alpha + \right.\right.$$

$$+ \frac{n}{2(l-3)}\left[\sin\alpha + \sin 2\alpha\left(1 - \frac{\alpha}{\pi}\right)\right] +$$

$$\left. + \frac{n}{2(l+3)}\left[\sin\alpha + \sin 2\alpha\left(2 - \frac{\alpha}{\pi}\right)\right]\right\}\sin 3x +$$

$$+ \left\{\left[\frac{m}{8}\sin 4\alpha - \frac{m}{12}\sin 6\alpha + \frac{1}{5}\cos 5\alpha + \frac{n}{2(l-5)}\left[-\sin\alpha + \sin 2\alpha\left(1 + \frac{\alpha}{\pi}\right)\right] - \right.\right.$$

$$\left.\left. - \frac{n}{2(l+5)}\left[\sin\alpha - \sin 2\alpha\left(3 - \frac{\alpha}{\pi}\right)\right]\right\}\sin 5x + \ldots\right\}.$$

Since the curve for total current is depicted, as is the furnace voltage curve, by two sine curves, both with a layer present and without a layer, the total current may in both cases be represented by a series of the same type as (12), the value of A being equal to the ordinate up to a horizontal straight line drawn through the point of intersection of the sine curves (Fig. 3).

The shape of the total current curve in an ore-reduction furnace does not therefore depend solely on the shape of the arc potential curve, as is the case with a steel melting furnace, but also on the correlation of arc, charge and layer resistances.

If the circuit is three-phase with no neutral conductor, as is the case in a three-phase ore-reduction furnace, with a symmetrical circuit there are no third and multiples-of-three harmonic components in the current curve.

Where the circuit is non-symmetrical, third and multiples-of-three harmonic current-components appear in the circuit even where there is no neutral conductor.

For example, if the arc lengths and potentials differ in individual phases of the circuit, currents with third and multiples-of-three harmonics will pass in these phases, their values being determined from the equations:

$$I_{(3\ldots)1}=(u_{(3\ldots)1}-u_{(3\ldots)0})\,y_1; \qquad I_{(3\ldots)2}=(u_{(3\ldots)2}-u_{(3\ldots)0})\,y_2;$$

$$I_{(3\ldots)3}=(u_{(3\ldots)3}-u_{(3\ldots)0})\,y_3; \tag{13}$$

$$U_{(3\ldots)0}=\frac{u_{(3\ldots)1}\,y_1+u_{(3\ldots)2}\,y_2+u_{(3\ldots)3}\,y_3}{y_1+y_2+y_3},$$

where $u_{(3\ldots)1}$, $u_{(3\ldots)2}$ and $u_{(3\ldots)3}$ are the voltages of the third and multiples-of-three harmonics of the first, second and third phases, and y_1, y_2, and y_3 are the conductivities of the separate phases, including the arc conductivities.

These currents will supplement the currents for the separate phases and distort the current curves of these phases.

The third harmonics will reach their maximum during two-phase short-circuiting of arcs in operation, when $u_{(3\ldots)2} = 0$, $u_{(3\ldots)3} = 0$ and the phase currents for $y = y_1 = y_2 = y_3$ are as follows:

$$I_{(3\ldots)1}=\frac{2}{3}\,u_{(3\ldots)1}\,y; \qquad I_{(3\ldots)2}=\frac{1}{3}\,u_{(3\ldots)1}\,y; \qquad I_{(3\ldots)3}=\frac{1}{3}\,u_{(3\ldots)1}\,y. \tag{14}$$

The determination of the size of the voltage between the neutral points of a furnace and furnace transformer with respect to the resistances of the charge and the layer is of practical interest, since this voltage can easily be measured in a working furnace and used for determining the resistance of the charge.

This voltage is formed by third and multiples-of-three harmonic voltage components and occurs where there are electric arcs in a circuit even when the circuit is completely symmetrical.

Its value is arrived at from the equation:

$$u_0=\sqrt{u_3^2+u_9^2+u_{15}^2+\ldots}, \tag{15}$$

where u_3, u_9, u_{15} etc. are the third, ninth, etc. voltage components for different circuit phases.

The form taken by the curve for this potential depends on the shape of the furnace potential curve.

Its value for different correlations between charge, arc and layer resistances may be calculated by the equations given above.

Fig. 4 shows curves for the relationship between this voltage and the charge current, drawn on the basis of calculations made for different charge and layer resistances. We can see that as the charge current increases the voltage of the third and multiples-of-three harmonics decreases, while the reduction follows different courses depending on the resistance of the layer.

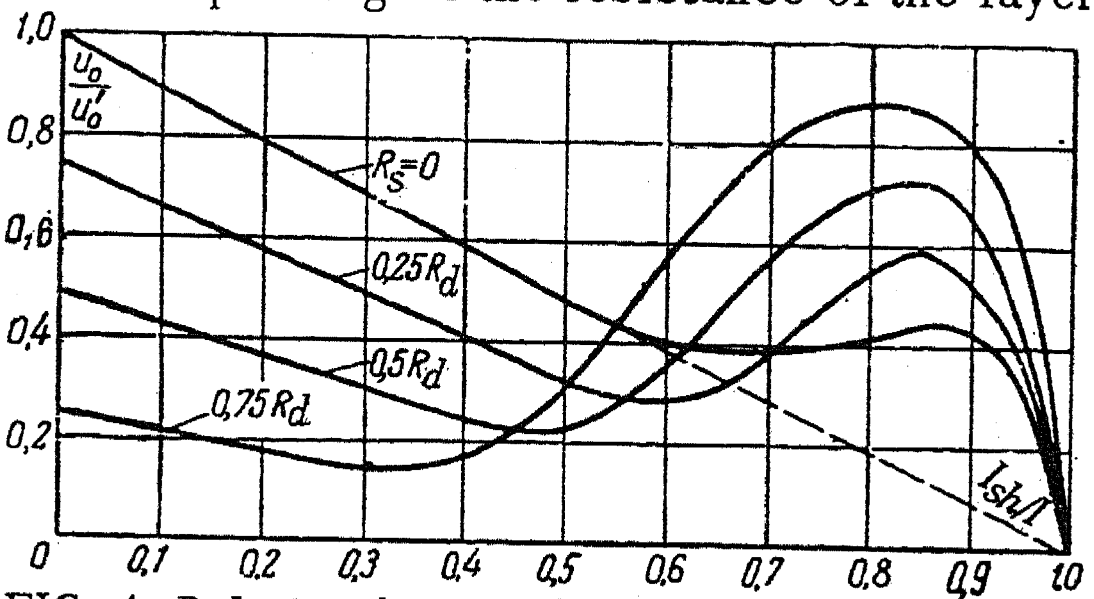

FIG. 4. Relationships of the voltages between the furnace and transformer neutral points to the charge current for a symmetrical circuit.

When the charge current is varied between 0 and 60 per cent of the total current, i.e. within the charge-current limits encountered in practice, the relationship of the voltage between the furnace and transformer neutral points, where no layer is present, is very close to linear and may be expressed as:

$$u_0 = u_0'(1 - I_{sh}/I), \qquad (16)$$

where u_0' is the voltage between neutral points without a charge ($R_{sh} = \infty$, $I_{sh} = 0$), and I = the total electrode current.

If there is no charge, then since the arc voltage curve is of square form, the voltage value u_0' will be one third of that at the arc ends. The arc voltage may be measured in the furnace when there is no layer, or may be calculated by equation (10) from the measured total furnace current.

The u_0 line can easily be drawn from equation (16) through two points: (a) the first point: $I_{sh} = 0$, $u_0 = \frac{1}{3} u_d$; (b) the second point: $I_{sh} = I$, $u_0 = 0$.

The curves in Fig. 4 and equation (16), may be used for determining values for charge resistance from electrical instrument measurements.

Fig. 5 is a circuit for the connexion of the electrical measuring instruments required for the determination of charge and layer resistances in a furnace.

To determine the charge resistance, where the furnace is symmetrically charged the voltage between the neutral points, the total current and the furnace potential must be measured. The charge current and charge resistance are determined from the upper curve in Fig. 4 by the equation:

$$R_{sh} = u_n/I_{sh}. \qquad (17)$$

The charge current may also be calculated from the equation:

$$I_{sh} = (1 - u_0' / \tfrac{1}{3} u_n)\, I. \tag{18}$$

If there is no charge, the resistance of the layer is determined from the readings of a voltmeter connected between the neutral points of furnace and transformer, by the well-known equation :

$$R_s = (u_n - 3u_0)\, /\, I. \tag{19}$$

However, where a charge is present, the resistance of the layer cannot be determined by this method, since the value of the potential u_0 depends on the charge resistance. In this case, if the charge resistance has been determined, the charge current can be calculated, and the resistance of the layer may be determined from the curves in Fig. 4 for a measured value of u_0 and the calculated charge current. Charge and layer resistances may only be determined by this method for voltage u_0 where the circuit is fully symmetrical and the furnace charging uniform.

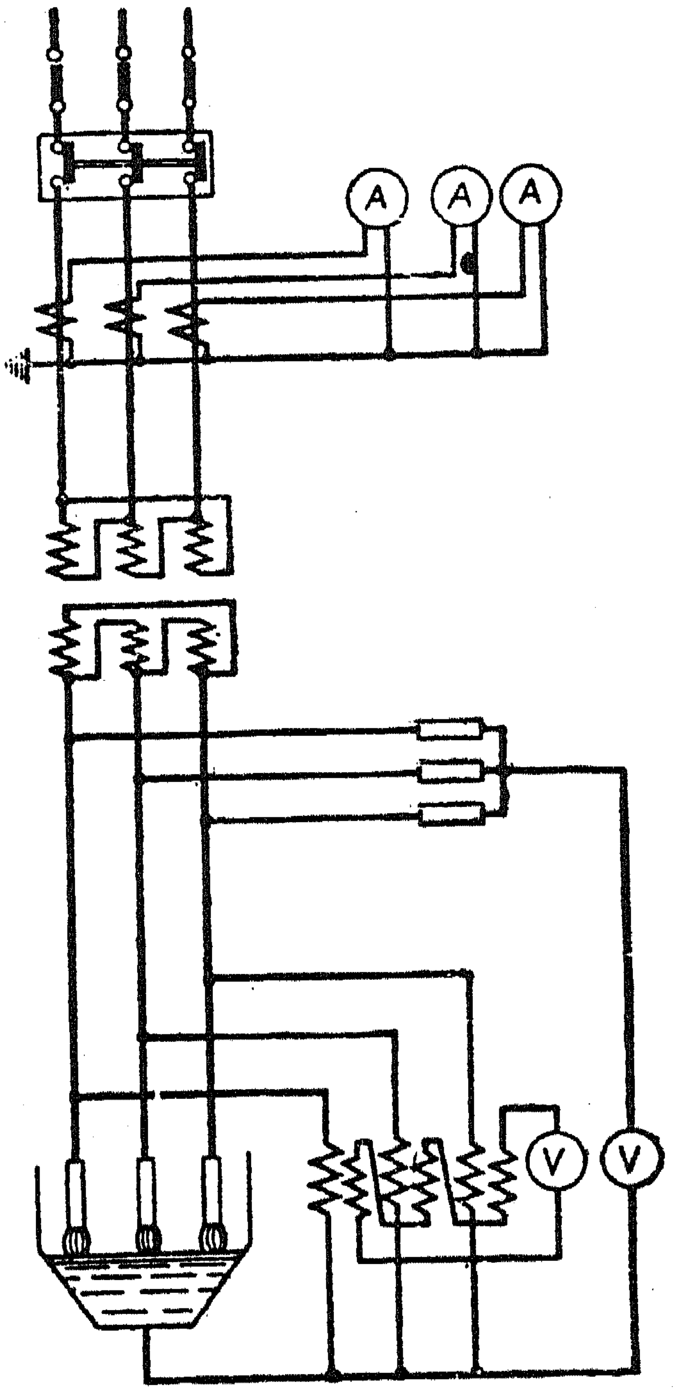

FIG. 5. Diagram for measuring charge and layer resistances.

Conclusions

(1) The non-sinusoidal nature of the curves for the furnace potential and the current in the electrical circuits of ore-reduction furnaces caused by the existence of charge and layer resistances has features distinguishing these curves from those for the electrical circuits in steel-melting furnaces.

(2) The problems of the theory of ore-reduction furnace electrical circuits which have been analysed enable us to increase the accuracy of the procedure for calculating these circuits; it becomes possible to calculate working currents and operating short-circuit currents, furnace characteristics and supply circuit impedances, the sinusoidal nature of the current curves being allowed for.

(3) The method proposed for determining the charge and layer resistances enables us to determine them from readings given by instruments set up outside the furnace.

Translated by J.H. Dixon

REFERENCES

1. S.I. Tel'nyi; Regulirovanie elektricheskovo rezhima raboty rudnotermicheskikh pechei (Control of the electrical conditions in operating ore-reduction furnaces), *Sborn. nauch. trud. Kuibyshevskovo industrial'novo inst.* No. 3 (1950).
2. S.I. Tel'nyi and I.T. Zherdev, Shuntirovannaia duga v elektricheskikh ferrosplavnykh pechakh (The shunted arc in electric ferroalloy furnaces). *Teor. i prakt. metallurg.* No. 9 (1937).

THE UNIVERSAL CHARACTERISTICS OF THE DYNAMIC BRAKING OF ASYNCHRONOUS MOTORS*

V.I. KLIUCHEV

Moscow Power Institute

(Received 29 April 1957)

The existing methods used for calculating the mechanical characteristics of the dynamic braking of asynchronous motors according to a scheme with separate excitation from a d.c. circuit are founded on the use of the motor magnetization curve $E_1 = f(I\mu)$. Use of the magnetization curve is made necessary by the saturation of the magnetic circuit which takes place in the great majority of cases in practice.

The saturation is allowed for in analytical methods of calculation by the use of a non-linear or piecewise-linear approximation of the magnetization curve. As a rule sufficient closeness of approximation over a wide range of magnetizing current values is not obtained, nor at the same time are correlations convenient for the calculation produced. Analytical methods of calculation have not therefore been applied in practice.

The graphic analysis method of calculation [2-4], which is based on direct use of the motor magnetization curve and equations (1) and (2) below, is at present the method most widely used in practice :

$$I_E^2 = \frac{E_1^2}{x_\mu^2}\left[1 + x_\mu \quad \frac{x_\mu + 2x_2'}{\frac{R_2'^2}{s^2} + x_2'^2}\right]; \tag{1}$$

$$M = \frac{3}{9.81\omega_0}\,\frac{E_1^2}{\frac{R_2'^2}{s^2} + x_2'^2}\,\frac{R_2'}{s}, \tag{2}$$

where I_E is the rated stator alternating current phase in amperes, equivalent to the direct current I_n, relating to the generated magnetizing force of the stator winding; E_1 is the atator phase e.m.f., in volts; I_μ is the magnetizing current in amperes; $x\mu = E_1 / I\mu$, the inductive reactance of magnetization, in ohms; x_2' is the reduced

---

* *Elektrichestvo* No. 1, 14 – 18, 1958 [Reprint Order No. EL 42].

rotor winding leakage inductive reactance, in ohms; $R_2' = r_2' + R_{d2}'$, the full reduced resistance of the rotor phase, in ohms; r_2' is the reduced resistance of the rotor winding phase, in ohms; $s = \omega/\omega_0$, the slip in dynamic braking; and M is the moment, in kg m.

The values of E_1 being known, $x\mu$ is determined from the magnetization curve; the slip is then found from equation (1). The corresponding value for the moment M is determined from equation (2). Calculations are made for points, and to draw the mechanical characteristic $M = f(s)$ takes a great time, particularly when calculating the static characteristics of dynamic braking in automatic control systems.

In this connexion, efforts to obtain universal mechanical characteristics in relative units, generalized for the greatest possible number of series of asynchronous motors, are of great practical interest. Much work was done in this direction at the Moscow Power Institute [2, 3].

It was shown to be possible, on the basis of analysis of the magnetization curves for isolated sizes in various series, to generalize the magnetization curves in relative units for motors in a given series to an accuracy of ± 5 per cent; it was found to be impossible to generalize the magnetization curves for different series with acceptable accuracy. At the same time, analysis of the parameters showed that it is not possible to generalize either the basic parameters or various combinations of them, even for motors in a single series, let alone for those in every series. Thus attempts to simplify the calculations by using universal curves have not yet led to the required results.

Analysis of the works indicated draws one to conclude that the relative units system adopted at present [2, 4] must be renounced if we are to obtain universal curves which are suitable for calculations of dynamic braking for motors in different series. A relative units system must be found which, when employing universal characteristics, will allow us to take into account the features of a particular machine both regarding its parameters and its magnetization curve. The first step in this direction was taken by Prof. A.T. Golovan in his published works. Dynamic braking characteristics are adduced in [1] in relative units which make it possible to take a number of specific motor characteristics into account; the applicability of these characteristics however, as the author remarks, is limited to low-power motors. The present article puts forward universal characteristics which can be used in the majority of cases in practice.

Generalization of the magnetization curves is based on a system of relative units in which the open circuit current I_0, for $V_{1\phi} = V_{1\phi N}$, and the stator phase e.m.f. $E_{1\phi 0}$ corresponding to this current are taken as the basic quantities of the magnetizing current and e.m.f. Here the difference between the magnetization curves for separate sizes and series is governed on the one hand by discrepancy in the magnetization curve shapes, and on the other hand by different levels of saturation of the magnetic circuit at specified voltage. It is impossible to eliminate the difference between the shapes of the characteristics by selecting other basic quantities; there are however grounds for supposing that this difference may not be important. The influence of the second feature can be fully eliminated if we take as basic quantities for each specific motor the rated e.m.f. E_{1p} and the rated open circuit current I_{0p} corresponding to that e.m.f. in conditions where the magnetic circuit is saturated to an equal degree:

$$E_{1p} = b_e E_{1\phi 0}\,;\; I_{0p} = b_i I_0\,. \tag{3}$$

Where a magnetization curve for $e = f(i\mu)$ exists which corresponds to the rated basic quantities, it is possible to proceed to the characteristic $e_p = f(i\mu_p)$ corresponding to the calculated basic quantities by using the following relationships:

$$e_p = \frac{E}{E_{1p}} = \frac{1}{b_e}\,e\,;\quad i_{\mu p} = \frac{I_\mu}{I_{0p}} = \frac{1}{b_i}\,i_\mu\,. \tag{4}$$

Thus universal dynamic braking characteristics calculated on the basis of some magnetization curve assumed as basic, may be used for specific motors with an accuracy determined by the degree to which the shapes of the magnetization curves coincide. The magnetization curve for the motor in question may serve as the basis for the selection of the coefficients b_e and b_i. However, in the majority of cases the person performing the calculations is not in possession of these data, and to obtain them is a very laborious process. The conclusion mentioned above that the $e = f(i\mu)$ magnetization curves can be generalized for motors of individual series is therefore of great practical interest.

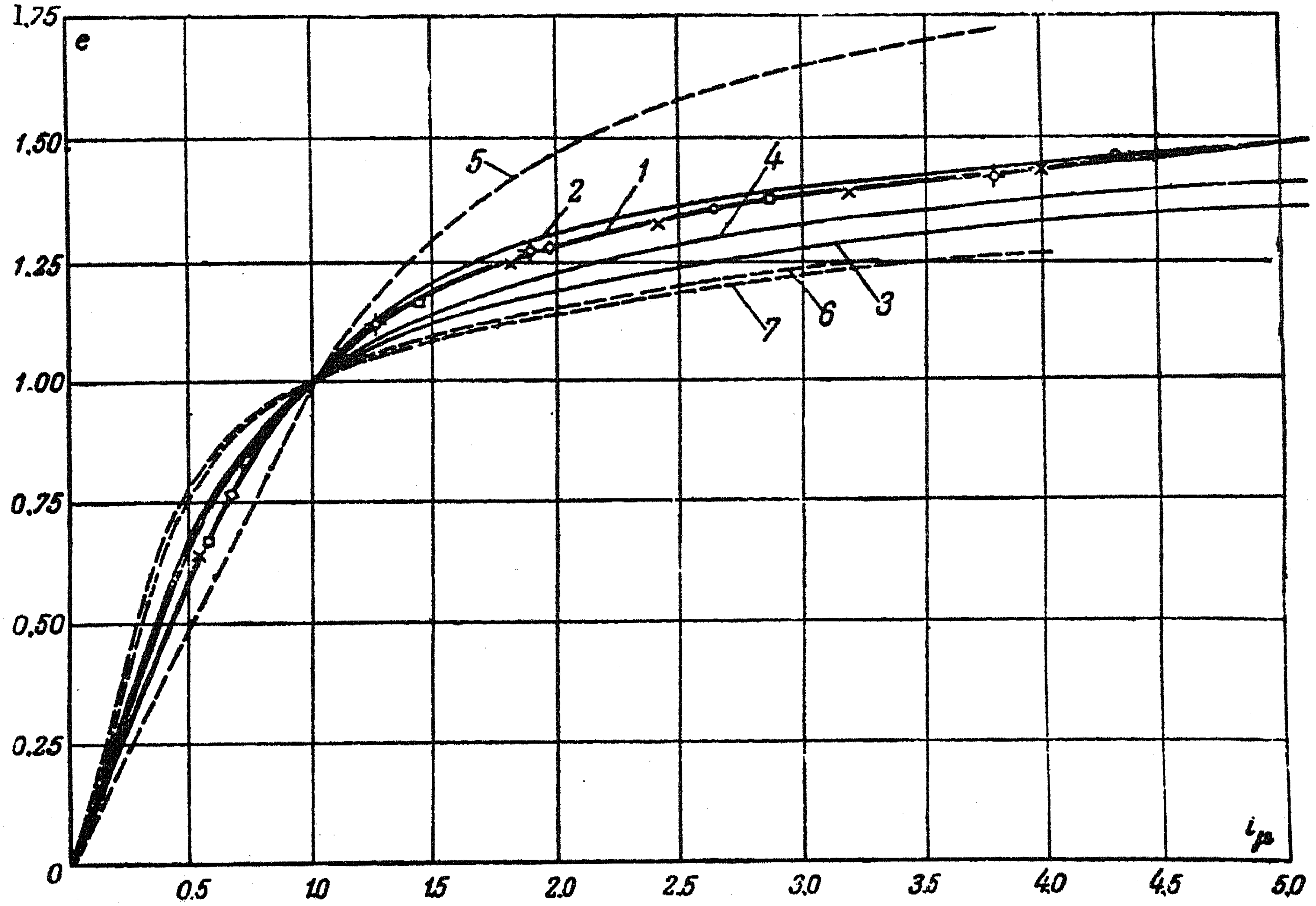

FIG. 1. Magnetization curves for asynchronous motors. 1 - FAMSO, AT, A; 2 - AM, DA; 3 - MT; 4 - MTK; 5 - KT-55/1003; 6 - AK61-6; 7 - AK61-4. ———— generalized relationships; — — — — — relationships obtained experimentally.

Generalized $e = f(i\mu)$ curves for series MT, MTK, AM [2] and FAMSO,DA, AT and A [3] are shown in Fig. 1. The $e = f(i\mu)$ curve may be used to advantage as the basic magnetization characteristics for FAMSO, AT and A series motors, the curve being common to this group of series. The values of the coefficients b_e and b_i selected from a state of equal saturation are set out in Table 1.

TABLE 1.

	FAMSO AT & A	DA, AM	MT	MTK	KT-55/1003	AK 61-1, AK 61-6
b_e	1.00	1.03	0.86	0.93	1.30	0.79
b_i	1.00	1.06	0.70	0.84	1.52	0.50

Points on the $e_p = f(i\mu_p)$ curves, calculated on the basis of equations (4) using the coefficients set out in Table 1, are plotted in Fig. 1. Over the whole range of magnetizing current these points lie in practice on the $e = f(i\mu)$ curve taken as the basic curve; this confirms that universal characteristics calculated from a basic curve can be used with equal accuracy for motors of all series enumerated.

Series AK and KT, whose generalized curves are lacking, are represented as examples by the experimental magnetization curves for the AK 61-4, AK 61-6 and KT-55/1003 motors. The values of b_e and b_i used for calculating the corresponding points on the $e_p = f(i\mu_p)$ curves for these motors are given in Table 1. These curves also practically coincide with the basic characteristic $e = f(i\mu)$. Thus, when the appropriate basic quantities are selected, on the one hand the limits within which the magnetization curves can be generalized become wider and on the other hand calculations from universal dynamic braking characteristics, where a magnetization curve exists for a given type of machine, become more accurate.

We will adopt the following basic unit system from now on:

$$e_p = \frac{E_1}{b_e E_{1g0}}; \quad i_{\mu p} = \frac{I_\mu}{b_i I_0}; \quad x_{\mu d} = \frac{e_p}{i_{\mu p}} = \frac{E_1}{b_e E_{1g0}} \times \frac{b_i I_0}{I_\mu} = \frac{x_\mu}{b_\mu x_0}; \quad i_E = \frac{I_{\text{э}}}{b_i I_0}; \quad x'_{2d} = \frac{x'_2}{b_\mu x_0}. \tag{5}$$

Using (5), equation (1) becomes:

$$i_E^2 b_i^2 I_0^2 = \frac{e_p^2 b_e^2 E_{1g0}^2}{x_{\mu d}^2 b_\mu^2 x_0^2} \times \left(1 + x_{\mu d} b_\mu x_0 \frac{x_{\mu d} b_\mu x_0 + 2x'_{2d} b_\mu x_0}{\frac{R_2'^2}{s^2} + x_{2d}'^2 x_0^2 b_\mu^2} \right).$$

From this we can obtain the following equation for the universal characteristic $e_p = f(i_E, s_0)$ by simple transformations

$$e_p^2 = \frac{i_E^2 x_{\mu d}^2}{1 + x_{\mu d} \frac{x_{\mu d} + 2x'_{2d}}{1/s_o^2 + x_{2d}'^2}}, \tag{6}$$

COLLEGE OF ENGINEERING LIBRARY BOOK No. GUINDY

where $s_0 = s/s_p$, the relative slip, and $s_p = R_2'/b_\mu x_0$, the calculated slip.

In a similar way we can obtain from equation (2) an equation for the universal characteristic $m = f(e_p, s_0)$:

$$m = \frac{s_0 e_p^2}{1 + s_0^2 x_{2d}'^2}, \tag{7}$$

where $m = M/M_p$, the relative moment value, and $M_p = 0.306/\omega_0 \, b_e \, b_i \times I_0^2 \, x_0$, the calculated moment value in kg m.

With the aid of the magnetization curve, relationships (6) and (7) establish the link between the relative values for the moment m, the slip s_0 and the direct current i_E for a given value of the parameter x_{2d}' tabulated in Table 2.

TABLE 2.

Series	x_{2d}'	
	Minimum	Maximum
MT	0.045	0.10
FAMSO	0.035	0.07
DA	0.040	0.09
AT, AM	0.025	0.06

The values of x_{2d}' lie between 0.025 and 0.1, while the lower values correspond to high-speed high-power motors. Taking this into account and using equations (6) and (7) and the magnetization characteristic selected above, two groups of universal $m = f(s_0)$ characteristics were calculated for a constant i_E, these groups corresponding to the intermediate values of x_{2d}' of 0.04 and 0.08 (Fig. 2). Comparison of the curves corresponding to these values of x_{2d}' confirms that to disregard the value of x_2', as is recommended in a number of published works, for low and average power machines, may involve errors of 10-12 per cent in determining the moment. On the other hand it is evident that the groups of curves shown in Fig. 2 enable us to take the effect of this parameter sufficiently accurately into account.

The value of the stator current I_n, ensuring the specified maximum braking moment $M_{\max}$ for a motor may be determined from the universal characteristics $m_{\max} = f(i_E)$, x_{2d}' being a constant, given in Fig. 3. For this purpose the relative value for the moment $m_{\max} = M_{\max}/M_p$ must be determined; the corresponding relative stator current i_E must then be found from the curves in Fig. 3.

The direct current magnitude is calculated from the equation

$$I_n = k_{sx} \, b_i I_0 i_E,$$

where $k_{sx} = I_n/I_E$, a coefficient depending on the stator winding circuit diagram [1,4].

The $M = f(s)$ characteristic, where i_E is constant, is calculated from the corres-

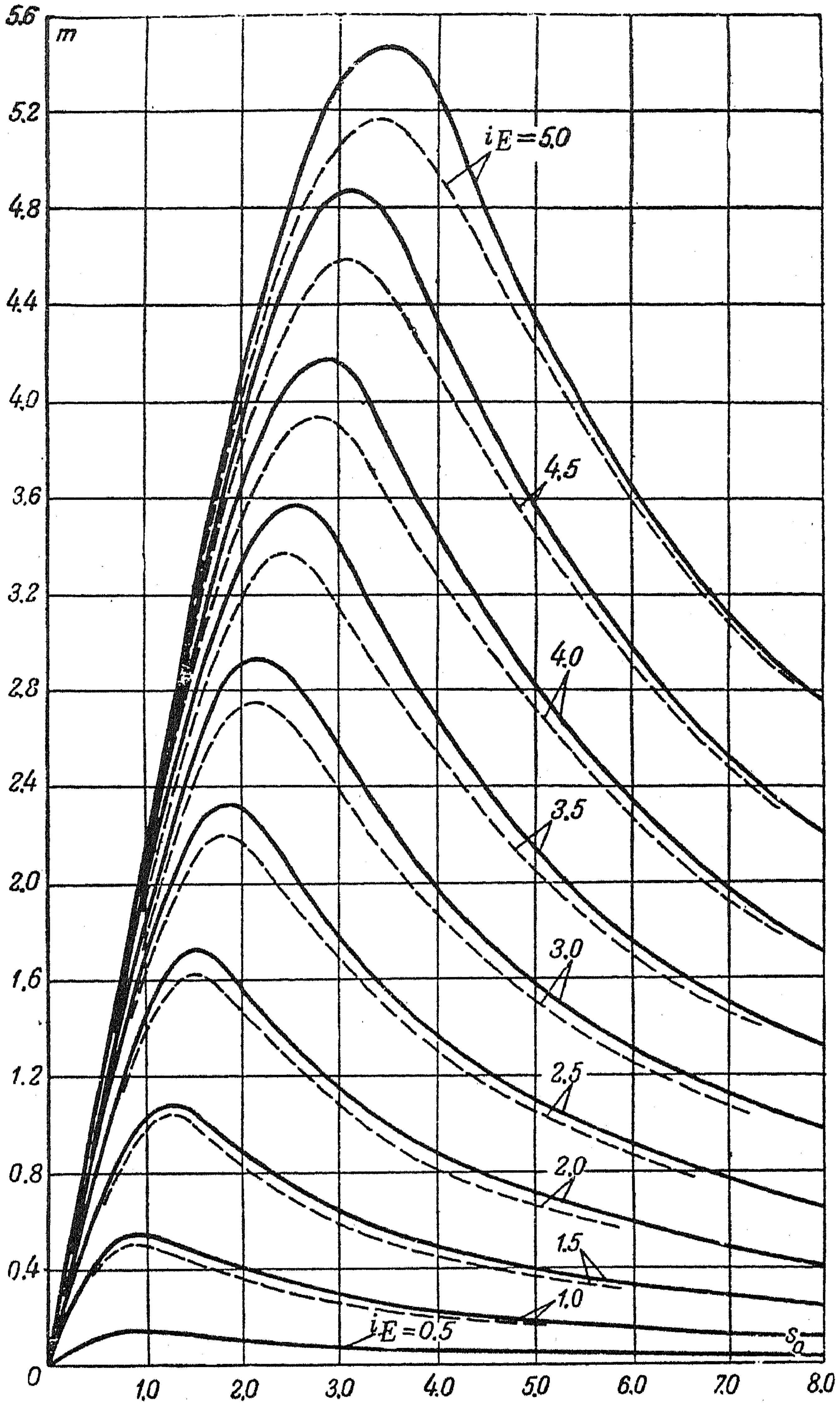

FIG. 2. Universal mechanical characteristics of the dynamic braking of asynchronous motors; —— for $x'_{2d} = 0.04$; – – – – for $x'_{2d} = 0.08$.

ponding universal $m = f(s_0)$ curve (i_E constant) from the following equations:

$$M = mM_p = m\frac{0{,}306}{\omega_0}\,b_e\,b_i I_0^2 x_0; \qquad s = s_o\,s_p = s_o \cdot \frac{R_2'}{b_\mu x_0}\,.$$

If it is necessary to determine the additional resistance of the rotor circuit R'_{d2}, for which the unknown characteristic passes through specific points M_1 and s_1, the corresponding slip s_{01} is determined, with the aid of the relative moment value $m_1 = M_1 / M_p$, from the universal characteristics.

The additional resistance R'_{d2} is calculated from the equation

$$R'_{d2} = b_\mu x_0 \frac{s_1}{s_{01}} - r'_2.$$

The static characteristics in control systems acting on the stator current magnitude during dynamic braking can be calculated in a minimum of time from universal characteristics. If for example $I_n = f(s)$, then this relationship can be expressed, using the correlations given above, in relative units by $i_E = f(s_0)$, and the points for the mechanical characteristics of control systems can be determined directly from the $m = f(s_0)$ curves (where i_E is constant).

It is necessary to dwell briefly on the recommendations met in technical literature, according to which the mechanical characteristic for the dynamic braking of an asynchronous motor can be deduced, for known values of maximum moment and the slip corresponding to them, from the well known simplified equation for the mechanical characteristics of asynchronous motors:

$$M = \frac{2M_{\max}}{\frac{s}{s_{\max}} + \frac{s_{\max}}{s}}. \tag{8}$$

Fig. 4 shows the $M = f(s)$ characteristics (where i_E is constant) for MT 31-6 motors, calculated using the universal curves according to the parameters for this motor given in [4], the characteristics obtained by equation (8) and also the corresponding experimental curves. We can see from comparison of the curves that saturation alters the shape of the characteristic; the error in determining the moment may reach 20-30 per cent for a given slip; calculations from equation (8) should there be considered to be approximate. The initial data necessary for calculation may be obtained from the curves given in Fig. 3.

Just as when using the initial graphic analysis method, it is necessary to know a number of motor parameters, r_1, r'_2 and I_0 in order to make calculations using universal curves. The effect of errors in the determination of each of these parameters on the accuracy of the calculations varies. For example, the value of r_1 is necessary for calculations for a d.c. circuit, and a certain amount of inaccuracy in its determination has no material effect. Errors in determining r'_2 involve inaccuracy in computation of the slip corresponding to a given moment value. The greater the additional resistance of the rotor circuit R'_{d2} the less the inaccuracy. Inaccuracy in determining the open circuit current I_0 involves the highest error in calculation, since it is used for determination of the moments M and the direct current I_n. Therefore calculations must be based, in important cases, on reliable motor parameter values, and their determination from catalogue data can only be recommended for rough calculations.

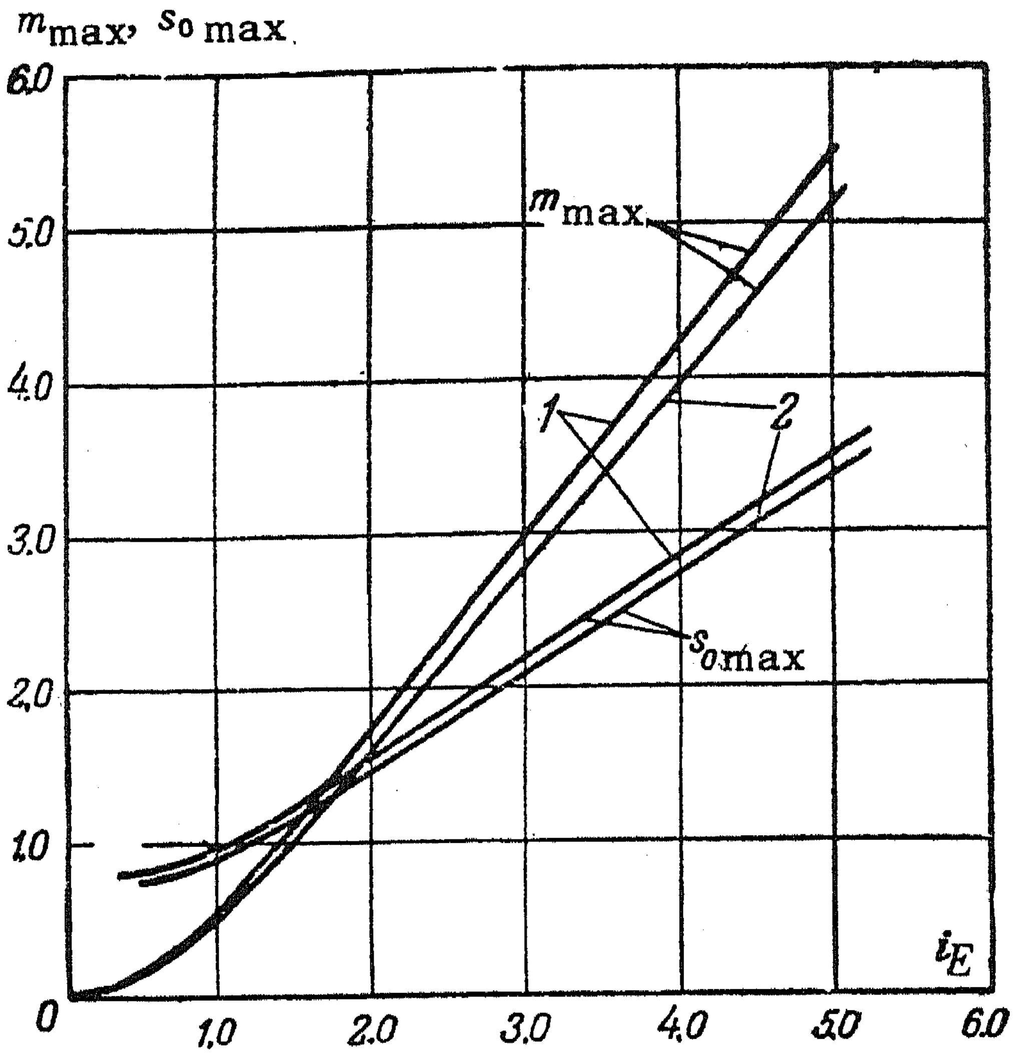

FIG. 3. The relationships $m_{max} = f(i_E)$ and $s_{0\,max} = f(i_E)$ for constant x'_{2d}. 1 - where $x'_{2d} = 0.04$; 2 - where $x'_{2d} = 0.08$.

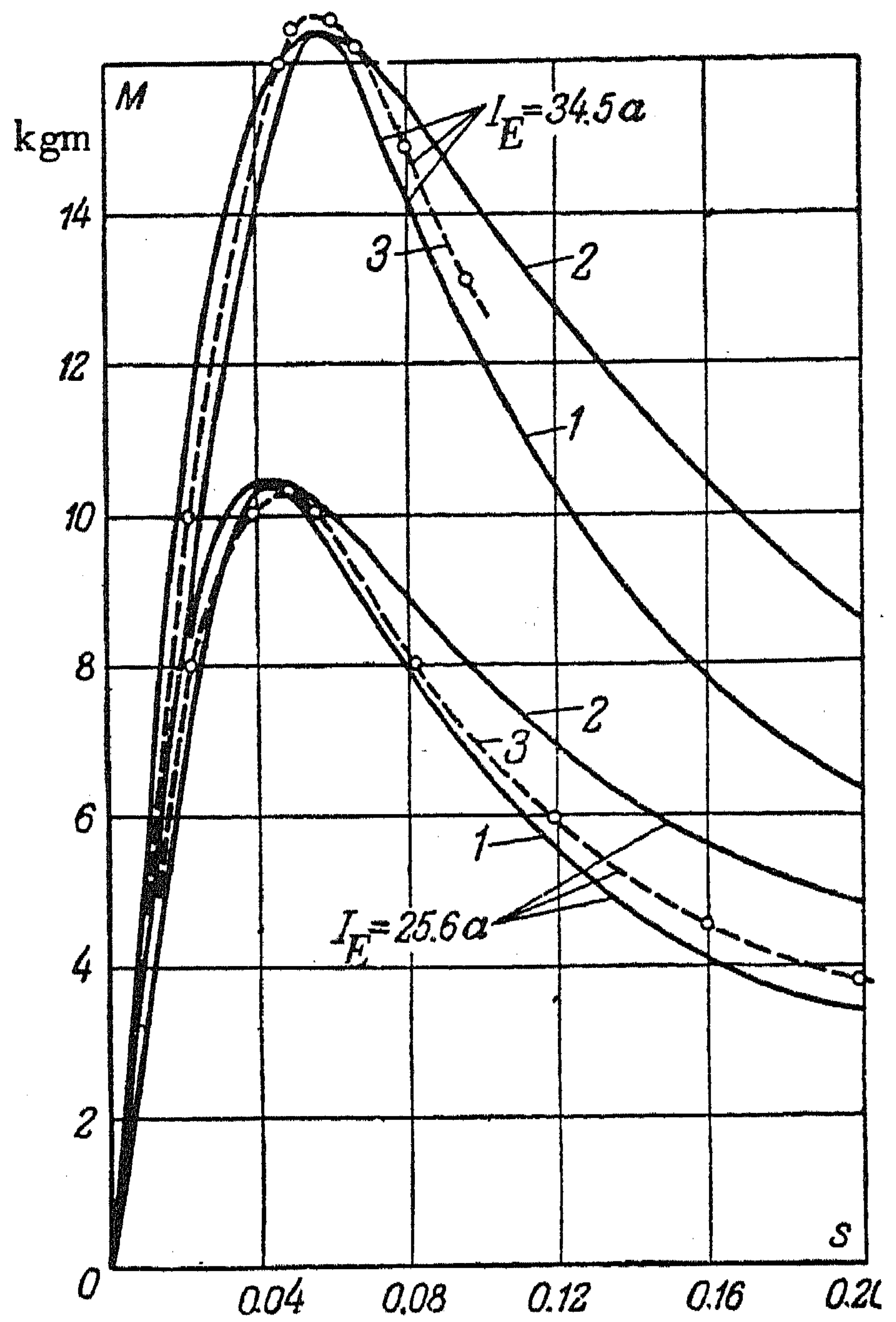

FIG. 4. The dynamic braking mechanical characteristics for the MT-31-6 motor. 1 - calculated from universal characteristics; 2 - calculated from equation (8); 3 - experimental curves.

When using the generalized magnetization curves given in Fig. 1, calculation of dynamic braking from universal characteristics cuts down the labour involved by many times and provides the same accuracy as is given by calculation from the initial equations (1) and (2) checked experimentally [2, 3]. At the same time, the great advantage of universal characteristics is that thay may also be used directly for the known magnetization curve for a specific motor or for a generalized curve for a series not given in Table 1. To do this, values for the coefficients b_e and b_i providing maximum coincidence between the $e_p = f(i_{\mu p})$ curve and the magnetization curve taken as basic must be selected. Thus the proposed curves can, in the majority of cases, in practice facilitate calculation of the static chacteristics of the braking of asynchronous motors.

Translated by J.H. Dixon

REFERENCES

1. A.T. Golovan; *Elektroprivod (Electric drive).* Gosenergoizdat (1947).
2. A.T. Golovan, I.P. Barbarash, A.P. Kuvaeva and V.I. Yakovlev; *Issledovanie i razrabotka metoda rascheta dinamicheskovo tormozheniia asinkhronnykh dvigatelei (Investigation and development of a method for calculating the dynamic braking of asynchronous motors),* Moscow Power Institute (1954).

3. A.T. Golovan, I.I. Levina, and V.I. Kliuchev; *Metodika rascheta dinamicheskovo tormozheniia shakhtnykh pod'emnykh mashin (Procedure for calculating the dynamic braking of mine hoist machines)*, Moscow Power Institute (1954).
4. S.N. Veshenevskii; *Raschet kharakteristik i soprotivlenii dlia elektrodvigatelei (Calculation of characteristics and impedances for electric motors)*, Gosenergoizdat (1954).

ARCING SHORT-CIRCUITS ON 400 kV TRANSMISSION LINES AND METHODS OF DEALING WITH THEM*

A.S. MAIKOPAR and N.N. BELIAKOV

Central Scientific and Research Electrotechnical Laboratory,
Moscow Electric Station

(Received 19 September 1957)

On 400 kV transmission lines with a solidly earthed neutral, we have to expect mainly single-phase short-circuits to earth. As opposed to the lines with lower voltages, the restoring of the electric strength of the path of the arc after switching off the phase becomes more difficult on 400 kV lines because of appreciable influence of the current at the point of damage caused by capacitive and electromagnetic connections between the disconnected phase and the working phases. The supply current which will flow at the point of the fault, after automatically switching off the faulty section of the line, will sustain the electric arc for a certain time. The next reclosing can be done only after the extinction of the arc and restoration of the electric strength. This circumstance not only defines the placing of protective relays but also exerts an influence on the total lay-out of switchgear on the 400 kV lines. In particular, the problem of connecting shunting reactors directly to the line or through the circuit-breakers is strictly connected with the extinguishing of the sustained current arc. Several works are known dealing with research on the sustained current arcs [1-5]. Nevertheless, they do not give a clear idea of the range of sustained currents, for which it is possible to use single-phase automatic reclosing. As a result of these works, it is assumed that the extinguishing of the sustained current arc is possible for the currents of the order of 12-15 A.

Research into powerful open arcs, carried out by the C.S.R.E.L., has shown that an electric arc is capable of self-extinction even for currents of a few hundred ampres, if the conditions exist for a substantial increase of its length [6]. On this basis the investigations of the sustained current conditions were undertaken. Experiments on a 6 kV model have shown that the extinction of the sustained current arc for gradients of 5-15 kV/m occurs for currents up to 75-100 A, and experiments on a 220 kV grid 750 km long have shown the possibility of extinction of the sustained current arc in the real conditions for currents of 30 A, [7]. Further experiments have been carried out on the 400 kV line from Kuibyshev Hydroelectric Power Station Moscow. The results are given in this article.

---

* *Electrichestvo* No.1, 19-25, 1958 [Reprint Order No. EL 43].

The values of the sustained currents and the restoring voltages at the place of flash-over determine to a considerable degree the time of burning of the arc.

In considering various separate cases, used for calculations, it is necessary to bear in mind that in the case of a single-phase automatic reclosing, the phenomenon of the sustained current is conditioned by the presence on the sound phases of the voltage of industrial frequency and of the working current, and, in the case of three-phase reclosing, by the presence of voltages varying in time on the sound phases during their capacitive discharge into the earth.

If a voltage transformer is connected to the 400 kV line, then the discharge of the line into it will have an aperiodic character. For a section of the line 200-500 km long the time constant of the aperiodic discharge is about 0.01 sec. The process of the discharge will be practically finished in 0.05 sec and will not produce any appreciable sustained current phenomenon. Therefore, in future, there is no need to consider this case. If the voltage transformer and the reactor are connected to the line, then the discharge process will be determined by the ratio of the capacitance of the line and the parameters of the reactor, in so far as the resistance of the reactor is smaller than the resistance of the voltage transformer by a few orders of magnitude. In this case, there will be an oscillatory discharge, and the constants of the discharge process will vary according to the length of the disconnected section. These constants are calculated by known formulae. The data, necessary for calculations of the amplitude values of the discharge current, proper frequency and time constant of discharge as a function of the length of the 400 kV line, are given in Table 1.

TABLE 1

Element of the electro-transmission	Values for one phase				
	Resistance of the positive sequence R (Ω)	Inductance of the positive sequence L (H)	Mutual inter-phase inductance M (H)	Phase capacitance with respect to earth C_0 (μF)	Interphase capacitance C_1 (μF)
Line (for 1 km)	0.2	0.93×10^{-3}	0.86×10^{-3}	8.6×10^{-3}	1.28×10^{-3}
Shunting reactor	5.3	3.4	–	–	–

As can be seen from the graphs on Fig.1, the values of the parameters characterizing the discharge of the line in relation to the length of the section vary rather considerably. Nevertheless, the current of discharge and its proper frequency are of the same order as the working current of the 400 kV line and its working frequency.

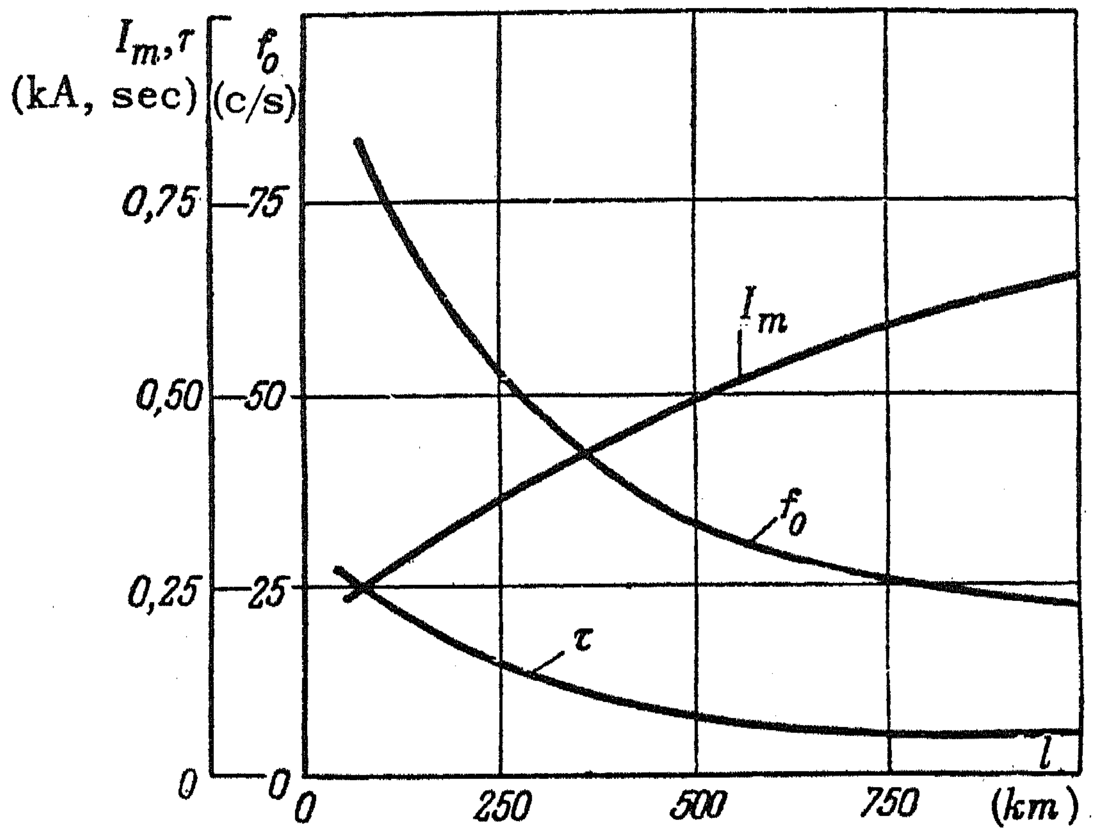

FIG.1. The values of the amplitudes of the discharge current I_m, time constant of the discharge τ and the proper frequency f_0 at the discharge of the line through the shunting reactor as a function of the length of the disconnected section.

The time constant of the discharge τ is equal to a fraction of a second; therefore we have to reckon with the fact that the voltage on the sound phases of the line and the discharge current will maintain sustained current conditions at the faulty place through the disconnected phase for 1 sec or more.

Thus, calculation of the sustained currents and of the recovery voltages should be done for two cases: switching off one phase and switching off all three phases in the presence of a reactor. The general formulae for these quantities are deducted on the basis of the simplified circuit of the line element with distributed constants, as shown in Fig.2. In this diagram, two sound phases are replaced by an equivalent single phase, the voltage along it being assumed constant. This assumption enables us to exclude consideration of the inductance and the resistance of the equivalent phase. The mutual inductance between the sound phases and the disconnected phase of the section is accounted for by the introduction into the faulty phase of the c.m.f. of the mutual inductance.

The differential equation of the line element has the following form:

$$\left.\begin{aligned} -\frac{\partial \dot U}{\partial l} &= j\omega L\dot I + j\omega M\dot I_A; \\ -\frac{\partial \dot I}{\partial l} &= j\omega C_0\dot U + (\dot U - \dot U_A)j\omega C, \end{aligned}\right\} \qquad (1)$$

where $\dot U_A = 0.5\ \dot U_f$; $\dot I_A = \dot I_f$; $C = 2C_1$;

$\dot U_A$ and $\dot I_A$ are the voltage and current in the phase equivalent to the two sound phases;

$\dot U_f$ and $\dot I_f$ are the voltages and currents in the sound phases; and

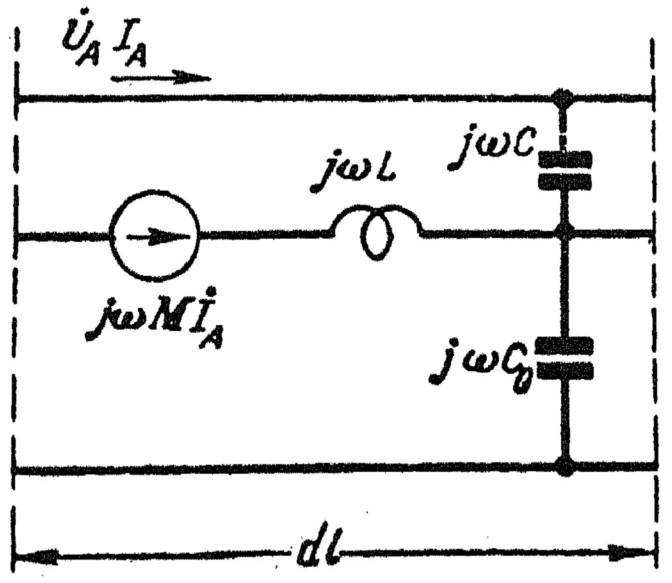

FIG.2. The diagram of the element of the line with distributed parameters for the calculated example.

$\dot{U}$ and $\dot{I}$ are the voltage and current in the disconnected phase.

Solving simultaneously the equations (1) for the section of the line of length l, we have:

$$\begin{aligned}\dot{U}_2 &= \dot{U}_1 \operatorname{ch}\gamma l - \dot{I}_1 Z_c \operatorname{sh}\gamma l + \dot{U}_A \frac{a}{\gamma^2}(1-\operatorname{ch}\gamma l) - \dot{I}_A \frac{j\omega M}{\gamma}\operatorname{sh}\gamma l;\\ \dot{I}_2 &= -\frac{\dot{U}_1}{Z_c}\operatorname{sh}\gamma l + \dot{I}_1 \operatorname{ch}\gamma l + \dot{U}_A \frac{a}{Z_c\gamma^2}\operatorname{sh} l - \dot{I}_A \frac{j\omega M}{Z_c\gamma}(1-\operatorname{ch}\gamma l),\end{aligned} \tag{2}$$

where $a = -\omega^2 LC$; $\gamma = j\omega\sqrt{L(C_0+C)}$; $Z_c = \frac{j\omega L}{\gamma}$;

$\dot{U}_1$ and $\dot{I}_1$ refer to the beginning of the section; and $\dot{U}_2$ and $\dot{I}_2$ refer to the end of the section.

Let us divide the section of the line in question into two parts: χ and l-χ. Let us establish for each of them the boundary conditions:

For the beginning of the part χ: $\dot{U} = \dot{U}_1$; $\dot{I} = 0$; for the end of the part χ: $\dot{U} = \dot{U}_\chi$; $\dot{I} = \dot{I}_\chi$; for the beginning of the part $l-\chi$: $\dot{U} = \dot{U}'_\chi$; $\dot{I} = \dot{I}'_\chi$; for the end of the part $l-\chi$: $\dot{U} = \dot{U}_2$; $\dot{I} = 0$; At the junction of two parts: $\dot{U}_\chi = \dot{U}'_\chi$; $\dot{I}_\chi = -\dot{I}'_\chi$

Using equations (2) and the boundary conditions we get the following expressions: for the recovery voltage on the disconnected phase

$$\dot{U}_x = \dot{U}_A \frac{C}{C_0+C} + j\dot{I}_A \frac{M}{\sqrt{L(C_0+C)}} \times \frac{\frac{1-\cos\gamma x}{\cos\gamma x} - \frac{1-\cos\gamma(l-x)}{\cos\gamma(l\quad x)}}{\tan\gamma x - \tan\gamma(l-x)};$$

for the magnetization current

$$\dot{I}_x = -j\dot{U}_A \frac{C}{\sqrt{L(C_0+C)}}[\tan\gamma x + \tan\gamma(l-x)] + \dot{I}_A \frac{M}{L}\cdot\frac{\cos\gamma(l-x) - \cos\gamma x}{\cos\gamma(l-x)\cos\gamma x}. \tag{3}$$

As can be seen from formulae (3), voltage $\dot{U}_\chi$ and current $\dot{I}_\chi$ have two components: the first of them depends on the voltage on the sound phases and is due to the capacitive connexion between sound and faulty phases, and the second depends on currents in the sound phases and is due to the mutual inductance.

On the basis of data given in Table 1, we obtain the distribution of the components of the recovery voltage and of the sustained current for different lengths of the disconnected section of the line in the case of an automatic single-phase reclosing after break. The value of the current I_A is assumed equal to 700 A.

The plotting of graphs of distribution in Figs 3 and 4 is done in such a way that the ordinate axis corresponds to the middle of the disconnected section, and the variable coordinate to the faulty place.

From graphs in Fig. 3 and 4, it is seen that the capacitive component of the recovery voltage does not vary along the section; we can also assume that the capacitive component of the sustained current remains constant along the section.

Inductive components of the sustained current and of the recovery voltage are equal to zero when the short-circuit occurs at the central point of the section, and for short-circuits at the ends of the section they have maximum values. The inductive component of the voltage has a positive value when the short-circuit occurs at one end of the section, and a negative one when it occurs at the other end of the section. The value of the resultant of the inductive and capacitive components depends upon the angle between the current, which produces them, and the voltage on the sound phases; the maximum value of the resultant also occurs at the end of the section.

The above method may also be used for calculations of the sustained current and of the recovery voltage in the case then a shunting reactor is connected at the end of the section of the line. Since, however, the maximum values of these quantities are of primary importance, we give below the formulae for calculations in the case when a short-circuit occurs at the end of the section opposite to that where the shunting reactor is connected. The boundary condition for this case will be: at the end of the section in which the fault occurred $U = U_d$; $I = 0$; at the end of the section with a reactor $U = I_{2j} X_p$; $I = I_2$ where $X_p = \omega L_p$ – inductive reactance of the reactor.

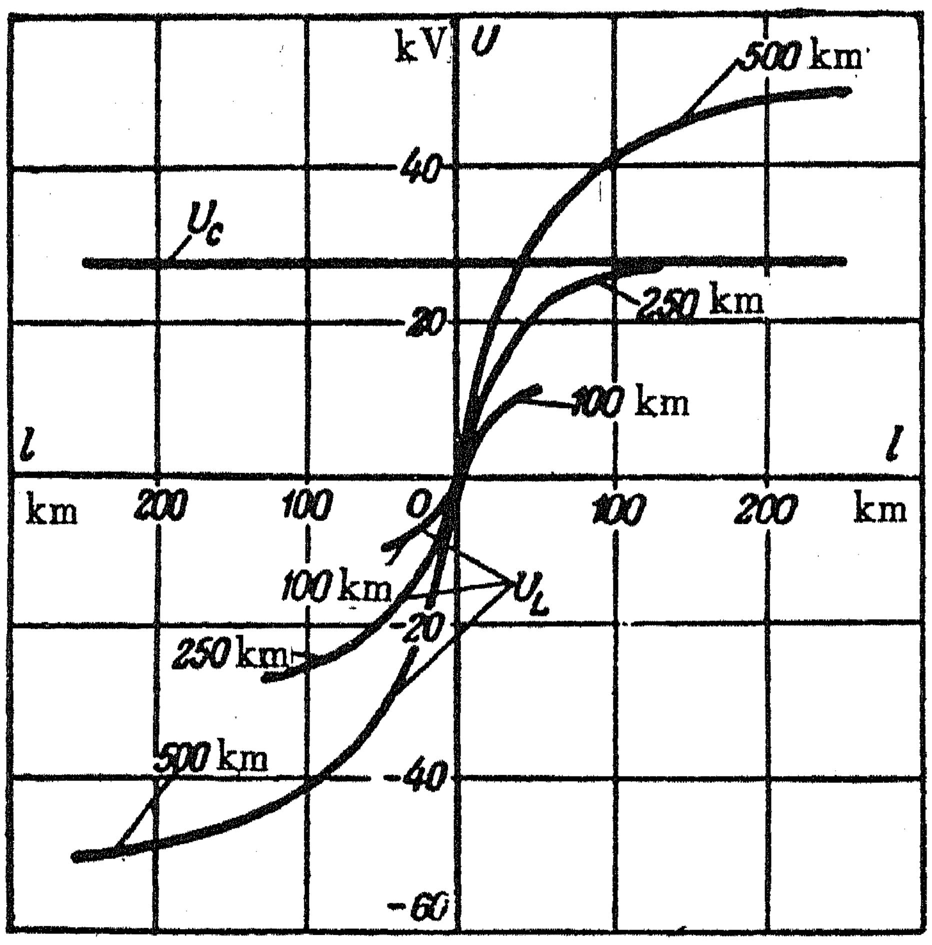

FIG.3. Capacitive U_c and inductive U_l component of the voltage on the disconnected phase (in the absence of the reactor).

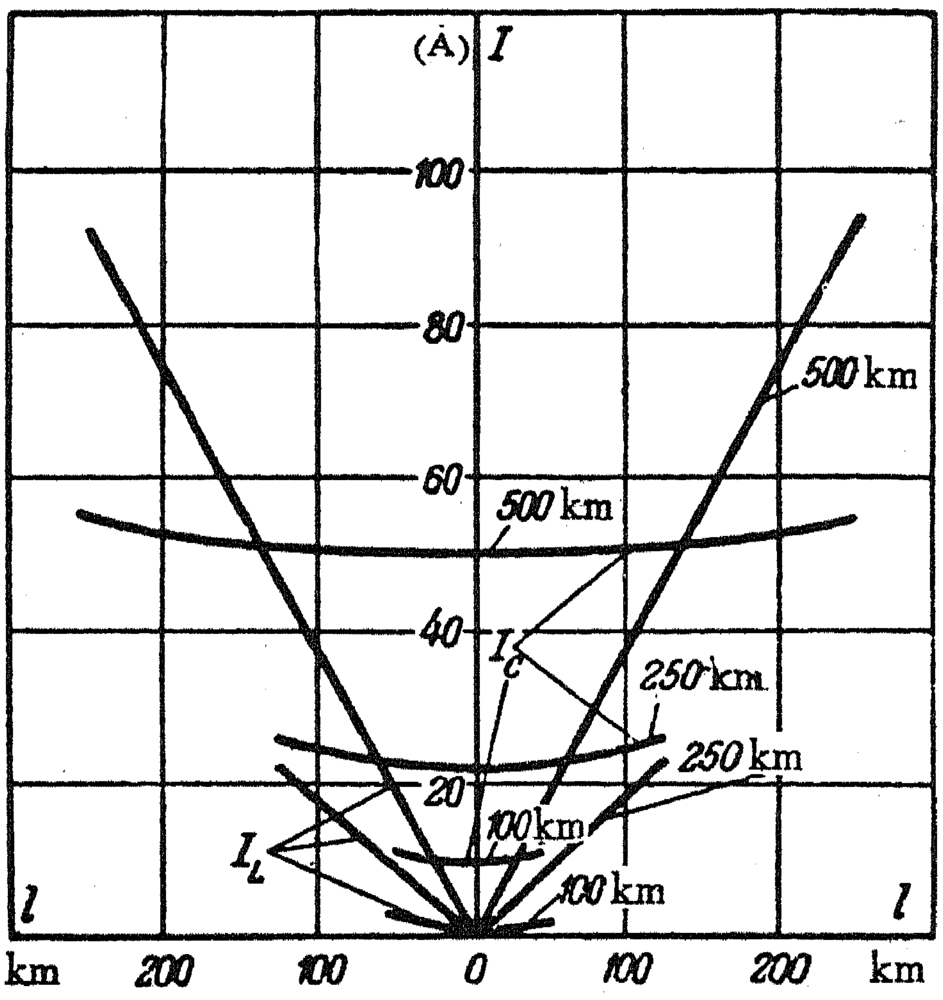

FIG.4. Capacitive I_c and inductive I_l components of the sustained fault current when one phase is disconnected (in the absence of the reactor).

Using equations (2) and the boundary conditions we get:

COLLEGE OF ENGINEERING LIBRARY BOOK No. GUINDY

$$\left.\begin{aligned}
\dot{U}_\partial &= \dot{U}_A \frac{C}{C_0+C} \frac{\sin\gamma l - \frac{Z_c}{x_p}(1-\cos\gamma l)}{\sin\gamma l - \frac{Z_c}{x_p}\cos\gamma l} + \\
&+ jI_A \frac{M}{\sqrt{L(C_0+C)}} \frac{1-\cos\gamma l - \frac{Z_c}{x_p}\sin\gamma l}{\sin\gamma l - \frac{Z_c}{x_p}\cos\gamma l}; \\
I_n &= -j\dot{U}_A \frac{C}{\sqrt{L(C_0+C)}} \frac{\sin\gamma l - \frac{Z_c}{x_p}(1-\cos\gamma l)}{\cos\gamma l - \frac{Z_c}{x_p}\sin\gamma l} + \\
&+ I_A \frac{M}{L} \frac{1-\cos\gamma l + \frac{Z_c}{x_p}\sin\gamma l}{\cos\gamma l + \frac{Z_c}{x_p}\sin\gamma l}
\end{aligned}\right\} \quad (4)$$

Here, the recovery voltage and the sustained current also have two components each, one of the components being capacitive and the other inductive.

For calculation of the resultant values of the current and voltage, despite the previously assumed values of different parameters, cos ϕ of the transmission was taken equal to unity, which approximately corresponds to the conditions of normal power. Fig.5 shows the results of calculations for the cases when the reactors are present and when they are absent.

I In the case of a single-phase automatic reclosing after the break and in the absence of a reactor, the recovery voltage varies within the limits 30-60 kV according to the length of the section. In the case when a reactor is present, its inductance and interphase capacitance appear as if connected in series; because of this, voltage resonance is possible, and, hence, a considerable increase of voltage on the faulty phase. Equating to zero the denominator of one of the terms for the voltage (4), we find that the resonance occurs for the length of the section

$$l_{res} = \frac{1}{\omega\sqrt{L(C_0+C)}} \tan^{-1} \frac{Z_c}{\omega L_p}.$$

Calculations show that l_{res} = 290 km. Although, in fact, resonance over-voltage is limited by the saturation of the reactor and the discharge, nevertheless it is necessary to reckon with a considerable increase of voltage. In the presence of a reactor, the sustained current also reaches a considerably higher value than in its absence.

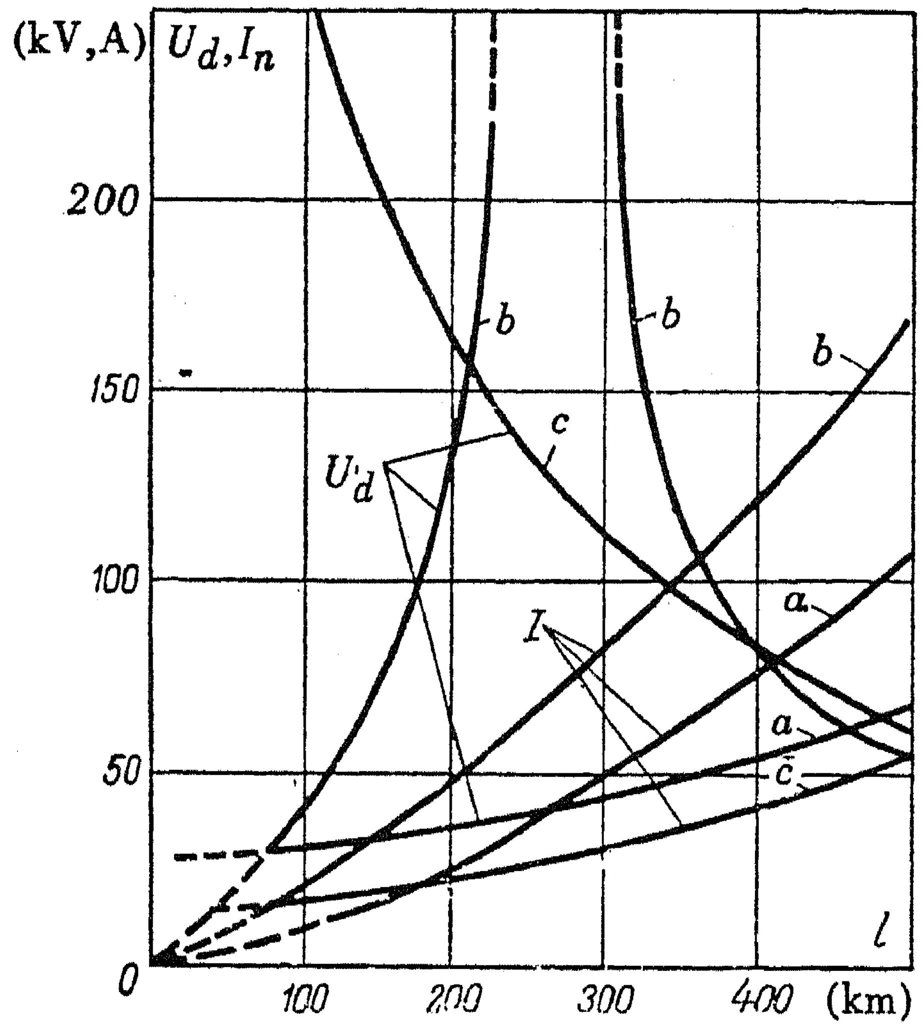

FIG.5. The sustained current and the recovery voltage on the disconnected phase for a point of the end at the section: (a) one phase disconnected, reactor absent; (b) one phase disconnected, reactor present; (c) three phases disconnected, reactor present.

In calculating the sustained current and the recovery voltage for conditions at the three-phase automatic reclosing after break, the values of the discharge current and of the proper frequency of the discharge for each length of the section were taken in accordance with graphs in Fig.1. Voltage on the sound phases was assumed to be equal to the nominal, the damping of the discharge current was disregarded, angles between vectors of the discharge currents and voltages of the sound phases were taken equal to 90 el. deg. The results of calculations are given on Fig.5. The sustained current was a little smaller, and the recovery voltage bigger than for conditions in the case of a single-phase automatic reclosing in the absence of a reactor. The sustained current in the case of a single-phase automatic reclosing in the presence of a reactor was approcimately equal to 0.3 A/km, and in the same case, in the absence of a reactor, to 0.2 A/km. In the case of the three-phase automatic reclosing in the presence of a reactor, the current equalled 0.1 A/km.

The diagram of the 400 kV line Kuibyshev - Moscow, during the experiments carried out by the C.S.R.E.L., is shown on Fig.6. Wind during these experiments was weak.

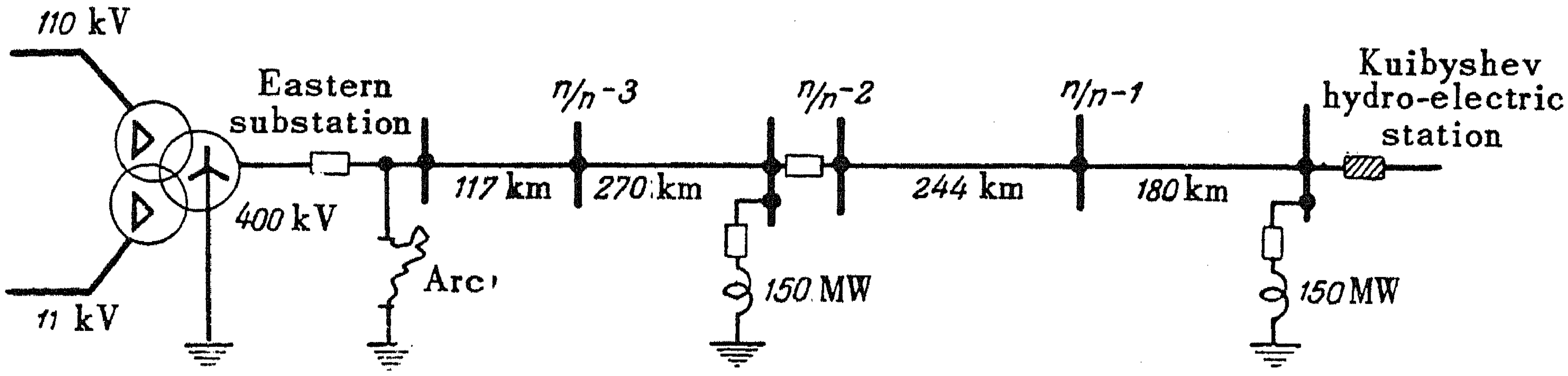

FIG.6. The diagram of the 400 kV Kuibyshev-Moscow line during the experiments with extinction of the sustained faulty current arc.

Arcing short-circuit on the group of insulators of the suspension type was produced by means of a copper wire of 1 mm^2 cross-section. After fixing the wire, all three phases were switched on and the arc was struck.

The damaged phase was disconnected by a breaker after 0.14 sec, and after this, the sustained current arc remained. The voltages of all three phases, the current of one sound phase, the short-circuit current and the sustained current were recorded by a magneto-electric ossillograph. The photographs of the arc were taken by a cine-camera at the rate of 32 frames/sec. Cine - frames of the experiment on the section of the line 815 km long, in the absence of reactors, are given in Fig.7, and the oscillograms of this experiment in Fig.8.

During the short-circuit stage, the arc on the film appears as a luminous cloud; later the luminous gases, surrounding the arc disperse and the patch of the sustained current arc can be clearly seen; this path gradually becomes longer, bending sideways and upwards, at the expense of thermal forces of the previous short-circuit and due to its own thermal effect; after this comes extinction.

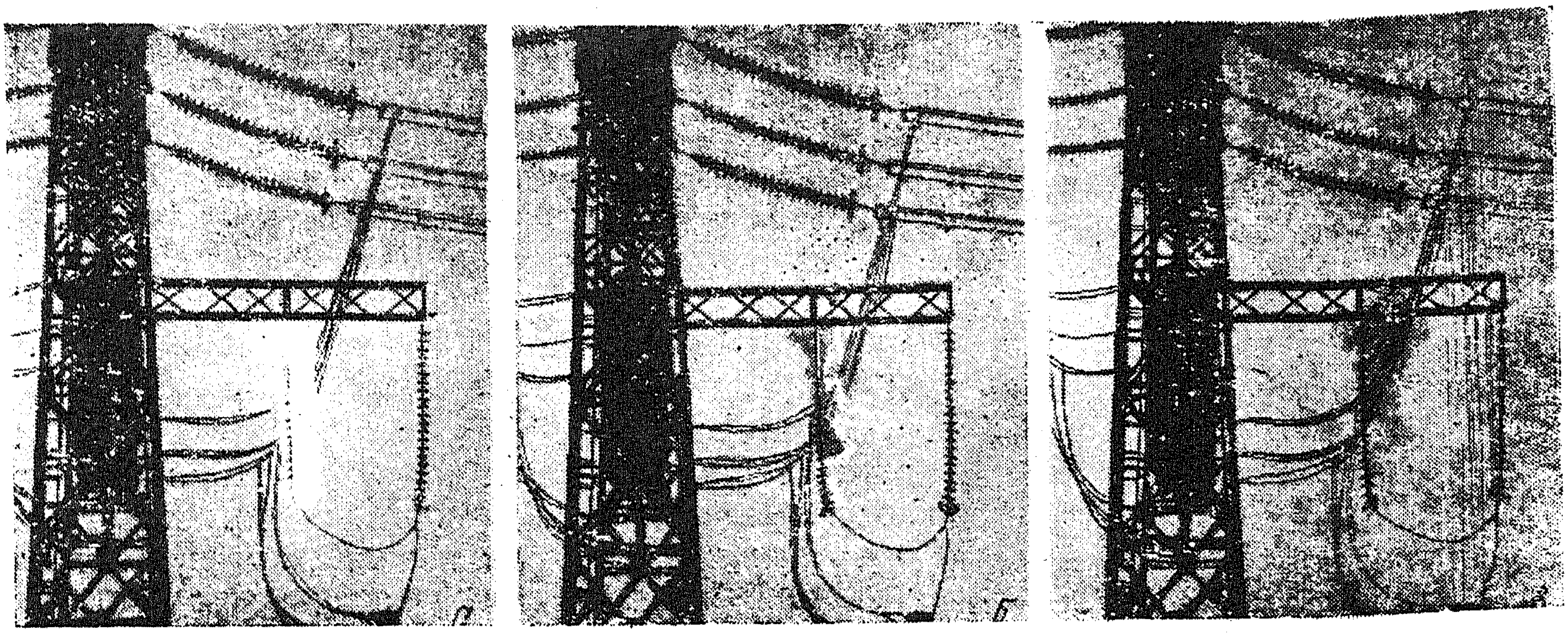

FIG.7. Separate cine-frames of the single-phase short-circuit with the following sustained current arc: (a) short-circuit arc; (b) the sustained current arc before the beginning of extinction; (c) cooling of gases after extinction of the sustained current arc.

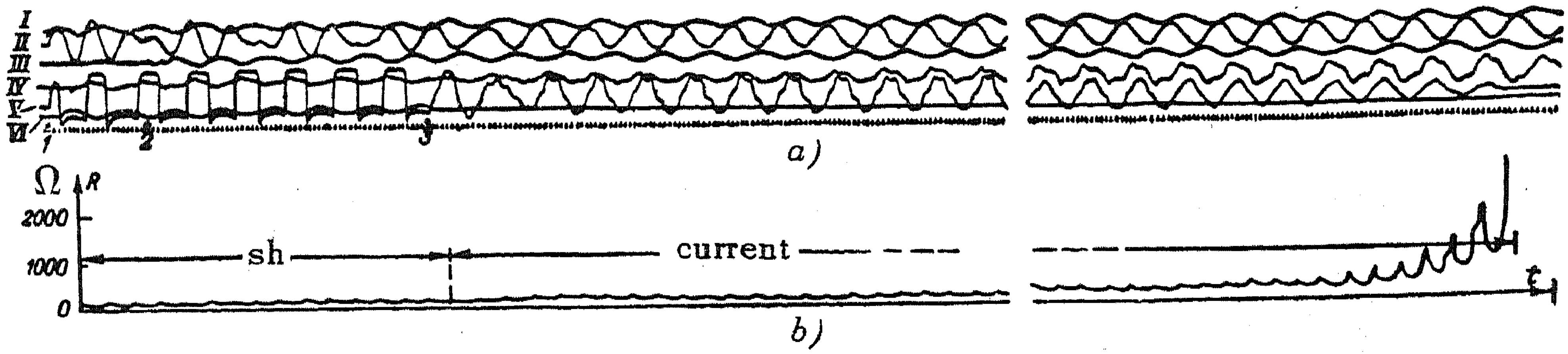

FIG.8. Oscillogram of the experiment (a) and the graph of the resistance of the path of the arc (b) on the single-phase short-circuit and switching off one phase. I – voltage of the "yellow" phase U_y. II – current of the "yellow" phase I_y. III – voltage of the "green" phase U_g. IV – voltage on the arc (of the "red" phase) U_r. V – current I_{su}. VI – short-circuit current I_{sh} (1) the beginning of the short-circuit; (2) connecting of the sound phase with a delay; (3) switching off the "red" phase (the end of the short-circuit).

As can be seen from the oscillogram in Fig.8, after switching off, the sustained current flows through the discharge channel; the current gradually decreases with the lengthening of the channel and the voltage increases on the arc gap. The resistance of the path of the sustained current arc, whose graph of variation is plotted using the oscillogram data, shows a steady increase during the whole process. This arc dies away due to the steady decrease of current caused by the increasing resistance of the path. This process of extinction occurred in all experiments and is typical for the sustained current arc. The extinction of open powerful arcs occurred in a similar way in all the experiments performed by Burgsdorf [6]. In a few cases in these experiments, single restrikes may be observed, these being peculiar to arcs in capacitive networks.

The oscillogram of the experiment on switching-off all three phases on a section of the line 117 km long, without a reactor, is shown in Fig.9a. In this case, the discharge of the sound phases of the line and the sustained current corresponding- to it have an aperiodic character. The discharge lasts only 1.5-2 periods of industrial frequency; therefore, reclosing with a delay of 0.3 sec proves successful.

The oscillograms of the experiment on switching off all three phases on a section of the line 635 km long with the reactor are shown in Fig.9b. In this case, the discharge of sound phases through the reactor, after they have been switched off, proceeds at a frequency of 31 c/s per sec and with small damping, and this agrees with calculations. The curve of the sustained current has an irregular shape, and the extinction of the arc occurs during 0.2 sec. The reclosing after 0.3 sec also proves succesful.

Table 2 shows the results of the experiments carried out on the line from Kuibyshev to Moscow. The experimental values of the sustained current are taken after the first half period after switching off the short-circuit, and the voltage on the disconnected phase is taken at its established value.

In all experiments, the short-circuit current was equal to 2.000 A, and the time of short-circuit 0.14 sec.

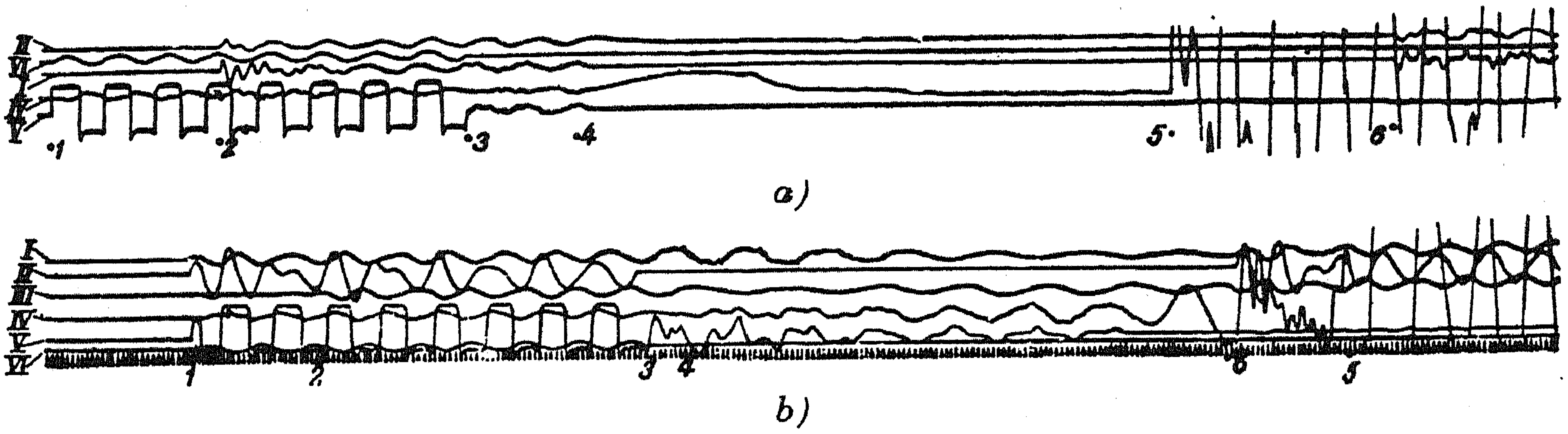

FIG.9. Oscillograms of the experiments with the three-phase switching off and reclosing. (a) section of the line with a voltage transformer; (b) section of the line with a voltage transformer and reactor. I – voltage of the "yellow" phase U_y; II – current of the "yellow" phase T_y; III – voltage of the "green" phase U_g; IV – voltage of the arc (of the "red" phase) U_r; V – current I_{su}; VI – short-circuit current I_{sh}. (1) the beginning of the short-circuit; (2) reclosing of the sound phase with a delay; (3) switching off the "red" phase (the end of the short-circuit); (4) switching off the "yellow" and "green" phases; (5) reclosing of the "red" phase; (6) reclosing of the "yellow" and "green" phases.

The data of the table show a satisfactory coincidence of calculated and measured values of the sustained currents and recovery voltages on the disconnected phase.

Experimentally obtained values of the times of arc extinction in relation to the sustained current for a single-phase automatic reclosing are plotted in Fig.10 as dots. As can be seen from this graph, these points show a considerable dispersion, due to the characteristic instability of the arc.

It is necessary to point out that the experiments were carried out on the line without load, and without the sustained current component, due to the inter-phase

TABLE 2

Kind of experiment	Length of the line (km)	Reactors on phases	Capacitive component of the:				Time of burning of sustained current arc (sec)
			Voltage on the disconnected phase (kV)		Sustained current (A)		
			Calculated	Measured	Calculated	Measured	
Single phase A.R.	117	—	28	28	15	17	0.05
" "	391	Y,G	28	28	40	38	0.26
" "	391		28	28	40	38	0.34
" "	391		28	28	40	38	0.38
" "	391		28	28	40	38	0.59
" "	635		28	28	67	62	0.25
" "	635		28	28	67	62	0.33
" "	635		28	28	67	62	0.40
" "	815		28	28	82	80	0.35
" "	815		28	28	82	80	0.76
" "	815		28	28	82	80	1.80
" "	391	Y,G,R	100	92	25	25	0.22
" "	391		100	92	25	25	0.24
" "	391		100	92	25	25	0.26
" "	635		45	50	47	45	0.84
" "	635		45	50	47	45	1.50
" "	635		45	50	47	45	1.88
Three phase A.R.	117		—	—	—	—	0.02*
" "	635	Y,G,R	—	—	—	35	0.1
" "	635		—	—	65	25	0.15
" "	635		—	—	65	75	0.20
" "	635		—	—	65	35	0.08**
" "	635		—	—	65	70	0.16***

* Reclosing succesfully done after 0.3 sec.
** " " " " 0.27 sec.
*** " " " " 0.26 sec.

mutual inductance. If the experiments were carried out on the line with a normal load, the sustained current would have been greater.

Taking into account the maximum durations of time for arc extinction and considering an additional interval of time of the order 0.05 sec, necessary for the recovery of the electric strength of the path after the arc extinction, we can assume, as an approximation, that the sustained current and the duration of the currentless interval for the single-phase automatic reclosing of the line without a reactor, are linearly dependent (straight line on Fig.10). Therefrom we can derive the relationship between the currentless interval and the length of the disconnected section, if the relationship between the length of the section and the sustained current has been determined earlier (see Fig. 7). The corresponding approximate formula is

$$t_{\mathrm{Sfar}} = 0.003\, l$$

where t_{Sfar} is the necessary currentless interval for the single-phase automatic reclosing (sec) and l is the length of the section (km)

With the reactor, which causes an increase in the recovery voltage, the necessary currentless interval will be appreciably longer than that obtained by formula (6).

In conditions approaching resonance the sustained current arc may remain unextinguished.

So far as the 400 kV line from Kuibyshev to Moscow is concerned, such conditions may occur on the section between the switching points 3 and 2, of length

274 km, and on the section between switching points 2 and 1, of length 244 km, if resonance occurs, as was found earlier, on the length of the disconnected 290 km section.

The resonant increase of the voltage on the disconnected phase can be dangerous for the insulation of the connected transformers and for the shunting reactor. The real value of the over-voltage may be found only experimentally.

For the successful use of the single-phase automatic reclosing on the sections considered of the line from Kuibyshev to Moscow, it is possible, for the single-phase short-circuit, to switch off the shunting reactor simultaneously with switching off the faulty phase. In designing 400 kV lines it is necessary to choose such distances between the switchgears that the conditions for the resonant increase of voltage should not arise when switching off one phase.

If the shunting reactors are sufficiently reliable and damage to them is less probable than serious damage to the line itself, excluding the possibility of its reclosing after break, then we can omit the breaker in the network of the reactor.

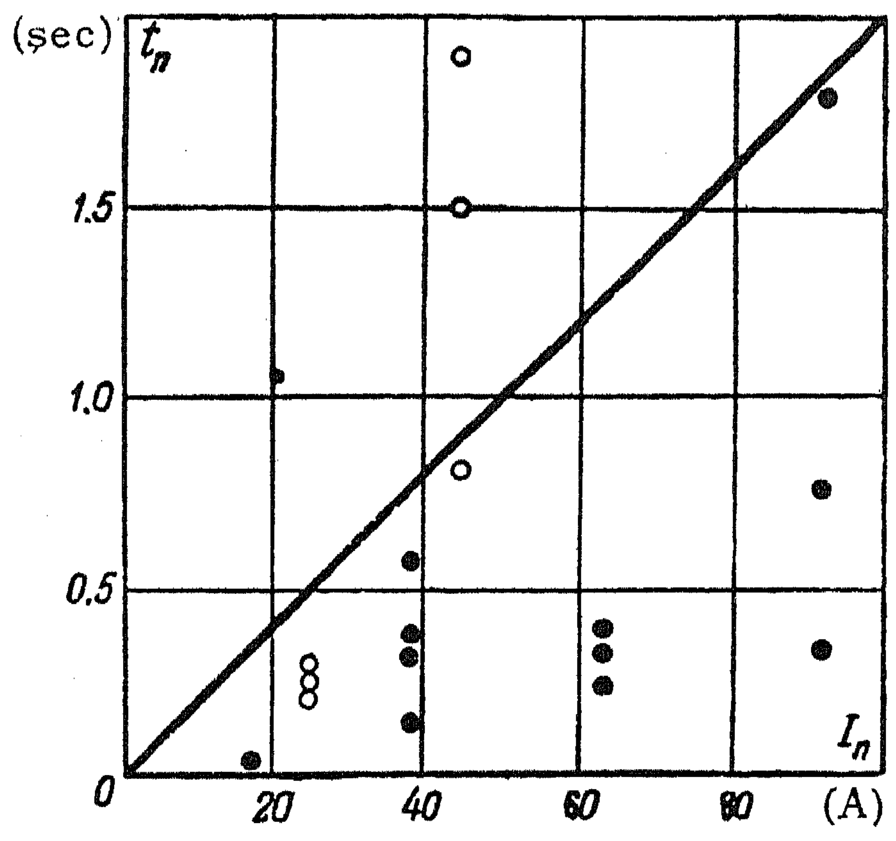

FIG.10. Experimentally found durations of the arc extinction in relation to the current:
● – on the section of the line without a reactor, ○ – on the section of the line with a reactor.

For the three-phase automatic reclosing with a reactor, the durations of arc extinction show a considerable dispersion, but the maximum duration does not exceed 0.2 sec. Therefore, in this case, we may successfully use the so-called quick-acting automatic reclosing, for which the interval is determined by the time of the separation of the arc breaking contacts of the air breaker and their consequent reclosing, this time being equal to 0.27 - 0.3 sec, as it was during the performed experiments.

In the conditions of dynamic stability of the electro-transmission it is desirable that the currentless interval for the three-phase automatic reclosing should be very small. Nevertheless, the further decrease of the interval of the quick-acting automatic switch-on is inadmissible with shunting reactors, since the relation between the maximum time of the burning of the sustained current arc (0.2 sec), and the maximum interval (0.3 sec) had a limiting value in the experiments. For deionization and the recovery of the electric strength of the path of the arc only 0.1 sec is left.

If, simultaneously with the disconnection of the three-phases of the line, we disconnect the three phases of the shunting reactor as well, then the interval of the quick-acting automatic reclosing will not be limited by the sustained current arc. In this case, the duration of the pause will be determined by the time of deionization and of the recovery of the electric strength of the path of the short-circuit arc. According to the published data, this time does not exceed 0.2-0.25 sec for a large range of short-circuit currents. Taking into consideration that for the 400 kV Kuibyshev - Moscow transmission line, the three-phase short-circuit current varies within the limits 1-10 kA, the reduction of the interval of the quick-acting automatic reclosing, the reactor being disconnected, may be brought down to the value of 0.25 sec. The possibility of the further reduction of the interval should be confirmed by additional experiments.

It is necessary to point out that on the section of the line between Moscow and switching point 3, where the reactor is absent, and the extinction of the sustained current arc takes only 0.05 sec, we may successfully use the single-phase quick-acting reclosing.

In conclusion it is necessary to point out that the effectiveness of the automatic reclosing on the 400 kV lines, judging from the experience gained from the exploitation of the 154 kV and 220 kV lines, having analogous electrical and mechanical characteristics, should be high. According to CSREL data, for the period from 1945 to 1954, on the lines with steel cables and the protective angle of 20° or less, there occurred about seventy cases of break - down. Damage due to lightning did not occur. 45 per cent of break-downs were of short duration (dirt, damp insulation in marshy regions, various deposits), and in 55 per cent of cases the break-downs were due to serious and lasting damage, followed by the conductors falling to the ground. It follows that approximately half of the short-circuit cases may be handled without prolonged disconnection of the line.

The authors wish to thank V.V. Burgsdorf for his valuable advice and help given during their work and colleagues who participated in the experiments.

Translated by S. Szymanski

REFERENCES

1. E. Mory; *Bull S.E.F.*, 8 (1945).
2. A. Amstat; *B.B.M.* 7/8 (1948).
3. E. Harrington and E. Starr; *Trans. Amer. Inst. Elect. Engrs. 2* (1949).
4. A. Matthey-Doret and A. Leuthold; *B.B.M.*, 9 (1954).
5. L. Norlin; *Tech. Tijdschro*, 40 (1953).
6. V.V. Burgsdorf; *Elektrichestvo*, No.10 (1948).
7. A.S. Maikopar; *Trud. TsNIEL (CSREL)*, No.2 (1953).

EARTHWIRE EARTHING SYSTEMS FOR LONG POWER-TRANSMISSION LINES*

N.A. MEL'NIKOV,

All-Union External Power Engineering Institute

A.I. GERSHENGORN and A.N. SHERENTSIS

Teploelektroproekt

(Received 13 July 1957)

At present, the lightning-protection wires of power transmission lines of all voltages are securely earthed at each tower.

During the design of long-distance 220-400 KV lines, it was established that a considerable amount of electrical energy can be lost via earth-wires earthed at many points. These losses are due to the presence of currents in the closed circuits of the wire-tower earthing systems, as a result of the electromagnetically induced e.m.f. in the earthwires. With the most widely adopted lightning-protection system using two earthwires, which are interconnected through the towers, the current obtained is greater than with one earthwire, in which case the circuit is completed only through earth.

Since the energy losses in the earthwires can reach considerable magnitudes, it is worthwhile considering the question of isolating them completely or partially from earth.

It should be pointed out that studies have been made in the U.S.S.R. in recent years on the question of using, as lightning-protectors, current-carrying conductors intended for supplying power to small-scale consumers [1], for driving electric motors when carrying out repair work on the line, melting ice-deposits and the like. The wires can also be used as communication wires, especially during erection of the power lines. In this connection, the need again arises to insulate the wires from earth. Isolation of the earthwire eases the conditions of repair work on the lines and also simplifies the measurement of the line-earth resistance at the towers.

Thus, the multiple earthing of earthwires could only be justified if the additional cost of isolating them were not covered by the saving in energy losses.

---

* *Ekektrichestvo* No.1, 25-30, 1958 [Reprint Order No. EL44].

An obligatory condition for the use of isolated earthwires is the maintenance of the same level of protection as is obtained with earthed wires. For this, the wires must be earthed through spark gaps which are bridged in the early stages of the leader stroke of a lightning discharge, to direct the latter on to the wire. Then when the spark gap has been bridged, the subsequent flow of the lightning current will proceed as with earthwires. Experimental work, carried out on a model, and also the experimental use of sections of 35 to 220 kV power lines with isolated earth wires, confirmed that the earthing of wires via spark gaps does not reduce their protective properties [2].

On the basis of the results of these investigations, the Technical Managemen of the Ministry for Power Stations decided to suspend the earthwires of 25 to 220 kV lines on insulators with spark gaps not exceeding 40 to 50 mm. The isolated earthwire system has since been extended somewhat to those sections of power lines, where the cables are used for reactive power take-off and consumer supply or the supply to protective relay circuits.

Electrical energy losses in earthwires

If a 400 kV line, for example, 1,000 km long, erected on towers such as are used on the Kuibyshev Power Station - Moscow line, has two steel earthwires 70 mm^2 in section, earthed at each tower, then the earthwires form a closed circuit over each pitch between the towers and the e.m.f. set up in the earthwires at a line load of 1,000 MW (on two circuits) is 52V/km, the current in each earthwire 27 A, the total loss of power in the earthwires about 3MW (in the two circuits) and the yearly energy loss of the order of 10 million kWh (Appendix la).

In a 350 MW transmission with the two 220 kV lines, 360 km long, the power loss in similar earthwires is 380 kW, and the yearly energy loss about 1.8 kWh.

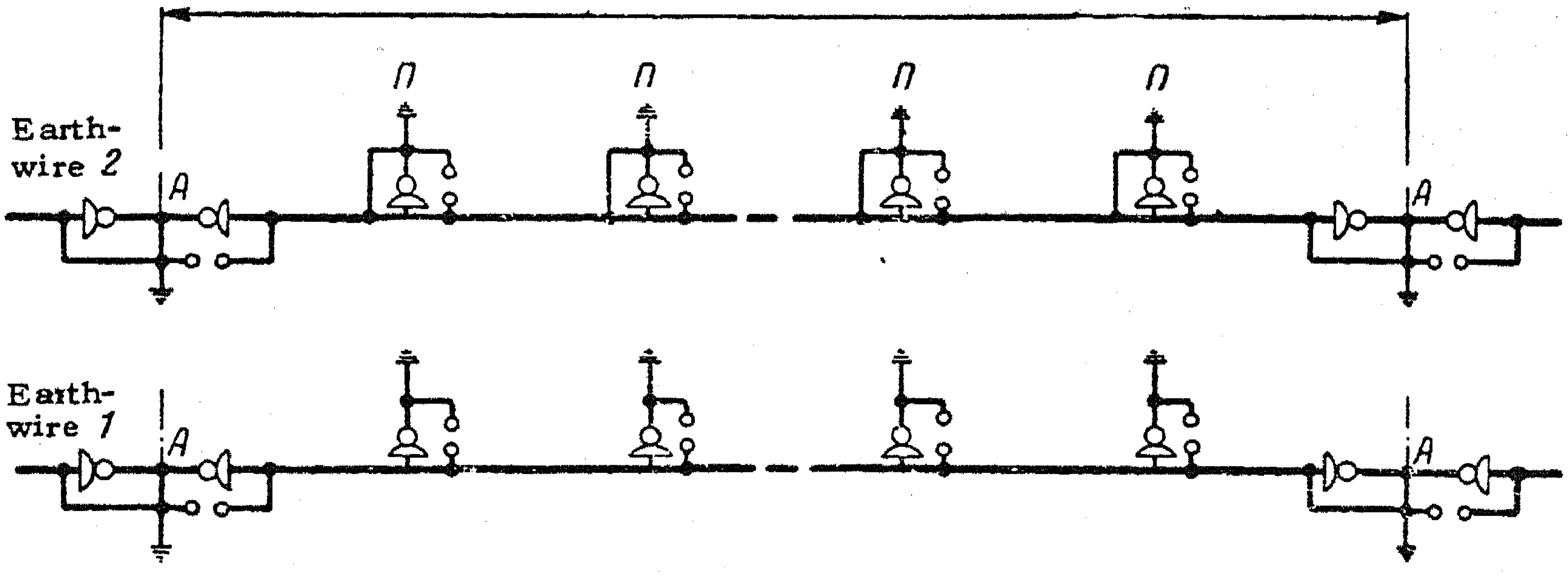

FIG. 1.

If the cost is taken as 10 kopecks per kWh, complete isolation of the earthwires in these lines would give a yearly saving of 1 million roubles in the first case and 180,000 roubles in the second. The saving due to isolating the earthwires on lower voltage lines would be considerably less, since such lines are comparatively short and the working currents are less.

If one of the earthwires is divided into sections, corresponding to the distance between strain towers, and each of these sections is isolated, as shown in Fig. 1. (earthwire), the closed earthwire circuit will be eliminated; current can flow only in the other earthwire and will return through earth. Since the distance between towers on long lines is quite considerable [3], we can ignore the current flowing at the ends of the sections and consider the earthwire-tower earthing system as a single-conductor earthwire-earth line. This system of earthing the wires gives a considerable reduction of the additional energy losses in the line, compared with the system of earthing both earthwires at many points. If this system is used on the 400 and 220 kV lines discussed above, the additional energy loss is reduced by 1.8 times (Appendix 1b).

Further reduction of the losses can be achieved by similarly dividing the second earthwire into sections and isolating them. In this case, in determining the loss on the distance between strain towers, the earthwire-tower circuit must be considered with full reference to the flow of current to earth at the separate towers (Appendix 1c). For example, in the 400 and 220 kV lines discussed above, this system of earthing the wires gives a reduction of approximately 3 times in the additional energy losses, compared with the system of earthing both wires at many points.

In accordance with the decision of the Technical Management of the MES, the distance between strain towers on 220 and 400 kV lines with receiving substiutions must not exceed 10 and 15 km respectively, whereas for lines with switching stations or stations of limited circuit-breaking capacity, this distance is not limited. The length of each section of earthwire in the latter case is determined by the distance between angle-strain towers and may exceed 20 to 30 km.

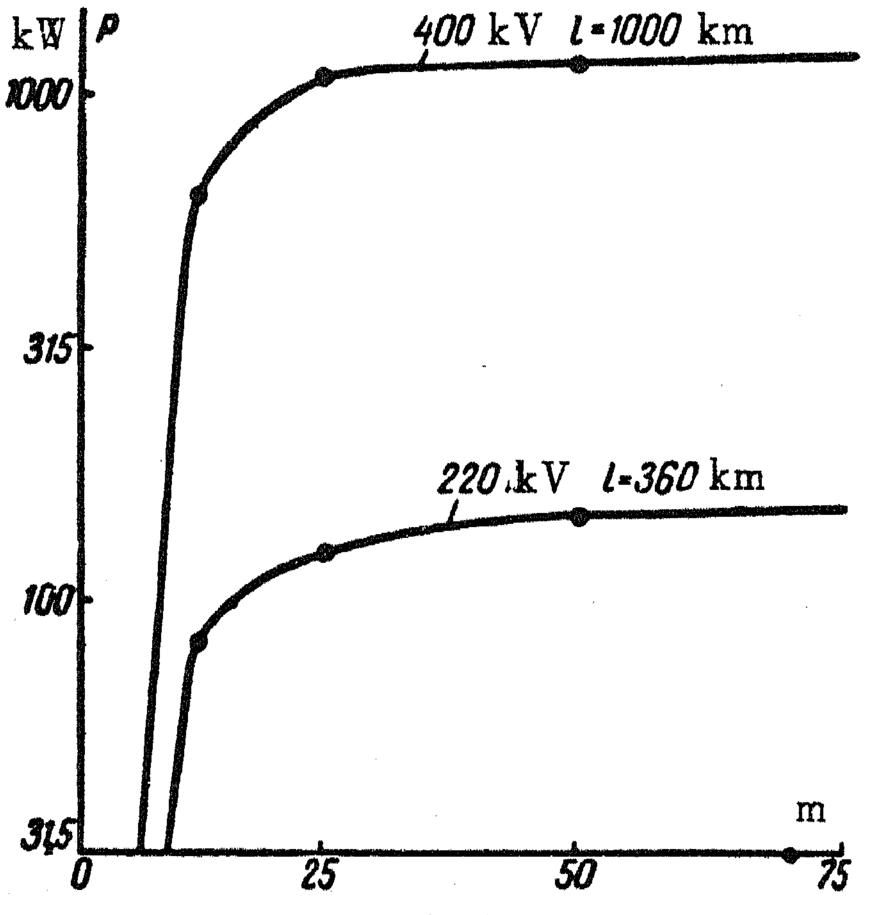

FIG. 2.

Fig. 2 shows the relationship between additional power losses in the earthwires and the section length with earthwires earthed at many points; the section length is plotted as the number of intermediate spans and the losses are plotted on a logarithmetic scale.

It follows from Fig. 2 that even at a section length of km, the additional energy losses with earthwires earthed at many points are considerable. This is explained by the fact that the current flow at the ends of the earthwire-tower circuits occurs over a relatively short length. At medium lengths of section, earthed at many points, the currents flowing in the earthwires are almost equal to those in earthwires of unlimited length, earthed at many points. Therefore, to eliminate additional losses of energy, it is also advantageous to avoid the use of sectionalized earthwires earthed at many points.

Earthwire isolation

If an earthwire is to be completely isolated, the insulator must be selected for the maximum voltage which can be set up in the earthwire in service. This voltage is that produced by the capacitative linkage between the earthwire and the line conductors (Appendix II).

Furthermore, the earthwire insulator must withstand the voltage set up by the longitudinal e.m.f., induced in the earthwire due to short-circuits on the line. This e.m.f. will be a maximum for an asymetric short-circuit to earth.

The e.m.f. induced in the earthwire of a three-phase line, when a single-phase short-circuit occurs in phase a, can be expressed by the following formula (Appendix Ia):

$$\dot{E} = j0.145 \cdot \dot{I}_a \log \frac{D_{am}}{D_e}.$$

This formula is equally valid for each of the earthwires on a line.

The maximum voltage due to the capacitative linkage, on the length between two towers, under normal working conditions, is 31 kV on 400kV lines, and 9 kV on 220 kV lines. Thus, the earthwire insulators on 400 kV lines may consist of strings of three insulators of the type P-4.5, and on 220 kV lines, of a single insulator of the same type.

Complete earthwire isolation on 400 kV lines is undesirable, since it complicates the tower design for these lines. In addition, the setting up of high voltages in the earthwires may make the use of such lines somewhat more difficult.

The total e.m.f. induced in an earthwire when there is a single-phase short circuit on the line, depends on the uninterrupted length of earthwire. Over the length of a complete transposition cycle, which may be taken as 250 km for a 400kV line the total longitudinal e.m.f. at a current of 5,000A may reach the comparatively high value of 45kV.

The size of the spark gap must be such as to ensure isolation of the earthwire under normal working conditions, whilst retaining the lightning-protection properties of the earthwire and ensuring self-extinction of the supplementary current arc after the spark gap has been bridged. For 400kV lines the required spark gap size must be determined experimentally.

The value of the total longitudinal e.m.f. can be reduced by dividing the earthwire into sections of shorter length. With a section length of earthwire earthed at one point equal to say 10km (distance between strain towers), the total longitudinal e.m.f. must not lead to voltages in the earthwire exceeding 1kv relative to earth. In this case also, the earthwire insulators on 400kV lines can consist of a single insulation of type P-4.5, with a 25 mm spark gap in parallel. In that case, the earthing system under consideration will be analogous, as regards its lightning-protection effect, to that used on 110 and 220 kV lines for equipment with reactive power take-off, and additional experimental confirmation of the lightning-protection effect of the earthwires is unnecessary. Reduction of the length of earthwire sections is also necessary, as will be shown below, on grounds of safety.

A current will flow from an earthwire earthed at one point through the earthing connexion to earth, owing to the capacitative linkage between the earthwire and line conductors, and a voltage difference with respect to earth will be set up at the corresponding tower or at several towers, connected to the other earthed wire.

The current in the earthwire earthing connection will be a maximum when the line is operating under unbalanced phase conditions. To determine it, it is sufficient to use the Maxwell equations for many conductor systems (Appendix II). The required current is

$$\dot{I} = j\omega\dot{q}_m,$$

where $\dot{q}_m$ is the charge on the earthwire, obtained from the combined solution of the system of Maxwell equations, which are set up under the assumption that the voltage in the cable is zero.

Calculations show that, over the distance between switching stations in a 400kV line, the current in the earthwire under unbalanced phase conditions may attain 12 A, so that the voltage on the tower, at a resistance of 10 Ω in the tower footing, may attain 120, which cannot be allowed from safety considerations. The current flowing in the earthwire over the distance between strain towers is less than 1.5 A; the voltage on the tower in this case does not exceed the permitted value even in the absence of a connection between it and the next tower through the other earthwire.

Comparison of earthwire earthing systems

A cost comparison, on the basis of the calculations made, established that the expense of isolating the earthwires on both 400 kV and 220 kV lines will be recovered within one year. Thus, the economic advantage of eliminating the earthing of the earth wires at many points throughout the length of 400 and 220 kV lines is quite obvious.

In connexion with increasing the resistance to current flow by isolating the earthwires, doubts arose during the design of the 400kV Kuibyshev-Moscow line, as to whether the selector devices on the single-phase circuit-breakers would operate normally in cases of a single-phase short-circuit. This consideration resulted in the decision not to divide both earth wires into sections corresponding to the distance between strain-towers, each section earthed at one point only.

The system adopted for earthing the earth-wires on the Kuibyshev-Moscow transmission line is shown in Fig. 1. It satisfies all the specified requirements; namely, reduction of additional losses of electrical energy, reduction of the additional costs of isolating the earth wires and retention of stable operation of the automatic control equipment. Earth wire 1 of each circuit is isolated by means of a single insulator of type P-4.5 and divided into line sections corresponding to the distance between strain-towers; each section is earthed at one point (at one of the strain towers). Earth wire (2) is divided into sections of the same length, earthed at each intermediate tower and at one strain tower. At the other strain tower, earth wire (2) is isolated by one insulator. To increase the degree of lightning protection for the 400 kV equipment at the approaches to substations and intermediate switching points, both earth wires on each circuit are directly earthed over a 5km section.

No diminution of lightning protection has been observed since the Kuibyshev-Moscow line has been in operation.

The doubt mentioned above, that the protective relay and automatic equipment would operate incorrectly, is not supported by experimental operation of transmission lines which have been working for a long time without earth wires. It must therefore be further recommended that on long 220 and 400 kV lines, the two earth wires on all the lines should be isolated, and divided into sections corresponding to the distance between strain-towers, since this system is the most economical.

It should be noted that earth wire (2) in Fig. 1, although earthed at each tower, is suspended on single insulators of type P-4.5 with spark gaps. On the Kuibyshev-Moscow line, this makes it possible to proceed to the system of isolating both earth wires.

The above calculations of the voltages which may arise in earthwires show that it is essential to earth the earthwire sections directly at one point on 400 kV lines. As for the earthwires on 220 kV lines, it is possible not to earth them, but merely to provide spark gaps.

It should be noted that to divide earth wires into sections and earth each at one point prevents their use as current-carrying conductors.

If only one earth wire is erected on a line, then to reduce additional energy losses it is also recommended to divide this into sections corresponding to the distance between strain-towers.

Appendix 1. Determination of energy losses

a) *Earthwires forming a two-conductor short-circuit loop.*

The flow of current in the line conductors induces an e.m.f. in the earthwires. At a frequency of 50 c/s, the induced e.m.f. in the earthwire [4] is

$$\dot{E}_e = j0.145 \sum_{p=1}^{3} \dot{I}_p \log \frac{D_{pe}}{D_r},$$

where D_{pe} is the distance between the phase conductor and the earth wire,

D_r is the depth of the equivalent earth return current (5);

I_p is the current in phase p.

As is well known, under normal symmetrical conditions of operation, the currents flowing in the different phase conductors are related as follows:

$$\dot{I}_a = a\dot{I}_b = a^2\dot{I}_c,$$

so that the e.m.f. induced in earth wire T_1 (Fig. 3) is:

$$\dot{E}_e = j0.145\dot{I}_a \left(a^2 \log \frac{D_{be}}{D_{ae}} + a \log \frac{D_{ce}}{D_{ae}} \right),$$

and in earthwire T_2:

$$\dot{E}'_e = j0.145\, \dot{I}_a \left(a^2 \log \frac{D_{be}}{D_{ae}} + \log \frac{D_{ce}}{D_{ae}} \right),$$

where I_a is the current in phase a conductor;

D_{ae} is the distance between the phase a conductor and the earthwire;

D_{be} is the same for phase b;

D_{ce} is the same for phase c.

It is assumed that the earth wires and conductors are arranged symmetrically on the tower with respect to the vertical axis.

If the earthwires are earthed at each tower on the line, then over each span the e.m.f. induced in the earthwires will produce currents in the earth-wires, towers and earth, since there are earthed wire-tower circuits.

The biggest energy loss will be due to currents flowing in the short-circuit loop formed by the earthwires.

The current in this loop is;

$$\dot{I}_e = \frac{\dot{E}_e - \dot{E}'_e}{2Z_e}.$$

Here Z_e is the impedance of the earth wire;

$$Z_e = r_e + j0.145 \ln \frac{D_e}{r_{e.e}} ,$$

where D_e is the distance between the earth wires;

r_{ee} is the equivalent radius of cross section of the earth wire [5].

The active power loss over 1km length of the loop is

$$\Delta P_e = -\mathrm{Re}(\hat{E}_e - \hat{E}'_e) \dot{I}_e =$$

$$= 1.5 \left(0\ 145 \cdot \dot{I}_a \log \frac{D_{ce}}{D_{ae}}\right)^2 g,$$

where

$$g = \frac{r_e}{r_e^2 + \left(0.145 \log \frac{D_e}{r_e}\right)^2}.$$

The approximate yearly loss of energy in the earthwires of a two-circuit line can be found in the normal way.

$$\Delta A = 2\Delta P_e l\tau.$$

where τ is the loss time from the loading curve at some average point (hr);

l is the length of the line, in km.

In its final form the formula for determining losses is:

$$\Delta A = \frac{3\left(0.145 I \log \frac{D_{ce}}{D_{ae}}\right)^2 r_e}{r_e^2 + \left(0.145 \log \frac{D_e}{r_e}\right)^2} \tau l,$$

where I is the load on one circuit of the line at some average point (A).

b) Earthwire – earth loop

Since the resistance of an earthwire – earth loop between towers is considerably greater than the footing resistances at the ends, particularly at substations and switching-points, where this resistance is at most 0.5 Ω, the earthwire – tower loops can be regarded as short-circuits. Then the e.m.f. is

$$\dot{E}_e = \dot{E}_e - \dot{I}_e Z_e = \dot{E}'_e + \dot{I}_e Z_e = \frac{\dot{E}_e + \dot{E}'_e}{2},$$

and the impedance of the earthwire - earth loop is

$$Z_{e.e} = \frac{r_e}{2} + 0.05 + j0.145 \log \frac{D_e}{r_e},$$

where

$$r_e = \sqrt{D_e r_{e.e}}$$

and the current of the loop is

$$\dot{I}_n = \frac{\dot{E}_e}{Z_{e.e}}.$$

The active power loss over 1km of the line is

$$\Delta P_n = -\operatorname{Re} \hat{E}_e \dot{I}_n$$

and the energy loss is

$$\Delta A = 2\Delta P_n \tau l = 2\left(0.145 \frac{I_n}{2} \log \frac{D_{be}^2}{D_{ae} D_{ce}}\right)^2 \times$$
$$\times \frac{(0,5r_e + 0,05)}{(0,5r_e + 0.05)^2 + \left(0.145 \log \frac{D_e}{r_e}\right)^2} \tau l.$$

If the line has only one earthwire earthed at many points, then

$$\Delta A'_n = 2\left(0.145 I \log \frac{D_{c\dot{e}}}{D_{ae}}\right)^2 \times$$
$$\times \frac{r_e + 0.05}{(r_e + 0.05)^2 + \left(0.145 \log \frac{D_e}{r_{e.e}}\right)^2} \tau l.$$

To determine the loss in the earthwire - earth loop it is borne in mind that long-distance power transmission lines are constructed with extended transposition cycles.

c) Earthwires - towers earthing system on sections between strain-towers

If a section earthed at many points is limited to the distance between strain-towers and is not electrically connected to other earthwire sections, then to calculate the energy losses it is necessary to take into account the flow of current in the whole earthwire - tower system [5].

Let an earthwire earthed at many points have n spans, i.e. earthed at $n+1$

COLLEGE OF ENGINEERING GUINDY
LIBRARY BOOK
No.

towers; the footing resistances of the towers can be taken to be identical and equal to R, whilst the resistance of the earthwire-earth loop for each span is

$$Z_{n.m} = Z_{me}\, l_m,$$

where l_m is the span length.

A chain of this type is active, uniform and finite.

The current in the span of earthwire between towers k and $k+1$ is

$$\dot{I}_{k,\,k+1} = -\dot{I}_{n-k-1,\,n-k} = \frac{E_m}{Z_m}\left(1 - B\,\frac{A^{k-n} + A^{-k-1}}{1-B}\right),$$

where A is the coefficient of voltage drop at each successive tower in an infinitely long chain:

$$A = \frac{Z^2}{RZ_{n.m}};$$

Z is the input resistance of an infinitely long chain with identical parameters for each unit:

$$Z = -\frac{Z_{n.m}}{2} + \sqrt{\left(\frac{Z_{n.m}}{2}\right)^2 + Z_{n.m}R};$$

B is the ratio between the currents at the two ends of a given finite chain, forming part of an infinitely long chain:

$$B = \frac{Z}{Z_{n.m}}\,A^n\,(1-A).$$

The active power loss in the chain considered is:

$$\Delta P = \sum_{k=0}^{n-1} P_{k,\,k+1} = E_m^2 \operatorname{Re}\frac{1}{Z_{n.m}}\left(n - 2B\,\frac{\sum\limits_{k=0}^{n-1} A^{k-1}}{1-B}\right) =$$

$$= E_m^2 \operatorname{Re}\frac{1}{Z_{n.m}}\left[n - \frac{2B(1-A^{-n})}{(1-B)(1-A^{-1})A}\right].$$

The energy loss for the entire two-chain line is

$$\Delta A = 2\Delta P\tau N = 2E_m^2 \operatorname{Re}\frac{1}{Z_{n.m}} \times$$

$$\times \left[n - \frac{2B(1-A^{-n})}{(1-B)(1-A^{-1})A}\right]\tau N,$$

where N is the number of strain towers for one circuit of the line; approximately:

$$N = \frac{l}{l_a},$$

where l_a is the distance between strain-towers.

Appendix II. Determination of the voltage on an isolated earthwire.

If the effect of the earth is replaced by the effect of mirror-image conductors with the same voltage but opposite sign, then each circuit of the line gives a system of six conductors with given voltages relative to earth, and the earthwire under consideration is in the electrical field thereby produced.

The charges q_a, q_b and q_c on the conductors can be found from the corresponding Maxwell equations [6]. In the case of a symmetrical system, in which the conductors are arranged in a right-handed sequence and symmetrical horizontally on the tower (Fig.3), the system of equations can be written in the following simplified form [4]:

$$\dot{U}_a = \frac{\dot{q}_a h_1 + q_b \dot{h}_2 + \dot{q}_c h_3}{2\pi\varepsilon_0};$$

$$a^2\dot{U}_a = \frac{\dot{q}_a h_2 + \dot{q}_b h_1 + \dot{q}_c h_2}{2\pi\varepsilon_0};$$

$$a\dot{U}_a = \frac{\dot{q}_a h_3 + \dot{q}_b h_2 + \dot{q}_c h_1,}{2\pi\varepsilon_0},$$

where

$$h_1 = \log\frac{2H}{r_e}, \quad h_2 = \log\frac{D'_{ab}}{D_{ab}}, \quad h_3 = \log\frac{D'_{ac}}{D_{ac}};$$

$D_{ab} = D$	is the distance between phase *a* and *b* conductors;
$D_{ac} = 2D$	is the distance between phase *a* and *c* conductors;
D'_{ab}	is the distance between phase *a* conductor and the mirror image of phase *b* conductor;
D'_{ac}	is the same for phase *c*.

As a result of the combined solution of the equations we obtain:

$$\dot{q}_a = 2\pi\varepsilon_0 \dot{U}_a \frac{h'}{h}, \quad \dot{q}_b = 2\pi\varepsilon_0 \dot{U}_a \frac{h''}{h}, \quad \dot{q}_c = 2\pi\varepsilon_0 \dot{U}_a \frac{h'''}{h},$$

where

$$h = \begin{vmatrix} h_1 & h_2 & h_3 \\ h_2 & h_1 & h_2 \\ h_3 & h_2 & h_1 \end{vmatrix}; \quad h' = \begin{vmatrix} 1 & h_2 & h_3 \\ a^2 & h_1 & h_2 \\ a & h_2 & h_1 \end{vmatrix};$$

$$h'' = \begin{vmatrix} h_1 & 1 & h_3 \\ h_2 & a^2 & h_2 \\ h_3 & a & h_1 \end{vmatrix}; \quad h''' = \begin{vmatrix} h_1 & h_2 & 1 \\ h_2 & h_1 & a^2 \\ h_3 & h_2 & a \end{vmatrix}.$$

COLLEGE OF ENGINEERING
LIBRARY BOOK
No.
GUINDY

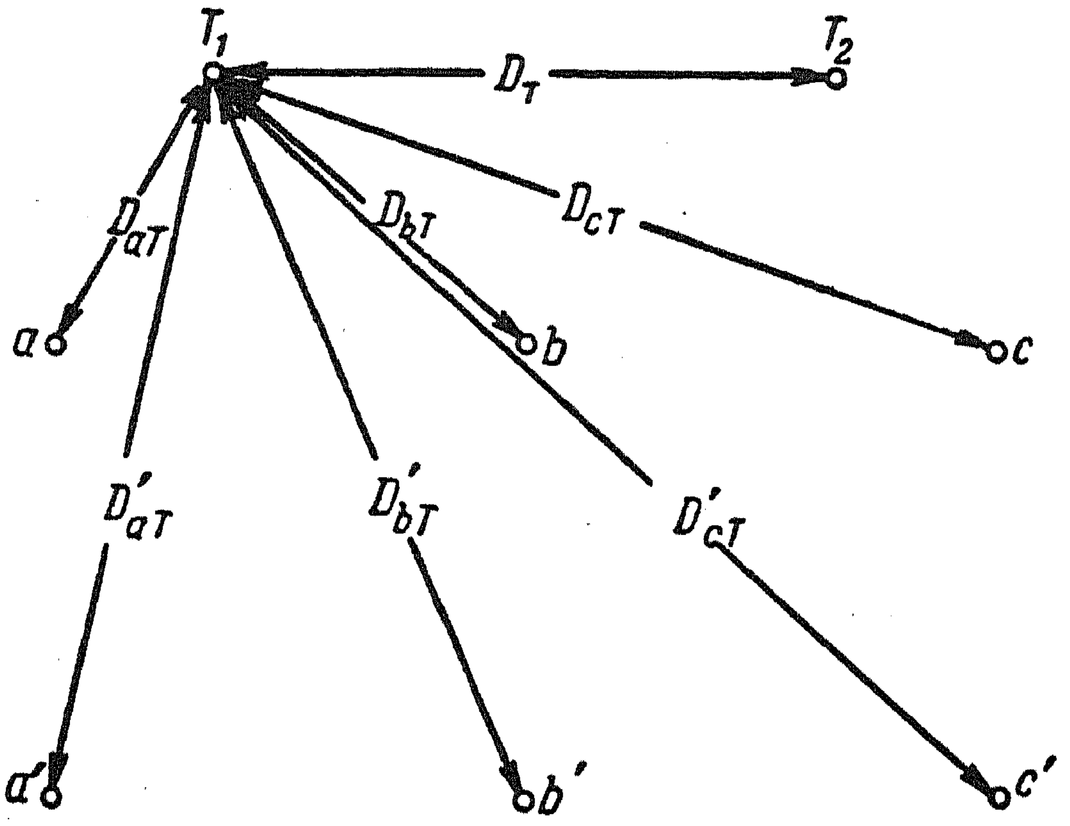

FIG. 3

Assuming that the earthwires are thin and arranged accurately along equipotential surfaces, the voltage in them relative to earth can be found:

$$\dot{U}_m = \frac{1}{2\pi\varepsilon_0}\sum_{k=a}^{c}\dot{q}_k \log\frac{D'_{mk}}{D_{mk}}.$$

Change in the order of sequence of the phases leads to conjugate values for the voltage in the earthwire.

The voltage in an earthwire when the line is operating under unbalanced phase conditions depends on the condition of the conductor which is out of the circuit. If the conductor is isolated then one must first determine some average voltage which will be produced in this conductor over the entire length of the transposition cycle, and then use the original equations to determine the charges q_a, q_b and q_c. If the conductor is connected to earth, the voltage in it can be taken as zero.

Translated by E. Bishop

REFERENCES

1. G.N. Baskakov; *Emkostnyi otbor moshchnosti ot vysokovol'tnykh linii elektroperedachi (Capacitative Power Take-off From High-voltage Transmission Lines)* Gosenergoizdat (1950).
2. A.I. Dolginov, I.G. Smirnov and V.D. Iurenkov; Earthing lightning-protection wires via spark-gaps, *Elektrichestvo*, No. 4 (1952).
3. A.I. Gershengorn, N.A. Mel'nikov and A.N. Sherentsis, The transposition of long transmission lines, *Elektrichestvo* No. 1 (1953).
4. N.A. Mel'nikov; *Raschety rezhimov raboty setei elektricheskikh sistem, (Calculation of Operating Conditions for the Circuits of Electrical Systems)*, Gosenergoizdat (1950).
5. N.F. Margolin; *Toki v zemle (Earth Currents)*, Gosenergoizdat (1947).

6. P.A. Ionkin and G.V. Zevekė; *Osnovy elektrotekhniki (Fundamentals of Electrical Engineering)*, Gosenergoizdat (1956).

EXPERIMENTAL DETERMINATION OF PARAMETERS OF ELECTRO - TRANSMISSION: KUIBYSHEV HYDRO - ELECTRIC POWER STATION – MOSCOW*

D.E. ARTEM'EV and S.S. SHUR

Science and Research Institute for Direct Current

(Received 15 April 1957)

For purposes of research, calculations, designing etc., it is necessary to know the parameters of electro-transmission not only for a frequency of 50 c/s, but also for frequencies within the range of variation of free oscillations in different transient processes and abnormal conditions.

The experiments the results of which are discussed in this article were conducted on two sections of the southern grid of the transmission line from Kuibyshev hydro-electric power station to Moscow; that is, Moscow-Vladimir, with a length of 117 km, and Moscow-Arzamas with a length of 391 km.

Let us mention the main characteristic features of the line from Kuibyshev hydro-electric station to Moscow.

The phases of this line are divided into three components, situated at the apices of an equilateral triangle with a distance between the components of $2d = 40$ cm. A mark ACO-480 cable is used for the line. The diameter of each on the three conductors is $2a = 302$ mm. The total cross-section of aluminium is in the phase 1,440 mm^2. The distance between phases is $D = 10.5$ m; the height of the cables above the earth is 21.85 m; the mean value of the sag equals 11.9 m and the mean length of the span equals 450 m. On each section of the line, that is between any two switchgear points ot sub-stations, there is a full cycle transposition. The line is protected by two steel lightning-cables of 70 mm^2 cross-section; one of them is earthed through the towers along the whole length of the line, and the second one is insulated by arcing gaps. The angle of the protection cone is equal to about 17°. The earthing resistance of most of the towers varies within the range 2-6 Ω. The dependence of the parameters of the transmission line on the frequency may be determined by two methods:

(1) by measuring these parameters in stabilized conditions when feeding the line from a generator with a large variation of frequency;

(2) by measurements in unstabilized conditions of the discharge of a battery of

---

* *Elektrichestvo* No. 1, 31 – 38, 1958 [Reprint Order No. EL 45].

capacitors into networks consisting of feeders of the line and earth ("method of damped oscillations").

The first method has the advantage that it is simple to use for interpreting experimental data. It disadvantages are that it is complex and expensive, that highly specialized equipment is required and that the exact measurement of resistance is difficult.

The second method has the advantages that it is simple to use, the equipment is readily available and reliable experimental data for determination of inductive reactances and resistances can easily be obtained. Its disadvantages are a rather cumbersome process of interpreting experimental data, and the necessity of arranging additional experiments for determination of capacitances of the system, since the error in finding them by the method of damped oscillations may be of the order of 10 - 15 per cent.

Taking into account the above advantages and disadvantages of the two methods, and the fact that for frequencies of less than 10 c/s per sec and height of the cables above the earth not exceeding a few tens of meters, the capacitances of the system are practically independent of the frequencies [1], and it is expedient to combine the two methods. We determine the proper and relative capacitances of the transmission system by the first method with a frequency of 50 c/s per sec and rated voltage. Inductive reactances and resistances for positive and zero sequences of the line, in a given range of frequencies, are measured by the second method.

Interphase capacitances and phase capacitances with respect to earth may be determined from the experiment, diagrammatically shown in Fig. 1. To ensure accuracy of the measurements, it is necessary to fulfil two conditions:

(1) the wave length of the section of line on test should be much less than $\frac{\pi}{2}$;

(2) the voltage graph during the test must not be distorted by the presence of higher harmonics. The more accurately these conditions are satisfied, the greater is the accuracy of the equations:

$$C_{11}+2C_{12}=\frac{I_A}{\omega l U_A}; \quad C_{12}=\frac{I_{BC}}{2\omega l U_A}, \tag{1}$$

where C_{11} is the capacitance of the phase with respect to earth per unit length of the line and C_{12} the interphase capacitance per unit length of the line.

The experiments made on the discharging of a battery of capacitors into the network consisting of phases of line and earth, enable us to determine the parameters of the equivalent circuit, representing the section of the line in question.

If the line is closed at one end and has a battery of capacitors at the other, then it may be shown, in the case of free oscillations of the system, that all harmonics with an index $k > 1$ are damped, approximately in accordance with the law $\exp(-R_k t/L_k)$ and harmonics with the index $k = 1$, in accordance with the law $\exp(R_1 t/2L_1)$; i.e. much more slowly, since for $k > 1$, because of the presence of skin - effect, $R_1/2L_1 < R_k/2L_k$. Therefore, after 2 - 3 half-periods of oscillations of

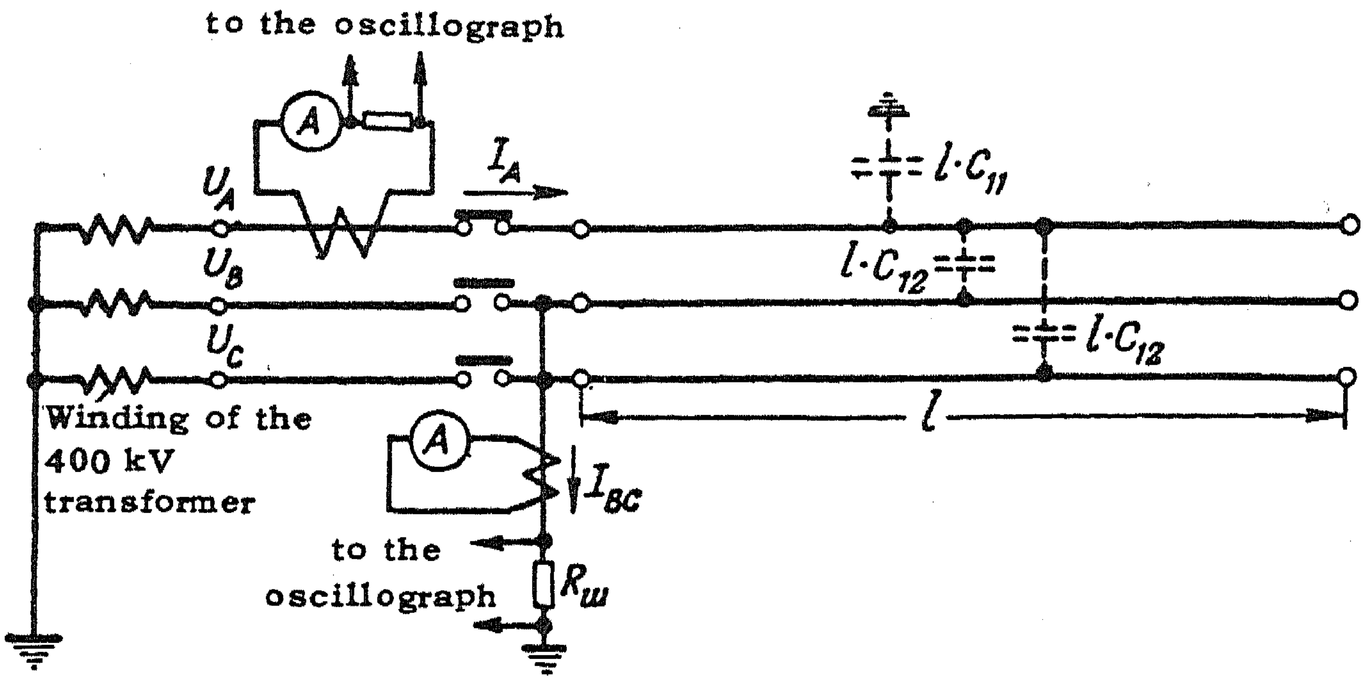

FIG. 1. Diagram for measurement of inductances of the line.

the lowest frequency, all high harmonics of the free oscillations, having index $k > 1$, will die out and the curve of discharge will practically become a damped sinusoid. Therefore, starting from a certain half-period, the line may be represented with sufficient accuracy by a single equivalent network, drawn for the lowest frequency of free oscillations, as shown in Fig. 2.

The equation characterizing the circuit in Fig. 2 will have the form :

$$C_nL_nR_dC_{\text{bat}}\,p^3+[L_n(C_n+C_{\text{bat}})+R_nC_nR_dC_{\text{bat}}]p^2+ \\ +[R_nC_n+(R_n+R_d)C_{\text{bat}}]p+1=0. \tag{2}$$

It is easy to show that, if the relations $R_d < R_n$ and $10\,C_n < C_{\text{bat}}$ are satisfied, then, up to the value of the operator $p \leqslant (-0.2+j1)\,10^3$ equation (2) may be replaced by a simpler one :

$$p^2+2\alpha p+\omega_0^2=0, \tag{3}$$

where

$$\alpha=\frac{1}{2L_n}\left[R_n+R_d\frac{C_{\text{bat}}}{C_n+C_{\text{bat}}}\right];\quad \omega_0^2=\omega^2+\alpha^2=\frac{1}{L_n(C_n+C_{\text{bat}})}\,. \tag{4}$$

The error resulting from this simplification will be less than 1 per cent. The ratio of two adjacent maxima of the curve will be equal to $\exp(2\pi\alpha/\omega)$, whence

$$\alpha=\frac{\omega}{2\pi}\ln\frac{i_{\max}^{(k)}}{i_{\max}^{(k+1)}}\,. \tag{5}$$

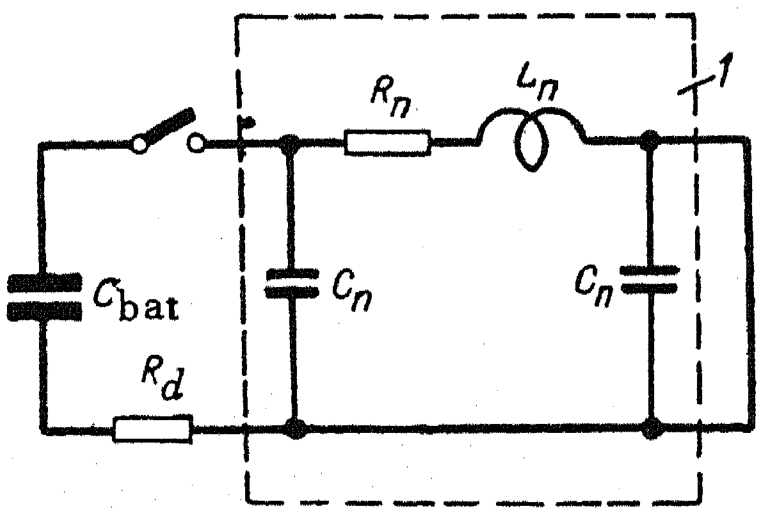

FIG. 2. Network of the experiment damped oscillations. 1. π - form equivalent circuit of the lines; R_d - total resistance of the connecting conductors and earthings.

On the basis of this discussion, we may formulate the following requirements, which must be satisfied to ensure the reliability of experimental results :

(1) resistances of connecting leads, earthings etc. should be small in comparison with the total resistance to be measured;

(2) capacitance of the battery should be at least to the order of one magnitude greater than

the total capacitance of the line;

(3) discharge currents should be sufficiently large, so that any occasional influences may be disregarded, and small enough, so that we may consider earthing resistances as linear and constant. The most suitable current to meet these conditions will be the current within the range of a few tens to a few hundreds of amperes.

Having found the discharge frequency ω from the oscillographs and the ratio of two adjacent maxima of the curve $i^{(k)}_{\max} / i^{(k+1)}_{\max}$ we determine by formulae (4) and (5) the resistance and inductive reactance of the circuit shown in the equivalent circuit diagram of the section of the line on test.

The parameters of the equivalent circuit Rn, Ln and Cn are expressed by the wave-length λ and wave impedance Z_B of the line, and, consequently, by the line parameters per unit length of the line.

In the case in question, the equivalent circuit of the line on test is set up for the operator $p = -\alpha + j\omega$; i.e. for a damped oscillations process. Because of this, the usual formulae relating line parameters per unit length and lumped parameters of the equivalent circuit R_n and L_n with quantities λ and Z_B, should be transformed. Deduction of these formulae is given in Appendix I. Only the final results and the order of calculation of the line parameters per unit length of the circuit in question are given here for the frequency ω and damping α.

We shall ignore the influence of the resistance on reactances of the equivalent circuit; it is well known that this simplification does not cause errors exceeding a fraction of 1 per cent, even for lines with a length of 60 – 70 el.deg. In this case, reactive components of the impedance and admittance of the equivalent circuit of the line network in question may be written in such a form:

$$j\omega L_n = jZ_B \sin\lambda; \quad j\omega C_n = j\frac{1}{Z_B}\tan\frac{\lambda}{2}, \tag{6}$$

where

$$Z_B = \sqrt{\frac{L}{C}}, \quad \lambda = \omega l\sqrt{LC};$$

L and C being inductance and capacitance per unit length of the line circuit on test.

By cross-multiplication of the first equation of (6) by the second equation of (4), we have

$$\frac{1}{C_n + C_{\text{bat}}} = \frac{\omega^2 + \alpha^2}{\omega^2}\,\frac{\lambda}{lC}\cdot\sin\lambda. \tag{7}$$

Multiplying equation (7) by the second equation of (6), and, substituting into the resulting expression the value $1/C_n + C_{\text{bat}}$ from equation (7), we obtain the following transcendental equation for the determination of λ:

$$\frac{\alpha^2}{\alpha^2 + \omega^2} = \cos\lambda - \frac{C_{\text{bat}}}{lC}\,\lambda\cdot\sin\lambda, \tag{8}$$

where C is a capacitance per unit length of the line, independent of a and ω, determined experimentally using asymmetrical idling.

For known λ and C, it is easy to find the inductance per unit length of the circuit in question :

$$L(\alpha;\ \omega)=\frac{\lambda^2}{l^2\omega^2 C}. \tag{9}$$

The resistance component of the impedance of the equivalent circuit (Fig. 2) is

$$R_n(a,\omega) = \mathrm{Re}\,[\,Z_{Ba} \sinh \lambda_a\,] \tag{10}$$

Formulae for determination of $Z_{Ba} = z_{Ba}e^{j\theta}$ and $\lambda_a = m + jn$ are given in appendix I.

Expanding expression (10), we have the transcendental equation

$$\frac{R_n(a,\omega)}{Z_{Ba}} + \sin\theta \sin n \cosh m = \cos\theta \cos n \sinh m \tag{11}$$

for determination of the resistance $R\,(a,\omega)$ per unit length of the circuit of the line on test.

The phenomena of skin effect, determining the dependence of line parameters on the frequency – other conditions being equal – differ for oscillations with constant amplitude, whose operator is $p = j\omega$, from damped oscillations, whose operator is $p = (-a + j\omega) = (-\eta + j)\,\omega$. The method of damped oscillations gives the corresponding parameters per unit length of the circuit in question.

Let us consider the relationship between parameters $R\,(a,\omega)$ and $L\,(a,\omega)$ for circuits phase-phase and phase-earth, and parameters of positive and zero sequences of the transmission line for the undamped process.

Having the results of the experiment of the battery discharge into the network phase-phase, we can, by formulae (8), (9) and (11), directly determine products of active resistance and inductance of the positive sequence by a double length of the section of the line on test, $R_1(a,\omega)\ 2\,l$ and $L_1\,(a,\omega)\ 2\,l$. The active resistance for the positive sequence for an undamped process can be calculated using the value of the active resistance for the positive sequence, obtained from formula (II, 17) for a given damped process.

The inductance of the positive sequence may be represented as a sum of two inductances: external L_e and internal L_i. The first one, L_e, is determined by geometric dimensions and depends neither on frequency nor on damping. For a three-phase transposition line with one phase divided into three components and with horizontal conductors, L_e may be found from the formula :

$$L_e = \frac{\mu_0}{2\pi} \ln \frac{D_1}{a_{\text{equ}}}, \tag{12}$$

where

$$D_1 = \sqrt[3]{2}D;\quad a_{\text{equ}} = \sqrt[3]{4ad^2}.$$

The influence of damping on the internal induction L_i may be found from formulae (II,18).

Calculations by formulae (II,17) and (II,18) show that the calculation of damping when $\eta < 0.2$, within the range of frequencies 10 - 200 c/s, is practically superfluous, since the corresponding correction is only of the order of a small fraction of 1 per cent of the active resistance and of inductance for the positive sequence.

From the results obtained experimentally by the discharge of the battery into the phase-earth network, we determine the active resistance, equal to the sum $R_1(a;\omega)+R_3(a;\omega)$, and the inductance, equal to the sum $L_i(a;\omega) + L_3(a;\omega) + L_2$, where $R_3(a;\omega)$ and $L_3(a;\omega)$ are the active resistance and inductance, introduced into the line by an imperfectly conducting earth; L_2' is the inductance of the network phase-earth, assuming perfect earth conduction.

Inductance L_2' is calculated from the following formula, which is derived from formulae (II,13) when $s = 3$.

$$L_2' = \frac{\mu_0}{2\pi(1+\delta)} \ln \frac{2h_{\mathrm{equ}}}{a_{\mathrm{equ}}},$$

where

$$\delta = \frac{a(h_2-h_1)}{2d^2}; \qquad h_{\mathrm{equ}} = \sqrt[3]{h_2 h_1^2}. \tag{13}$$

Formulae for calculation of $R_3(\omega)$ and $L_3(\omega)$ for given values of $R_3(\omega)$ and $L_3(\omega)$ are given in Appendix II. It can be seen from formulae (II,19) and (II,20), that the ratio of the active resistances $\dfrac{R_{er}(a;\omega)}{R_{er}(\omega)}$ depends only on damping, characterized by parameter η. The ratio of the inductances $\dfrac{L_{er}(a;\omega)}{L_{er}(\omega)}$ depends on damping and on the parameter κ, the value of which depends on an unknown quantity σ_e, specific earth conductance. Therefore, to be able to use expression (II,20), it is necessary to determine κ, and consequently σ_e, from an auxiliary transcendental equation. This equation is derived by a transformation, leading to expression (II,20); when $s = 3$, we can ignore all terms in this equation with κ raised to a power greater than unity, since the error will not exceed 0.5 per cent. The equation has the following form:

$$\begin{gathered}\frac{\sqrt{2}}{3}\left[\sqrt{\sqrt{1+\eta^2}-\eta}-\eta\sqrt{\sqrt{1+\eta^2}+\eta}\,\right]\varkappa - \\ -\ln\varkappa = \frac{2\pi(1+\delta)}{\mu_0} L_{\mathrm{er}}(\alpha;\ \omega) - \eta\psi - 0{,}6166.\end{gathered} \tag{14}$$

Equation (14) may have one or two roots, but only the smaller root has a real meaning.

After having found values $R_3(\omega)$ and $L_3(\omega)$, we can determine the parameters of the zero sequence from relations

$$R_0(\omega) = R_1(\omega) + 3R_3(\omega); \quad L_0(\omega) = L_i(\omega) + 3\,[L_3(\omega) + L_2], \tag{15}$$

where L_2 is the inductance of the circuit three phases-earth, assuming a perfect earth conductance.

Inductance L_2 is calculated by the formula

$$L_2 = \frac{\mu_0}{2\pi(1+\delta)} \ln \frac{D'_{\text{equ}}}{D_{\text{equ}}}, \tag{16}$$

where

$$D_{\text{equ}} = \sqrt[3]{a_{\text{equ}} D^2}.$$

The asymmetrical idling experiment was carried out on the Moscow-Vladimir section of the line from Kuibyshev hydro-electric power station to Moscow, at the rated line voltage. A scheme of the experiment is shown in Fig. 1.

The wave-length for this section at the frequency of 50 c/s is approximately equal to 0.75 $\pi / 2$; consequently, voltages at the beginning and end of the idle phase differed one from the other by less than 0.5 per cent. The use of formulae (1) is therefore justifiable.

Table (1) shows the result, obtained by reading index instruments and from oscillographs, one of which is shown for purposes of illustration in Fig. 3.

TABLE 1.

Experiment	U_A (kV)	I_A (A)	I_{BC} (A)	C_{11} (μF / km)	C_{12} (μF / km)	C_{work} (μF / km)
27*	230	91.4	17.7	0.00872	0,001047	0.01187
		96.0	18.25	0.00922	0.001077	0,01244
28*	225	89.9	16.7	0,00884	0.001011	0.01186
		94.5	17,1	0,00935	0.001033	0,01245

* The first line gives the results obtained from oscillographs (first harmonic), and the second line those obtained by the reading of instruments.

The working capacitance of the line was calculated by the formula

$$C_{\text{work}} = C_{11} + 3C_{12}. \tag{17}$$

As is seen from the oscillograph in Fig. 3 there all small per cent distortions present in the current of the order of 5 - 6 per cent are caused by the presence of higher harmonics. Because of this, capacitances calculated from index readings are slightly too large. Therefore, those values of capacitance calculated from the fundamental harmonic of current and voltage are accepted as the mean values (Table 5).

The experiments with damped oscillations were carried out on the phase - phase circuit on the Moscow - Vladimir section and phase - earth circuits on two sections, Moscow - Vladimir and Moscow - Arzamas.

During the experiments, the capacitances of batteries varied from 15 to 650 μF. The sum of resistances of earthing and of connecting conductors (R), was on the Moscow end of the line 0.51 Ω, Vladimir 0.8 Ω and in Arzamas 0.24 Ω. Phases not used in the experiment were disconnected from both ends. The amplitudes of the discharge currents varied from 25 to 230.

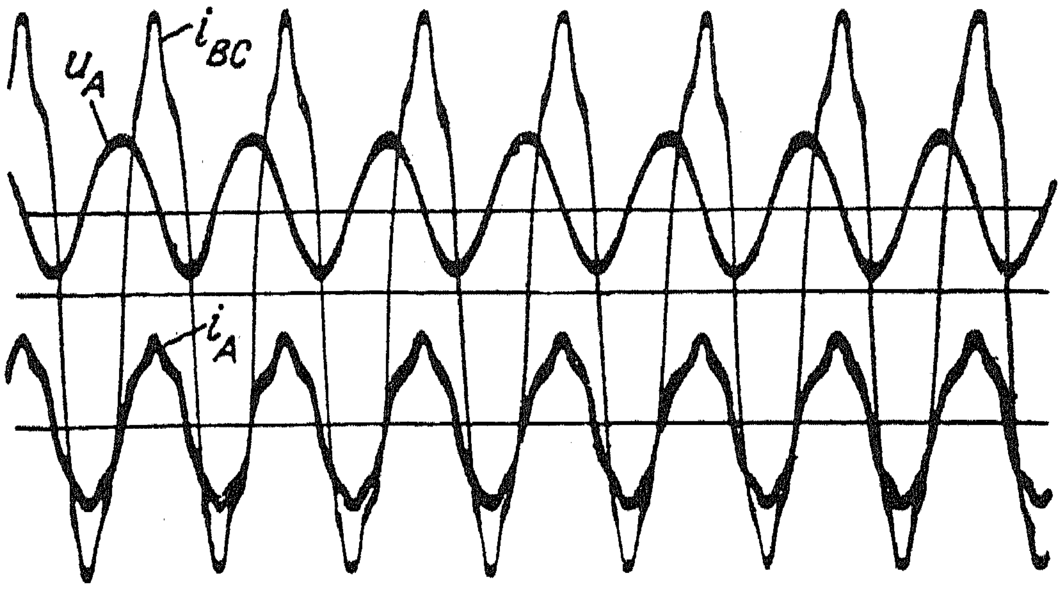

FIG. 3. The oscillographs of currents and voltages obtained from the experiment of asymmetrical idle running.

TABLE 2.

f (c/s)	α (1/sec)	Parameters of the positive sequence	
		$L_1(\omega)$ (μH/km)	$R_1(\omega)$ (Ω/km)
14.3	9.51	0.968	0.0207
17.4	9.54	0.967	0.0207
24.9	9.46	0.964	0.0206
35.3	10.1	0.955	0.0217
60.2	11.67	0.944	0.0251
77.0	12.59	0.935	0.0268
90.3	13.51	0.930	0.0289
118.7	15.05	0.928	0.0327

From the above conditions of these experiments, it follows that the use of the above formulae was justifiable.

For purposes of illustration, Fig. 4 shows oscillographs obtained from experiments with damped oscillations.

The results of experiments of the discharge of a battery of capacitors into the phase - phase network are given in Table 2. The experiments were carried out at temperatures of 0 - 2° C.

Graphs of dependence R_1 and L_1 on frequencies, plotted using the data of Table 2 are shown in Fig. 5. The external inductance L_e, calculated by formula (12), is also shown in this figure (horizontal dotted line). The difference $L_1(a, \omega) - L_e = L_i$ gives the value of the internal inductance of the bundle of three conductors, which is necessary for the calculations.

The results of the discharge of a battery of capacitors into the phase-earth network are given in Table 3 (Moscow-Arzamas section) and in Table 4 (Moscow-Vladimir section) and the corresponding graphs in Fig. 5 and 6.

TABLE 3.

f (c/s)	α (1/sec)	$R_1(\alpha;\omega)+$ $+R_{er}(\alpha;\omega)$ (Ω/km)	$L_i(\alpha;\omega)+$ $+L_2'+L_e(\alpha;\omega)$ (μH/km)	Parameters of the zero sequence	
				$R_0(\omega)$ (Ω/km)	$L_0(\omega)$ (μH/km)
7.3	6.41	0.03385	1.850	0.0571	3.979
13.9	7.91	0.04143	1.830	0.0783	3.918
20.1	10.72	0.05425	1.754	0.1155	3.685
34.4	15.75	0.07968	1.718	0.1866	3.559
48.3	20.2	0.10440	1.679	0.2553	3.479

For the frequency 50 c/s the inductances of the positive and zero sequences were also measured under static conditions of short-circuit. The results obtained were very near to those obtained by the method of damped oscillations for the same frequency.

Table 5 gives the values

of the parameters of the line from Kuibyshev HEPS to Moscow, obtained experimentally at the frequency of 50 c/s. For comparison, it also gives values of these parameters, calculated by the Carson formulae and from the Maxwell equations, with and without consideration of the earthed steel cable. The values calculated, disregarding the earthed cable, are taken from those of the project of electro-transmission, designed by the *Teploelektroproekt* (Electric power and heat generating project). As can be seen from Table 5, the values of inductance of the positive sequence and of the partial capacitance of the phase with respect to earth are near to the values assumed in the design.

The interfacial capacitance obtained experimentally differs from the value assumed for the design by 24 per cent, but practically coincides with that obtained from calculations, taking into account the earthed cable. Therefore, the experimental value of the working capacitance is near enough to that used for design calculations.

T The experimental value of the active resistance of the positive sequence exceeds the value taken for

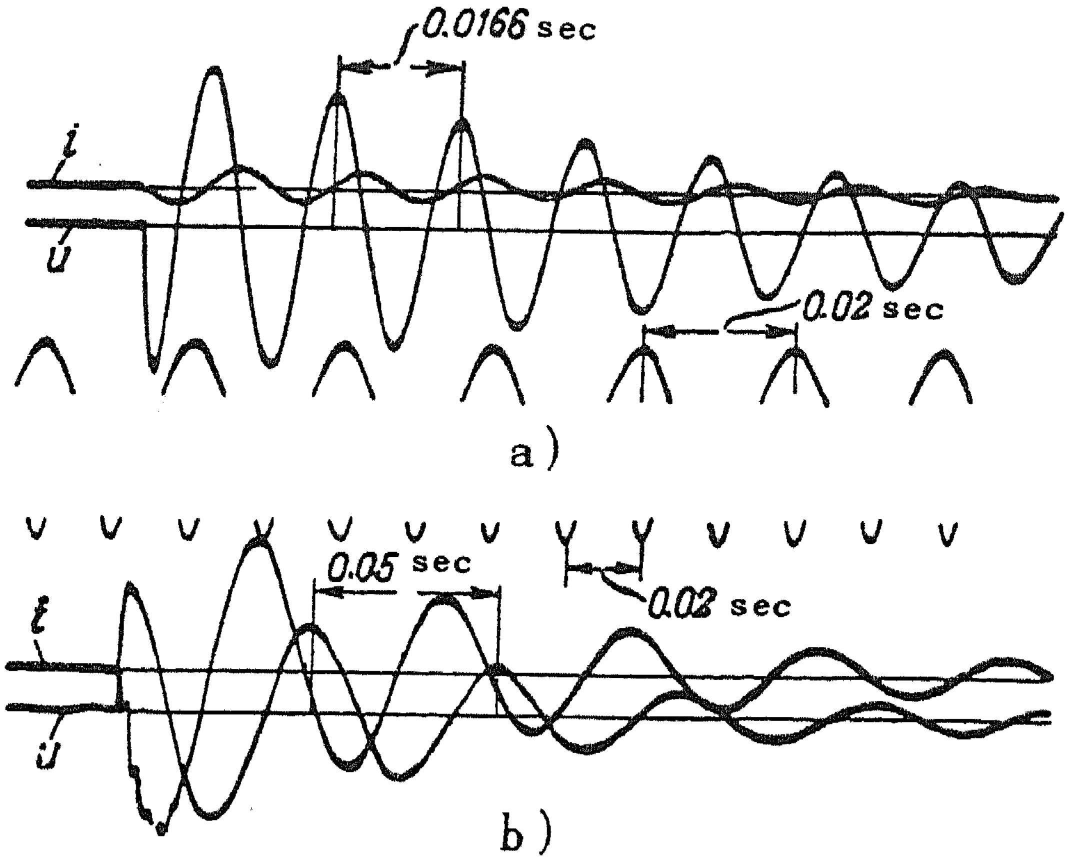

FIG. 4. The oscillographs of current and voltage obtained from the experiment with damped oscillations. (a) discharge of the battery into the network phase - phase; (b) discharge of the battery into the network phase - earth.

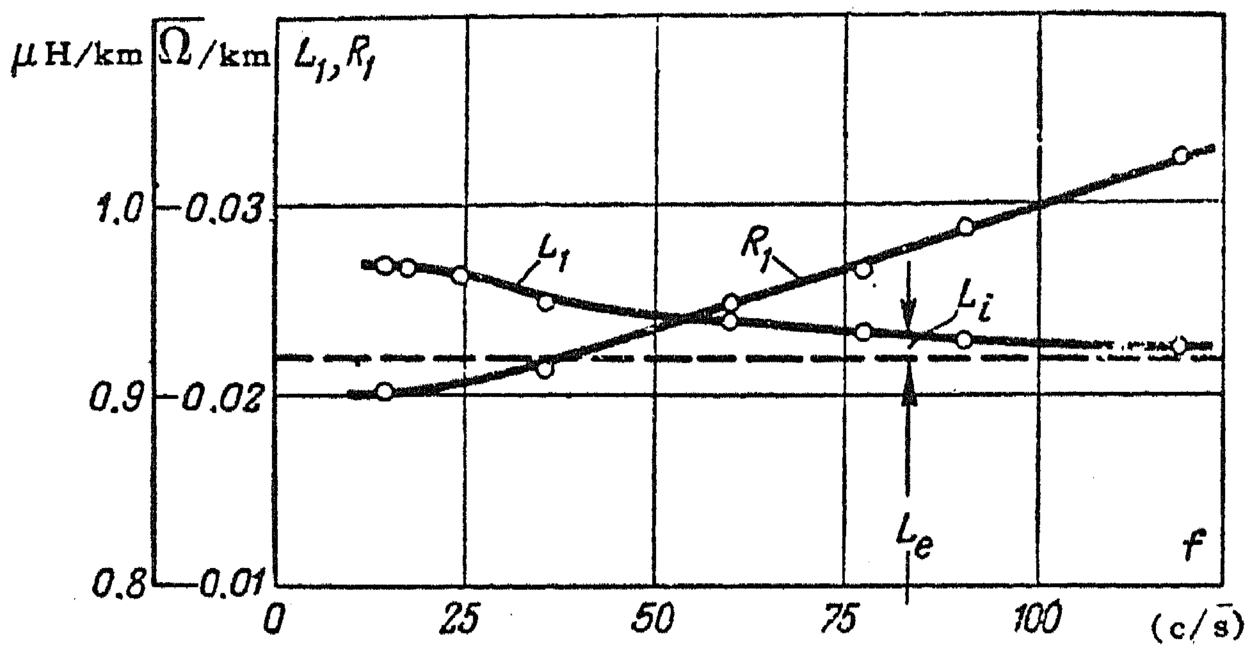

FIG. 5. Dependence of parameters of the positive sequence on the frequency.

TABLE 4.

f (c/s)	α (1/sec)	$R_1(\alpha;\omega) + R_{er}(\alpha;\omega)$ (Ω/km)	$L_i(\alpha;\omega) + L'_2 + L_e(\alpha;\omega)$ (μH/km)	Parameters of the zero sequence	
				$R_0(\omega)$ (Ω/km)	$L_0(\omega)$ (μH/km)
13.5	11.57	0.0550	1.883	0.1137	4.040
14.5	12.10	0.0576	1.888	0.1212	4.056
17.9	13.15	0.0628	1.860	0.1365	3.961
26.1	16.37	0.0772	1.760	0.1781	3.667
37.5	21.07	0.0939	1.700	0.2395	3.511
52.9	29.02	0.1471	1.685	0.3681	3.474
65.1	35.46	0.1710	1.648	0.4359	3.379
84.6	42.41	0.1990	1.602	0.5147	3.253
100.8	56.61	0.2630	1.573	0.6857	3.172
135.5	70.78	0.3115	1.486	0.8447	2.920

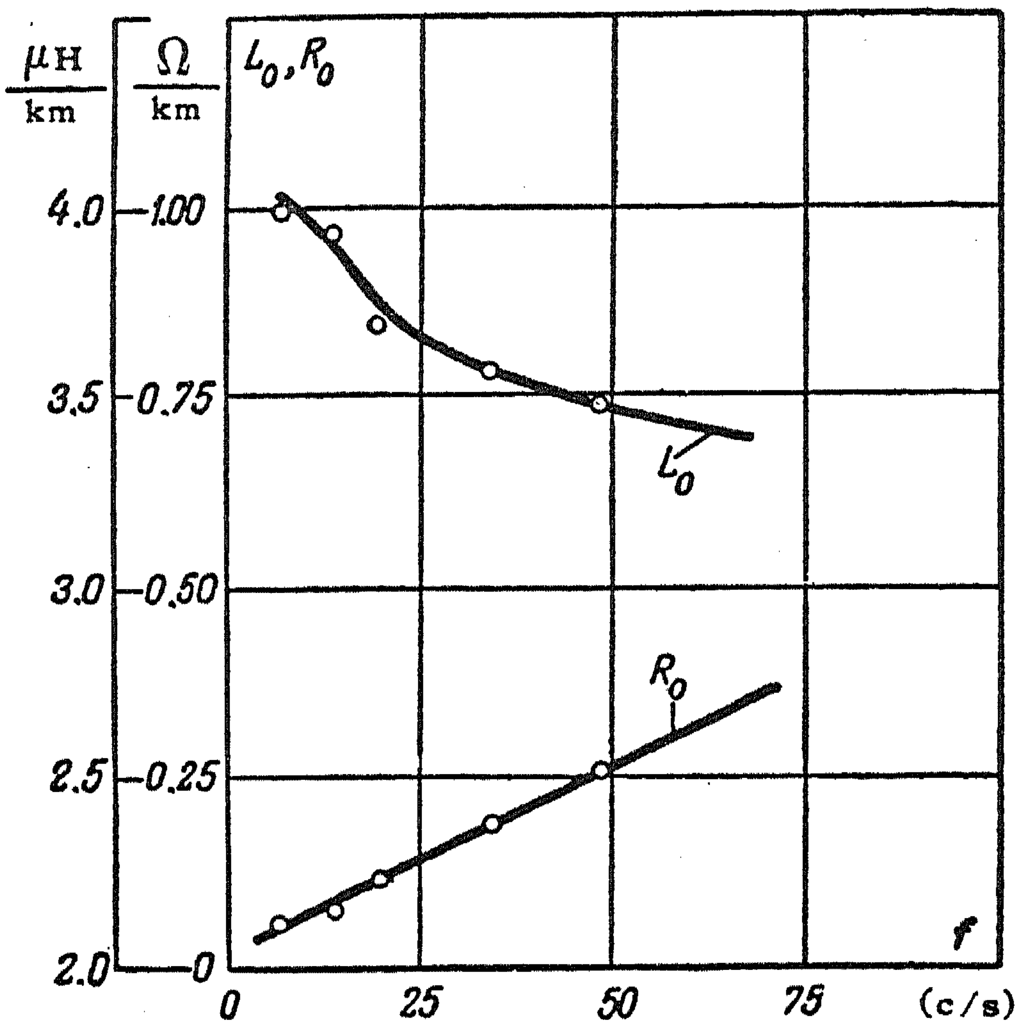

FIG. 6. Dependence of parameters of the zero sequence on the frequency for the Moscow - Arzamas section of the line.

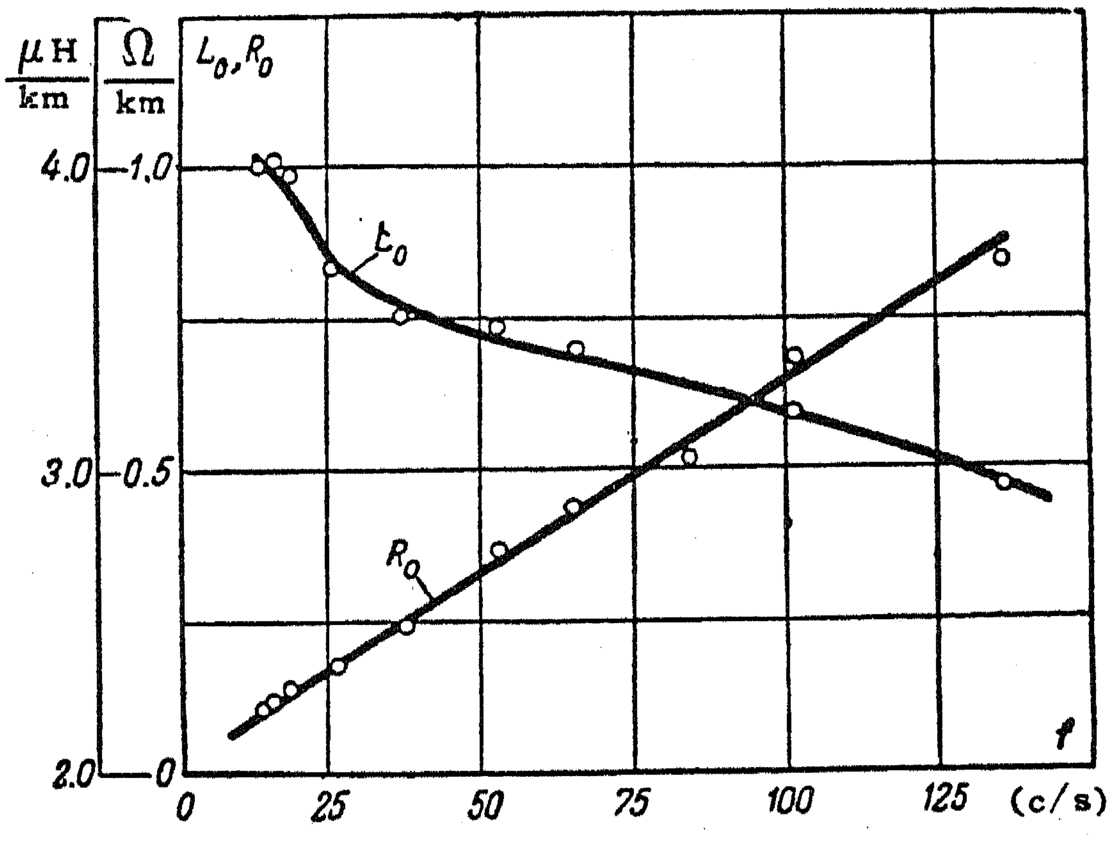

FIG. 7. Dependence of parameters of the zero sequence on the frequency for the section of the line from Moscow to Vladimir.

design purposes approximately by 7.5 per cent, and this can be attributed to the influence of tie beams, terminal fittings and other parts fixed on split feeders of the line. Measurements taken in the Science and Research Institute for direct current and in the central science and research laboratory of the Moscow Electric Station have shown that tie-beams and other fittings are a source of additional losses in the line.

Experimental values of the active resistance of the zero sequence differ considerably from those assumed in the design project and differ slightly less from those obtained from calculations, considering the influence of the steel cable. From this, the influence of the earth conductance is also clearly seen on different sections.* According to Carson's theory, this should not occur at low frequencies. The dependence of line parameters on frequency, found from experiments, is sufficiently near to the dependence given by Carson [for low frequencies $R_0(\omega)$ is practically a straight line]. Evidently, Carson's assumption about unbound and homogeneous earth is valid for high frequencies and good for the determination of the character of the function $R_0(\omega)$, but is inadmissible for purely quantitative calculations for frequencies within the range of a few hundred c/s.

---

* According to regulations [2], the earth conductance on the Moscow - Vladimir section is approximately equal to 65×10^{5} 1/Ωcm, and on the Moscow - Arzamas section to 35×10^{5} 1/Ωcm.

TABLE 5.

Description of parameter	Value of the parameter obtained from experiment	Value of the parameter obtained from calculations	
		Taking into account the earthed steel cable	From the transmission design
Partial phase capacitance with respect to earth C_{11} (μF/km)	0.00878	—	0.00867**
Interphase capacitance C_{12} (μF/km)	0.001030	0.001060	0.001276
Working capacitance C_{work} (μF/km)	0.01187	0.01185	0.01250
Active resistance of the positive sequence R_1 (Ω/km)	0.0236	—	0.0220
Inductance of the positive sequence L_1 (μH/km)	0.946	—	0.948
Active resistance of the zero sequence R_0 (Ω/km)			
for section 117 km long	0.365	0.282/0.359*	0.171
for section 391 km long	0.257	0.275/0.348*	
Inductance of the zero sequence L_0 (μH/km)			
for section 117 km long	3.466	3.410	2.970
for section 391 km long	3.446	3.560	

* Value in the numerator for steel cable resistance R cable = 2.0 Ω/km, in the denominator for R cable = 1.5 Ω/km.

** Taking into account the steel cable.

As can be seen from Table 5, the inductance of the zero sequence, calculated by Carson's formulae, taking into account the influence of the steel cable, is sufficiently accurate for practical purposes.

With the variation of frequency from 10 to 130 c/s, the active resistance of the positive sequence increases approximately 1.5 times, and that of the zero sequence 8 to 10 times. Inductances, as could be expected, increase less (by 20 - 25 per cent), therefore, in practical calculations and in research, we can disregard variation of inductance with frequency, if the wave-length of the line for a given frequency is not too near to $\pi/2$. It is desirable to take into consideration the variation of the active resistances with frequency, particularly for the determination of surge currents and voltages.

Thus, with free oscillations, damping manifests itself in effect only by the influence on the active resistance of the zero sequence. Nevertheless, increase of R_0 due to damping is small, and for practical calculations we may use the simplest formula (II,19).

In conclusion, it is necessary to point out that the experimental data discussed are related only to the region of comparatively low frequencies. For calculation of transient processes in long-distance lines it may be necessary to know the resistances at higher frequencies, of the order of hundreds of c/s. For determination of these resistances it may be expedient to perform additional experiments.

The authors express their gratitude to the employees of the transmission line from Kuibyshev hydro-electric station to Moscow, to E.P. Belov and to P.I. Gedinia for their daily help in carrying out these experiments.

Appendix I.

Expressions for wave resistance and wave length of the line during the damped sinusoidal process.

Let the process occurring in the line correspond to the law

$$\dot{U}e^{(-\alpha+j\omega)\,t} \text{ and } \dot{I}e^{(-\alpha+j\omega)\,t}. \qquad (I,1)$$

Substituting expressions (I,1) into the equation of a long-distance line, after simple transformations we have:

$$\frac{d^2\dot{U}}{dx^2} - \gamma^2\dot{U} = 0; \quad \frac{d^2\dot{I}}{dx^2} - \gamma^2\dot{I} = 0,$$

where (I,2)

$$\gamma^2 = (R - \alpha L + j\omega L)(g - \alpha C + j\omega C). \qquad (I,3)$$

From expressions (I,2) and (I,3) it is seen that the transformation of the known formulae, giving the relation between parameters λ_α and Z_B for a damped wave $\exp[(-\alpha + j\omega)\,t]$ and undamped sinusoidal oscillations, consists in replacing R by $R^1 = R(a, \omega) - a\,L(a, \omega)$ and g by $bg' = g - aC$. Let us perform this substitution.

$$Z_{B\alpha} = z_{B\alpha}\,[\cos\vartheta + j\sin\vartheta] \approx \sqrt{\frac{R - \alpha L + j\omega L}{-\alpha C + j\omega C}}; \qquad (I,4)$$

$$\lambda_\alpha = m + jn \approx l\sqrt{(R - \alpha L + j\omega L)(-\alpha C + j\omega C)}.$$

In expressions (I,4) it is taken into consideration that, as a rule, $10\, g < a\, C$.

Separating on the right-hand side of expressions (I,4) the real and imaginary terms, we have the components of the wave impedance:

$$Z_{B\alpha} = \sqrt[4]{\frac{(R-\alpha L)^2 + \omega^2 L^2}{C^2(\alpha^2+\omega^2)}}; \quad 2\vartheta = \tan^{-1} \frac{-\omega R}{L(\alpha^2+\omega^2) - \alpha R} \tag{I,5}$$

and the components of the wave length

$$\left.\begin{matrix} m \\ n \end{matrix}\right\} = l \sqrt{\frac{C}{2}} \times$$
$$\times \sqrt{\mp L(\omega^2-\alpha^2) \mp \alpha R + \sqrt{(\alpha^2+\omega^2)\,[(R-\alpha L)^2 + \omega^2 L^2]}}. \tag{I,6}$$

Remembering that for frequencies $f > 5\text{-}7$ c/s the inequality $(R - \alpha L) \ll \omega^2 L^2$ holds good, it is easy to reduce formulae (I,6), to a form more convenient for calculations. For this purpose, we expand the internal square root in the formulae (I,6), into the power series

$$\frac{\omega^2 (R - 2\alpha L)^2}{[L(\omega^2 - \alpha^2) + \alpha R]^2} \ll 1.$$

Restricting ourselves to the first two terms of the expansion we have

$$m = \frac{\omega l \sqrt{C}}{2} \cdot \frac{R - 2\alpha L}{\sqrt{L(\omega^2-\alpha^2)+\alpha R}}; \quad n = \frac{l\sqrt{C}}{2} \sqrt{\frac{4\,[(\omega^2-\alpha^2)L + \alpha R]^2 + \omega^2 (R - 2\alpha L)^2}{L(\omega^2-\alpha^2)+\alpha R}}. \tag{I,7}$$

Appendix II

The relation between parameters of the transmission line for the sinusoidal processes dying away with time.

The solution of the problem is applicable to the three-phase line with phases divided into three conductors (Fig. 8) for a sinusoidal time-attenuated process.

$$e^{pt} = e^{(-\eta + j)\,\omega t}, \quad 0 \leqslant \eta < 1, \tag{II,1}$$

It is convenient to carry out this solution exactly by the methods of Grinberg and Bonshtedt [1], ignoring the influence of the proximity of phases; i.e., representing a system of s conductors-earth, as s separate conductor-earth systems, and to find field components in air and in earth by superimposing s fields, corresponding to s separate conductor-earth systems. In future we shall use the following notation: medium 1 – conductors, medium 2 – air, medium 3 – earth. Remaining notations are clear from Fig. 8, or are given in the text.

Expressions for field components of the conductor-earth system inside any of the three media (conductor, air, earth), for sinusoidal processes are derived in [1]. The derivation of these expressions for processes of type (II,1) shows that they will have the same form, the only difference being that $j\omega$ should be replaced by

$p = (-\eta + j)\omega$. Therefore, we shall not give this derivation; we shall write only these expressions of field components, which are the constants of integration of the Maxwell equations obtained from boundary conditions of the given problem. We shall also give the equations for determination of the complex propagation constant, which will be necessary for further discussion.

The intensity of the electric field in air may be represented in such a form as this:

$$\overline{E}^{(2)} = \overline{E}^{(2)\,0} - \overline{E}_1^{(2)}, \qquad \text{(II,2)}$$

where $\overline{E}_1^{(2)}$ is the intensity of the secondary electric field in air, due to the presence of earth; $\overline{E}^{(2)\,0}$ is the intensity of the electric field of the conductor, situated in an infinitely homogeneous medium (air).

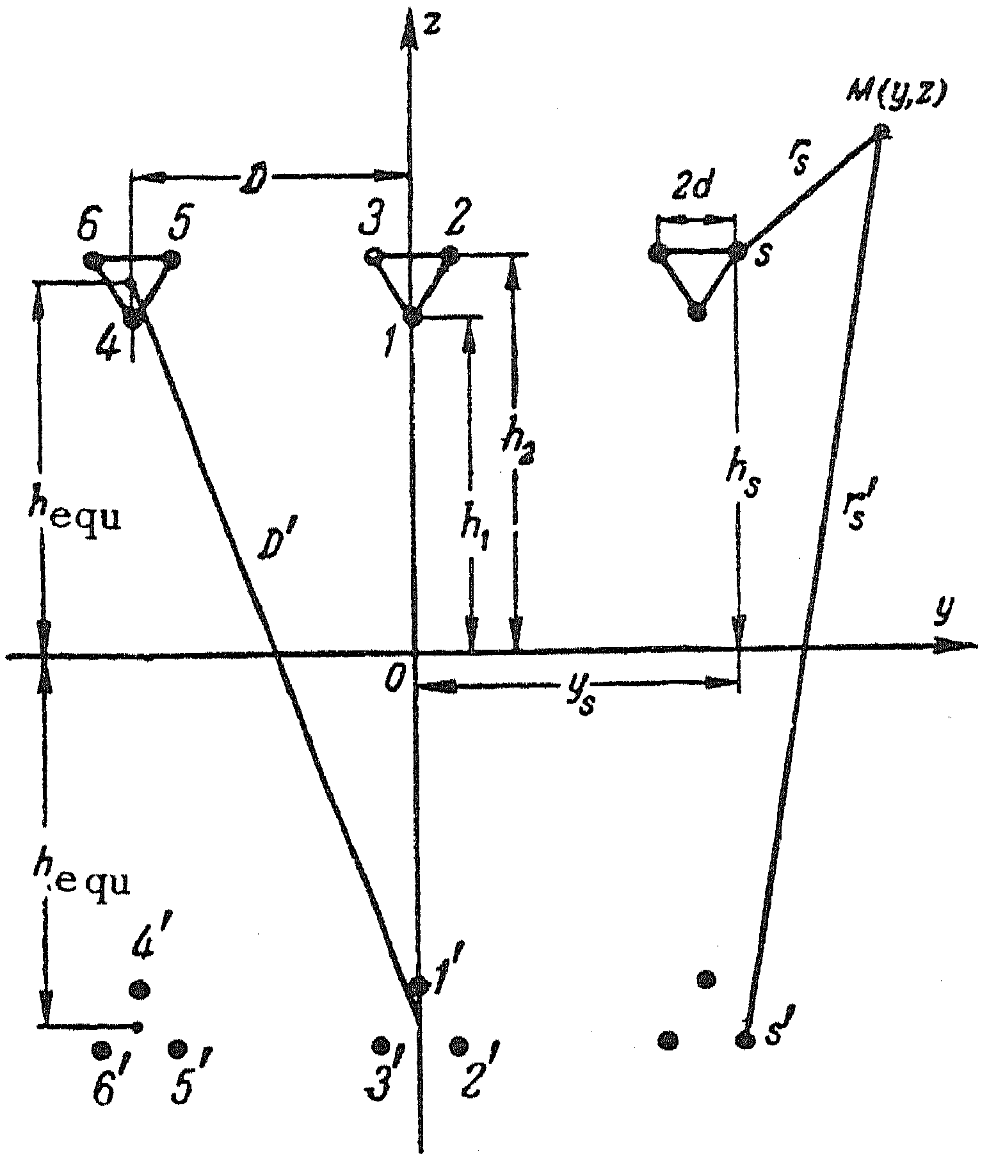

FIG. 8. Layout of the conductors of the line.

The components of the field intensity of separate conductors along the z axis are given by the following expressions written in the Gauss system of units.

$$E_{sz}^{(2)\,0} = -\frac{jq}{m_2^2} C \frac{\partial}{\partial z} H_0(m_2 r_s); \qquad \text{(II,3)}$$

$$E_{sz}^{(2)} = \frac{2qC}{\pi m_2^2} \int\limits_0^\infty \frac{\varepsilon_3' \eta_2 - \varepsilon_2' \eta_3}{\varepsilon_3' \eta_2 + \varepsilon_2' \eta_3} e^{-\eta_2 (z+h_s)} \cos \nu (y - y_s)\, d\nu,$$

where (II,4)

$$\eta_i = \sqrt{\nu^2 - m_i^2}\,; \quad \mathrm{Re}\, \eta_i > 0;$$
$$m_i = \sqrt{k_i^2 - q^2}\,, \quad \mathrm{Im}_i > 0;$$
$$k_i = -j \frac{p}{C} \sqrt{\varepsilon_i' \mu_i}, \quad \mathrm{Im}\, k_i > 0,$$

$\varepsilon_i' = \varepsilon_i + \frac{4\pi\sigma_i}{p}$ is the complex dielectric constant; σ_i is the specific electric conductance of the ith medium; H_0 is the Hankel function of the first kind of zero order.

The resultant field in the second medium (air) will be determined if we add the component fields of all nine conductors.

The constant of integration C is expressed by the parameters of the system and by the current in one conductor I_1:

$$C=\frac{I_1 m_2 \varepsilon_1'}{2ra\sigma_1}\times\frac{1}{H_1(m_2 a)+\frac{2(h_2-h_1)}{\sqrt{d^2+(h_2-h_1)^2}}H_1(m_2\sqrt{d^2+(h_2-h_1)^2}}. \tag{II,5}$$

Using the above quoted method of Grinberg and Bonshedt we can deduce the following equation for the approximate determination of the complex propagation constant q of the system in question:

$$\left(\frac{m_2}{k_2}\right)^2\frac{1}{1+\delta}\left(\ln\frac{2h_1}{a}+\sum_{s=2}^{9}\ln\frac{\sqrt{y_s^2+(h_s+h_1)^2}}{\sqrt{y_s^2+(h_s-h_1)^2}}\right.=\frac{1}{1+\delta}\sum_{s=1}^{9}F_s-\frac{1}{ak_1}\frac{J_0(ak_1)}{J_0'(ak_1)}, \tag{II,6}$$

where

$$\delta=\frac{2a(h_2-h_1)}{d^2+(h_2-h_1)^2};\quad F_s=2\varepsilon_2'\int_0^\infty\frac{\eta_2\eta_3-\nu^2}{k_3^2\eta_2+k_2^2\eta_3}e^{-\eta_2(h_1+h_s)}\cos\nu y_s d\nu.$$

The calculation of the integral F_s, within the limits $\omega<10^5$, $\sigma_3>10^7$, with an error not exceeding 0.25 per cent, gives as the first approximation

$$\begin{aligned}F_s=2\Bigg\{&-\frac{(h_1+h_s)^2-y_s^2}{[(h_1+h_s)^2+y_s^2]^2}\cdot\frac{1}{k_3^2}+\frac{1}{2}\frac{1}{\varkappa_s'}\Bigg[\frac{\pi}{2}\Upsilon_1(\varkappa_s')-\\&-\sum_{n=1}^{\infty}(-1)^{n-1}\frac{(\varkappa_s')^{2n}}{1^2\cdot3^2\ldots(2n-1)^2(2n+1)}\Bigg]+\frac{1}{2}\frac{1}{\varkappa_s''}\Bigg[\frac{\pi}{2}\Upsilon_1(\varkappa_s'')-\\&-\sum_{n=1}^{\infty}(-1)^{n-1}\frac{(\varkappa_s'')^{2n}}{1^2\cdot3^2\ldots(2n-1)^2(2n+1)}\Bigg]\Bigg\},\end{aligned} \tag{II,7}$$

where

$$\varkappa_s'=k_3[y_s-j(h_1+h_s)],\quad \varkappa_s''=k_3[-y_s-j(h_1+h_s)],$$

$\Upsilon_1(\varkappa)$ is the Bessel function of the second kind and of the first order.

Let us determine the parameters of the zero sequence per unit length of the line.

The equations for the long-distance line for time-damped sinusoidal processes, ignoring the active conductance of the earth, can be written in the following form:

$$jqU=\left(R_0'+\frac{p}{c^2}L_0'\right)I;\qquad pC_0'U=jqI, \tag{II,8}$$

where R_0', L_0', C_0' are active resistance, inductance and capacitance, respectively, per unit length of the line, when the currents flowing in all conductors are in the same phase. The total current flowing in all conductors of the line $I = 9 \sum I_1$, voltage

$$U = -\int_{0}^{h_1-a} E_z^{(2)}\Big|_{y=0}\, dz. \tag{II,9}$$

Let us substitute into equation (II,9) expressions (II,3) and (II,4) for the components of the field intensity. For frequencies $\omega \leqslant 10^6$, earth conductance $\sigma_3 \geqslant 10^7$, the height of the conductors above the earth being of the order of a few tens of metres, we can derive the following expression for the voltage:

$$U = \frac{jqI}{9p}\,\frac{1}{1+\delta}\left[\ln\frac{2h_1}{a} + \frac{1}{2}\sum_{s=2}^{9}\ln\frac{y_s^2+(h_s+h_1)^2}{y_s^2+(h_s-h_1)^2}\right]. \tag{II,10}$$

The error in using formula (II,10) will not exceed 0.5 per cent.

From the second equation of (II,8), taking into consideration (II,10), we have

$$C_0' = \frac{9(1+\delta)}{2\left[\ln\frac{2h_1}{a} + \frac{1}{2}\sum_{s=2}^{9}\ln\frac{y_s^2+(h_s+h_1)^2}{y_s^2+(h_s-h_1)^2}\right]}. \tag{II,11}$$

Substituting into the first equation (II,8) expressions (II,10) and (II,11), we have the equation which, in view of (II,6), is reduced to this form:

$$\begin{aligned} c^2R_0' + pL_0' = {} & \frac{2p}{9(1+\delta)}\left[\ln\frac{2h_1}{a} + \frac{1}{2}\sum_{s=2}^{9}\ln\frac{y_s^2+(h_s+h_1)^2}{y_s^2+(h_s-h_1)^2}\right] - \\ & - \frac{2p}{9(1+\delta)}\sum_{s=1}^{9}F_s + \frac{1}{9}\,\frac{2p}{ak_1}\cdot\frac{J_0(ak_1)}{J_0'(ak_1)}. \end{aligned} \tag{II,12}$$

Equation (II,12), can be written in the form

$$Z_0' = pL_2' + Z_{er} + Z_1,$$

where L_2' is the external inductance, of the line assuming ideal earth conductance

$$L_2' = \frac{1}{C_0'}\,; \tag{II,13}$$

Z_{er} is the total impedance, introduced into the line by non-ideal earth conductance:

$$Z_{er} = -\frac{2p}{9(1+\delta)}\sum_{s=1}^{9}F_s; \tag{II,14}$$

Z_1 is the total impedance of line conductors for time attenuated alternating current (impedance of the positive sequence):

$$Z_1 = \frac{1}{9}\,\frac{2p}{ak_1}\,\frac{J_0(ak_1)}{J_0'(ak_1)}\,. \qquad \text{(II,15)}$$

For practical calculations it is convenient to use the following formulae for determination of the active resistance and inductance of the zero sequence:

$$R_0 = 3R_0' = \frac{1}{3}\,(R_1 + R_{\mathrm{er}}); \qquad L_0 = 3L_0' = \frac{1}{3}\,(L_i + L_{\mathrm{er}} + L_2). \qquad \text{(II,16)}$$

Dependences of resistances R_1 and R_3, and of inductances L_i and L_3 on the damping parameter η, may be conveniently represented as the dependence on damping of the ratios of these values to the corresponding values (say R_1', R_3'; L_i', L_3'), measured when damping is absent, i.e. when $\eta = 0$. For real lines, when radius, height of conductors above earth and frequency of the process are not too large, formulae (II,14) and (II,15) may be considerably simplified, if we expand into the power series the transcendental functions of these equations and restrict ourselves to a few terms of expansion. In this case, the error will not exceed 0.5 per cent. For $m = \frac{1}{4}\,a^2\omega\,\mu_0\sigma_1 < 2$, the following expressions can be obtained for active resistance and internal inductance of the conductor:

$$\frac{R_1(\alpha;\,\omega)}{R_1(\omega)} = 1 + \eta^2\,\frac{m^2}{12} + \eta\,(1+\eta^2)\,\frac{m^3}{24} + \eta^2\,(1+4\eta^2)\,\frac{m^4}{240} - \eta\,(1+\eta^2)\,(8-5\eta^2)\,\frac{m^5}{862}\,; \qquad \text{(II,17)}$$

$$\frac{L_i(\alpha;\,\omega)}{L_i(\omega)} = 1 + \eta\,\frac{m}{3} + \eta^2\,\frac{m^2}{8} - \eta\,(5-8\eta^2)\,\frac{m^3}{180} - \eta^2\,(5-3\eta^2)\,\frac{m^4}{240}\,. \qquad \text{(II,18)}$$

For $X < 9.3$ and distances between the conductors of adjacent phases not exceeding the distances between the conductor and earth, for active resistances and inductances in the line to earth, we can use the formulae:

$$\frac{R_3(\alpha;\,\omega)}{R_3(\omega)} = \frac{4}{\pi}\,(1+\eta^2)\,\psi; \qquad \frac{L_3(\alpha;\,\omega)}{L_3(\omega)} = 1 + \frac{2\eta\phi}{1 - 2\ln\frac{\gamma\rho\varkappa}{2}} - \qquad \text{(II,19)}$$

$$-\,\frac{2\sqrt{2}}{3}\,\frac{\varkappa}{1 - 2\ln\frac{\gamma\rho\varkappa}{2}}\left[1 - \frac{2\eta\psi}{1 - 2\ln\frac{\gamma\rho\varkappa}{2}} - \sqrt{1-\eta} + \eta\sqrt{1+\eta}\right], \qquad \text{(II,20)}$$

where $\phi = \tan^{-1}\sqrt{\dfrac{\sqrt{1+\eta^2}+\eta}{\sqrt{1+\eta^2}-\eta}}$; $\varkappa = 2h_{\mathrm{equ}}\sqrt{\omega\mu_0\sigma_3}$;

$\rho = \dfrac{D'_{\mathrm{equ}}}{2h_{\mathrm{equ}}}$; $D'_{\mathrm{equ}} = \sqrt[3]{2h_{\mathrm{equ}}(D')^2}$; $h_{\mathrm{equ}} = \sqrt[3]{h_2 h_1^2}$.

If the formulae (II,19) and (II,20) are used, the error will not exceed 0.5 per cent.

REFERENCES

1. G.A. Grinberg and B.E. Bonshteot; Asnovy tochnoi teorii volnovogo polga linuu peredachi (Basis of an accurate theory of the wave field of transmission lines), *Zh. tekh. fiz.*, 24, 1 (1954).
2. *Pravila ograhdeniia sooruzherii soiazi u signalizatsii ot vrednogo deistviia ustanovok silnogo toka (Rules for the protection of communication installations and the indication of faults).*

COLLEGE OF ENGINEERING
LIBRARY BOOK
No.
GUINDY

PARTIAL CAPACITIES (CONDUCTIVITIES) OF A SYSTEM OF ELECTRODES AND SEPARATE FLUXES OF THE RESULTANT FIELD *

E.A. MEEROVICH and V.K. RED'KIN

Moscow

(Received 25 April 1957)

The point of view has been put forward that partial fluxes of the electrical displacement vectors in charged conductors, in the general case, are numerically equal to the charges in the partial capacities. This point of view is erroneous, and in engineering calculations it can lead to inaccuracies.

Let us consider the electrostatic field of n conducting charged bodies in a linear dielectric medium (Fig. 1).

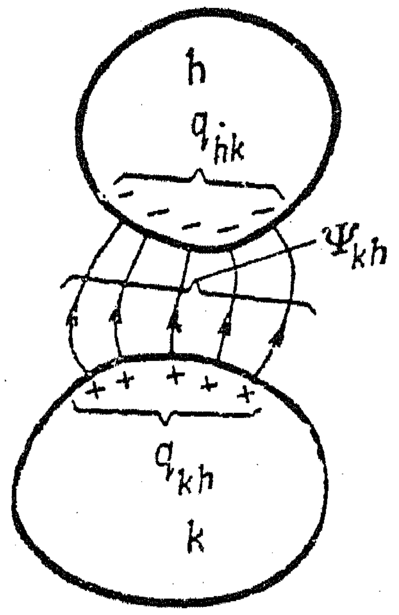

FIG. 1.

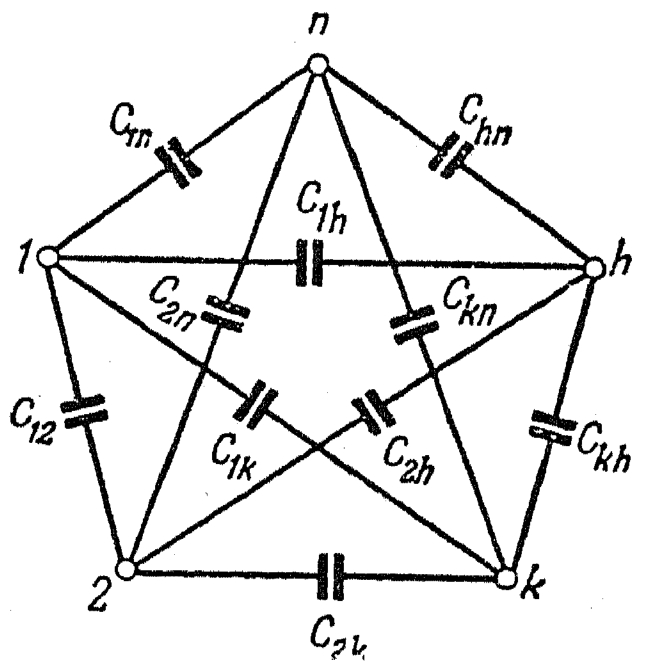

FIG. 2.

The following symbols are used:

q_k	the excess charge on body k;
ϕ_k	the potential of the body;
D	the lectrical displacement vector;
S_k	the surface area of body k;
ψ_k	the flux due to the electrical displacement vector across the surface area S_k;

---

* *Elektrichestvo* No. 1, 54-57, 1958 [Reprint Order No. EL 46].

ψ_{kh} the partial flux due to the electrical displacement vector across surface area S_k, linked only to area S_h;
q_{kh} that part of the charge on body k, relating to the partial flux ψ_{kh};
C_{kh} the partial capacitance between k and h.

The flux of the electrical displacement vector across the surface of body k equals the excess charge on this body:

$$\psi_k = q_k.$$

The partial flux ψ_{kh} resides on parts of the surfaces of bodies k and h, on which there are charges, equal in magnitude and opposite in sign, $q_{kh} = - q_{hk}$.

Let the sign of the partial flux ψ_{kh} correspond to the sign of the charge on that portion of the body k on which this charge resides. In this case the following equations are valid:

$$q_{kh} = \Psi_{kh} \text{ and } \Psi_{kh} = - \Psi_{hk},$$

whilst the fluxes of the electrical displacement vectors and the excess charges are determined by the equations:

$$\left.\begin{aligned} \Psi_k &= \sum_{h=1}^{n} \Psi_{kh}, \quad (h \neq k); \\ q_k &= \sum_{h=1}^{n} q_{kh}, \quad (h \neq k). \end{aligned}\right\} \tag{1}$$

The excess charges on the bodies can also be determined from the equations containing the partial capacities:

$$q_k = \sum_{h=1}^{n} C_{kh}(\varphi_k - \varphi_h), \quad (h \neq k). \tag{2}$$

To equations (2) there corresponds an equivalent circuit in the form of a closed network (Fig. 2), the elements of which are condensers equal to the partial capacities of the system of bodies.

This network may be regarded as analogous to the system of n bodies in the sense that if to each body there corresponds a given node, and if the excess charge on each body equals the sum of the charges on the plates of the condensers connected to the node representing that body, the potential difference between any two bodies will be identical to the potential difference between the nodes corresponding to those bodies. On the other hand, if the potential differences between nodes and between the bodies to which they correspond are equal, then the excess charge on each body will equal the sum of the charge on the plates of the condensers connected to the node representing this body.

Another system of indices is sometimes used in literature to denote the partial capacitances. It is normally used in those cases when the fields of bodies are considered in the presence of the earth. The earth is regarded as the $(n+1)$th body, of infinitely large size and at zero potential [1, p.85]. In this case the partial capacities of the bodies relative to earth are denoted by two identical indices (C_{kk}) and are called self-capacities, whereas the other partial capacities (C_{kh}) are called mutual.

Since the set of bodies under consideration need not include a body of infinite size and the potential may be taken as zero at any desired point, the partial capacities will not be divided into self and mutual in this paper. It should be noted that the index system has no effect on subsequent deductions.

From equations (1) and (2) if follows that

$$\sum_{h=1}^{n} q_{kh} = \sum_{h=1}^{n} C_{kh}(\varphi_k - \varphi_h), \quad (h \neq k). \tag{3}$$

However a number of authors consider that there is also a further relationship, as follows:

$$\Psi_{kh} = q_{kh} = C_{kh}(\varphi_k - \varphi_h). \tag{4}$$

This is equivalent to the assertion that the partial fluxes of the electrical displacement vectors are numerically equal to the corresponding terms on the right hand side of equations (2), i.e. to the charges on the corresponding condensers in the equivalent circuit.

For example, it is stated [1, p. 86] that the separate terms on the right hand side of the equations containing the partial capacities determine the respective parts of the displacement fluxes emanating from the charged bodies. Thus, for example, that part of the flux emanating from the first body equal to $C_{11}(u_1 - 0)$ represents the total number of unit tubes of flux passing from the first body to the surface of the earth. Another part of the same flux, equal to $C_{12}(U_1 - U_2)$ represents the total number of unit tubes of flux passing from the first body to the second and so on. In fact, a similar assertion is made in [2, 3].

No less definite statements are found in foreign publications. For example in [4] formulae are given for calculating the partial capacities in the equivalent circuit, which correspond to relationship (4):

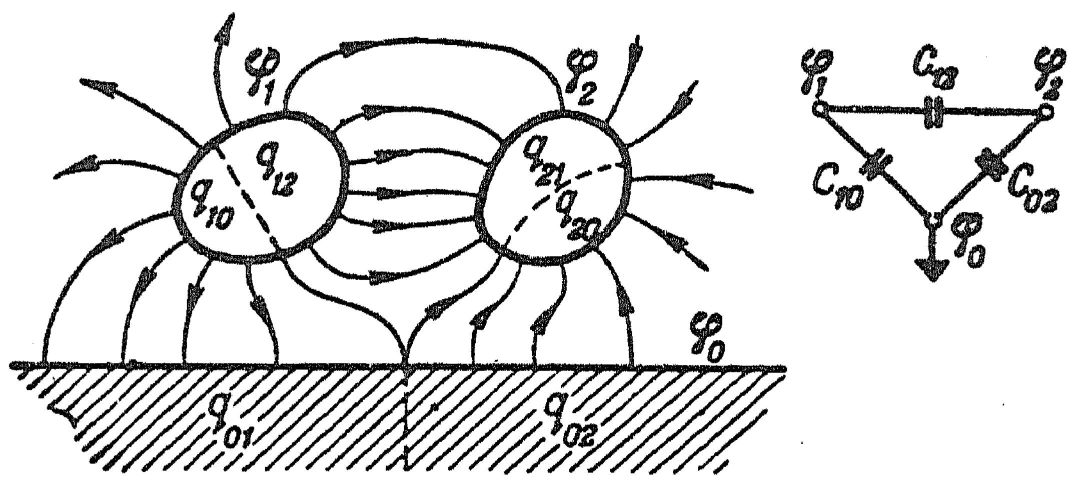

FIG. 3.

This relationship is illustrated in Fig. 3 taken from [4] *.

We shall show that this point of view is erroneous. We assume that the medium is uniform, the sum of all the charges on the bodies is zero, all the surfaces S_k are smooth and none of them completely encloses any other surface.

Under these conditions the following propositions may be established for a system of n charged bodies.

1. On the surfaces of the bodies which have a maximum or minimum potential in the given field, the values of the modulus of the electrical displacement vectors exceed some positive number. The validity of this proposition follows from the general theory of harmonic functions [5].

2. None of the partial capacities is zero. This corresponds to the Maxwell proposition [6] that the mutual electrostatic induction coefficients of a system of bodies are negative if the condition is observed that none of the surfaces completely encloses any other surface.

The second proposition is easily derived.

In fact, the partial capacities are equal to the mutual electrostatic induction coefficients, with the signs reversed. To determine the partial capacities C_{kh}, relating to body k, it is necessary, for example, to impart to it a potential of ϕ_k; and to the remaining bodies a potential of ϕ, equal on them all, but such that $\varphi_* \neq \varphi_k$. Then, in accordance with the first proposition, all the charges ϕ_{kh} will differ from zero.

In these conditions, we have for the partial capacities:

$$C_{kh} = \frac{q_h}{\varphi_* - \varphi_k} > 0.$$

Without disturbing the general nature of the proof, we shall further consider fields in which the bodies, except k and h, can be replaced by a single body Σ (Fig. 4).

---

* Fig. 3 (also corresponds to Fig. 4-9, in [2].

The method of proof will be by *reductio ad absurdum.* Assume that equation (4) is valid whatever potentials the bodies are at. Take the case when the potentials are different for each body, i.e.

$$\phi_h \neq \phi_k \neq \phi_\Sigma \text{ whilst } \phi_k > \phi_\Sigma \text{ and } \phi_h > \phi_\Sigma.$$

Since none of the partial capacities is equal to zero, the following picture must be set up of the flux distribution. Two partial fluxes emanate from the surface of each body, whilst the total number of partial fluxes is equal to three, since $|\psi_k| = |\psi_{hk}|$. The partial fluxes emanating from the body with a potential intermediate between those of the other two will clearly have opposite directions relative to the normal direction outwards from the surface of the body in question.

The selected potential distribution can be regarded as resulting from the superimposition of two conditions, shown schematically in Fig. 4a, b, the values e' and e'' of the e.m.f. being taken as follows:

$$e' = \varphi_k - \varphi_\Sigma; \quad e'' = \varphi_h - \varphi_\Sigma.$$

In each of these cases two bodies in the system are at the same potential, and consequently there is no partial flux between them.

According to the first proposition, it follows that for any value of $(\phi_k - \phi_\Sigma)$ a value of $(\phi_h - \phi_\Sigma)$ can be found such that the value of the modulus of the electrical displacement vectors at any points on the surfaces S_k and S_h will be greater for the condition of Fig. 4b, than for that of Fig. 4a. In that case, after superimposition, the electrical displacement vector will not change direction relative to the normal direction outwards from one of the surfaces; in other words, the flux distribution corresponds to Fig. 4c, and is not in accordance with the assumption made.

Thus on the bases of equation (4) we have reached a contradiction, proving that this equation is not valid.

The result obtained is to some extent analogous to those obtained in considering the magnetic field due to a number of current-carrying coils [7, 8, 9]. The idea existed earlier that the dispersal fluxes, figuring in transformer calculations, can be found directly from the picture of the flux-coupling of the resultant magnetic field. In actual fact, there is generally no correspondence between the real partial flux distribution and the representation of the separate dispersion fluxes.

The use of an equivalent circuit makes the calculations easier. Having found the partial capacities by one method or another and built up from them the equivalent circuit, it is possible to calculate the input capacities on the part of any two bodies, to find the distribution of excess charges and potentials on the bodies and so on. All the calculation methods for electrical networks are applicable to the equivalent circuit.

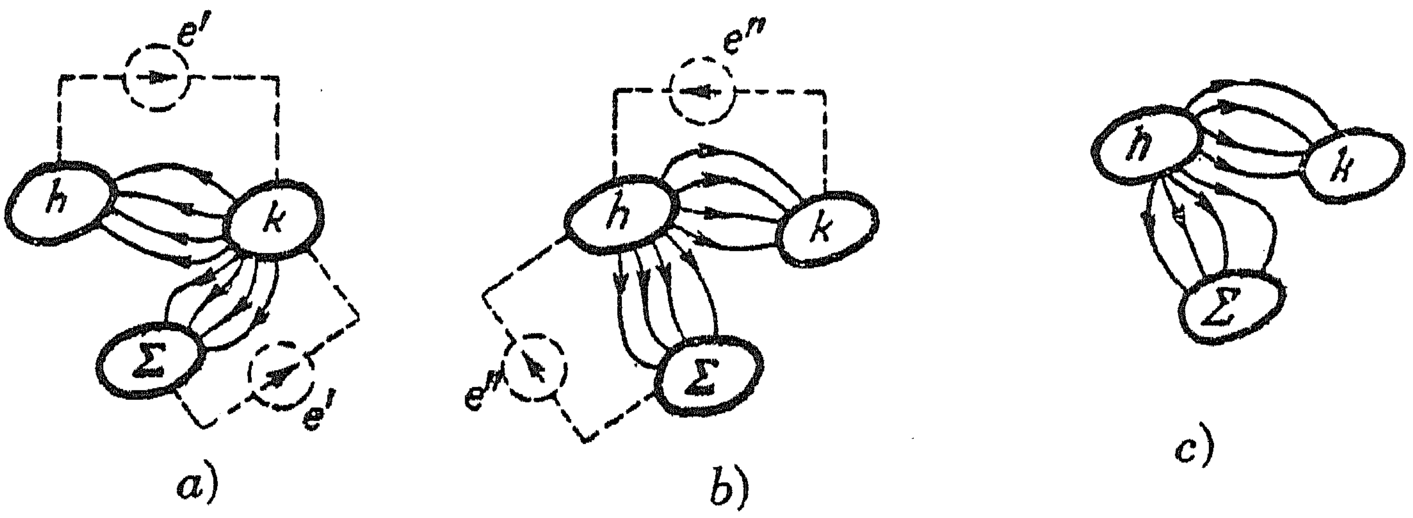

a) b) c)

FIG. 4.

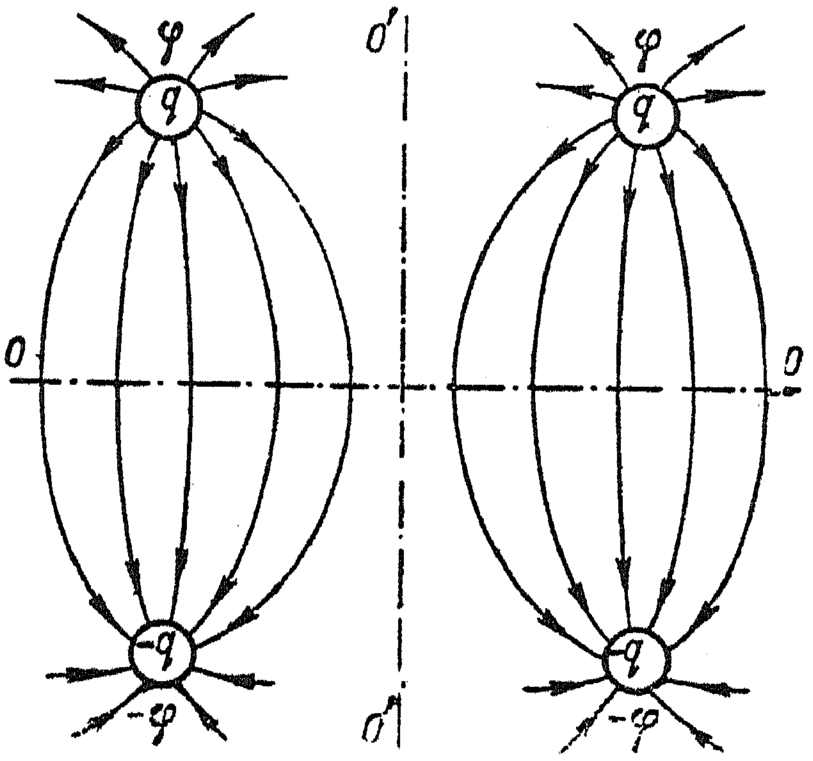

FIG. 5.

The partial capacities can be found from equations (2), in which the values of the excess charges and potentials are substituted. Since the total number of unknown capacitances in $\frac{1}{2}n\ (n-1)$, whereas only $(n-1)$ equations correspond to each condition, it is necessary to consider a number of conditions which can be the most convenient.

In the special case when the charges on all the bodies other than k are equal, the value of the charge on these bodies is numerically equal to the electrical displacement vector flux. For each such condition, the partial capacitances relative to body k are found directly from equation (4).

Calculation of the stationary field of the electric current in a system of electrodes in a conducting medium is carried out in an analogous manner, if it is assumed that the electrodes have infinite conductance. Since there is an analogy between current fields and charge fields, such fields can be used as models for each other; the analogues of the electric displacement vector fluxes will be the currents flowing in the conducting medium, the partial conductances will correspond to partial capacities, and so on. Consequently, all the preceding arguments relating to partial capacities and fluxes can be related to partial conductances and currents. The equivalent circuit in this case will be a closed network in which the node potentials correspond to the electrode potentials and the elements are partial conductances.

Example Consider the plane-parallel electrostatic field of four circular conductors (Fig. 5). Assume that all the conductors have the same cross-section, and that their centres are at the corners of a rectangle. All values will relate to unit length of the conductors in a direction normal to the plane of Fig. 5. The medium is taken to be uniform.

In this case, equations (2) take the form:

$$q_1 = C_{12}(\phi_1 - \phi_2) + C_{13}(\phi_1 - \phi_3) + C_{14}(\phi_1 - \phi_4);$$

. . . .

. . . .

whilst none of the partial capacities is equal to zero.

We shall study the condition in which:

$$\phi_1 = \phi_2 = \phi\ ;$$
$$\phi_3 = \phi_4 = -\phi\ .$$

In this condition the line of symmetry O-O is the intercept of the equipotential surface, whilst the line of symmetry O′-O′ is the intercept of the surface of equal electrical displacement vector flux. Since there can be no unit tubes of displacement across the line O′-O′, the resultant field contains only two partial fluxes, equal in magnitude:

$$\Psi_{14} = \Psi_{23} = q = (C_{14} + C_{13})\, 2\phi\ .$$

If the formulae (4) are assumed correct, then, for example, to calculate the partial capacity C_{14} we have:

$$\Psi_{14} = q = 2C_{14}\phi\ .$$

Thus the error in calculating C_{14} from formula (4) is determined by the value of the partial capacity C_{13}.

Translated by E. Bishop

REFERENCES

1. L.P. Neiman and P.L. Kalantarov; *Teoreticheskie osnovy electrotekhniki (Theoretical Principles of electro-technology)*, III, 4, Gosenergoizdat (1954).
2. G.V. Zeveke and P.A. Ionkin; *Osnovy elektrotekhniki* (Principles of Electro-technology) 1, Cosenergoizdat (1955).
3. A.V. Netushil and K.M. Polivanov; *Osnovy elektrotekhniki (Principles of Electro-technology)*, 3, Gosenergoizdat (1956).
4. E. Weber; *Electromagnetic Fields*, New York, 1 (1950).
5. V.I. Smirnov; *Kurs vysshei matematiki (Course of Higher Mathematics)* GITL IV, 3 (1953).
6. Maxwell; *Electricity and magnetism*, Oxford, 1 (1904).

7. Hemmeter; *A. f. E.*, 32, 167 (1927).
8. E.G. Markvardt; *Elektromagnitnye raschety transformatorov* (Electromagnetic Transformer Calculations), ONTI (1938).
9. E.A. Meerovich; "On the problem of electromagnetic dispersion in transformers", *Izv. ENIN Akad. Nauk SSSR*, 1, 1-2 (1935).

COLLEGE OF ENGINEERING
LIBRARY BOOK
No.
GUINDY

THE HEAT EMISSION OF RECTIFIER STACKS MADE OF LARGE SELENIUM CELLS*

F.F. SOKOLOV

Scientific Research Institute of Cinema Photography

Special thermal tests have been carried out here to calculate the heat emitted by rectangular selenium plates of large dimensions, particularly under forced-draught cooling; the results of these tests are given below.

Method of testing

The cells were heated by losses of forward currents when passing d.c. through the stacks, The stacks consisted of cells specially selected in order as far as possible to exclude non-uniform heating owing to differences in cell characteristics. Losses were measured by the voltmeter-ammeter method. The excess heating was measured by copper-constantan thermocouples soldered to the cells (the mean of six cell-stacks). The excess heating was measured 15 mm from the upper edge of the cells (the point of maximum heat of a cell). Where cooling was natural, the stacks were set 150 mm above the test-bench. With forced-draught cooling, the stacks were set up in a container-duct of cross-section 365 × 312 mm. An electric motor and fan were installed at the top; the cooling air velocity could be regulated over a wide range. The stacks were installed in such a way as to fill the entire cross-section of the container. The air velocity was measured by vane anemometer in the bottom opening of the container. These tests were reduced, when processing the results, to the air velocity between the cells.

Natural cooling

Tests were made on stacks of selenium cells, 6 to 18 mm apart, on 100 × 200 and 100 × 300 mm aluminium base-plates. The heat emission data were determined for cell excess temperatures of from 0 to 40°C, and with a surrounding air temperature of about 20°C. All the thermal regimes were repeated for two stack positions: "vertical" (the long side of the cell being vertical) and "horizontal" (the long side horizontal). The experimental data obtained are given in Figs. 1 and 2 in the form of graphs for the relationship between τ, the excess heating of the cells and the specific losses q (W/dm^2).

---

* *Elektrichestvo* No. 1, 58 – 63, 1958 [Reprint Order No. EL 47].

Analysis of the results obtained enables us to draw the conclusion that the heat emissivity of the rectangular cells tested is better than the known data for circular cells [2, 3, 4]. The improvement in heat emission should be attributed primarily to the difference in materials: the data for circular cell-stacks were mainly obtained when testing rectifiers on steel base-plates; in my case aluminium plates with better heat-conductivity were tested, this reducing the amount by which the most heated parts of cells (at the top) were overheated, while somewhat raising the overheating of the less-heated parts. In addition, the parameter of rectangular cells is greater than that of circular cells and, as we know, the regions of a cell close to the periphery are the more effective as to heat emission [3].

For the purpose of generalization, the experimental data on the heat emission of stacks of rectangular cells were expressed in dimensionless form [5]. The logarithmic coordinate curve in Fig. 3 expresses the graphical relationship of the Nousselt number:

$$Nu = \frac{\alpha b}{\lambda}$$

to the product of the three numbers:

The Grasshof:

$$Gr = \frac{\beta g b^3 \tau}{\nu};$$

The Prandtl:

$$Pr = \frac{\nu}{a}$$

and the dimensionless number:

$$\frac{b}{H},$$

where α is the coefficient of heat emission of the surface of the cell, (kcal/m^2/hr/°C);
λ is the coefficient of heat conductivity , f the cooling medium, (kcal/m/hr/°C);
β is the coefficient of volumetric expansion of the cooling medium (/°C);
ν is the coefficient of kinometric viscocity of the cooling medium (m^2/sec);
a is the coefficient of temperature conductivity of the cooling medium (m^2/sec);
g is the gravitational acceleration (m/sec^2);
b is the gap between cells (m);
and H is the cell height (m).

A temperature of 35° was taken as the specific temperature, in making calculations for the physical constants used in the numbers; this temperature of 35° corresponds to 30°C mean excess cell temperature and a surrounding medium temperature of 20°C.

If we substitute the following values for the constants:

$$\lambda = 0.0225; \qquad \beta = \frac{1}{273}; \qquad \nu = 17.1 \cdot 10^{-6}; \qquad a = 2.33 \cdot 10^{-5}$$

and for the convenience express b and H in mm and α in W/dm^2/°C, the equations for calculating the numbers are simplified:

$$Nu = 3.82 \alpha b; \qquad (1)$$

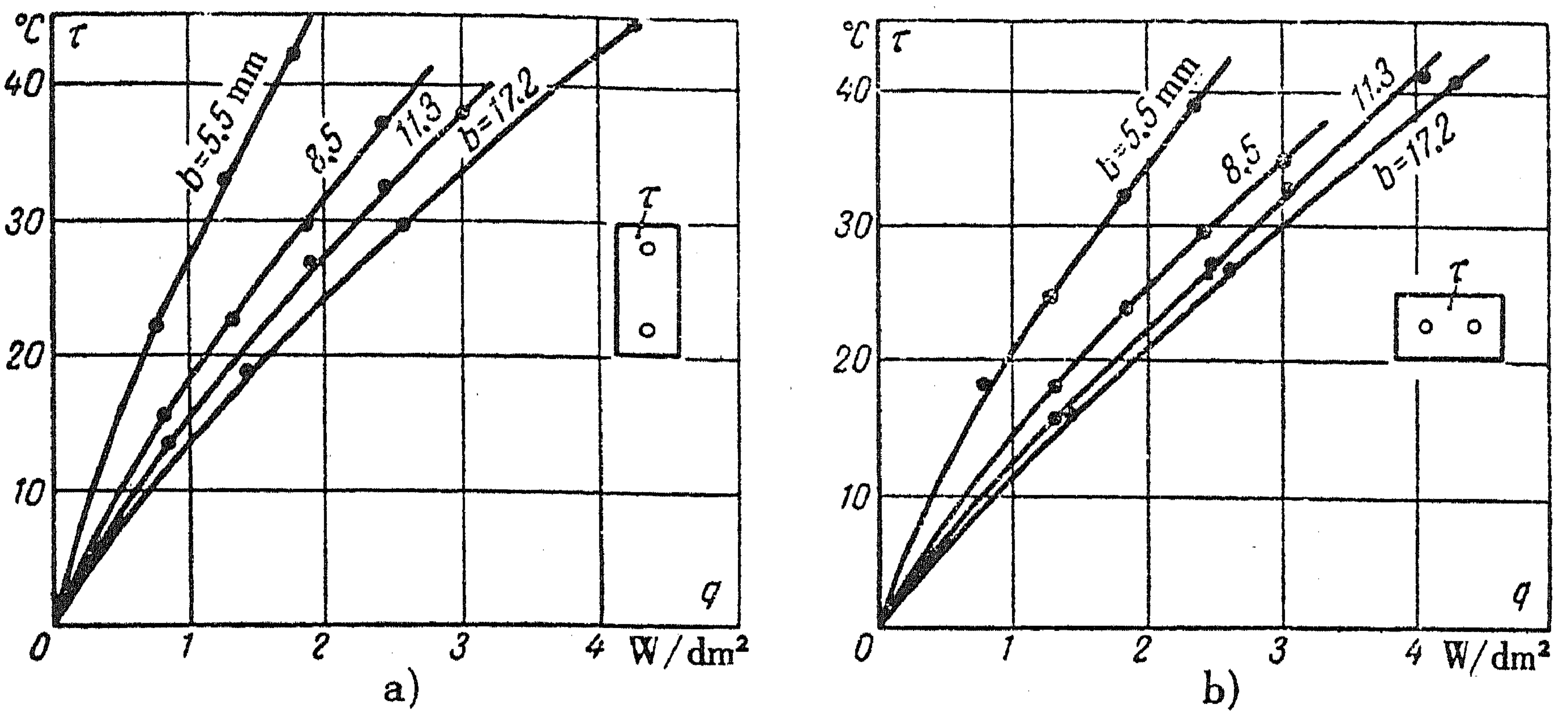

FIG. 1. The heat emission of 100 × 200 mm selenium cells, naturally cooled in stacks with different gaps (b is the gap between cells). (a) vertical and (b) horizontal cell arrangement.

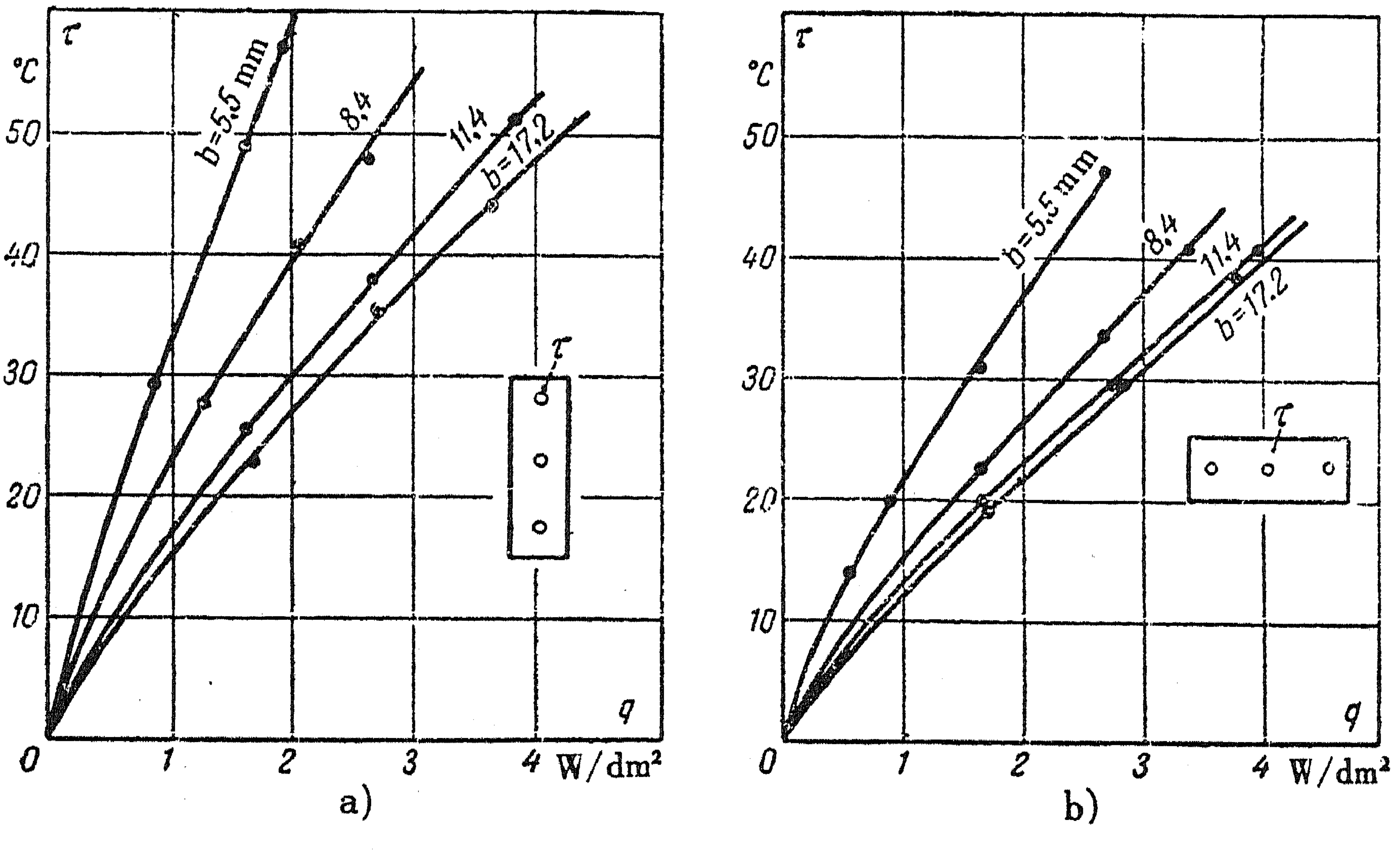

FIG. 2. The heat emission of 100 × 300 mm selenium cells, naturally cooled in stacks with different gaps (b is the gap between cells). (a) vertical and (b) horizontal cell arrangement.

$$Nu = 3.82\,\alpha\,\beta$$

$$Gr\,Pr\,\frac{b}{H} = \frac{0.089b^4\tau}{H}. \tag{2}$$

The curve in Fig. 3 is drawn according to equations (1) and (2) by substituting the values for b, H, τ and $\alpha = q/\tau$ from the curves in Figs. 1 and 2.

It is clear from the curve that the results of my tests on stacks with cells of dimensions 100 × 200 and 100 × 300 mm (in the vertical and horizontal positions)

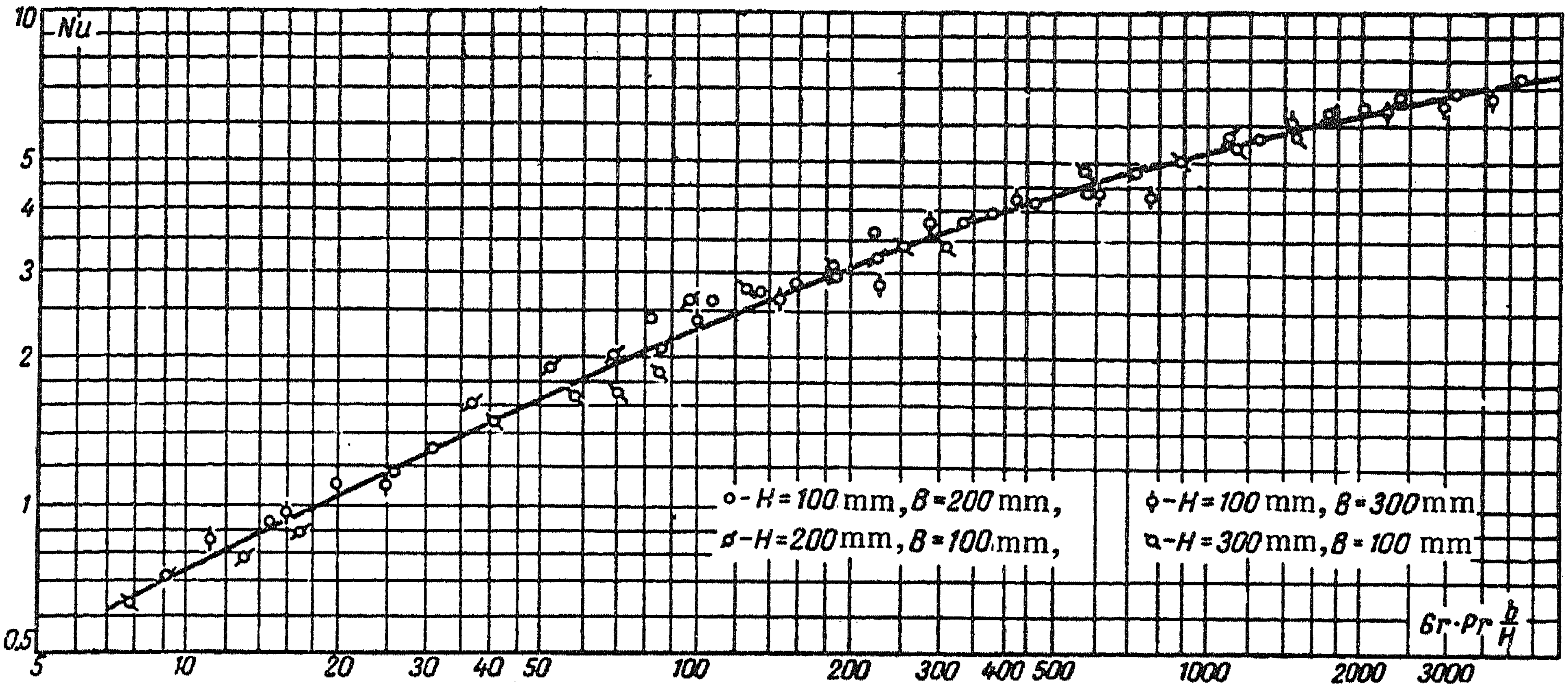

FIG. 3. Heat emission of selenium stacks composed of rectangular cells naturally cooled, in numerically generalized arrangement.

6 - 18 mm apart fit quite well on one curve (the error does not exceed 10 - 12 per cent). This result may be counted fully satisfactory particularly if we take into account that in the preceding analysis the proportion of the heat emission falling to radiation was not deducted,* for convenience in making use of the data obtained, and also that the test results combined by processing were obtained using selenium stacks which differed considerably in geometrical dimensions.

The generalized relationship represented in Fig. 3 can clearly be applied successfully to other stacks composed of rectangular cells of dimensions almost the same as those of the tested stacks, and with any gap encountered in practical cases in calculations for separated stacks cooled naturally. The generalized relationship obtained may also be applied in principle to cases of the heat emission of stacks in other mediums, for example in oil (by substituting appropriate values for the physical constants in the dimensionless numbers).

When the stacks are arranged in any specific layout (in a housing, together with other parts, several stacks beneath one another, etc.) the heat emission conditions obtained for separately arranged stacks (Figs. 1 - 3) may alter substantially. In these cases other methods for the thermal calculation [3], and the data obtained with forced-draught cooling, should be used.

---

* Specially conducted experiments have shown [3] that 12 - 16 per cent of the total heat emission fell to radiation in selenium stacks with natural cooling. The assumption made for the excess temperatures in the narrow range in which I was interested is therefore fully justifiable.

Forced draught cooling

Stacks of 100 × 300 mm cells were tested in two series. In the first series (Fig. 4a) the stacks were arranged with the long sides of the cells vertical, tests being carried out with gaps of 6, 12 and 18 mm between cells. In the second series (Fig. 4b) the stacks were arranged with their long sides horizontal, tests being carried out with a gap of 12 mm between cells, but for one, two and three stacks arranged above one another (stacked); the excess heat was measured for the cells in the upper stack.

Tests were carried out with air velocities up to about 5 m/sec. The data obtained were processed in the form of the graphical relationship between the heat emission coefficient a and the air velocity between plates ω. Tests were made for stack excess temperatures of close to 30°C and at surrounding air temperatures of about 20°C.

The test-results show that the coefficient of heat emission for identical cooling-air velocities depends to a great extent on the gap between cells (Fig. 4a), the height of the cell (comparing the mean curve in Fig. 4a and the upper curve in Fig. 4b) and on the number of stacks set one above the other (Fig. 4b).

The conclusion can be drawn, from analysis of the experimental data obtained, that the heat emission data obtained for stacks of cells 300 mm high can also be applied to stacks of cells of different heights if a correction is made for the excess heating of the cooling air corresponding to the difference between the cell heights. Let us examine the thermal balance of a rectifier cooling-channel under set conditions.

The thermal energy liberated into the channel from the walls of the cells (per unit of cell width), $Q = 2qH$;
the same energy is carried away with the cooling air

$$Q = b\omega\gamma c_p \tau_v,$$

whence

$$\tau_v = \frac{2qH}{b\omega\gamma c_p},$$

where q is the specific loss in the cells (W/dm^2), H is the height of the cell (mm), τ_v is the mean excess temperature of the air in the cooling channel at height H (°C), b is the width of the cooling channel (mm), ω is the velocity of the cooling air (m/sec), γ is the specific gravity of the air (kg/mm^3), and c_p is the thermal capacity of the air in kcal/kg/°C.

Substituting the values $\gamma = 1.164$ and $c_p = 0.242$, and taking 1 kcal/sec as being equal to 4184 W, we get:

$$\tau_v = \frac{0{,}17qH}{b\omega} \text{ (° C)}. \tag{3}$$

If a_n, the coefficient of heat emission of the cells, is known by experiment (for example from Fig. 4b) for a given stack of cells of height H_n for any conditions, and

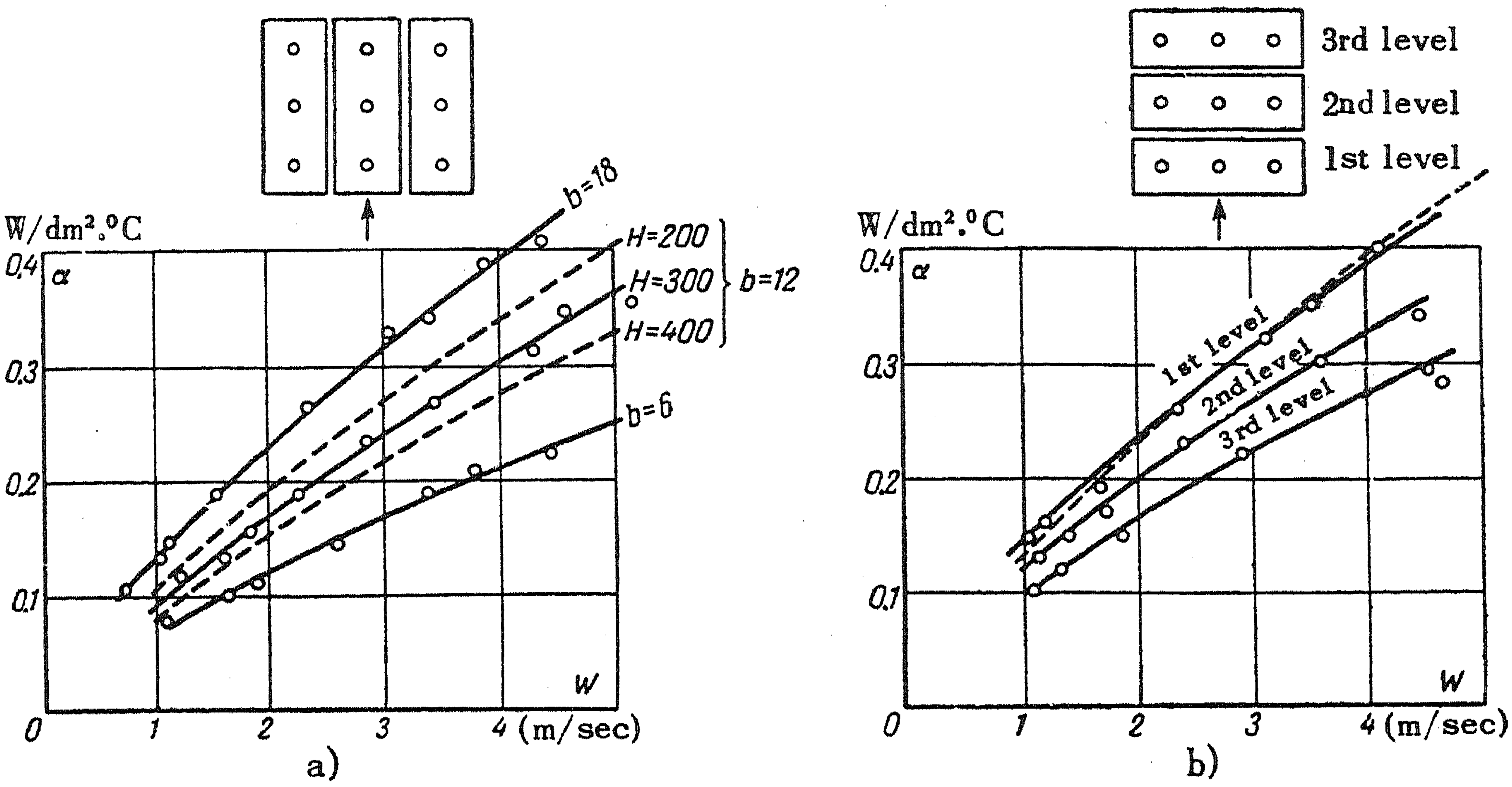

FIG. 4. Heat emission of forced-draught air-cooled selenium stacks of 100 × 300 mm rectangular cells. (a) "vertical" stacks with 6, 12 and 18 mm gaps *b* between cells (the dotted curves are calculated heat emission curves for stacks of heights $H = 200$ and 400 mm with a 12 mm gap *b* between cells); (b) "horizontal" stacks with 12 mm gaps *b* between cells; stacks arranged in 1st, 2nd and 3rd levels (the dotted curve is that for the heat emission of a stack of height $H = 100$ mm, calculated by equation (5) from data for a stack of $H = 300$ mm).

so for any given specific load q, we also know the excess temperature of the cells

$$\tau_n = \frac{q}{\alpha_n}, \qquad (4)$$

then the excess temperature of cells of height H_m can be found for the same load q from (3) and (4) as follows:

$$\tau_m = \tau_n + \tau_{v(m-n)} = \frac{q}{\alpha_n} + \frac{0,17q(H_m - H_n)}{b\omega},$$

where $\tau_{v(m-n)}$ is the excess temperature of the cooling air in the rectifier channel at a height H_m-H_n above the lower edge of the cell.

Consequently the coefficient of heat emission for cells of height H_m

$$\alpha_m = \frac{q}{\tau_m} = \frac{1}{\frac{1}{\alpha_n} + \frac{0,17(H_m - H_n)}{b\omega}}. \qquad (5)$$

Equation (5) enables us to determine the coefficients a_m for stacks of height H_m, which may be either less or more than H_n, from the coefficients of heat emission a_n obtained experimentally for stacks of height H_n.

Heat emission curves are drawn according to this equation in Fig. 4a, from data for stacks of height 300 mm, for stacks of cells 200 and 400 mm in height (the gap $b = 12$ mm, the dotted curves). To confirm the correctness of these calculations, a heat emission curve is drawn in Fig. 4b from the same data for a stack with cell height 100 mm (dotted); this curve coincides extremely well with the experimental curve (unbroken line) obtained with cells of height 100 mm.

Equation (5) does not take into account the phenomenon of thermal conductivity in the body of a cell which, generally speaking, should also be taken into consideration when determining the relationship between heat emission and height of cell. However, as specially conducted experiments showed, this factor is not of great importance. Fig. 5 shows isotherms (lines of identical excess temperature) for a selenium cell on an aluminium base of dimensions 1 × 100 × 300 mm, in a stack with 18 mm gaps, with an air velocity of 3.6 m/sec, specific load of 9.8 W/dm^2 and surrounding air temperature of 22°C; the isotherms are drawn for the excess temperatures measured at 10 points on the cell (see the measurement points on Fig. 5). The temperature gradient, with a general downward direction, is clearly visible in the illustration; however, calculations show that the levelling effect of the thermal conductivity is not great, owing to the small thickness of the cell, and may be ignored. Thus only about 2.4 per cent of the heat liberated above the line AA is transmitted downwards across the section AA, and correspondingly less than 2 per cent across the section BB.

On comparing the mean curve in Fig. 4a (single level arrangement, gap 12 mm, height 300 mm) with the lower curve in Fig. 4b (the same gap of 12 mm but three-level arrangement, and total height also 300 mm), it can be concluded that, other things being equal, for a multi-step arrangement the coefficient of heat emission is somewhat reduced (by roughly 10 per cent in the given specific case). To some extent the reason for this is the difference noted above in the heat conductivity conditions in the body of a cell; in addition very probably there are other factors which I have not examined connected with the conditions under which the air flows in the channels between cells (stagnant zones, etc).

On analysing the particular experimental relationships, given in Fig. 4, between the coefficient of heat emission and parameters such as cell height, width of gap between cells and number of levels, it is easy to satisfy oneself that for a given air velocity these relationships are of an almost linear nature and therefore lend themselves well to interpolation for other close values of the parameters. The data obtained can thus be used in the thermal calculations for rectifiers of the most varied designs, also in the comparative analysis of different types of rectifier for different specific cases.

Let me give an example to illustrate the use of the heat emission data obtained for forced draught cooling. The cost and dimensions of very powerful selenium rectifiers are the most important characteristics of their design.

We can assume as a first approximation that the cost of a rectifier is directly proportional to the area S of the selenium cells; this can easily be expressed through Q, the losses in the rectifier or, if we introduce η the efficiency of the rectifier, through the rectifier output power P (*et*):

$$S = \frac{Q}{\alpha\tau} = \frac{P\left(\frac{1}{\eta} - 1\right)}{\alpha\tau}. \qquad (6)$$

It follows from this that for a given rectifier output P the area of the cells, and also the cost of the rectifier, are in inverse proportion to α, the coefficient of heat emission (since r, the excess temperature of the cells, and η are given by the technical data for the selenium cells).

Turning to the rectifier dimensions, it can be affirmed that, besides the height, the plan area of the rectifier is of particular interest, for with forced draught cooling this area determines the fan output, and to a great extent its dimensions and power.*

Fig. 6 gives a network of intersecting curves drawn from the data in Fig. 4a and compiled using equation (5), showing how the height of the cells H and the gap between cells b affects alterations in α, the coefficient of heat emission for the cells, and A, the "field" coefficient of heat emission; A is expressed by:

$$A = \frac{\alpha 2H}{b+\delta},$$

where δ is the thickness of a cell, usually 1mm for large cells.

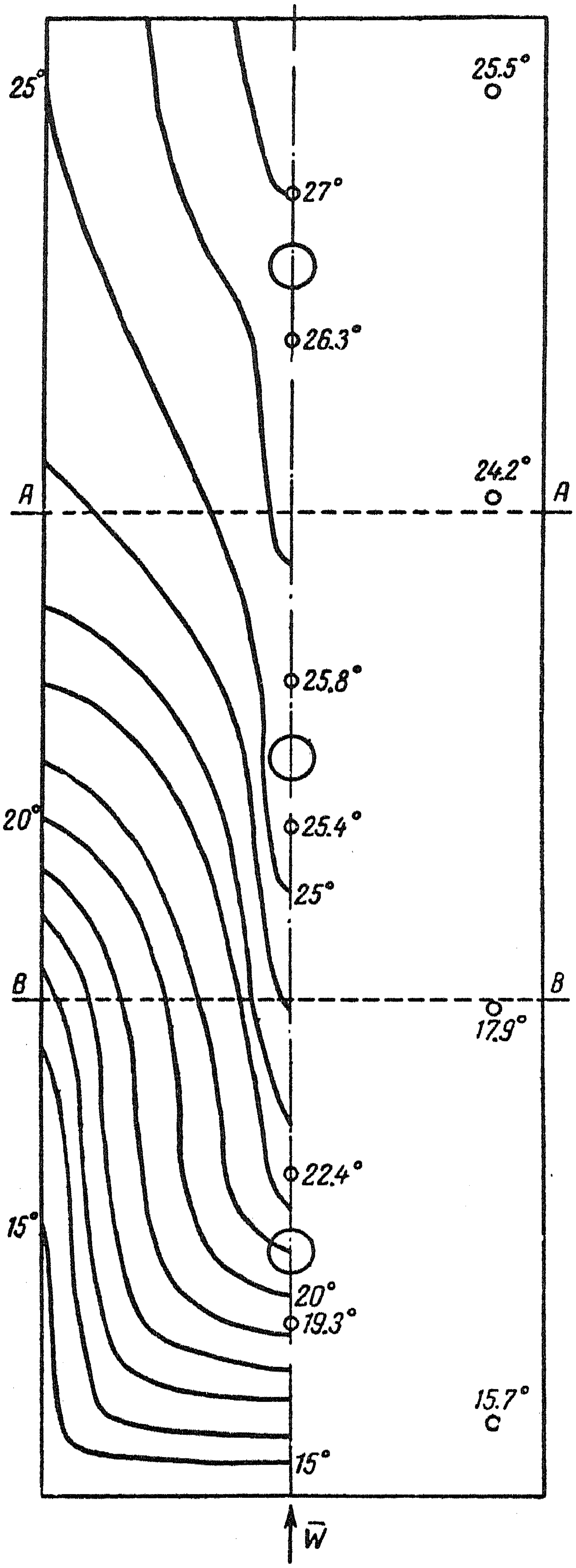

FIG. 5. Excess temperature isotherms for a selenium cell on an aluminium base, dimensions 1 × 100 × 300 mm, in a stack with 18 mm gaps, air velocity 3.6 m/sec, specific load 9.8 W/dm², surrounding air temperature 22° C.

---

* Losses due to friction are usually low in the general fan pressure balance; fan power is therefore little dependent on the height of the cells.

For specific losses, or from output power and efficiency, the coefficient A enables us easily to determine the area of the field occupied by a rectifier (its vertical projection), S_n(dm²):

$$S_n = \frac{Q}{A\tau} = \frac{P\left(\frac{1}{\eta} - 1\right)}{A\tau}. \qquad (7)$$

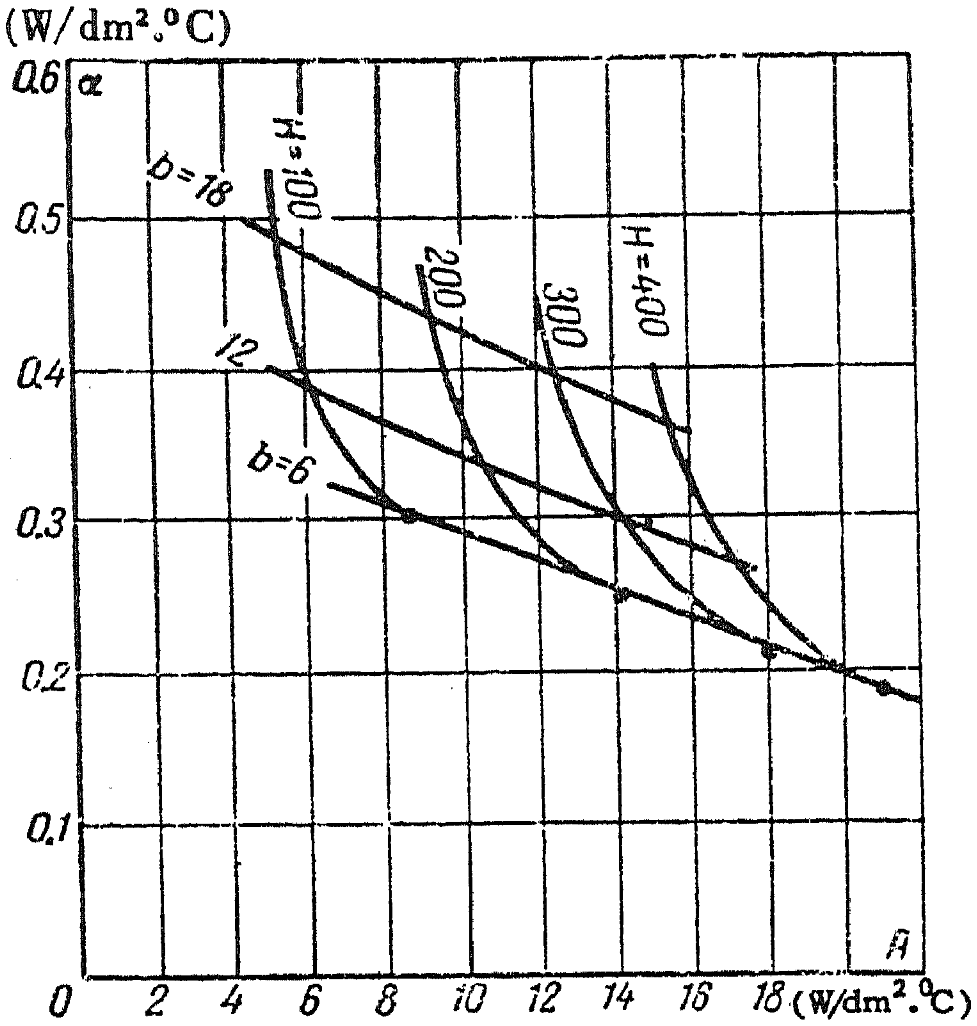

FIG. 6. Relationship of a, the coefficient of heat emission, and A, the coefficient of specific load of the rectifier vertical projection, to b, the gap between cells.

Thus the graph in Fig. 6 has ordinates a which are in inverse proportion to the area of the cells (and so to their cost); the abscissae A are in inverse proportion to the vertical projection area of the rectifier; these facts facilitate selection of the most acceptable compromise between these parameters with relation to the specific requirements in the case of calculations for different rectifiers.

It is also quite evident from Fig. 6 how important it is to use large-dimension cells when constructing powerful rectifiers; for acceptable rectifier dimensions can only be obtained by increasing the height of a rectifier (or by increasing the number of levels which is, however, worse than was shown in Fig. 4) and simultaneously increasing the gap b; this is equivalent to sufficiently increasing the specific field load (the coefficient A) without materially reducing the utilization of the elements (the coefficient a).

Translated by J.H. Dixon

REFERENCES

1. F.F. Sokolov; Iz. Opyta ekspluatatsii selenovykh vypriamitelei (Experience in the operation of selenium rectifiers), *Elektrichestvo* 3 (1953).
2. V.G. Komar; Raschet selenovykh vypriamitelei (Calculations for selenium rectifiers), *Elektrichestvo* 9, 46 (1946).
3. F.F. Sokolov; *Teplovoi raschet selenovykh vypriamitelei (Thermal calculations for selenium rectifiers)*, Moscow, NIKFI, dissertatsiia (1949).
4. V.G. Komar; *Rabota poluprovodnikovykh vypriamitelei v tsepiakh upravleniia (The operation of semi-conductor rectifiers in control circuits)*, Gosenergoizdat (1952).
5. M.A. Mikheev; *Osnovy teploperedachi (The fundaments of heat transfer)*, Gosenergoizdat, 53—78 (1947).

THE USE OF 220 kV LINES WITH SPLIT CONDUCTORS*

A.N. ZEILIGER and B.P. NOVGORODTSEV

Leningrad Teploelektroproekt Department**

(Received 4 October 1957)

This article presents the results of the technical and economic comparison of 220 kV lines with split conductors and transmission lines of the same voltage without split conductors.***

As we know, there are two purposes in splitting the conductors in 220 kV lines: (1) to increase the carrying capacity of long-distance lines when the transmitted power is limited by voltage drop or by their stability limits; (2) to reduce the number of parallel lines when the rated load of one line exceeds the economic load of the maximum gauge single conductor available.

In the first case, a single large section conductor is replaced by two or more conductors of smaller section with the same total conductor section per phase. In the second case, the single conductor is replaced by two or more conductors whose total cross-section per phase exceeds the maximum cross-section of the single conductor. In the first case the reactance of the line can be reduced at the expense of making its mechanical part somewhat more costly; carrying capacity is thereby raised. In the second case the reactance of the single line with split conductors and the reactance losses in it are considerably higher than in lines consisting of the corresponding number of parallel lines containing single conductors of the same total cross-section.

However, the splitting of conductors is not the only method of ensuring the required electrical transmission properties. Increase in the carrying capacity and reduction in the reactance losses in long-distance lines may also be obtained by the use of compensating installations; reduction in the number of parallel lines may be achieved by the use of double-circuit lines. In view of this, the question of the expediency of using split conductors for 220 kV electric power transmission

---

* *Elektrichestvo* No. 2, 9-12, 1958 [Reprint Order No. EL 48].

** *"Teploelektroproekt":* "Electric Power and Heat Generating Project".

*** The article has been compiled from the results of work done by the authors with K.P. Kriukov and S.N. Ruzanov at the Leningrad Teploelektroproekt Department.

lines in different cases must be solved on the basis of the technical and economic comparison of different transmission line design variants. In this comparison, the following must be taken into account as well as the cost of the mechanical part of the line: the cost of the compensating installations installed on the power line itself, or in the power transmission system, to compensate the additional reactance and reactance losses, where a line of high reactance is used.

Analysis of the problem of the expediency of splitting conductors has been made for three groups of 220 kV electric power transmission lines. The first group comprises lines whose total conductor single phase cross-section is (for aluminium) 480 mm^2. The economic load corresponding to this cross-section is about 200 MVA at an economic current density of 1 amp/mm^2. Single circuit lines with single ASO-480 conductors and split 2 × ASO-240 conductors belong to this group. The second group comprises lines of a total conductor cross-section of 960 mm^2 (economic load about 400 MVA). Single circuit lines with 2 × ASO-480 split conductors and double circuit lines with single ASO-480 conductors belong to this group. The third group comprises lines of a total conductor cross-section of 1920 mm^2 (economic load about 800 MVA). Double circuit lines with 2 × ASO-480 split conductors belong to this group.

Calculations for the supports and foundations for all these lines have been made for climatic regions I and II. The rated wind velocity was taken as 25 m/sec. The wind velocity in the zone 30-50 m above the earth was taken as 110 per cent of the velocity in the first zone. The supports were made of type St-3 steel and low-alloy type NL-2 steel. The latter was used in every case where it resulted in reduction of the weight of the support. The stresses permitted for the type St-3 steel were, according to the *Rules for the Construction of Electrical Engineering Installations*, with the emergency stress permitted for intermediate supports, reduced to 2000 kg/cm^2.

The permitted tension, compression and bending stresses in NL-2 steel components were taken as being: for normal conditions, 2250 kg/cm^2, and for emergency conditions 2600 kg/cm^2 (anchorage supports), and 2800 kg/cm^2 (intermediate supports).

The normal condition support plans were made in accordance with the *Rules for the Construction of Electrical Engineering Installations*. The conductor breaking stress at intermediate supports was reduced for lines without split conductors to 0.75, and for lines with split conductors to 0.6 times the reduced breaking stress for the full phase. This reduction was taken into account in making the calculations for all the types of support, except the "barrel" type twin-circuit support which was supplied until the relative MES Technical Directorate instruction came into force. Twin-circuit "barrel" type supports were designed for the total reduced conductor breaking stress.

In cases where breaking conductors may fall on to part of the support structure, it was specified that supports with releasing terminals were to be reinforced by clamping terminals.

When comparing lines with releasing and clamping terminals, it was taken into consideration that the distances between the anchorage supports of the former must not exceed 10 km; the distance between anchorage supports in the second case is unlimited; ie., supports of the anchorage type are only used for important crossings.

When designing the foundations, a pressure of 2 kg/cm^2 on the ground, ground weight of 1.6 tons/m^3 (when calculating for excavation) and 1. 8 tons/m^3 (when calculating for compression) were allowed. It was assumed that the ground water-level was below the base of the foundation and that the angle of slope of the ground was less than 35°. Concrete type 200 was used for built-up foundations.

The most economic variants for the construction of the different types of lines (single circuit or double circuit with single or split conductors) were taken for comparison.

The development work by Teploelektroproekt showed that the most suitable metal supports for double-circuit 220 kV lines are supports of the "barrel" type with clamping terminals, made of low-alloy steel. According to the working drawings, the weight of an intermediate support with clamping terminals is only 375 kg, or 5 per cent, greater than that of an intermediate support with releasing terminals. This is explained by the fact that normal conditions are assured when calculating for the support body cords, and therefore, the assortment of body cords is identical in both cases. For the lattice-work of the body, conductor breaking conditions in clamping terminals on the upper cross-arm are taken for calculations in the case of releasing terminals, and conductor breaking conditions in clamping terminals on the middle cross-bar in the case of clamping terminals. Since the number of anchorage supports is lower on lines with clamping terminals than on lines with releasing terminals, practically identical weights of metal are used per kilometre of line in both cases. The greater reliability of lines with clamping terminals during operation forces us to give preference to this type of line.

Till recently "wine-glass" or "hinged portal" type supports were used for single circuit 220 kV lines. However, the work by Teploelektroproekt on developing new types of support, designed for the suspension of type ASO-480 zero conductors in climatic regions I and II, have proved that the Crimea type support is the most economical. The use of low-alloy steel for these supports considerably reduces the amount of metal used, while the use of this steel for 220 kV portal-type supports provides practically no economy.

The weights of intermediate supports for the three types compared and the amounts of metal and concrete used per km of line are given in Table 1.

The foundation reinforcement is included in the amount of metal used per kilometre of line. The amounts of metal and concrete used are taken for the most economical variants of the lines (those on "hinged portal" and "wine-glass" type supports with releasing terminals, and those on Crimean type supports with clamping terminals).

TABLE 1

Type of support	Calculated span	Weight of support (kg)		Material used per km of line	
		with releasing terminals	with clamping terminals	metal (tons)	concrete (m^3)
"Hinged portal"	400	4300	5800	17.3	17.8
"Wineglass"	450	4900	6200	16.9	8.5
Crimean	450	4500	4800	13.6	8.0

It was also established, when developing supports for single circuit lines with split conductors, that Crimean type supports are the most economical. We used 16.7 tons of metal and 10.6 m^3 of concrete per kilometre of line on Crimean type supports, 21.7 tons and 15.5 m^3 respectively per kilometre of line on "hinged portal" type supports, and 22.4 tons and 15.0 m^3 respectively per kilometre of line on "wineglass" type supports, using A-P type anchorage and corner supports.

We will now therefore compare single circuit lines on Crimean type supports and double circuit lines on "barrel" type supports. It is conditionally assumed that all the lines being compared have the following: intermediate supports with clamping terminals, 90 per cent; intermediate corner supports (2-20°), 5 per cent; and corner supports (20-60°), 5 per cent. K, the coefficient of utilization, is taken as being 0.9 for all the lines being compared.

Fig. 1 provides a schematic representation of the supports of the lines being compared. Table 2 gives the technical and economic figures. The costs per kilometre of line are given in comparative figures.

It is evident from comparison of lines in the first group that a single circuit line with single type ASO-480 conductors (line (*a*)) is cheaper than a single circuit line with split conductors of type 2 × AS-240 (line (*b*)). This is explained by the fact that the wind pressure on the line and the sag of the conductors in line (b) is higher than in line (a), leading to reduction in the economic span and an increase in the metal and concrete used per kilometre in line (b), and therefore to an increase in the cost of this line per kilometre.

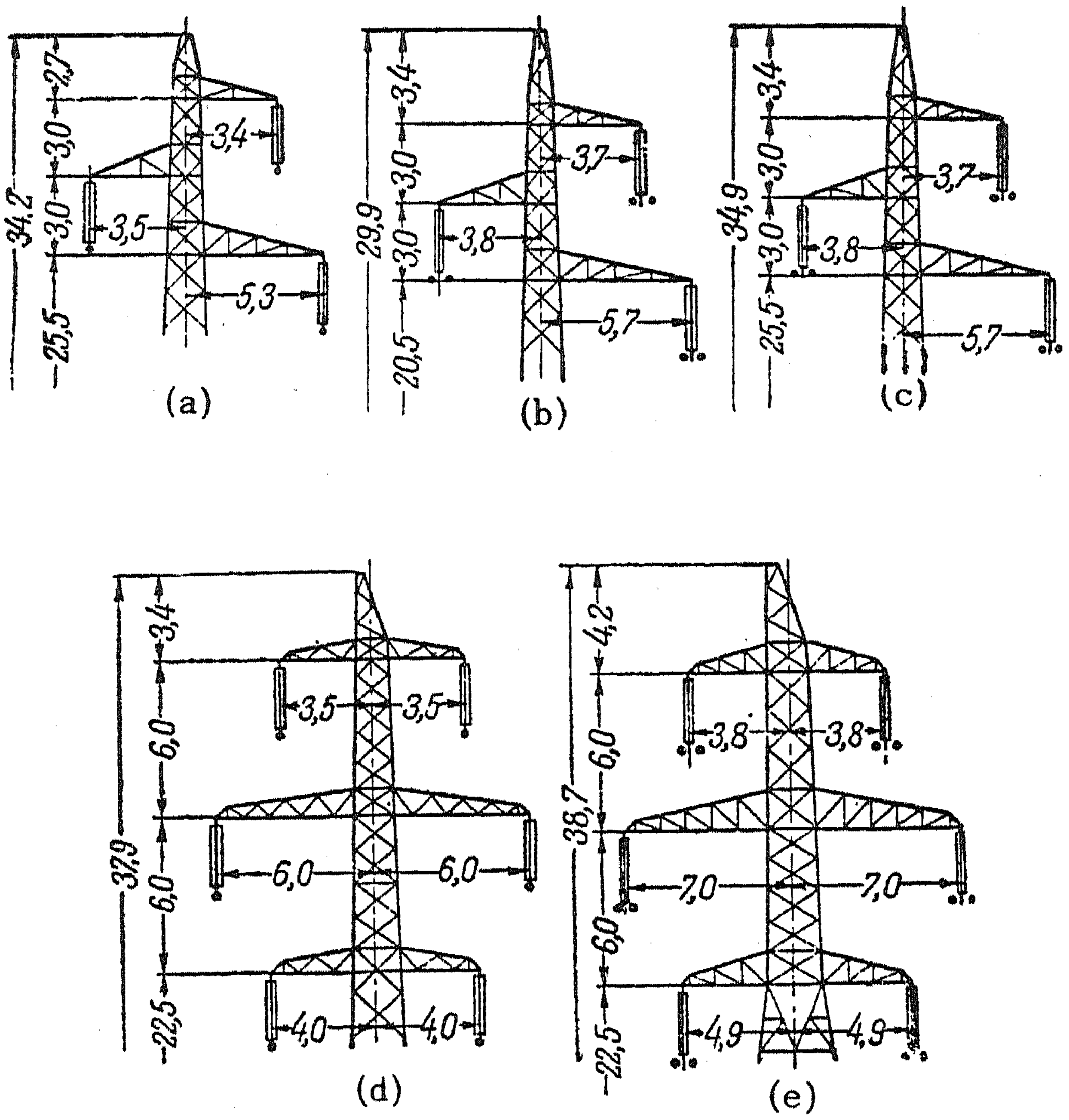

FIG. 1. Schematic representation of the supports of the lines being compared.

TABLE 2

Line lettering (see Fig. 1.)	Conductor types	Supports	Calculated span (m)	Expenditure per km of line		Cost of 1 km of line (1000 roubles).
				Metal (tons)	Concrete (m^3)	
Line (a)	ASO-480	Crimean type	450	13.6	8.0	154.8
Line (b)	2 × AS-240	Crimean type	340	15.6	10.4	172.8
Line (c)	2 × ASO-480	Crimean type	450	16.7	10.6	246.3
Line (d)	ASO-480	"Barrel" type (narrow body)	400	21.2	12.4	262.7
Line (e)	2 × ASO-480	"Barrel" type (wide body)	400	27.6	15.3	383.3

It should be noted that comparisons between single circuit lines with single and split conductors made abroad have produced the same results. For example, it was established in Sweden that a single circuit 220 kV line with split conductors is 18 per cent more costly than a single circuit line with single conductors.

The total wind pressures on the conductors of single circuit lines with 2×ASO-480 split conductors (line (c)) and on those of double circuit lines with single ASO-480 conductors are identical, since in both cases six conductors of the same type are suspended from the supports. However, the double circuit support is heavier than the single circuit support, owing to its greater height and greater number of cross-arms. The amount of metal used for 1 km of double circuit line is therefore greater than that for 1 km of single circuit line. More concrete is used for double circuit lines, also because of the greater height from which the conductors are suspended and their consequently greater moment. Thus, the double circuit line with single conductors is more costly than the single circuit line with split conductors.

It was stated above that the double circuit supports examined were calculated for total reduced conductor breaking stress, and Crimean type supports for 0.75 times the reduced stress. When converting to the new calculation conditions, the weight of the "barrel" type intermediate supports is reduced, and in consequence the difference between the costs of the lines being compared becomes less.

It should be noted that single circuit lines with split conductors are only cheaper than double circuit lines with single conductors in cases where Crimean type supports with a triangular arrangement of conductors are used. Single circuit lines with split conductors on portal-type supports, with the conductors horizontally arranged, are more costly than double circuit lines on "barrel" type supports.

Of the lines in the third group, with a total cross-section of the conductors of 1920 mm^2 per phase, we can compare a single double-circuit line with split conductors on wide-bodied "barrel" type supports (line (e)), with two single circuit lines with split conductors or two double circuit lines with single conductors. The amount of metal used for one double circuit line with split conductors is 17 per cent less than the amount used for two single circuit lines, and 35 per cent less than that used for two double circuit lines; the amounts of concrete used are respectively 27 and 38 per cent less, and the costs 22 and 26 per cent less.

In order to make a full technical and economic comparison of the various 220 kV lines, taking into account the expenditure on compensating installations, a number of factors for 220 kV lines with single and split conductors are given in Table 3. The line reactance losses were determined, starting from the utilization factor, in accordance with the economic current density at an average voltage level of 230 kV.

It is evident from Table 3 that, for identical rated loads, the reactance losses are different for the lines being compared.

The vast majority of present-day electric power systems have no excess reactive power, and each increase in the line reactance losses makes it desirable as a rule to install additional compensating devices of corresponding capacity. Table 3 provides the capacity of the additional compensating devices which must be installed, to ensure identical reactive power equalization, on the electric power lines under comparison. The additional compensating installations are as a rule installed in the power system receiving-end circuits in the form of synchronous or static compensators.

In cases where the reactance of a line must be compensated in order to raise its carrying capacity, part of the capacity of the compensating devices may be arranged in the form of longitudinal compensation. The use of any system of compensation has no effect on the results of the technical and economic comparison, since the total of the compensating device capacities and their specific costs are not materially affected in either case.

Comparison of the economic figures for the lines, taking the expenditure on additional compensating devices into account, is made in Table 4.

Comparison of the lines in Group I shows that, even when the cost of the compensating devices is taken into account, the total cost of electric power transmission by single conductors is lower than that for split conductors.

Comparison of the lines in Group II shows that the costs of the additional devices for compensating the increased reactance losses of lines with split conductors cover the difference in the cost of the mechanical part of the lines; in this connexion, single circuit lines with split conductors of large section are less economic than double circuit lines with single conductors of the same section. In addition, double circuit lines with single conductors are more reliable and convenient to operate than single circuit lines with split conductors. Therefore it may prove expedient to use single circuit lines with split conductors only in particular isolated cases, for example, with the simultaneous installation of two parallel lines in power systems with no excess reactive power.

Comparison of the lines in Group III shows that the use of double circuit lines with split conductors is economically very effective, since it enables us to reduce the number of parallel lines. The use of double circuit lines with split conductors can be recommended in every case where the transmission of such high power on a single double-circuit line is permissible from the point of view of power supply reliability.

CONCLUSIONS

1. Phase-splitting, on 220 kV lines, into two or more conductors of smaller

TABLE 3

Name of factor	Group I		Group II		Group III	
	Single circuit line, ASO-480 conductor	Single circuit line, 2 x AS-240 conductors	Single circuit line, 2 x ASO-480 conductors	Double circuit line, ASO-480 conductor	Two double circuit lines, ASO-480 conductors	Double circuit line, 2 x ASO-480 conductors
Economic loading (MVA)	200	200	400	400	800	800
Resistance (Ω/km)	0.064	0.064	0.032	0.032	0.016	0.016
Inductive reactance (Ω/km)	0.4	0.314	0.304	0.2	0.1	0.152
Capacitive susceptance, (1/Ω/km)	2.75×10^{-6}	3.6×10^{-6}	3.7×10^{-6}	5.5×10^{-6}	11×10^{-6}	7.4×10^{-6}
Inductive losses at economic load (kVAR)	302	237	920	605	1210	1840
Capacitive power, for $V_{av} = 230$ kV (kVAR)	-145	-190	-196	-291	-582	-392
Total reactance losses (kVAR)	157	47	724	314	628	1448
The capacity of the additional compensating installations necessary to equalize the reactive capacity of lines in each group (kVAR)	-110	-	-410	-	-	-820

TABLE 4

	Group I		Group II		Group III	
Name of factor	Single circuit line, ASO-480 conductor	Single circuit line, 2 × AS-240 conductors	Single circuit line, 2 × ASO-480 conductors	Double circuit line, ASO-480 conductor	Two double circuit lines, ASO-480 conductors	Double circuit line, 2 × ASO-480 conductors
Cost of line (1000 roubles /km)	154.8	172.8	246.3	262.7	525.4	383.3
Cost of installing additional compensating devices (costing 75 roubles/kVAR) 1000 roubles/km	8.2	-	30.8	-	-	61.6
Total costs (10 roubles/km)	163.0	172.8	277.1	262.7	525.4	444.9

COLLEGE OF ENGINEERING LIBRARY BOOK No. GUINDY

section, for the purpose of reducing the reactance of lines, is not economically justifiable, since a similar effect may be achieved at lower cost by the use of compensating devices.

2. The splitting of each phase of a single circuit 220 kV line into two conductors of greater section, in order to raise the total conductor cross-section, results in most cases in an increase in the total capital outlay, including the cost of compensating appliances, in comparison with double-circuit 220 kV lines. In view of this, the use of single circuit 220 kV lines with split conductors of larger cross-section is not as a rule expedient.

3. The use of double-circuit 220 kV lines with split conductors of large cross-section is economically justifiable, since the capital expenditure for erecting such lines is considerably lower than that for the erection of two parallel double-circuit lines with single conductors.

Translated by J.H. Dixon

COLLEGE OF ENGINEERING
LIBRARY BOOK
No.
GUINDY

CALCULATIONS OF SHORT-CIRCUITS IN UNBALANCED PHASE TRANSMISSION SYSTEMS*

G.G. KOSTANIAN

Tbilisi Scientific Research Institute of Building and Hydroelectrics

(Received 22 June 1957)

As a result of researches carried out in recent years, calculations of complicated asymmetric faults in electrical systems have been materially simplified. Thanks to this research, it is now possible to study combinations of any asymmetric faults at two points in a system, and in particular combinations of short circuits in systems with unbalanced phase transmission [1, 2]. However, calculations of such faults, particularly in complex systems with ring connexions, are none the less laborious and can be materially simplified if treated as an extension of calculations dealing with a fault at one point of the system.

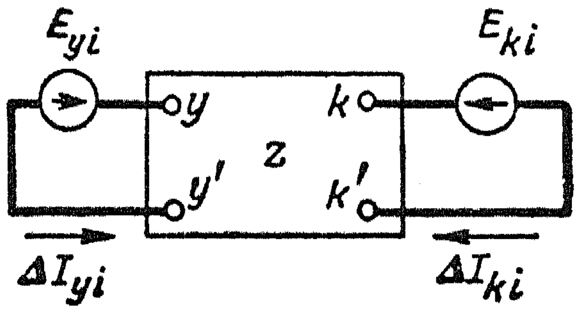

FIG. 1. Circuit for any sequence at a phase break.

Actually, all the changes introduced by the second fault in each sequence of the circuit can be represented, as shown in Fig. 1, by two e.m.f.'s only: E_{ki}, the e.m.f. at the point of the first fault, and E_{yi}, the e.m.f. at the point of the second fault. The resulting components of current and voltage in the sequences of the circuit can be found by superimposing the components calculated for a fault at one point of the circuit on to the components determined from the circuit of Fig. 1. This approach to calculations of asymmetric faults at two points in a circuit makes it possible to use the methods and results already obtained in calculations for faults at one point of a circuit; the changes introduced by the second fault are taken into account in these circuits by the e.m.f.'s E_{ki} and E_{yi}.

The basic ideas of the proposed method are described below, as applied to the calculation of various combinations of short-circuits in unbalanced phase transmission systems. One of the special types of fault at two points in the system is considered, namely various combinations of short-circuit at one point in the system with a break on one phase at another point.

From now on, values referring to the short-circuit branch will be denoted by the

---

* *Elektrichestvo* No. 2, 13 – 18, 1958 [Reprint Order No. EL 49].

subscript k, those referring to the break branch by y; to the corresponding phases, by A and B respectively; to the corresponding sequences, by 1, 2 and 0; and to any sequence, by i. The superscript (3) denotes that the value in question refers to the case of a three-phase short-circuit; (1.1) to the case of a short to earth on two phases; (1) to the case of a short to earth on one phase.

The problem of calculating the components of the two e.m.f.'s referred to above is considerably simplified by the method proposed in this paper of transferring all the e.m.f.'s operating in the system to the one branch being studied.

Consider the relationship between the e.m.f.'s E_y and the current in the branches of the passive quadripole shown in Fig. 2.

In the presence of a single e.m.f. in the branch y - y', the current in the branch k - k' is

$$I_k = \frac{\alpha E_y}{z_y} = \frac{\beta E_y}{z_k} = pE_y\,, \tag{1}$$

where $1/z_y = g_y$; $1/z_k = g_k$, the intrinsic conductivities in branches y-y' and k-k' respectively; $\rho = g_{yk} = g_{ky}$, the mutual conductivity between the branches y-y' and k-k'; $\alpha = g_{ky}/g_y$; $\beta = g_{yk}/g_k$ are coefficients.

The coefficients α, β and ρ are values which are reciprocals of the known coefficients of quadripoles. They depend only on the parameters of the quadripole, and are related as follows :-

$$\beta = \frac{z_k}{z_y} . \alpha = \rho z_k \,. \tag{2}$$

The coefficient β shows what fraction of the total e.m.f. in the branch y-y' is equal to the e.m.f. in branch k-k', and what fraction of the current in branch k-k' is equal to the current in branch y-y'. This assumes that the e.m.f. occurs only in branch y-y' and the current source only in the branch k-k'. The coefficient α, on the other hand, shows what fraction of the e.m.f. in branch k-k' is equal to the e.m.f. in branch y-y' and what fraction of the current in branch y-y' is equal to the current in branch k-k'.

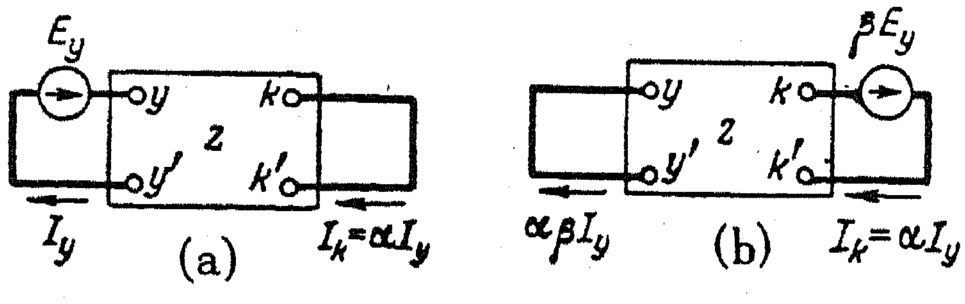

FIG. 2. Relationships between currents and e.m.f.'s in a passive quadripole, on transferring them from one branch to another.

The transfer of e.m.f. E_y from branch y-y' to branch k-k', as shown in Fig. 2, does not change the current in branch k-k'.

As applied to an active quadripole, expression (1) determines the component of current due to e.m.f. E_y, whilst the full current in branch k-k' of such a quadripole is found by superimposing the currents due to all the e.m.f.'s (at an e.m.f. $E_y = 0$) on to the current due to e.m.f. E_y. In this case, expression (2) and the assumption that when e.m.f. E_y is transferred to branch k-k' the current in the latter is unchanged, are valid not only for the passive quadripole shown in Fig. 1 but also for an active quadripole with other e.m.f.'s in its branches in addition to E_y.

Extending this to active networks, it can be shown to be valid to account for the effect of an e.m.f. in branch n-n' on the current in any other branch p-p' by taking E_n from branch n-n' and transferring the fraction which is numerically equal to $g_{np}/g_p\ E_n$ over to branch p-p', where g_{np} is the mutual conductivity between branches n-n' and p-p' and g_p is the intrinsic conductivity of branch p-p'.

The coefficients β, ρ and α between the branches containing two faults in the circuits of two separate sequences can be measured on a calculating machine, e.g. by methods known from the theory of quadripoles, or found from the results of previous short-circuit calculations. Below is given only the latter method of determining them, as applied to the calculations of a short-circuit with a phase break.

The circuits and expressions from which to start out in the determination of coefficients β_i, ρ_i and α_i for the individual sequences are shown in Table 1.

The data required for determining the coefficients are taken from the results of a calculation of any type of asymmetric short circuit in branch k-k', in the absence of a fault in branch y-y'.

The coefficients β_i and ρ_i are the most interesting, since they enter into the expressions determining E_{yi} and E_{ki}, whereas the coefficient α_i does not figure in these expressions.

Coefficient α_i has only subordinate value and serves to simplify the calculation of the circuit conductivities of the sequences at the point of phase rupture, which is of most importance in calculating complex circuits with ring connexions.

For example, the sum of the circuit conductivities of all the sequences can be determined using this coefficient as follows :-

$$g_{y\Sigma} = \frac{1}{z_{y1}} + \frac{1}{z_{y2}} + \frac{1}{z_{y0}} = \frac{\rho_1}{\alpha_1} + \frac{\rho_2}{\alpha_2} + \frac{\rho_0}{\alpha_0}\,. \tag{3}$$

The sums of coefficients β_i and α_i, given in Table 1, merit particular attention; to determine them we need the total currents in the phases when one phase is short-circuited and the total e.m.f.'s in the phase when two phases are shorted to earth. These sums define the connexion between the components of current and e.m.f. in the calculations which are to be made.

The equations relating currents and e.m.f.'s, given in the circuit of Fig. 1, can be put in the following form :-

$$\Delta I_{yi} = I^*_{yi} - I_{yi} = \rho_i \Delta E_{ki} - \frac{E_{yi}}{z_{yi}}\,; \tag{4}$$

$$\Delta I_{ki} = I^*_{ki} - I_{ki} = \rho_i E_{yi} - \frac{\Delta E_{ki}}{z_{ki}}\,, \tag{5}$$

where I^*_{yi} and I^*_{ki} are the current components in branches y-y' and k-k' after phase

TABLE 1.

Initial Circuits	Expressions for coefficients in the circuits			Expressions for finding the sums of coefficients
	Direct sequence	reverse sequence	zero sequence	
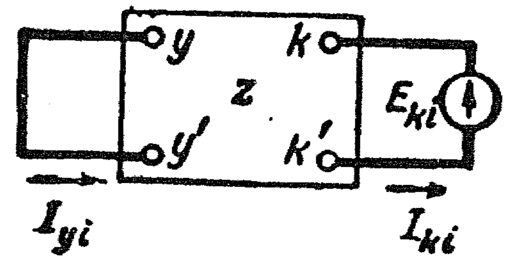 Circuit *A* Any asymmetric short-circuit between *k - k'* in the condition prior to phase rupture in section *y - y'*	$\beta_1 = \frac{I_{y1} - I_y^{(3)}}{I_{k1} - I_k^{(3)}}$	$\beta_2 = \frac{I_{y2}}{I_{k2}}$	$\beta_0 = \frac{I_{y0}}{I_{k0}}$	$\beta_1 + \beta_2 + \beta_0 = \frac{3\left(I_{yA}^{(1)} + \beta_1 I_k^{(3)} - I_y^{(3)}\right)}{I_{kA}^{(1)}}$ $a^2\beta_1 + a\beta_2 + \beta_0 = \frac{3\left(I_{yB}^{(1)} - a^2\beta_1 I_k^{(3)} - a^2 I_y^{(3)}\right)}{I_{kA}^{(1)}}$
	$\rho_1 = \frac{I_{y1} - I_y^{(3)}}{E_{k1}}$	$\rho_2 = \frac{I_{y2}}{E_{k2}}$	$\rho_0 = \frac{I_{y0}}{E_{k0}}$	$\rho_1 + \rho_2 + \rho_0 = \frac{3\left(I_{yA}^{(1.1)} - I_y^{(3)}\right)}{E_{kA}^{(1.1)}}$ $a^2\rho_1 + a\rho_2 + \rho_0 = \frac{3\left(I_{yB}^{(1.1)} - a^2 I_y^{(3)}\right)}{E_{kA}^{(1.1)}}$
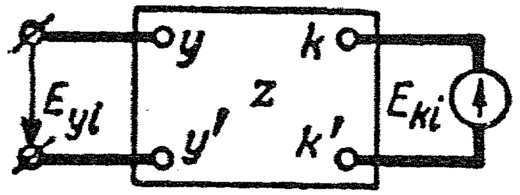 Circuit *B* Any asymmetric short-circuit between *k - k'* with three-phase cut-off section *y - y'*.	$\alpha_1 = \frac{E_{y1}}{E_{k1}}$	$\alpha_2 = \frac{E_{y2}}{E_{k2}}$	$\alpha_0 = \frac{E_{y0}}{E_{k0}}$	$\alpha_1 + \alpha_2 + \alpha_0 = \frac{3E_{yA}^{(1.1)}}{E_{kA}^{(1.1)}}$ $a^2\alpha_1 + a\alpha_2 + \alpha_0 = \frac{3E_{yB}^{(1.1)}}{E_{kA}^{(1.1)}}$

Note: 1. In the circuits, only e.m.f. currents and frequencies at the point of short-circuit are noted. E.m.f. currents and frequencies of the generators are excluded from the direct sequence circuits.

2. Phase *A* is taken as the main phase in the indices.

rupture in the sequence circuits; I_{yi}, I_{ki} are the corresponding values before phase rupture; z_{yi}, z_{ki} are the intrinsic resistances of the branches y-y' and k-k' in the sequence circuits.

Equations (4) and (5) are valid for each sequence and are not limited by the conditions of short-circuit in branch k-k' or of phase break in branch y-y'.

As applied to the faults under consideration, E_{yi} can signify the component of e.m.f. at the phase break point and ΔE_{ki}, ΔI_{ki} and ΔI_{yi} the changes in the components of e.m.f. and current produced by the phase break. The relationships between these values (boundary conditions) are given in Table 2. They are analogous to the known boundary conditions characterizing the relationships between the currents and voltages in separate sequences with asymmetric short circuits and phase breaks. As regards ΔI_{ki} and ΔE_{ki}, they are determined only by the type of fault in branch k-k'; ΔI_{yi} and ΔE_{yi} are determined both by the type of fault in branch y-y' and by the conditions under which the fault arises.

Equations (4) and (5) can be limited by the special conditions of various combinations of short-circuits and phase ruptures; for each combination it is necessary to solve twelve equations, six of which are given by equations (4) and (5), the other six by the special limiting conditions for the short circuit or phase break, as shown in Table 2. The simplest solution to this problem is obtained by using the known complex substitution circuits in place of the short-circuit and in place of the phase break, transferring all the effective e.m.f.'s caused by the phase break, first into the short-circuit branch and then into the phase break branch.

Fig. 3a shows the complex substitution circuit in place of a short to earth on phases B and C. Figs. 3b, 4b show the same circuits after subtracting the currents and e.m.f.'s acting before the break, and transferring the e.m.f. E_{yi} to the circuit branch. These circuits determine the current and e.m.f. at the point of short-circuit, due to the phase break.

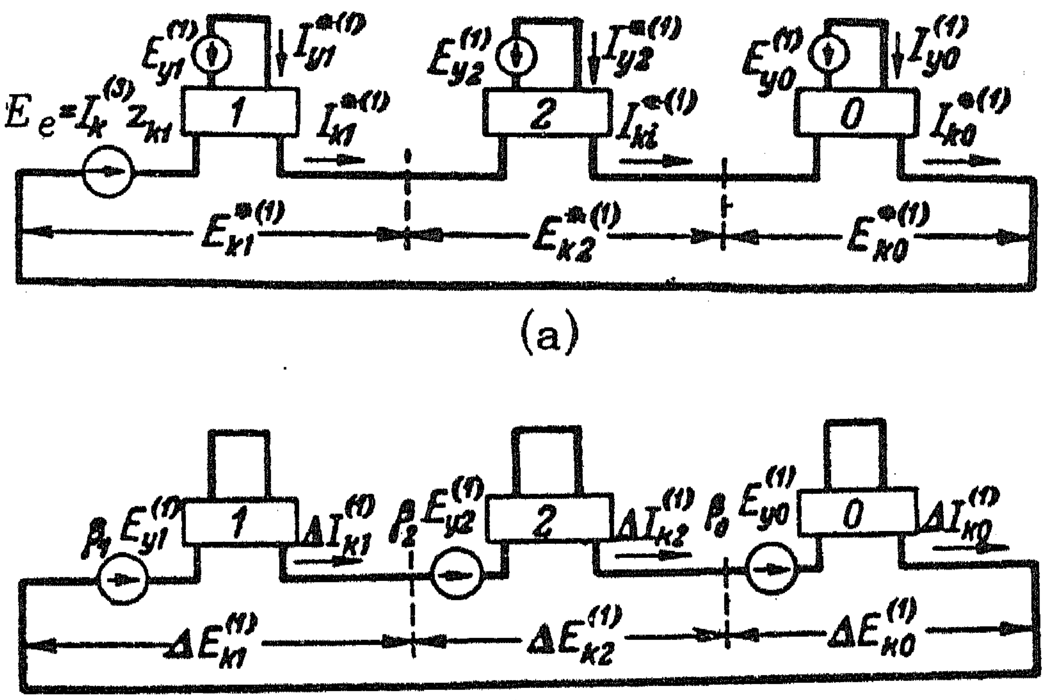

(a)

(b)

FIG. 3.

In finding the current in the circuit of Fig. 3b and the voltage in that of Fig. 4b it can be shown that:

$$\Delta I_{k1}^{(1)} = \Delta I_{k2}^{(1)} = \Delta I_{k0}^{(1)} = \tag{6}$$

$$= \frac{B_1 E_{y1} + \beta_2 E_{y2} + \beta_0 E_{y0}}{z_{k1} + z_{k2} + z_{k0}} = nE_{y0};$$

$$\Delta E_{k1}^{(1.1)} = \Delta E_{k2}^{(1.1)}, = \Delta E_{k0}^{(1.1)} = \frac{\rho_1 E_{y1} + \rho_2 E_{y2} + \rho_0 E_{y0}}{\frac{1}{z_{k1}} + \frac{1}{z_{k2}} + \frac{1}{z_{k0}}} = mE_{y0}, \tag{7}$$

where n and m are coefficients which are determined, for a break on any phase, by

TABLE 2.

In short-circuit branch (branch k-k' in Fig. 1).		In phase rupture branch (branch y-y' in Fig. 1).	
Type of fault	Boundary conditions	Phase broken	Boundary conditions
Three-phase to earth	$\Delta E_{k1}=\Delta E_{k2}=\Delta E_{k0}=0$	A	$I_{yA}+\Delta I_{y1}+\Delta I_{y2}+\Delta I_{y0}=0$ $E_{y1}=E_{y2}=E_{y0}$
Two-phase (phases B and C) to earth	$\Delta E_{k1}+\Delta I_{k2}+\Delta I_{k0}=0$ $\Delta E_{k1}=\Delta E_{k2}=\Delta E_{k0}$	B	$I_{yB}+a^2\Delta I_{y1}+a\Delta I_{y2}+\Delta I_{y0}=0$ $a^2E_{y1}=aE_{y2}=E_{y0}$
Single-phase (phase A) to earth	$\Delta I_{k1}=\Delta I_{k2}=\Delta I_{k0}$ $\Delta E_{k1}+\Delta E_{k2}+\Delta E_{k0}=0$	C	$I_{yC}+a\Delta I_{y1}+a^2\Delta I_{y2}+\Delta I_{y0}=0$ $aE_{y1}=a^2E_{y2}=E_{y0}$

Note: 1. Phase A is taken as the main phase.
2. In interphase damage without earthing short-circuits, in the expressions cited $\Delta E_{k0}=0$; $\Delta I_{k0}=0$.

the coefficients β and ρ and by the phase differences between E_{y1}, E_{y2} and E_{y0}. Expressions for the coefficients n and m, for various combinations of short-circuit and phase rupture are shown in Table 3.

Having used the complex substitution circuit in place of the phase break in an analogous manner, we obtain*:

$$E_{y0}=E'_{y0}+E''_{y0}=\frac{I}{g_{y\Sigma}}+E''_{y0}, \tag{8}$$

where E_{y0} is the e.m.f. at the phase rupture point in the zero sequence circuit; I is the current in the phase to be broken, before the rupture; $g_{y\Sigma}=1/z_{y1}+1/z_{y2}+1/z_{y0}$ is the sum of the conductivities of all the sequence circuits at the phase rupture point; E''_{y0} is the component of e.m.f. E_{y0}, due to the voltage changes at the short-circuit point resulting from the phase break.

If phase A is broken

$$E''_{y0}=\frac{\rho_1\Delta E_{k1}+\rho_2\Delta E_{k2}+\rho_0\Delta E_{k0}}{g_{y\Sigma}};$$

and if phase B,

$$E''_{y0}=\frac{a^2\rho_1\Delta E_{k1}+a\rho_2\Delta E_{k2}+\rho_0 E_{k0}}{g_{y\Sigma}}.$$

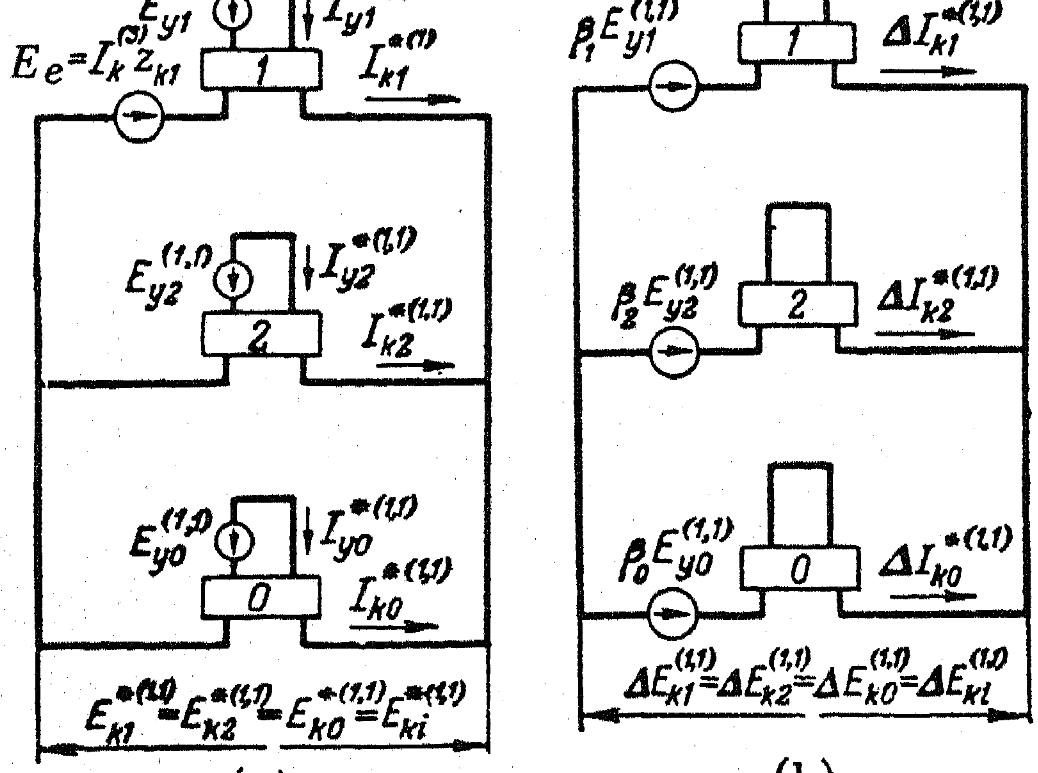

(a) FIG. 4. (b)

* Equation (8) can also be obtained by solving equation (4) together with equations defining the boundary conditions for the phase break (Table 2).

TABLE 3.

Type of short-circuit to earth	Phase broken	Expressions for coefficients	
		Δ	m and n
Three phase	A	$\Delta_A^{(3)} = 0$	—
Two phase (B and C)	A	$\Delta_A^{(1.1)} = -\frac{(\rho_1 + \rho_2 + \rho_0)^2}{g_{k\Sigma}}$	$m_A = \frac{\rho_1 + \rho_2 + \rho_0}{g_{k\Sigma}}$
	B	$\Delta_B^{(1.1)} = \Delta_A^{(1.1)} + \frac{3\,(\rho_1\rho_2 + \rho_2\rho_0 + \rho_1\rho_0)}{g_{k\Sigma}}$	$m_B = \frac{a\rho_1 + a^2\rho_2 + \rho_0}{g_{k\Sigma}}$
Single phase (A)	A	$\Delta_A^{(1)} = \frac{(\beta_1 + \beta_2 + \beta_0)}{z_{k\Sigma}} - \left(\frac{\beta_1^2}{z_{k_1}} + \frac{\beta_2^2}{z_{k_2}} + \frac{\beta_0^2}{z_{k_0}}\right)$	$n_A = \frac{\beta_1 + \beta_2 + \beta_0}{z_{k\Sigma}}$
	B	$\Delta_B^{(1)} = \Delta_A^{(1)} - \frac{3(\beta\ \beta_2 + \beta_1\beta_0 + \beta_2\beta_0)}{z_{k\Sigma}}$	$n_B = \frac{a\beta_1 + a^2\beta_2 + \beta_0}{z_{k\Sigma}}$

Note: Phase C in any form of short-circuit has no special characteristics in relation to phase B; for this reason combinations which include an interruption of phase C are not cited.

Equation (8) is not limited by the conditions of the short circuit in the branch. For a three-phase short-circuit, $E''_{y0} = 0$, and equation (8) takes the following form:

$$E_{y0} = \frac{I^{(3)}}{g_{y\Sigma}},$$

where $I^{(3)}$ is the current in the phase to be broken (before the break) in a three-phase short-circuit. For other forms of short-circuit, $E''_{y0} \neq 0$ and takes various values, depending on the combination of short-circuit and phase rupture.

For any combination of short-circuit and phase break, equation (8) can be written in the following form:-

$$E_{y0} = \frac{I}{g_{y\Sigma} + \Delta}, \tag{9}$$

where Δ is a coefficient determined by the boundary conditions of the short-circuit and phase break and having the dimensions of conductivity. Values of Δ, obtained as a result of the combined solution of equations (6) - (8) for various combinations of short-circuit and phase rupture, are given in Table 3.

Given the values of E_{y0}, $\Delta I_{k0}^{(1)}$ and $\Delta E_{k0}^{(1.1)}$, we can find their values for straight and reverse sequence circuits (Table 2), and determine $\Delta E_{ki}^{(1)}$ and $\Delta I_{ki}^{(1.1)}$ according to equation (5), and ΔI_{yi} according to equation (4), for all the sequence circuits. This completes the calculation of the current and e.m.f. components shown in Fig. 1.

Thus, all the current and e.m.f. components shown in Fig. 1, for any combination of short-circuit and phase break, can be expressed in terms of E_{y0} and the coefficients g_{ki}, g_{yi}, ρ_i, β_i. Together with this it can be seen from equation (9) that, whatever the combination of short circuit and phase break, E_{y0} is always determined only by the magnitude and direction of the current in the break phase and by coefficients $g_{y\Sigma}$ and Δ, which have the dimensions of conductivity. Current I depends on the e.m.f. in the circuit prior to the phase break, whilst the sum of $(g_{y\Sigma} + \Delta)$ is determined independently of the e.m.f. parameters of the circuit.

If only the inductive resistance is taken into account, the coefficient Δ for any combination of faults considered, is in phase with $g_{y\Sigma}$ and can be regarded as a correction to the conductivity $g_{y\Sigma}$, accounting for the special features of various combinations of faults. In the general case $\Delta_A^{(1)} \neq \Delta_B^{(1)} \neq \Delta_A^{(1.1)} \neq \Delta_B^{(1.1)}$.

In fact this correction accounts for the changes in the e.m.f. E_{y0} due to a phase rupture, with various forms of short-circuit. In cases of rupture in the phase damaged by the short-circuit, these changes are small. Calculations show that if $2z_{ki} < z_{yi}$, even under the most unfavourable conditions, Δ does not exceed 4 per cent of the conductivity $g_{y\Sigma}$ and drops rapidly as β_1, β_2 and β_0 fall. Thus in practical calculations of E_{yi} for any combination of phase breaks, with a short circuit at $2z_{ki} < z_{yi}$, a coefficient Δ can be assumed to be zero.

It should be noted that the combinations of faults considered are of great practical interest, since they introduce the maximum change in the e.m.f. and current values before the break.

Calculations of these combinations can be simplified still further if we neglect not only ΔE_{ki}, but also the inequality between the direct and reverse sequences. In this case expression (4) takes the form:-

$$I_{yi} = I_{yi} - q_i I, \tag{10}$$

where I is the current in the break phase prior to rupture; q_i are coefficients in the direct (q_1), reverse (q_2) and zero (q_0) sequence circuits, depending only on $k = z_{y0}/z_{y1}$ and on which phase is broken; if phase A,

$$q_1 = q_2 = kq_0 = \frac{k}{2k+1};$$

and for a break in phase B,

$$a^2 q_1 = aq_2 = kq_0 = \frac{k}{2k+1}.$$

By analyzing expression (10), it can be shown that in real circuits I^*_{y0} cannot exceed 0.6 I in a three-phase short-circuit and 0.6 $I - I_{y0}$ in a single- or two-phase short-circuit to earth. On this basis it can be found, without any calculation, whether deliberate incomplete phase transmission endangers the protective relays or whether more detailed calculation is required to examine their safety.

Expression (10) makes it possible to find without trouble the significant values of the components for combinations giving the maximum distortion, and, for $2z_{\hat{k}i} < z_{yi}$, to determine them to the accuracy normally allowed for practical calculations.

Example It is required to find the current and voltage components for a short to earth in phases A and B at point k, with a simultaneous break in phase A in the y-y' branch. The data required for this determination are given in Fig. 5.

Replace the given combination of faults by another, easier to consider: namely, shorts to earth in phases B and C with a break in phase B in the y-y' branch. The return step from this combination to that given is not difficult, since for this the current and voltage vectors found must be rotated through 120°.

In order to simplify the example and working, we assume that the circuit contains only active resistances.

The coefficients α_i, β_i and ρ_i, and their sums as in the expressions in Table 1 are:

$$\beta_1 = 0.25;\ \beta_2 = 0.25;\ \beta_0 = 0.5;\ \rho_1 = 0.5;\ \rho_2 = 0.25;$$
$$\rho_0 = 1;\ \alpha_1 = 0.66;\ \alpha_2 = 0.66;\ \alpha_0 = 1;\ \rho_1 + \rho_2 + \rho_0 = 1.75;$$
$$\rho_1\rho_2 + \rho_1\rho_0 + \rho_2\rho_0 = 0.875;\ a\rho_1 + a^2\rho_2 + \rho_0 = 0.5 - 0.25a^2.$$

The resistances at the point of rupture in the separate sequence circuits are:

$$z_{y1} = \frac{\alpha_1}{\rho_1} = 1.33\ \Omega;\quad z_{y2} = \frac{\alpha_2}{\rho_2} = 2.66\ \Omega;\quad z_{y0} = \frac{\alpha_0}{\rho_0} = 1\ \Omega.$$

The total conductivities of the sequence circuits at the point of phase rupture and the point of short-circuit are:

$$g_{y\Sigma} = 2.12 = \frac{1}{\Omega};\qquad g_{k\Sigma} = \frac{I_k^{(2)}}{E_k^{(1.1)}} = 5\,\frac{1}{\Omega}.$$

The total coefficient Δ for the combination of faults considered (Table 3) is:

$$\Delta_B^{(1.1)} = -0.086 \cdot \frac{1}{\Omega}.$$

The e.m.f. of the zero sequence, according to expression (9), is:

$$E_{y0} = \frac{I_B^{(1.1)}}{g_{y\Sigma} + \Delta_B^{(1.1)}} = -1\,053\,a^2 + 147.$$

The e.m.f.'s in the direct and reverse sequences, taking into account the boundary conditions of the phase break, are:

$$E_{y1} = aE_{y0} = -147\,a^2 - 1\,200;\ E_{y2} = a^2E_{y0} = 1\,053 + 1\,200\,a^2.$$

The change in e.m.f. at the point of short-circuit, according to equation (7) is:

$$\Delta E_{k1}^{(1.1)} = \frac{a\rho_1 + a^2\rho_2 + \rho_0}{g_{y\Sigma}.} E_{y0} = (-165a^2 + 38).$$

The resultant e.m.f. at the point of short-circuit is:

$$E_{ki}^{*} = E_{ki} + \Delta E_{ki} = 438 - 165\,a^2.$$

The change in current at the point of short circuit, according to expression (5) is:

$$\Delta I_{k1} = 257a^2 - 524;\ \Delta I_{k2} = 301 + 465a^2 \text{ н } \Delta I_{k0} = 223 - 722\,a^2.$$

The resultant current at the point of short-circuit is:

$$I_{k1}^{*} = 676 + 257\,a^2;\quad I_{k2}^{*} = 465\,a^2 - 99;\quad I_{k0}^{*} = -722a^2 - 577.$$

The change in current at the point of the phase break, according to expression (4) is:

$$\Delta I_{y1} = 28a^2 + 884;\ \Delta I_{y2} = -493a^2 - 406 \text{ and}$$
$$\Delta I_{y0} = 888a^2 - 185.$$

The resultant current at the point of phase break is:

$$I_{y1}^{*} = -1\,166 + 28\,a^2;\ I_{y2}^{*} = -306 - 493\,a^2;\quad I_{y0}^{*} = 215 + 888\,a^2.$$

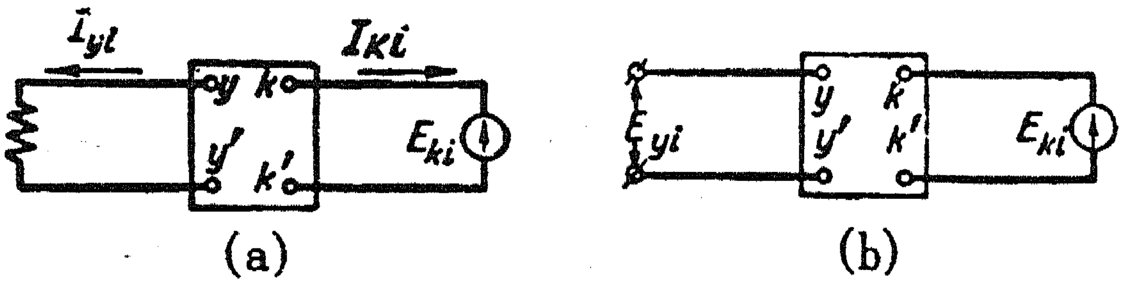

FIG. 5. (a) branch y - y' included; I_{y1} = 2050 A; I_{y2} = 100 A; I_{y0} = 400 A; I_{k1} = 1200 A; I_{k2} = 400 A; I_{k0} = 700 A; $E_{k1} = E_{k2} = E_{k0}$ = 400 V; Z_{k1} = 0.5 Ω. Z_{k2} = 1 Ω; Z_{k0} = 0.5 Ω; $I_k^{(3)}$ = 2000 A; $I_y^{(3)}$ = 2200 A. (b) branch y - y' excluded; $E_{y1} = E_{y2}$ = 95 V; E_{y0} = 143 V; $E_{k1} = E_{k2} = E_{k0}$ = 143 V.

The amount of calculation required to find the values needed is quite independent of the complexity of the circuit. In this respect the proposed method differs usefully from all the other known methods, in which the calculations become more complicated as the circuit becomes more involved.

To find z_{yi} in the absence of calculations shown by the scheme B in Table 1, it is possible to use the data given in Fig. 6. Fig. 6a corresponds to a short-circuit at one end of branch y-y', and Fig. 6b at the other.* On the basis of these data it is possible to find the intrinsic resistance of the y-y' branch in the absence of a short circuit in the system, if the following expression is used:-

$$z_y' = \frac{ab}{b - ac},$$

* As applied to the direct sequence circuit, the data shown in Fig. 6 denote the currents and voltages due solely to the e.m.f. at the point of short-circuit, assuming that the generator e.m.f. is zero. These currents and voltages are found by the superimposition of the conditions for any asymmetric short-circuit on those for a three-phase short circuit.

where

$$a = \frac{z_n^2}{z_n - \frac{U_k''}{I_k''} + \frac{U_k' U_k''}{U_k' I_k''}}; \quad b = \frac{U_k'}{I_y'}; \quad c = \frac{I_y'}{I_k'}.$$

The changes produced by a short-circuit in the value of intrinsic resistance for the y-y' branch can be taken into account, bearing in mind that:

$$\frac{1}{z_y} = \frac{1}{z_y'} + \frac{\beta^2}{z_k},$$

where β shows what fraction of the total current at the point of short-circuit constitutes the current in the y-y' branch (Table 1); z_k is the resistance introduced at the point of short-circuit.

Conclusions

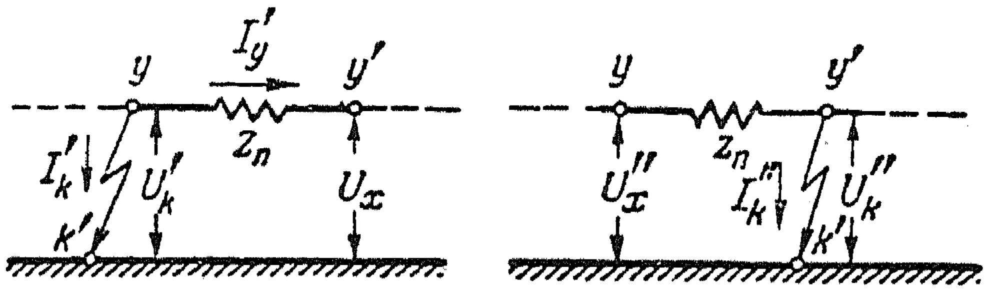

(a) (b)

FIG. 6.

The described method of calculation affords: (1) substantial simplification of the calculation of asymmetric faults by use of the results of calculations of short circuits in full-phase conditions. The changes brought about by unbalanced phase transmission are expressed in terms of the current for the full-phase condition and are independent of the e.m.f. parameters of the system; (2) simplification of calculations in systems with deliberately selected coefficients of current distribution. This refers in particular to combinations of any complex faults not considered in the paper, to the calculation of short circuits in power systems in connexion with changes in the generator e.m.f. and so on; (3) simplification of the calculation of complex asymmetric faults, when carried out on computing machines, by the superimposition of current components determined for full-phase conditions on to the current components due to the e.m.f.'s E_{yi} and ΔE_{ki}.

Translated by E. Bishop

REFERENCES

1. N.N. Shchedrin and S.A. Ul'ianov; *Zadachi po raschetu korotkikh zamykanii (Problems in the Calculation of Short-Circuits)*, Gosenergoizdat, (1955).
2. A.B. Chernin; *Korotkie zamykaniia pri nepolnofaznykh rezhimakh elektricheskikh setei (Short-Circuits in Unbalanced Phase Conditions in Electric Circuits)*, Gosenergoizdat, (1952).

COLLEGE OF ENGINEERING
LIBRARY BOOK
No.
GUINDY

A NEW CIRCUIT FOR HIGH-SPEED PULSE CONTROL IN SYSTEMS CONTAINING IONIC INVERTERS*

D.P. MOROZOV, M.G. CHILIKIN, N.G. LYSENKOV and L.M. TVERDIN

(Received 22 July 1957)

Modern electric drive is characterized by wide use of controlled ionic inverters. The use of control systems containing magnetic and electronic amplifiers ensures the development of high-quality electric drive systems satisfying the increased demands made on automatic control for precision and speed of effective action.

The introduction of ionic inverters in the electric drive systems of metallurgical shops, where a large number of different systems using controlled mercury rectifiers as inverters operate, is most significant. Practical experience in the operation of these installations has been accumulated both here and abroad. Our design and scientific research organizations have developed various different systems for grid control by ionic inverters (systems containing peak transformers and chokes, etc.).

The rectified voltage is regulated, in systems in use at present which contain ionic inverters, by the phase displacement of the control peaks. The ionic inverter mean rectified voltage is determined from the well-known equation $V_d = V_{d0} \cos \alpha$. A number of intricate and important units are used for changing the grid control system firing angle: grid supply and phase shift systems, and systems summing, shaping and amplifying the control signals [1-3]. The use of modern grid control systems enables us to exercise control by means of powerful mercury rectifiers with high-speed rectified voltage build-up [3].

Study of the systems containing ionic inverters used at present and the experience accumulated in their operation permits us to formulate the following basic tasks which must now be performed in order that these installations may be put to wider use.

(1) The improvement of $\cos \phi$ and the efficiency of systems with a wide range of rectified voltage control.

(2) Increase in the speed of effective action of control systems, this increase

* *Elektrichestvo* No.2, 22-27, 1958 [Reprint Order No. EL 50].

being particularly important for powerful rolling mills and other important industrial plant.

(3) Further increase in the operating reliability of installations containing ionic inverters, and maximum simplification of the control system, as a necessary condition for the use of these inverters.

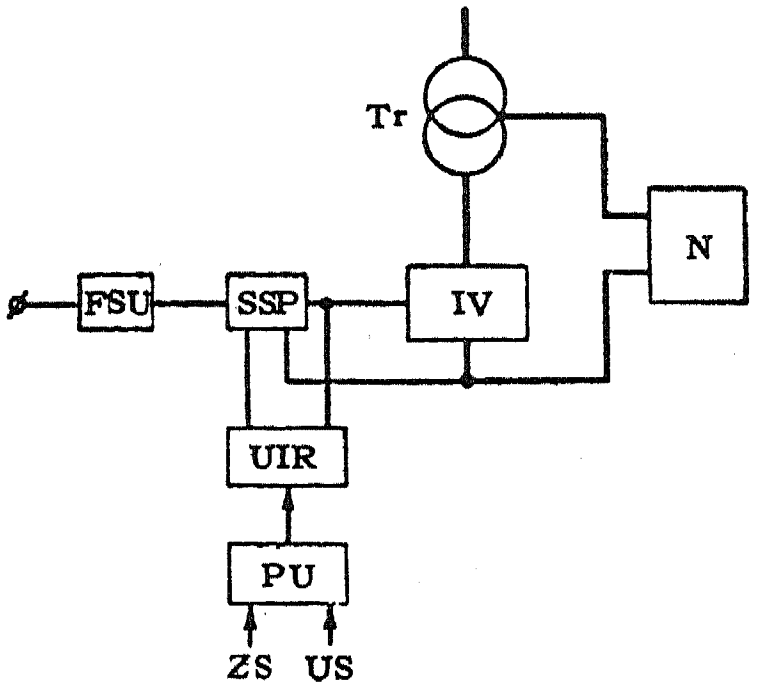

FIG.1. Diagram of the principle of high-speed pulse regulation. Tr - transformer; IV - ionic valve; N - load; FSU - phase-shifting appliance; SSP - grid feed system; UIR - pulse regulation unit; PU - intermediate installation; ZS - specified signal; US - controlling signal.

The grid control systems containing ionic inverters used at present do not fully satisfy these requirements. Where the rectified voltage regulation range is wide, the phase-shifting and summing units are complicated and definitely sluggish.

Regulation of rectified voltage by altering the firing angle over a wide range considerably worsens the power factor, this making the introduction of ionic inverters in powerful installations difficult.

The authors of this article have developed and investigated several variants of a new way of regulating the mean rectified voltage of an ionic inverter (Fig.1).

The basis on which the system operates is the pulse method of regulating the mean rectified voltage; here, change in the regulated quantity is caused not by phase displacement of the positive control peaks, but by how frequently and for how long the ionic inverter is applied.

Pulsatory ionic inverter working conditions are obtained by introducing a new unit into the grid control circuit. The main purpose of this unit is to blank-off and trigger the ionic inverter in accordance with the required regulation conditions. The principle components of this unit are the controlled low-power valves which ensure the blanking-off and triggering of the ionic inverters at the necessary intervals and for the necessary lengths of time. Magnetic or mechanical appliances can be used in place of the controlled valves. All these installations must satisfy the condition of low voltage drop when the control peaks fed to the ionic inverter are applied.

Let us examine the working of this system in the example of an installation with a 3-phase mercury rectifier (Fig.2), in order to clarify the principle on which the proposed new high-speed pulse regulation system operates.

When there is no control signal V_{vkh} on the grids of the pulse regulation high-speed unit control valves UV, these valves are blanked off by the blanking voltage V_{sm} (the bias voltage).

The positive triggering peaks, produced by the mercury rectifier in the grid control circuit, are fed to its grids in the usual way. The mercury rectifier is opened and the rectified voltage determined by a, the angle of regulation.

When a control signal V_{vkh}, sufficient for triggering, is fed to the grids of the valves UV, these valves fire and clip the positive pulses fed to the grids of the rectifier RV. The mercury rectifier is blanked-off.

The cessation of the input signal V_{vkh} corresponds to the blanking-off of the valves UV and the triggering of the mercury rectifier.

Depending on the frequency of transmission and the duration of the signals fed to the grids of the valves UV, rectified voltage pulses of the corresponding frequency and duration are produced at the output of the ionic inverter. The mean mercury rectifier rectified voltage depends on the time of conduction and the spacing, where a is constant.

The new ionic inverter high-speed pulse control unit may be introduced into certain systems in use for regulating ionic inverters by various means, depending on the nature and purpose of the systems.

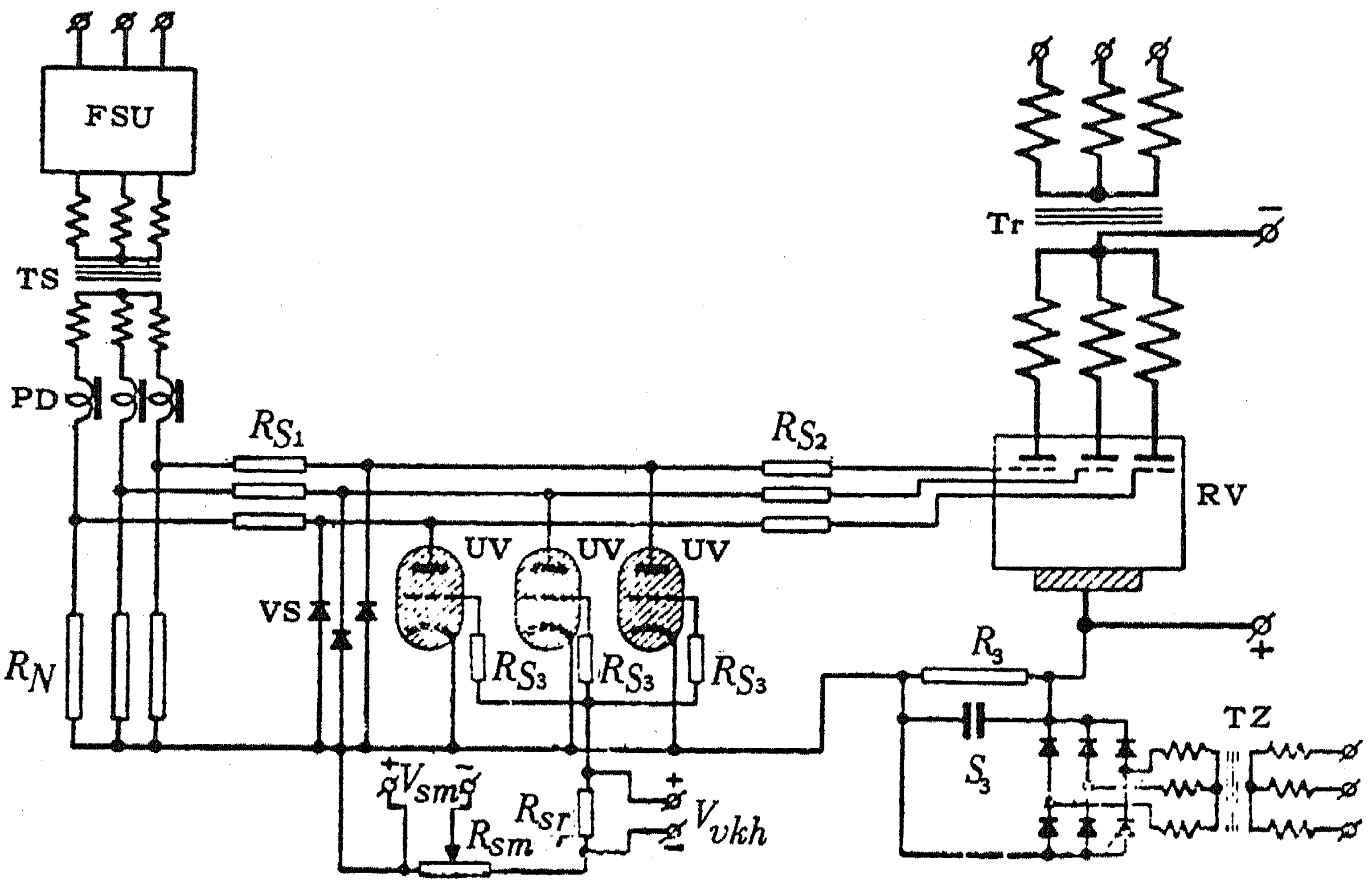

FIG.2. Circuit illustrating the principle of pulse regulation of rectified voltage. Tr - transformer; RV - mercury rectifier; FSU - phase-shifting appliance; TS - grid transformer; PD - peak choke; RN - load resistance; R_{S1}, R_{S2} - grid resistances; VS - semiconductor rectifiers; TZ - mercury rectifier locking voltage unit transformer; R_3 - locking potential unit resistance; UV - controlled valves of the pulse control unit; R_{S3} - grid resistance in the controlled valve grid circuits; R_{sm} - grid bias; R_{sr} - comparing resistance in the controlled valve grid circuits.

In the new system, the rectified voltage can be regulated both where $a \neq 0$ and where $a = 0$. In the first case, the high-speed impulse regulation unit is made an additional link in the circuits in use. In the second case, the phase-shifting appliance may be removed from the circuit and all the necessary signals fed only to the pulse regulation unit.

The control signal V_{vkh}, the frequency and duration of which correspond to the specified mean rectified voltage, may be obtained:

(a) from the independent switchgear, for instance, a mechanical switch with conducting plates and slide contact (an open circuit regulating system), or

(b) from intermediate gear providing equalization of the specified and regulated magnitudes (a closed regulating system).

Oscillation or electronic regulators, also magnetic amplifiers, can be used as the intermediate equipment, working on the input of the pulse regulation unit. The summing of the various signals, their comparison with the specified value, and also the shaping of the signal supplied to the input of the pulse regulation unit, are performed in the intermediate equipment.

In a number of cases, the intermediate equipment may be omitted. In these circuits the control signals are fed direct to the pulse regulation unit.

A number of circuits using the high-speed pulse regulating unit were investigated in the laboratories of the Moscow Power Institute Industrial Undertaking Electrical Equipment. In particular, the circuit shown in Fig.3 was examined. The circuit provides forced generator voltage build-up, generator voltage "cut-off", and the maintenance of a specified voltage; the control signal is fed directly to the high-speed impulse regulation unit.

A PN-550 type generator was used; $P_N = 88$ kW, $V_N = 230$V, $I_N = 383$A, $n_N =$ 1440 rev/min an RM-200 mercury rectifier with grid supply unit was used, and the controlled valves were TR 1-2.5/2 thyratrons.

In the supply circuit, feed to the field windings of the generator was accomplished by the inclusion of a two-pole contactor K. A negative potential, exceeding their blanking-off potential, was fed to the grids of the valves UV by a potentiometer P. Whilst starting the motor, the rectifier RV was open and a voltage $a_0 V_{vN}$ (a_0 being the forcing coefficient) was applied to the field windings of the generator. The controlled valves were blanked-off until the generator voltage had reached a value such that $| V_{sm} | - | V_{vkh} | \leqslant | V_{otn} |$, where V_{otn} is the triggering voltage for UV. The valves UV come into operation. The positive peaks fed to the grids of the rectifier RV are cut off, and extinguished. The current in the generator field windings begins to drop. The generator field winding self-induction e.m.f. will maintain the current in the discharge resistance and at one of the mercury rectifier anodes (until the anode current passes zero). Reduction of the generator voltage causes reduction in the signal V_{vkh}; UV thereupon is extinguished and RV comes

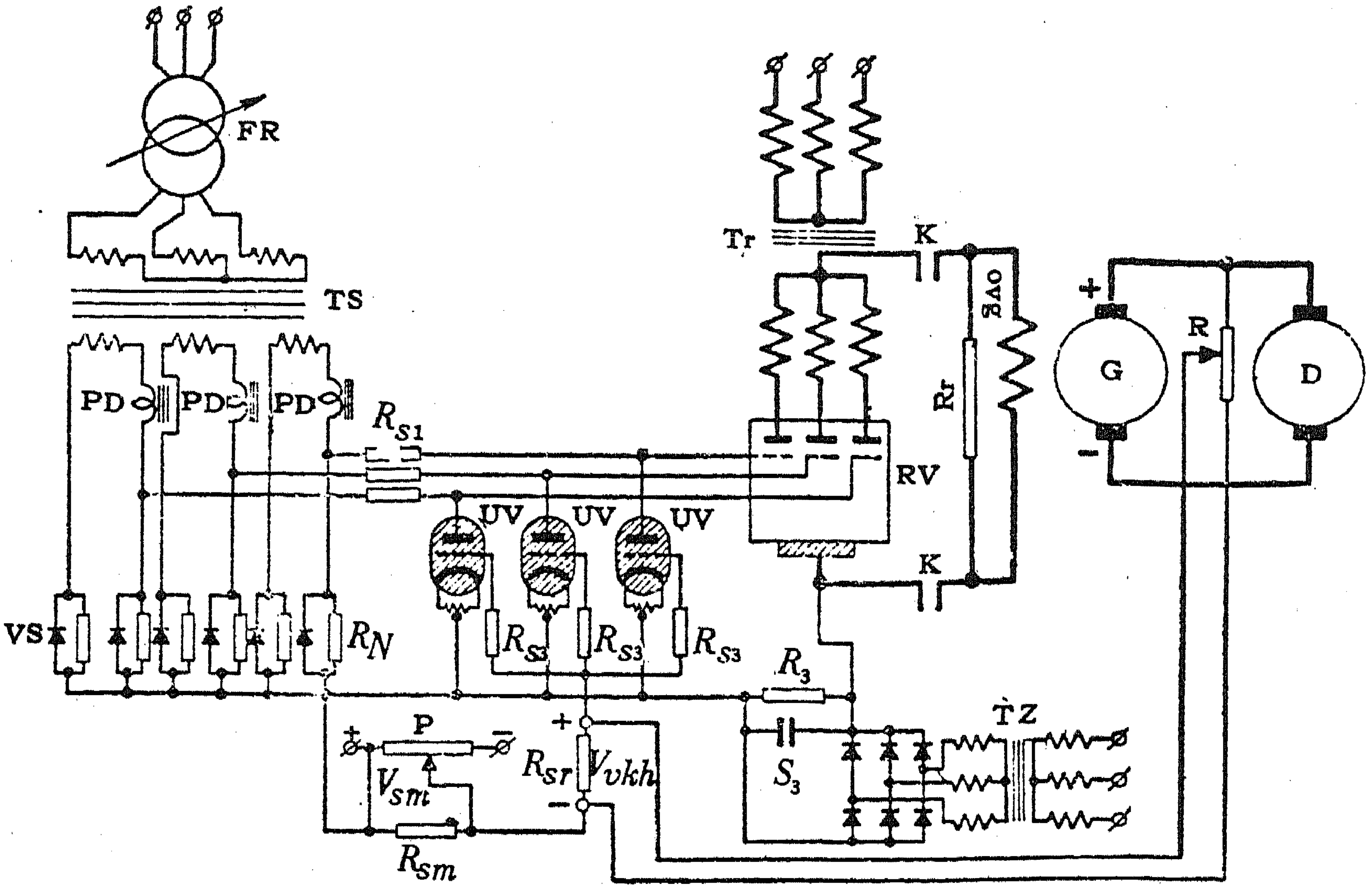

FIG.3. Diagram illustrating the principle of the pulse regulation of generator excitation current in a generator-motor system.

into action. Thus, the mercury rectifier is working on a system of impulses and the generator voltage is maintained at a specified level, fluctuating around its mean value.

The "cut-off" voltage is determined by the bias voltage V_{sm} and $\beta = \frac{V_{vkh}}{V_g}$ (Rheostat R contact position).

The control circuit (Fig.3) is extremely simple, notwithstanding the complicated tasks which it performs. Ideal voltage "cut-off" is very simply accomplished. The change in time of generator voltage, generator excitation current and field winding voltage for various levels of voltage regulation are shown in the oscillographs in Fig. 4-6. The recording in Fig. 4 shows the process of transition to the rated generator excitation current and voltage. The ultimate values for these quantities are equal to 0.66 of the rated values in the recording in Fig. 5, 0.33 in

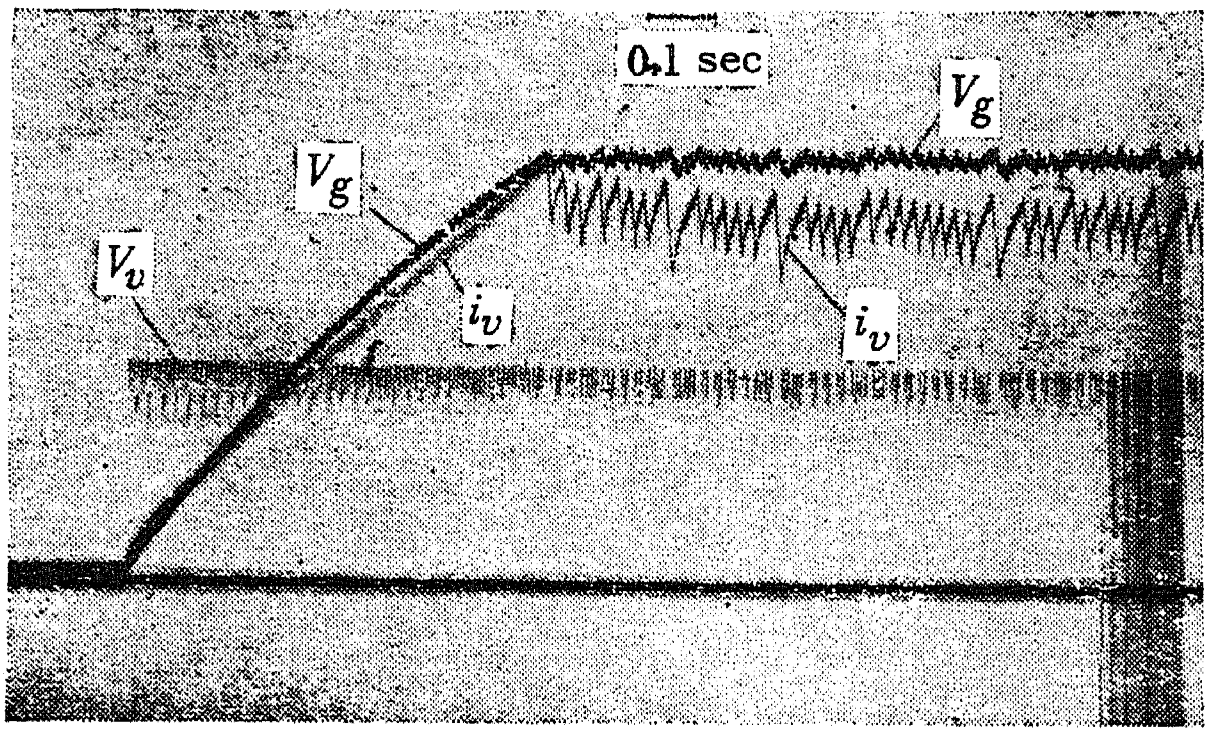

FIG.4. Oscillograph recording of the transitional generator excitation process where the forcing coefficient $a_0 = 2$; $i_{vu} = i_{vn}$.

Fig.6. In spite of the considerable deviations of thyratron-actuating characteristics and the lack of an intermediate appliance ensuring a steep signal front at the input of the pulse regulation unit, the circuit provides small generator voltage fluctuations at various excitation levels.

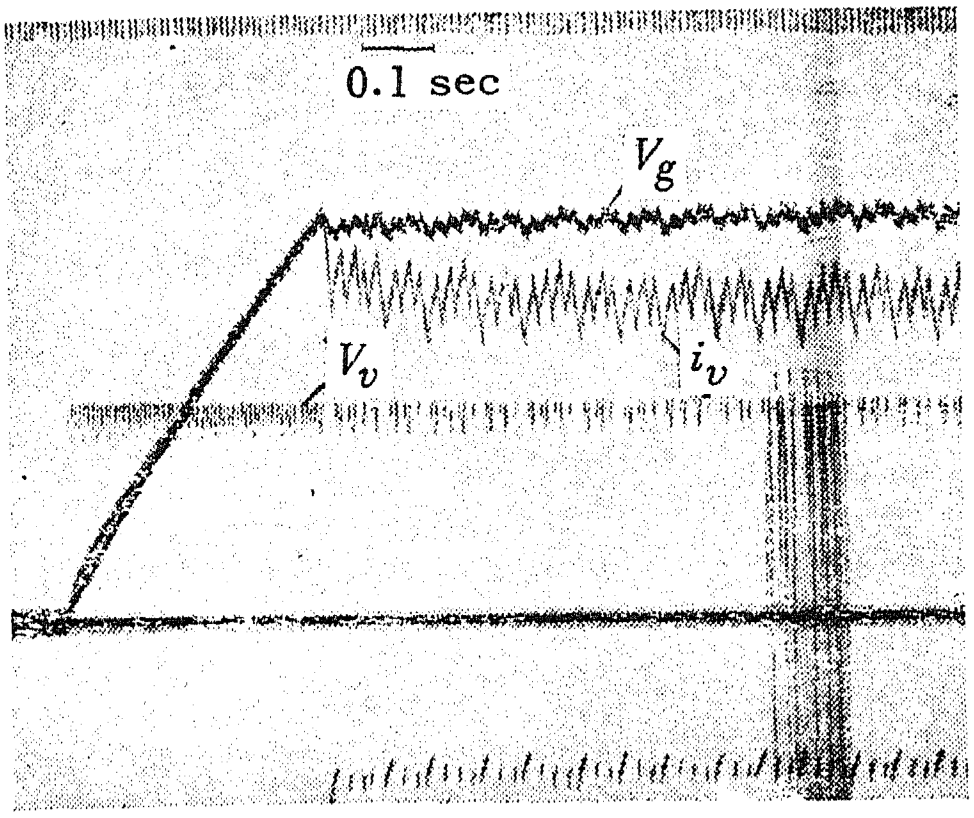

FIG.5. Oscillograph recording of the generator excitation transitional process for forcing coefficient $\alpha_0 = 2$; $I_{vu} = 0.66\ I_{vn}$.

Since regulation of the rectified voltage takes place at a firing delay angle $\alpha = 0$, the circuit ensures a high power coefficient and efficiency. The circuit is quick-acting; the operating time is determined solely by the time taken by the thyratrons UV to fire and extinguish. Their firing time is practically zero; the time they take to extinguish depends on the moment at which the signal is fed to the fired thyratron and cannot, for a three-phase circuit, exceed 8.33×10^{-3} sec (for a six-phase rectifier it is 66.6×10^{-3} sec).

It must be noted that the qualitative and quantitative factors of the new circuit are subject to further theoretical and experimental research. It will also be necessary to study a number of physical phenomena and processes which accompany the working of the new regulation circuit. The preliminary results show that the new circuit can be employed in various intricate electrical drive circuits requiring: (a) a wide range of regulation; (b) speedy action; (c) precise regulation with high power coefficients and efficiencies.

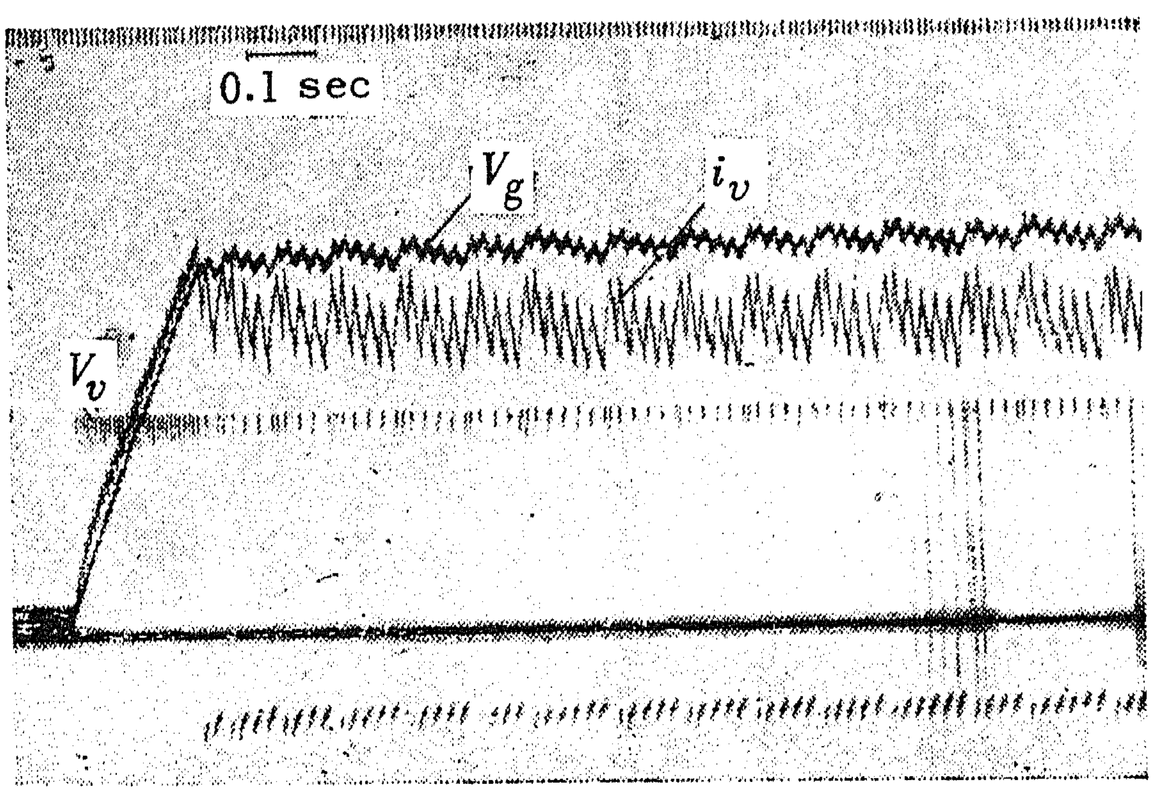

FIG.6. Oscillograph recording of the generator excitation transitional process for forcing coefficient $\alpha_0 = 2$; $i_{vu} = 0.33\ I_{vn}$.

Ionic inverters operating in pulse systems may be used for the supply of: (a) electric motor and generator starter circuits, and (b) electric motor armature circuits.

Without enumerating all the possible types of mechanism for which the new high-speed pulse regulation circuit may be used, we will give some examples to illustrate its use.

Fig.7 shows the principles of the control of the generator-motor system for a reversing blooming mill stand. The generator and motor field windings are supplied from ionic inverters operating in impulse systems. Reversing of the motor is accomplished by changing the generator excitation polarity, using a reversing switch. The motor rotation rate is regulated up to basic by the effect on the ionic inverter feeding the generator excitation circuit, and above basic by the effect on the ionic inverter feeding the motor excitation circuit.

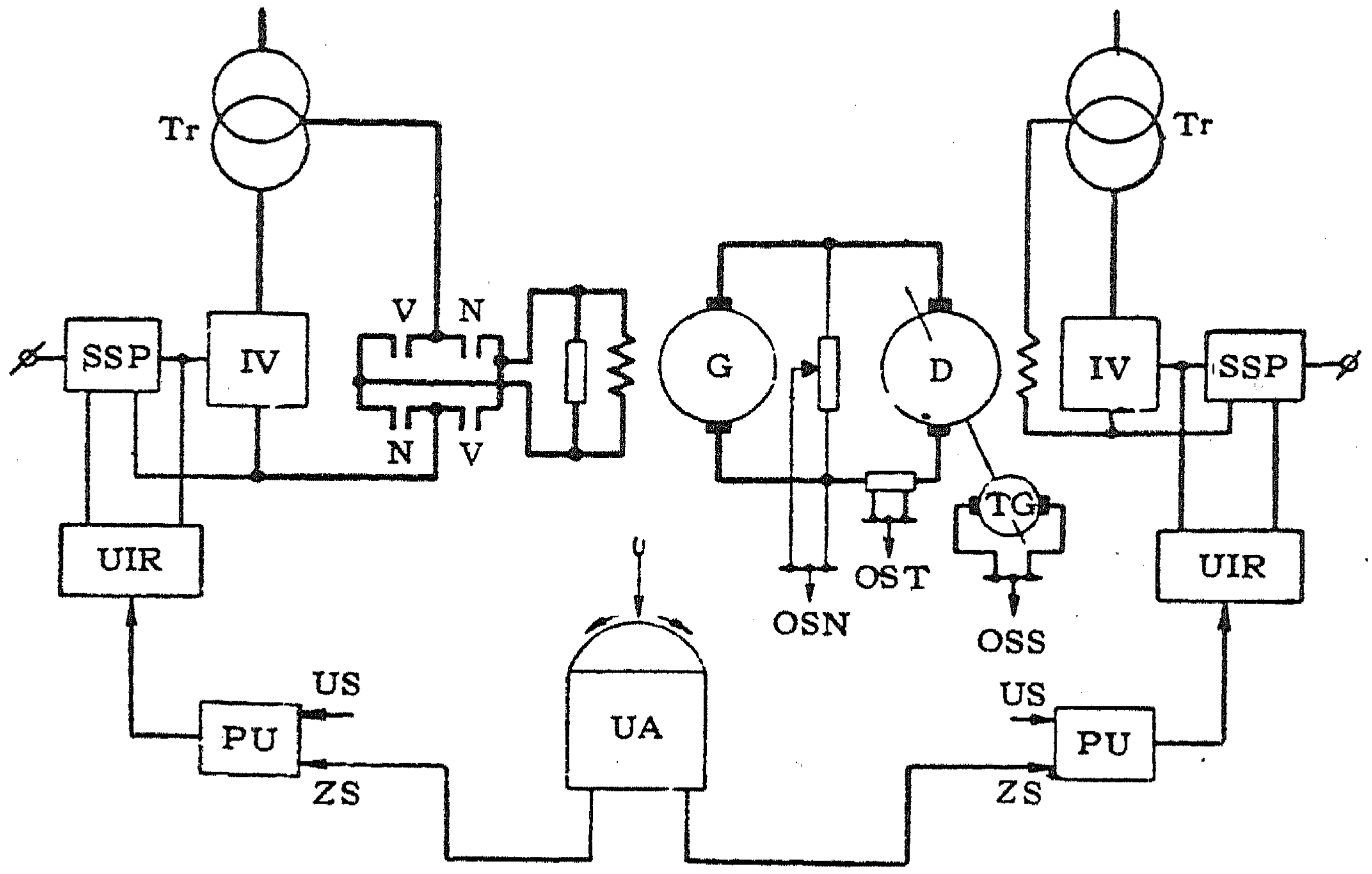

FIG.7. Diagram illustrating the principle of the pulse control of the excitation of large machines from ionic inverters in the generator-motor system of a reversing mill. Tr - transformer; IV - ionic valves; G - generator; D - motor; TG - tacho-generator; V,N - reversing contacts "forward", "back"; UA - controlling gear; SSP - grid supply system; UIR - pulse regulation unit; PU - intermediate installation; ZS - specified signal; US - controlling signal; OSN - voltage feed-back; OSS - rotation feed-back; OST - current feed-back.

There are no complicated phase-shifting devices in the diagram for control using mercury rectifiers. All the control functions in the steady-running and transitional states are performed by the pulsatory regulation unit. Although the pulsatory control unit can be made on the basis of magnetic appliances (high-speed magnetic amplifiers and relays, etc.) the use of thyratrons may be considered a sufficiently reliable solution. We know that thyratrons are widely used in practice at home and abroad (in the U.S.A. and Germany) in electric drive control circuits. Certain designs of thyratron being introduced into industry at the present time are very reliable and hard-wearing (service life of 15,000 hr). The elimination of phase-shifting and other intricate units simplifies and improves mill control circuits in comparison with existing circuits, and facilitates their operation.

The mercury rectifiers in the given circuit operate with an angle of regulation $\alpha = 0$. Calculations show that for constant electrical motor or generator field winding times $T_v = 3 - 4$ sec, forcing coefficient $\alpha_s = 3 - 4$ and tolerated regulated quantity variations (generator voltage, field current, motor rate) of 4 - 5 per cent of the rated values, the resting and working times of the mercury rectifier RV vary between 0.04 and 0.1 sec (in a three-phase rectification system this corresponds to the firing or misfiring of six to fifteen anodes in succession). The extinction of the rectifier RV in pulsatory ionic excitation circuits is determined by the discharge resistance selection condition:

$$k_p \leqslant \frac{\alpha_{\Omega}\pi}{m \sin \frac{\pi}{m}},$$

where $k_p = R_p/r_v$, R_p is the discharge resistance in the field winding circuit, and m is the number of rectification phases.

For the rectifier RV pause and firing-period intervals indicated above, the impulse system of this rectifier hardly worsens the shape of the circuit current curves, and ensures that cos ϕ is close to unity. Where the anodes fire and misfire in quicker rotation, the coefficient of power is affected by the worsened shape of the current curve and the firing of the last (prior to extinction of RV) anode in the transformer secondary e.m.f. negative value region. However, in this case also, the power coefficient is considerably higher in impulse control circuits than in RV continuous control circuits. In an experimental installation with frequent rotatiou of anode firing and misfiring, pulsatory RV control improved cos ϕ (for identical conditions), in comparison with continuous control by up to 60-70 per cent (0.34 to 0.58; 0.51-0.72; 0.62-0.85, etc).

The simplicity, economy and precision with which the regulated value is maintained (less than 1 per cent when T_v = 3-4 sec), and high-speed action enable us also to recommend pulsatory RV control circuits for the excitation of the principle electrical machinery in the generator-motor transmission systems of powerful continuous mills (reconstructed and under construction), and of less powerful plant.

The use of ionic inverters operating in impulse systems for supplying the armature circuits of blooming mill motors is shown in Fig.(8). The motor is reversed in this circuit by a switch in the motor armature circuit. The introduction of an impulse regulation unit into the control circuit hardly makes this circuit more complicated in view of the simplicity of the proposed unit, and enables the armature to be supplied at reduced rates of rotation (up to basic rate), with a regulation angle $\alpha = 0$. At the lowest motor rotation rates, in order to reduce the armature current pulsations and improve motor working conditions, it is advantageous to work at $\alpha = \cos nt \neq 0$, but at lower regulation angles than in the case of continuous RV control. The employment of a pulse regulation unit ensures a high power coefficient and is more advantageous than intricate circuits with artificial anode communication, non-symmetrical control, etc.

The proposed pulse control by mercury rectifiers feeding the motor armature can be very widely applied (with or without phase-shifting equipment) in the electric drive systems of less powerful plant, (rolling mill auxiliary mechanisms, metal-working machines, etc.), where the motors work under better conditions. It should be possible, in order to confirm the proposal that an RV impulse system may be employed for the supply to a motor armature, to refer to the details given in

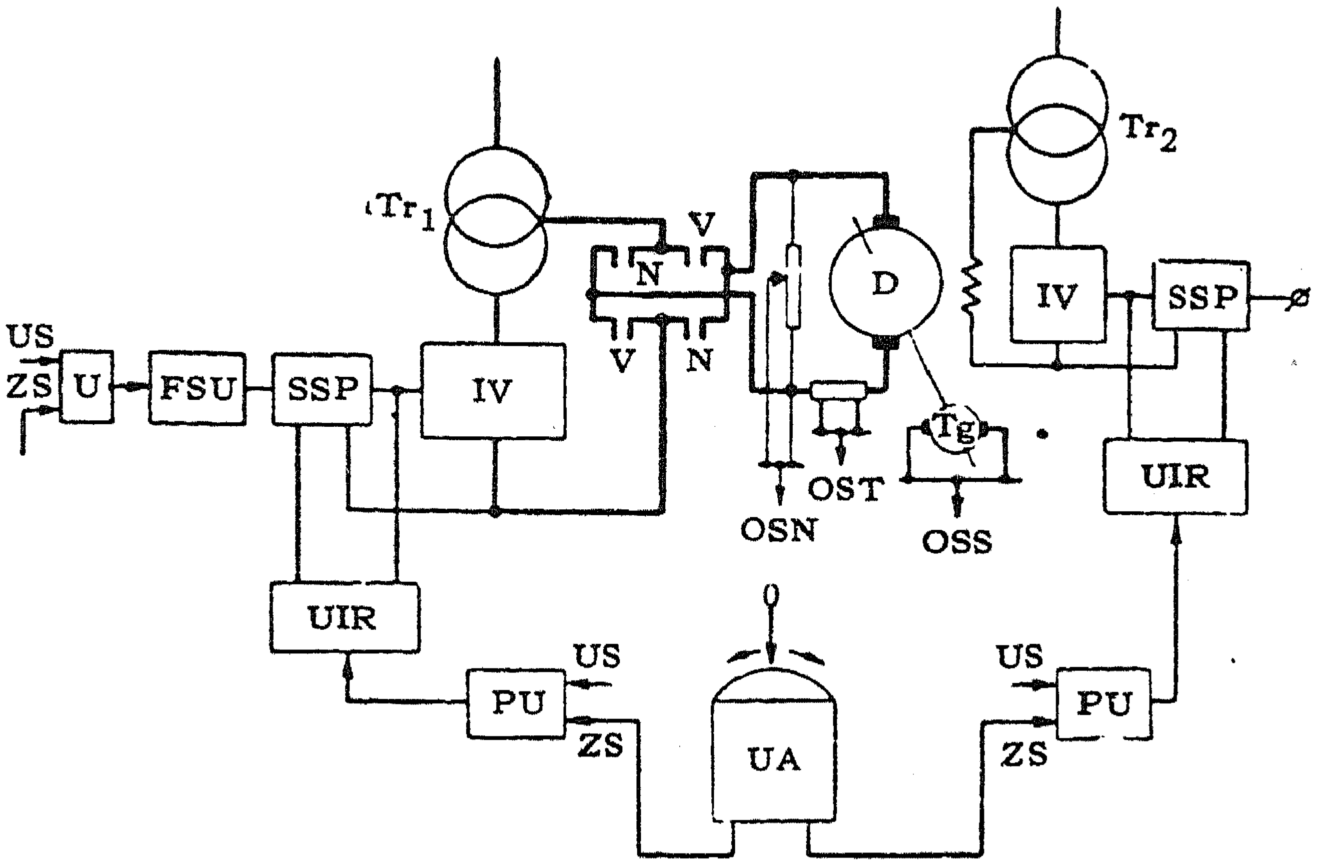

FIG.8. Diagram illustrating the principle of reversing mill motor feed from a mercury rectifier using pulse regulation. Tr_1 - main inverter transformer; Tr_2 - motor excitation circuit ionic inverter transformer; D - motor; IV - ionic valves; SSP - grid feed system; FSU - phase-shifting appliance; U - amplifier; UIR - pulse regulation unit; PU - intermediate installation; US - controlling apparatus; ZS - specified signal; US - controlling signal; OSN, OST, OSS - voltage, current and rate feed-backs; V, N, - reversing contacts, "forward", "back".

foreign literature [4], on practical experience abroad of the use of mercury rectifiers working in a system of impulses in the electric drives of the pressure roll and other auxiliaries in powerful rolling mills.

Finally, yet one more important field for the employment of the pulse regulating unit must be indicated: that is, the electric drive of continuous mills, (the armature and excitation circuits of the motor supplied from mercury rectifiers), where speedy action and precision of regulation are required with a narrower range of regulation (narrower than, for example, in a blooming mill).

The use of pulse regulation in circuits where synchronous motor field windings are supplied from ionic inverters is of great interest.

Conclusions

The practical introduction of powerful controlled rectifiers for electric drive is a progressive trend in the development of automatic regulated industrial installations. Considerable reduction in capital outlay, increased labour productivity and lower power consumption are associated with this.

The reconstruction and modernization of installations already in use should be undertaken incorporating ionic inverters just as these are used in installations now being constructed.

The new system of high-speed pulse regulation described in this article will result in the fulfilment of the highest technical and economic production standard, in installations using ionic inverters. These standards are primarily high coefficients of power and efficiency, and the high speed and comparative simplicity of the automatic control circuit.

Translated by J.H. Dixon

REFERENCES

1. I.L. Kaganov; *Elektronnye i ionnye preobrazovateli (Electronic and ionic inverters)*, III, Gosenergoizdat (1956).
2. F.I. Butaev and E.L. Ettinger; *Ventil'nyi elektroprivod (Valve electric drive)*, Gosenergoizdat (1951).
3. E.L. Ettinger, B.M. Gutkin and P.M. Borodavchenko; Sovremennye skhemy ventil'novo elektroprivoda (Modern valve electric drive circuits), *Elektrichestvo* 9 (1956).
4. F. Holters; Stromrichteranlagen fur Walzwerksantriebe, *AEG M:* 44, 9-10, 364 (1954).

THE CONTROLLED PHASE-TYPE COMPOUND WINDING OF SYNCHRONOUS GENERATORS WITH CORRELATION AS TO VOLTAGE *

O.M. KOSTIUK and V.E. RYBINSKII

Ukr. S.S.R. Electrical Engineering Institute of the Academy of Sciences

(Received 21 February 1957)

The controlled compound winding of synchronous motors and generators with correlation as to voltage is at present widely used. At the same time, the possibilities of improving the compounding circuits by achieving a relationship between the excitation of synchronous machines and not only the stator current, but also the stator voltage, taking the phase angle between them into account (phase compound winding), and also by achieving circuits with parameters which change under the action of an automatic corrective device, have been under examination for quite a long time.

In 1945, circuits for controlled (not phase) compound winding were developed by Moscow Regional Power System Administration, and simultaneously by the Moscow Electric Power Institute and the State Trust for the Organization and Efficiency of Electric Power Plants. Control was accomplished by the excitation of an intermediate transformer [1], or shorting choke [1, 2], in a normal compound winding circuit. An electronic voltage corrective device was used for this purpose in both the articles referred to. The shortcoming of this circuit is the lack of automatic regulation in low generator load conditions. In the second circuit they used what was, essentially, an additional corrective device creating a supplementary voltage drop at the shunt rheostat, to eliminate this shortcoming. This made the construction of the regulator more complicated.

For the first time, controlled phase compound winding with electro-mechanical corrective devices was then achieved on a 35 MW turbo-generator at Kievenergo [3,4].

Controlled phase compound winding was thereafter used to improve a circuit with electronic and ionic regulators [5], but this circuit was not widely adopted owing to the comparative complexity of the regulators themselves.

---

* *Elektrichestvo* No. 2, 27-34, 1958 [Reprint Order No. EL 51].

A phase (uncontrolled) compound-winding circuit for self-exciting generators of low power was developed in 1940 at the Lenin All-Union Electrical Engineering Institute [6]. In recent years, circuits for the phase combination of controlled compound winding with the field current, not controlled from the voltage [7 and 8], have been used for this purpose. The circuit for the phase combination of uncontrolled compound winding with the field current controlled from the voltage should be noted [9].

Controlled compound winding was also achieved for low-power generators with mechanical exciters, but in these circuits there is no automatic regulation in low generator load conditions, and the voltage regulation accuracy is not high [10].

This article sets out briefly the results of the development of a system for the automatic regulation of synchronous generator excitation, with phase compound winding controlled from the stator current and voltage. The industrial production of the regulators described in the article commenced in 1956.

Circuit and principle of operation

Fig. 1 contains diagrams showing the principles on which generators with mechanical exciters operate.

The main compount of the regulator is an all-mains transformer for controlled-phase compound winding, which in construction is a transformer-type magnetic amplifier. Fig. 2 is a schematic diagram of the all-mains transformer for low-voltage generators.

All the transformer windings are sited around the central bars of two III-shaped magnetic circuits (1), while the a.c. windings cover both magnetic circuits, and the field windings (2) cover each magnetic circuit individually. The primary series winding (3) is connected to the stator current circuit, phase A for example; the primary parallel winding 4 is connected to the stator voltage through an additional resistance of choking coil.

Taking into account the possibility of non-symmetrical generator states, it is desirable to perform compound winding on the current of at least two stator phases. A second series winding (5), connected for example to phase B, is provided for this purpose. The geometric sum or difference of the magnetizing forces in windings (3) and (5) is obtained, depending on the connexion polarity. With three-phase compound winding, thers may be a third series winding connected to phase C. The polarity of the two windings must then correspond to the sum of the magnetizing forces, and that of the third to the difference between them. This type of double or triple connexion of a single all-mains transformer is more expedient than the corresponding use of two or three separate transformers, one for each phase.

An e.m.f proportional to the resultant magnetizing force of the series and parallel primary windings is induced in the secondary (output) winding (6) of the

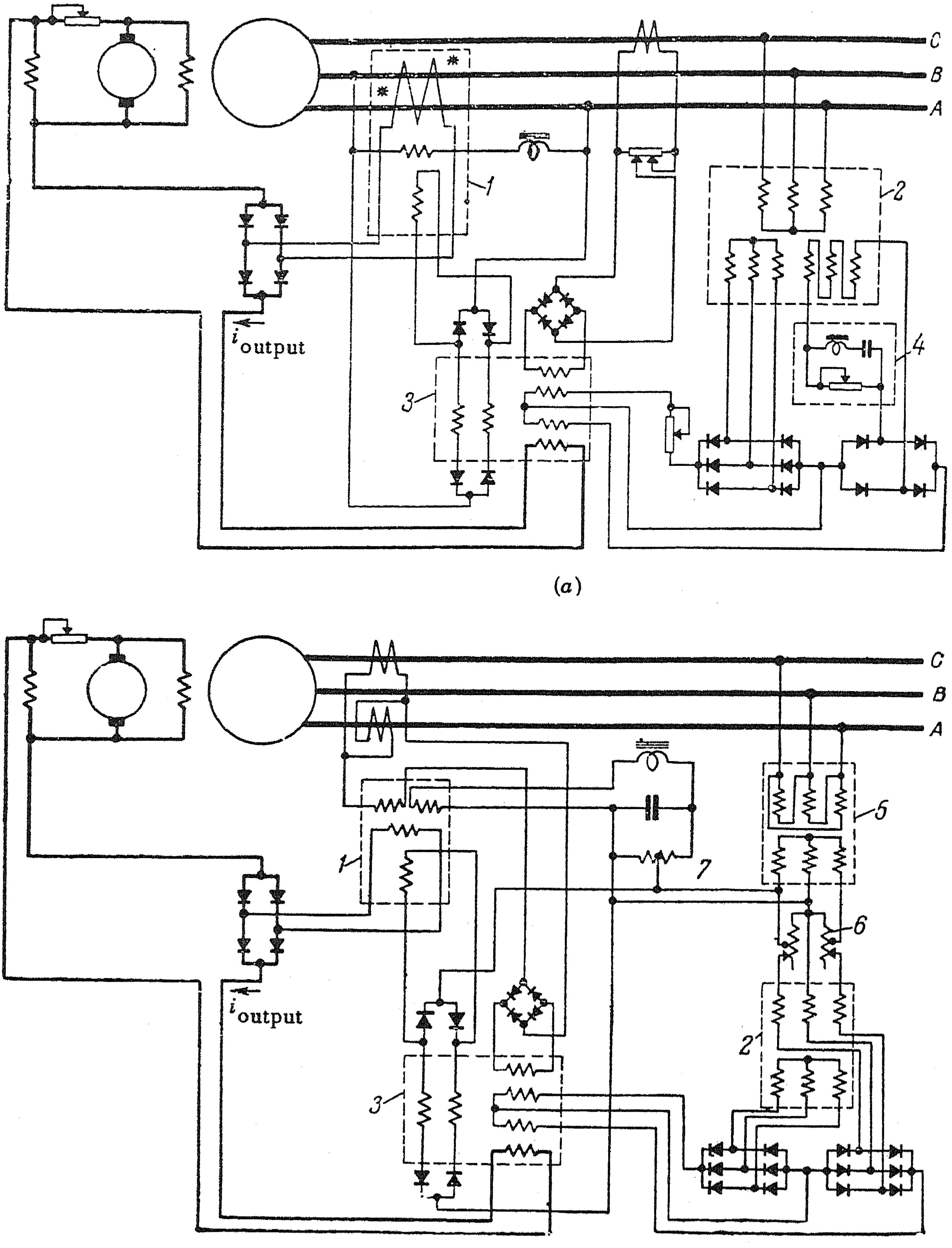

(a)

(b)

FIG. 1. Circuit for controlled phase compound winding with electro-magnetic voltage corrector.
(a) – for low-voltage synchronous generators; (b) – for high-voltage synchronous generators; 1 – all-mains controlled phase compound winding transformer; 2 – measuring device saturable transformer; 3 – magnetic amplifier; 4 – tuned circuit for frequency correction; 5 – voltage transformer; 6 – adjusting compensator; 7 – step-up compensator.

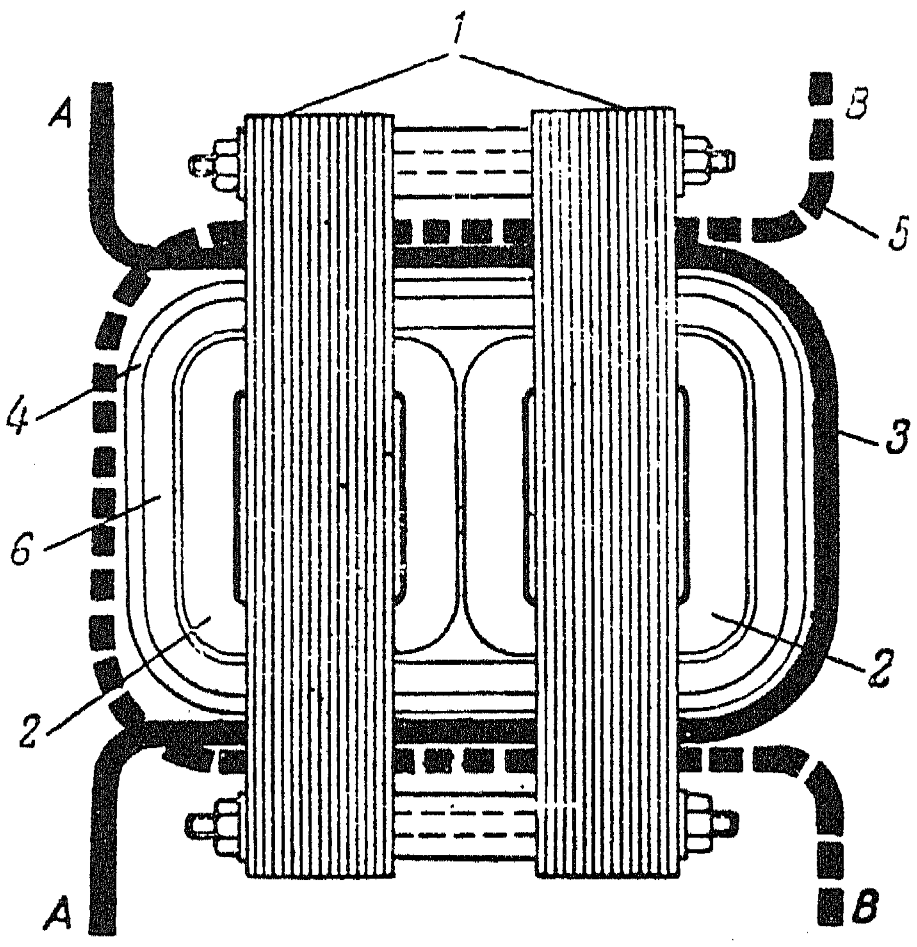

FIG. 2. Core and winding distribution in the all-mains controlled phase compound winding transformer.

all-mains transformer. The secondary transformer winding current is rectified and fed to the exciter-excitation circuit (Fig. 1).

It is expedient to connect a filler-type condenser in parallel with the magnetizing winding (2) (Fig. 2).

The phases to which the transformer parallel winding must be connected are determined with respect to the circuit diagram for the series windings of the all-mains controlled phase compound winding transformer and to the type of additional resistance in the parallel winding circuit (choke or rheostat). The phases selected must be such that, for an almost inductive load, where $\cos \phi \approx 0$, the magnetizing forces in the primary windings, which are proportional to the stator current and voltage, coincide as to direction, while for a load, where $\cos \phi \approx 1$ they should be displaced by an angle of 90° and the magnetizing force proportional to the stator voltage must lag.

The most expedient and constructionally convenient circuit is that of the double connexion for the difference in magnetizing forces of two phases. When connecting for the sum of the magnetizing forces of two phases, there will be no forced excitation in these phases on short circuit.

The electro-magnetic voltage corrective device has a three-phase measuring appliance at its input side, which acts on the single-phase intermediate magnetic amplifier. The output side of the voltage corrective device is connected to the field winding of the all-mains transformer. The possibility of additional correction of voltages as to frequency, by means of a tuned circuit connected to the non-linear component circuit, has been foreseen for low-power generators (Fig. 1 a). In this case, to reduce the size of the tuned circuit, the non-linear component circuit is made on the frequency tripler system.

The regulator shown in Fig. 1 b has been developed for powerful high-voltage generators. To increase the available regulation power and further improve the dynamics of the regulator, double-circuit regulation may be introduced; here a magnetic amplifier, counter-connected to an additional de-magnetizing field winding in the exciter, is also controlled from the corrective device measuring appliance. No additonal correction for frequency is required for powerful generators or for generators working in parallel in a powerful electric power system.

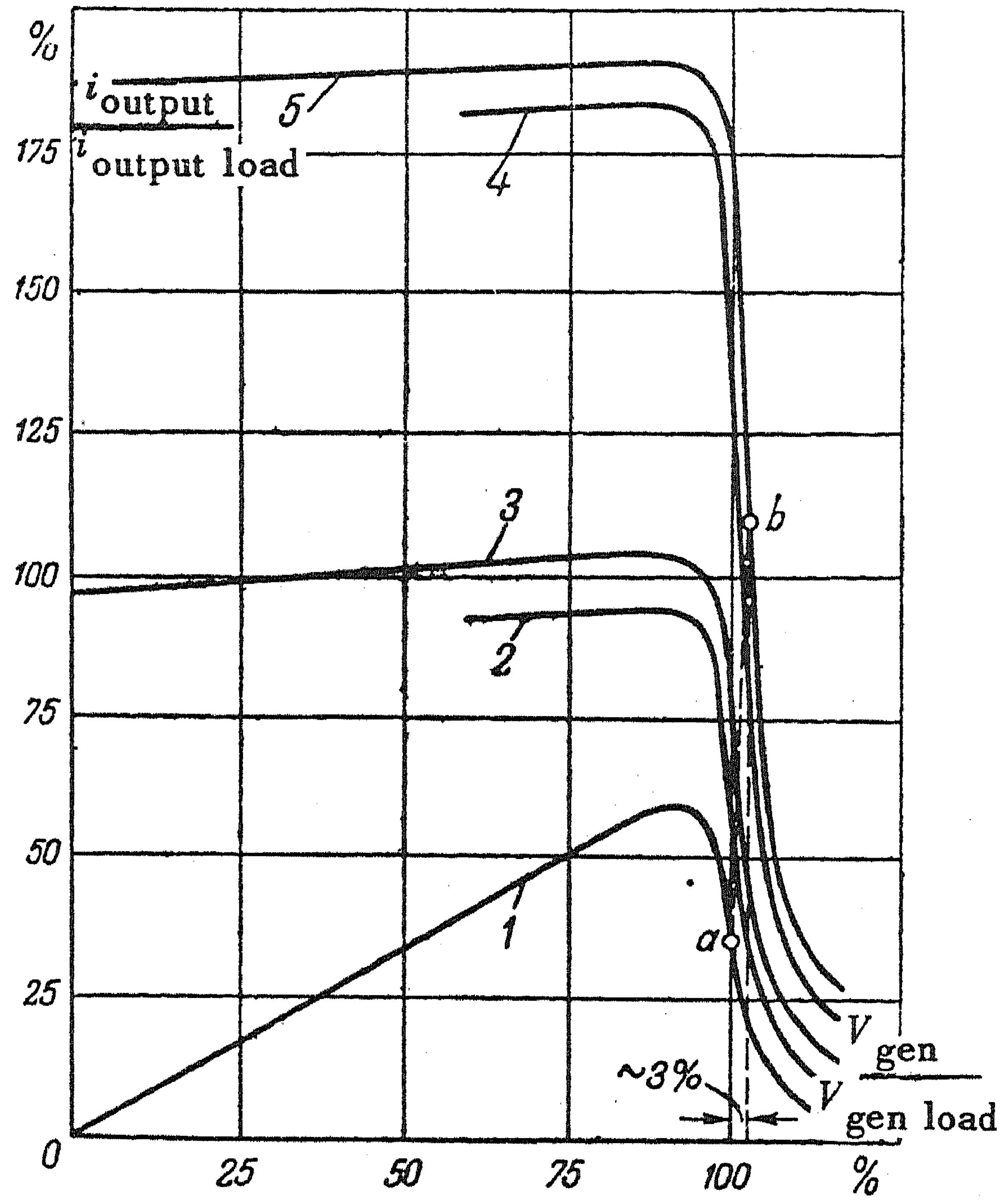

FIG. 3. The relationship between regulator output current and voltage. 1 – Generator open circuit; 2 – High power factor, $I_{gen} = 0.5\ I_{gen\ load}$; 3 – Low power factor, $I_{gen} = 0.5\ I_{gen\ load}$; 4 – high power factor, $I_{gen} = I_{gen\ load}$; 5 – low power factor, $I_{gen} = I_{gen\ load}$.

Owing to the development of a phase compound-winding circuit, the amplification coefficient of the voltage corrective device may be considerably less than for simple compound winding. In this connexion, the lag of the magnetic amplifier and control circuit of the all-mains transformer is also less than the lag in electro-magnetic voltage correctors; this increases regulation stability. In this case, there is no need for additional regulator stabilization appliances; this simplifies the regulator circuit and still further increases the difference between its speed of action and that of the electro-magnetic correctors at present in use, in which a flexible negative feed-back (a stabilizing transformer) slows down the regulation.

The resultant regulator working characteristics are given in Fig. 3 for various generator states. For generator short-circuit and low loads, automatic regulation is accomplished by voltage compound winding (curve 1). The relationship between the regulator output current and the generator voltage, load current and power factor is characterized by a set of curves (2-5), from which it is clear that generator excitation increases with reduction of the power factor.

The spring feed-backs from the stator current and the regulator output current necessary for adjusting the regulator to the required statism and also for increasing the accuracy of the voltage regulation are provided in the regulator circuit (Fig. 1). In installations where very high voltage correction accuracy is not required, the stator current feed-back need not be used. In addition, it is possible to amplify or weaken the magnetic amplifier internal positive feed-back by using the normal additional external feed-back from the amplifier output current (not shown in Fig. 1).

Additional magnetic amplifier feed-back alters the steepness of the characteristics in Fig. 3. Increase in accuracy, and also decrease in regulation stability, correspond to the increase in steepness, which is limited by the possibility

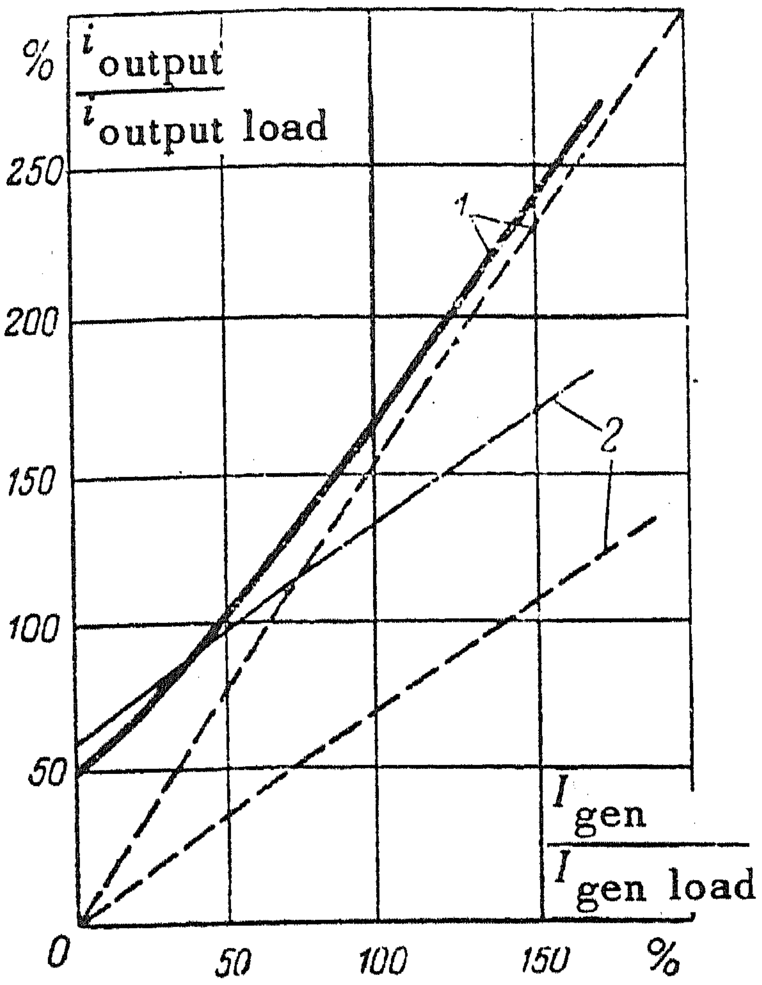

FIG. 4. Relationship between regulator output current and stator current in forcing conditions for steady reduction of 15 per cent in voltage (unbroken curves) and steady three-phase generator short circuit (dotted).

1 – controlled phase compound winding;

2 – normal compound winding with slow-acting electro-magnetic corrector (UK and EMK).

of a relay effect. Feed-back from the stator current is connected with polarity such that curves (2-5) are displaced to the left of curve 1.

In the case of feed-back from the stator current, the feed-back from the regulator output current is connected with polarity such that curves 1-5 are displaced to the right and their steepness increased. Here, accuracy of voltage correction increases with changes in the frequency and heating of the generator and exciter. Feed-back from the regulator output current also changes the phase sensitivity of the regulator; here the high and low power factor curves are displaced vertically in relation to one another.

The type of feed-back is selected when adjusting the regulator with respect to the generator and exciter parameters and the voltage correction requirements.

It is also clear from Fig. 3 that the regulator described without additional feed-backs can easily ensure adjustment with regative statism.

For example, if the regulator output current is altered, in different generator conditions, between open circuit and full load with a low power factor, the negative regulation statism between values *a* and *b* is about 3 per cent. In order, for example, to produce positive regulation statism, it is necessary for curves (2-5) to be displaced to the left of curve (1). This can be achieved by feed-backs.

It should be emphasized that the widespread idea that positive statism is necessary is based on the premise that a regulator setting of that sort ensures parallel working stability. Meanwhile we know that, from the point of view of maintaining constancy of voltage at the receiving terminal, it is most expedient to use a negative statism setting for automatic voltage regulators. The existence of the equalizing connexions, described below, enables us to recommend the negative statism adjustment of regulators as being more correct in principle; this adjustment is easily achieved without introducing any additional equipment into the circuit.

Positive statism adjustment is easily achieved, on the other hand, in regulators of the compensator type, reacting to differences in the quantity being regulated. To create negative statism, essentially, a regulator compound winding is used; this, however, requires additional equipment.

Fig. 4 shows the forcing capacity characteristic of a regulator at generator voltage drops of 15 and 100 per cent (short circuit). Similar characteristics for a type UK-EMK regulator are plotted for comparison (simple compound winding with an electro-magnetic voltage corrector), on the assumption that, in the second case, the component of the resultant regulator current determined by the corrective device for a rated generator state, is 30 per cent. It is clear from Fig. 4 that the forcing capacity of the regulator being described is considerably higher. This is associated with the fact that it is necessary for this regulator, at rated voltage, other things being equal to take an all-mains transformer coefficient of transformation such as to compensate the field effect, which may be regarded as an additional transformer error. Therefore, with a drop in voltage, when the transformer magnetization is sharply reduced, the compounding coefficient quickly increases; this is a feature characteristic of controlled compound winding circuits.

The increased forcing capacity, which has been indicated for the regulator described, makes the reactive load distribution stability condition more difficult, when generators are working in parallel. In order to achieve reliable stability, particularly for the generator voltage bus-bars when they are working in parallel, it is desirable that there should be an equalizing coupling between the generators working in parallel. This is achieved by the parallel connexion, either directly or through a spacing transformer, of sections, of the secondary windings themselves, of the all-mains transformers. In many cases, this circuit is more expedient than the use of equalizing connexions between the excitation circuits. In the proposed circuit, the excitation circuits are not electrically connected, and the possibility of using the coefficient of transformation in the equalizing circuit enables us to operate various types of generator in parallel. The elasticity of the equalizing coupling can be regulated at will by a small impedance connected in series.

It is possible, for low voltage generators, to confine ourselves to only one equalizing conductor between the primary (parallel) windings of the all-mains transformers on the choking coil side (Fig. 1a), since in this case the equalizing coupling closes the primary commutation circuit of the generators working in parallel.

It should be pointed out that the compound winding and voltage correction circuit described, is very valuable for self-exciting synchronous generators. In this case, in order to ensure the necessary compound winding capacity, all-mains transformers may be connected to the three phases. If additional frequency correction is not applied, the voltage corrector may be still more simply constructed in the form of a saturable choke and rectifier. The choke is connected to the generator through a step-down transformer. The core of the choke should preferably be of permalloy (a type UTT-6 current transformer is used as the choke in the regulator we have constructed), but satisfactory results may also be obtained when using high quality electrical engineering steel. In this circuit the corrector is practically without inertia.

For comparatively powerful generators, controlled phase compound winding may be combined with uncontrolled phase compound winding, ensuring 70-80 per cent of the required excitation capacity. This makes it possible greatly to reduce the size of the all-mains controlled phase compound-winding transformers.

Basic relationships

Let us examine the steady working conditions for a phase compound winding circuit with all-mains transformers, assuming as a preliminary that the compound winding is uncontrolled.

Using the super-imposition principle, we can find the current in the secondary winding of the all-mains transformer:

$$I_2 = \sqrt{I_{2k}^2 + I_{2kh}^2 + 2 I_{2k} I_{2kh} \cos \gamma}\ , \tag{1}$$

where I_{2k} and I_{2kh} are the currents in the transformer secondary winding for short circuit (at the specified stator current and open circuit conditions, and γ is the angle between the currents I_{2k} and I_{2kh}.

Currents I_{2k} and I_{2kh} are determined as follows :

$$I_{2k} = \sigma_k \ I_1 \omega_{i1}/\omega_{2e} ;\ I_{2kh} = \sigma_{kh}(V/z_e)/(\omega_{u_1}/\omega_2) \tag{2}$$

where I_1	is the current in the all-mains transfomer primary winding,
V	is the generator voltage (Fig. 1a), or the voltage on the secondary side of the compensator (Fig. 1b),
σ_k and σ_{kh}	are coefficients allowing for the all-mains transformer current errors for generator short-circuit and open circuit conditions,
ω_{i1}, ω_{v1}, ω_2	are the number of turns in the series and parallel primary windings and the secondary (output) winding of the all-mains transformer,
ω_{2e}	is the equivalent number of secondary winding turns in short-circuit conditions (taking into account the effect of the primary parallel winding),
z_e	is the equivalent resistance of the compound winding circuit due to voltage in open circuit conditions.

The values of ω_{2e} and z_e are determined from the following equations:

$$w_{2e}=\sqrt{w_2^2+\left(\frac{r_v'}{\nu_k z_n}\right)^2+2w_2\frac{r_{\text{в}}'}{\nu_\kappa z_n}\cos\xi}\,; \tag{3}$$

$$z_e=\sqrt{\left(r_n+\frac{r_v'}{kh}\right)^2+x_n^2}\,, \tag{4}$$

where

$$r_v'=\frac{\beta_i}{\beta_u}\ \mathrm{x}\ \frac{\omega_{u1}^2}{\omega_2^2}\,r_v\,,$$

the load resistance at the output side of the compound winding circuit, reduced to the number of windings in the all-mains transformer primary parallel winding (β_i and β_u are relationships of the mean rectified current and voltage values to the effective values for alternate current and voltage at the rectifier);

$\bar{z}_n = r_n + jx_n$, the resistance in the all-mains transformer primary parallel winding circuit,

ξ is the difference between the impedance angles of the all-mains transformer primary parallel winding circuit and secondary winding circuit,

and ν_k and ν_{kh} are coefficients allowing respectively for the difference between the different voltage drops in the all-mains transformer secondary and primary parallel windings and the transformer voltage error in open circuit conditions.

The current fed to the all-mains transformer primary parallel winding circuit in generator short-circuit conditions is determined by the equation:

$$I_{nk} = (r_v/z_n)\,(\omega_2/\omega_{u1})\,I_{2k} \tag{5}$$

Fig. 5 gives the vector diagram for the case where an all-mains transformer is connected with the difference in currents between two generator phases and its linear voltage. The direction of the vector I_{2kh} is determined by the impedance angle ψ of the equivalent resistance z_e, the direction of the vector I_{2k} by the angle a which allows for the angular error of the all-mains transformer as regards the current reaching its primary parallel winding circuit (the direction OM is parallel to the vector $I_{1a} - I_{1b}$).

When the angle π alters, the end of the vector I_2 moves along the time curve which represents a circle of radius I_{2k}, its centre lying at the ends of the vector I_{2kh}.

The basic relationships of the linearized phase compound winding circuit which have been obtained can also be applied to controlled compound winding with the proviso that the magnetic state of the all-mains transformer is specified,

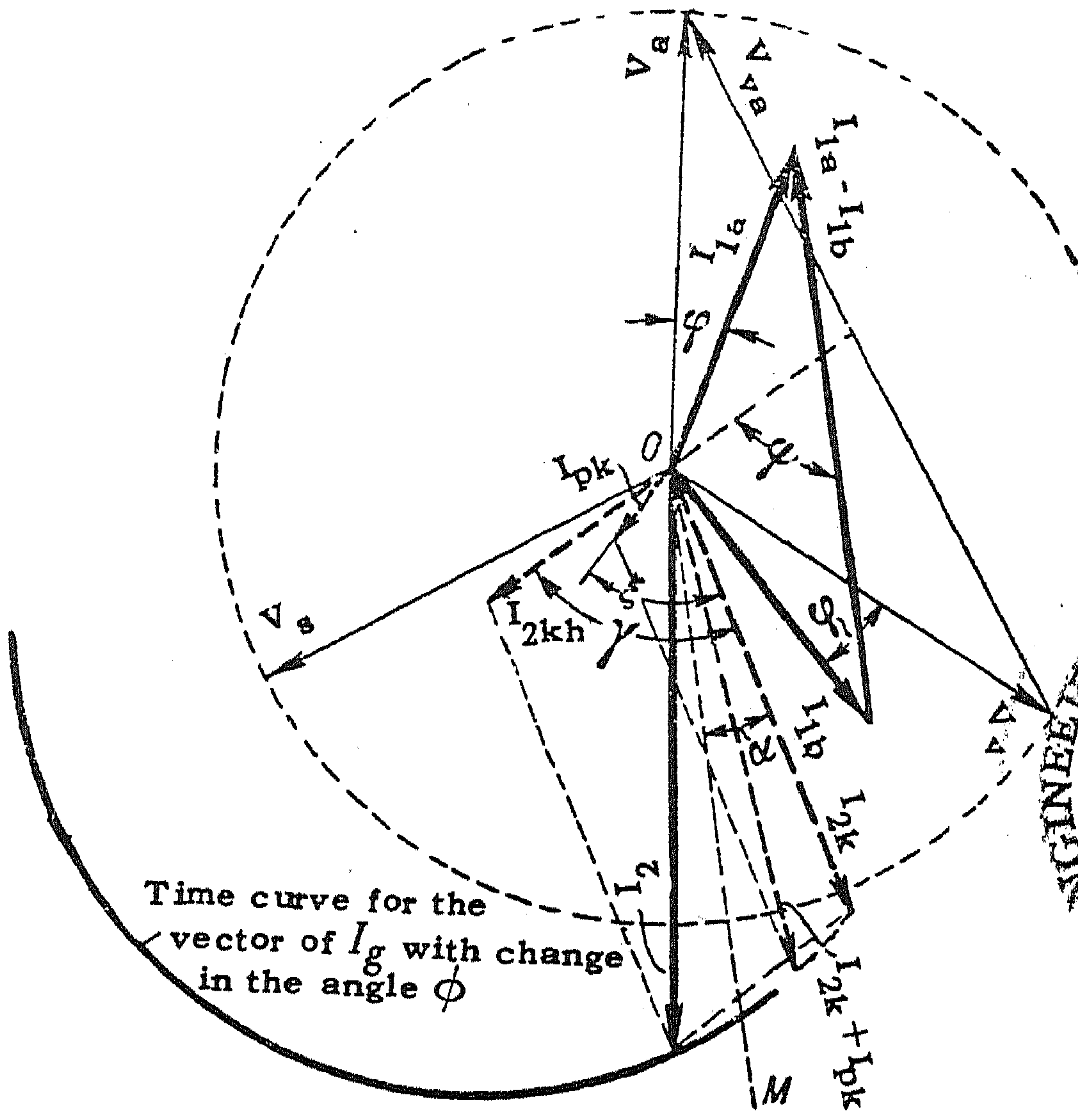

GUINDY
LIBRARY BOOK
No.
COLLEGE OF ENGINEERING

FIG. 5. Phase compounding vector diagram.

taking into account the constant magnetization corresponding to the specific generator voltage. The values of the parameters σ_k, σ_{kh}, ν_k, ν_{kh}, ψ and α must correspond to the given regime.

The sensitivity of the phase compound winding circuit $dI_2/d\phi$ depends on the correlation of the currents I_{2k} and I_{2kh} and the initial phasing angle, generally equal to $\gamma + \phi$. For each phase compound winding circuit this angle is a constant quantity.

On increase of this angle, the phase sensitivity rises, but, as analysis and tests showed, where the initial phasing angle exceeded 90° there was intensification of the undesirable non-linearity of the synchronous generator external characteristics, when loaded at a high power factor. It is expedient, therefore, to limit the initial phasing angle roughly between 70° and 110°.

Phase sensitivity is still not unduly lowered at the lower limit, and at the upper limit the non-linearity of synchronous generator external characteristics is within the tolerated limits.

A phase compound winding-circuit sensitivity ensuring that the external characteristic of the generator being regulated is independent of the power factor may be called normal. For astatic adjustment of a circuit for the automatic regulation of excitation, the phase sensitivity must approximate to the normal value. If adjustment with negative statism is being made (back regulation, to compensate for the voltage drop in the circuit supplying the consumer), it is expedient to have phase sensitivity above normal. Then the negative statism will be higher with inductive generator loading and with lower operating load; this is a requisite for

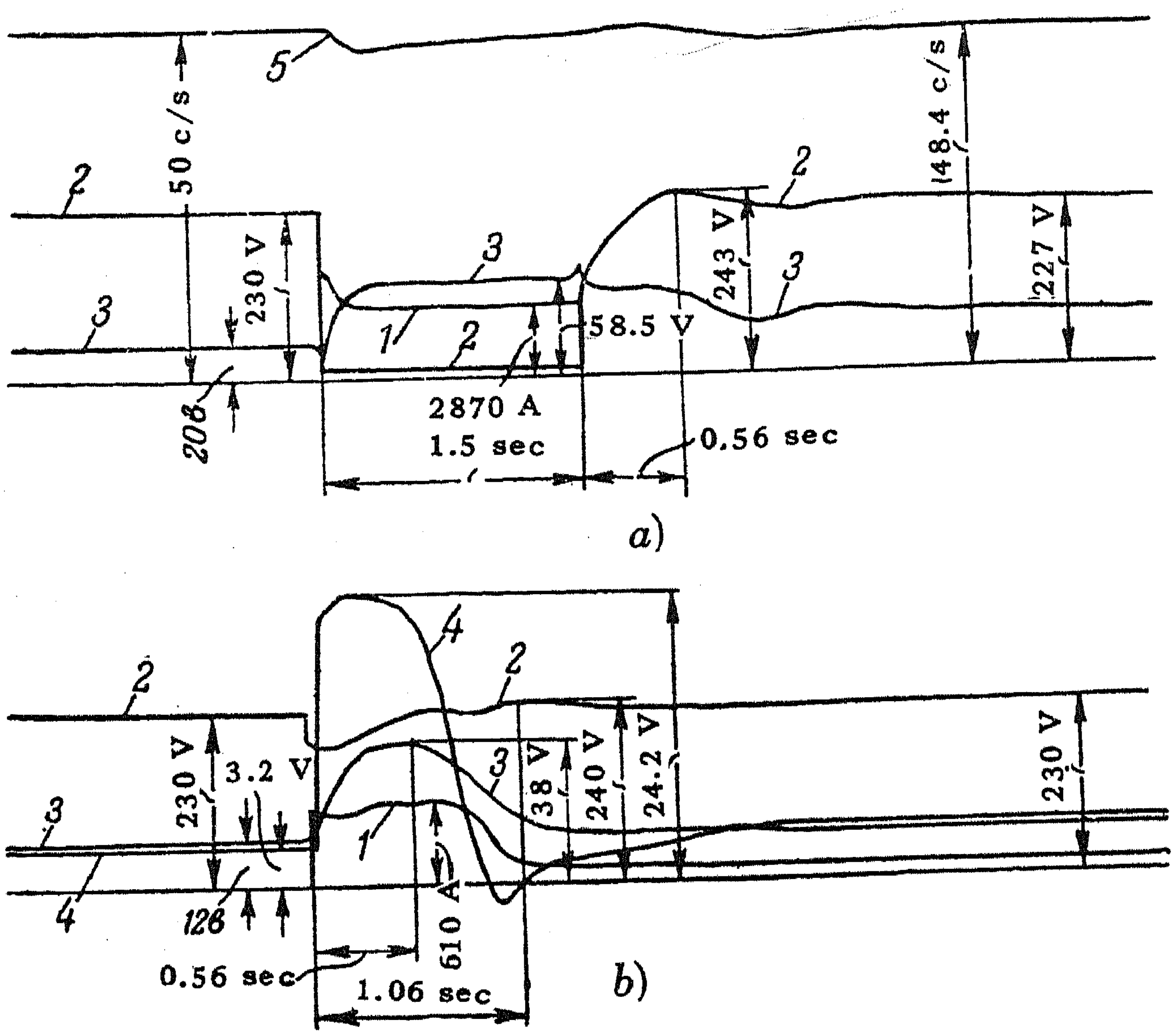

FIG. 6. Oscillograph recording of transitional processes.
(a) three-phase short circuit of MS-126-4 generator;
(b) short-circuited induction motor started from MS-126-4 generator, engine power about 30 per cent of generator power.
1 – generator current; 2 – generator voltage; 3 – generator excitation voltage; 4 – generator exciter excitation voltage; 5 – frequency.

obtaining a better approximation of astatic characteristics at the consumer's end or at a nodal point in the circuit.

Test results

Production models of the regulator were made according to the controlled phase compound winding circuit described. The Electrical Engineering Institute of the Ukr. S.S.R. Academy of Sciences assisted by the "Elektroprivod" (Moscow) Central Design Bureau, tested the regulators on MS-126-4 (150 kW) and MS-92-4 (50 kW) synchronous generators working separately and in parallel.

The external characteristics of the generators being regulated deviated with wide variations in the power factor between 0.1 and 0.8 (inductive load), by not more than ± 1 per cent from the mean value. Adjustment corresponded to a negative statism of 1 - 2 per cent. The phase sensitivity of the compounding circuit was above normal, since with low power factors, the negative statism was higher than with high power factors.

The generator operation was extremely stable when working in parallel, where there were equalizing couplings. Opening the equalizing coupling shortly disrupted the stability in an aperiodic manner, one of the generators passing to

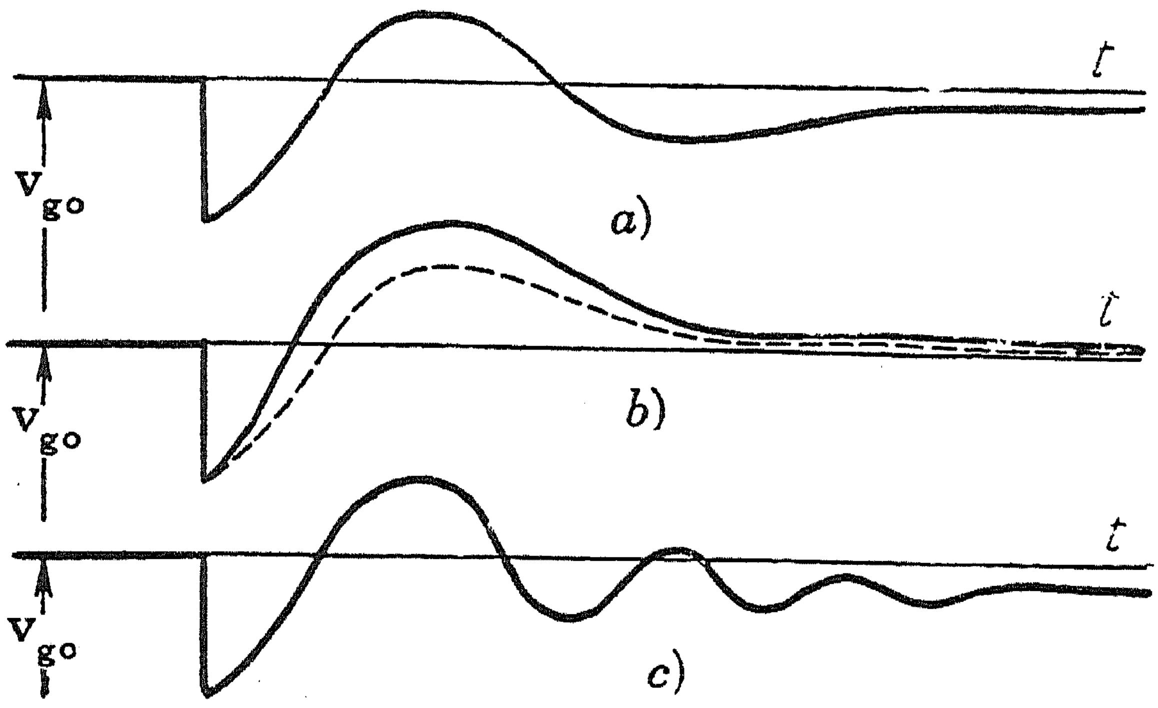

FIG. 7. Typical transitional processes in a circuit with weak damping without special equipment for changing statism (generator and exciter).
(a) compensation type regulator with artificial damping.
(b) controlled compound winding without artificial damping.
(c) compensation type regulator without artificial damping.

conditions with a capacitive power factor.

Oscillograph recordings were made of the transitional processes when static loads (about 50 and 100 per cent of the rated power of a generator with high and low power factors) were cut in and out, when starting short-circuited induction motors (about 30 and 90 per cent of the generator rated power), and for a number of generator short-circuits lasting for up to 1.5 sec.

Oscillograph recordings, for cases of the short-circuiting of a 150 kW generator and the starting of an induction motor connected to that generator, are given in Fig. 6; it is evident from these that the regulator ensures high-speed action and that the transitional processes are of a favourable nature. The low regulator lag is typified by the fact that the voltage at the regulator output (at the exciter shunt excitation winding) rose practically simultaneously with the stator current, and then in addition rose, owing to the removal of the excitation of the corrector, to maximum value in about 0.2 sec.

Tests made on a 50 kW generator with self-excitation through a regulator of the type described showed that the nature of the transitional processes is still more favourable in this case.

Fig. 7a shows the change in voltage when a static load is applied to a generator fitted with a compensation voltage regulator, with positive regulator statism and no special equipment for altering the statism. Fig. 7b shows a similar transitional process for the regulator described with natural negative statism. We can see from comparison of the curves that, in the second case, the first normal regulated voltage value is reached quicker, and the nature of the transitional process is more favourable.

Where sufficiently effective means of damping, which complicate the design of compensation regulators, are not available, the transitional process shown in Fig. 7c is typical of these regulators; here, the time for the first restoration of voltage is somewhat shorter, but the oscillations are more intense.

The transitional process on reduction in the compound winding coefficient is shown by the dotted line in Fig. 7b. Here the over-regulation is reduced, but so is the forcing capacity of the regulator. It should be emphasized that over-regulation for a single shock, and the consequent sufficiently fast aperiodic steadying of the conditions, may be regarded, when we consider the essential factors which make the post-shock conditions more difficult, as a favourable form of transitional process. Such factors are respective loads, for example, the alternate running of motors, changes in the slip of induction motors(which are braked on initial reduction of voltage and accelerated when it is subsequently restored) etc.

The considerations set forth were well supported by the tests. In particular on eliminating the short circuit of a 150 kW generator running idle, the over-regulation was 19.5 per cent of the rated voltage, but when a loaded 40 kW induction motor had previously been connected, this over-regulation was reduced to 5.6 per cent (Fig. 5a). Similar tests were successfully carried out on a MS-1250-750 (1000 kW) generator. A regulator constructed according to the circuit in Fig. 1b was tested on a 25 MW type T2-25-2 turbo-generator.

Translated by J.H. Dixon

REFERENCES

1. N.I. Sokolov and N.V. Chernobrokov; Kompaundirovanie vozbuzhdeniia sinkhronnykh generatorov v Mosenergo (The compounding of synchronous generator excitation at Mosenergo), *Elektricheskie stantsii,* 4, 5 (1946).
2. I.I. Kodkind; Reguliator napriazheniia dlia kompaundirovannykh sinkhronnykh generatorov (A voltage regulator for compounded synchronous generators), *Elektricheskie stantsii,* 4, 5 (1946).
3. V.L. Inosov and L.V. Tsukernik; Kompaundirovannoe vozbuzhdenie sinkhronnykh generatorov s elektromekhanicheskym korrektorom napriazheniia(The compounded excitation of synchronous generators with an electro-mechanical voltage corrector) *Elektricheskie stantsii;* 4, 5 (1946).
4. L.V. Tsukernik; Metodika rascheta kompaundirovaniia sinkhronykh generatorov s elektromekhanicheskym korrektorom (The procedure for calculating the compounding of synchronous generators with an electro-mechanical corrector) *Sborn nauch-tekhnich. statei elektrotekh. Akad. Nauk. Ukr. S.S.R.,* No. 1 (1948).
5. G.R. Gertsenberg; Avtomaticheskie reguliatory napriazheniia sistemy VEI (VEI system of automatic voltage regulators) *Sborn. "Avtomatika i telemekhanika v energosistemakh"*, Gosenergoizdat (1950).
6. S.B. Iuditskii; *Sinkhronnye mashiny s poluprovodnikovymi vypriamiteliami (Synchronous machines with semiconductor rectifiers),* Gosenergoizdat (1954).
7. H.F. Storm; A static magnetic exciter for synchronous generators, *Trans. Amer. Inst. Elect. Engrs.* 70 (1951).

8. A. Lang; Samoreguliruemye sinkhronnye generatory bez mashinnykh vozbuditelei (Self-regulating synchronous generators without mechanical exciters), *ETZ-A* 10 (1955).
9. P.A. Meshchaninov; Fazovaia skhema kompaundirovaniia s elektromagnitnym korrektorom (A phase compounding circuit with electro-magnetic corrector), *Elektricheskie stantsii,* 4 (1955).
10. N.A. Nechaev; Avtomaticheskii reguliator vozbuzhdeniia dlia generatorov maloi energetikoi (An autcmatic excitation regulator for low power generators). *Energetik,* 12 (1955).

TRANSISTOR AMPLIFIERS OF THE ALLOY TYPE *

A.A. MASLOV

(Received 23 September 1957)

An ordinary flat transistor amplifier consists of two electron- or hole-conducting junctions, situated in a single monocrystal and separated by a distance w; this distance should be considerably less than the diffusion length at the non-base carriers in the middle region. If a triode is made in such a way that an electron semiconductor, conventionally denoted by n, is fixed in the middle and a hole semiconductor, denoted by p, on the sides, then such a triode is called a *p-n-p* type as opposed to the triode of the *n-p-n* type, in which the mid section is the hole type of semiconductor. As is generally known, the semiconductor amplifier is connected in a circuit in such a way, that a forward biased voltage is applied to one junction; this junction is called the emitter junction. To the other junction a reverse biased voltage is applied; this junction is called the collector. The mid-part of the triode between the two junctions is called the base or the base region.

The circuit of a *p-n-p* triode is shown on Fig. 1. Consider the mode of operation of the *p-n-p* type amplifier. The emitter is biased on the forward direction and in certain conditions it will cause the injection of holes into the base region. Since the width of the base w is considerably less than the diffusion length of the holes in this region, the holes injected into the n region will be diffused to the collector and only a part of them will recombine with electrons in the base layer. The collector is biased in the reverse direction; the electric field is in such a direction that it will attract holes which entered in the base region. Consequently, these holes will reach the output network of the collector and produce the current of the output signal. If the value of the emitter current varies, the value of the current in the collector network will vary as well. Usually triodes are constructed in such a way that a considerable part of the emitter current enters the collector network. Therefore we can assume that the change in the emitter current is approximately equal to the change in the collector current, i.e.

$$\Delta I_e \approx \Delta I_c .$$

* *Electrichestvo* No. 2, 46-51, 1958 [Reprint Order No. EL 52].

Since the collector junction has a reverse bias and consequently a high load impedance, the change of current in the collector occurs in a network of high resistance, and this will produce a large change of voltage, tens of times greater than the change of the voltage in the emitter network, which produced the change in the emitter current. As a result, there will be a voltage and power gain, which can be taken from the load resistance. To get a good gain it is necessary that ΔI_c should differ from ΔI_e as little as possible. The ratio $I_c/I_e = a$ is called the current amplification or current gain of a crystal triode. The current amplification depends on the quantities given below.

1. Emitter efficiency

The current flowing through the emitter junction has two components: the hole, and the electron components. In amplifying operations of the *p-n-p* triode only the hole component of the current takes part. The ratio of the change of the hole component (ΔI_{eh}) to the total emitter current (ΔI_e) is called the emitter efficiency and is designated γ. Obviously

$\gamma = \dfrac{\Delta I_{eh}}{\Delta I_e}$. By simple calculations we can find that $\gamma = 1 - \dfrac{w\sigma_b}{L_e\sigma_e}$

where σ_b is the base region conductance

σ_e is the emitter region conductance, and

L_e is the diffusion length of the non-base hole carriers in the emitter region. In order that γ should be near to unity it is necessary that

$$w\,\sigma_b \ll L_e\,\sigma_e\,.$$

2. The ability of the base region to transfer the holes leaving the emitter to the collector (β)

This quantity is determined as the ratio of the change of the hole component of the collector current to the change of the hole component of the emitter current,

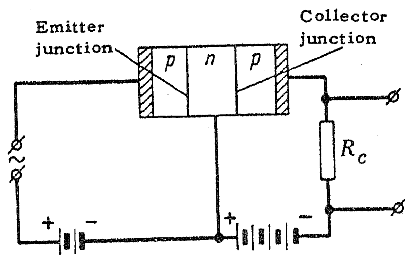

FIG. 1. *p-n-p* triode in a common base network

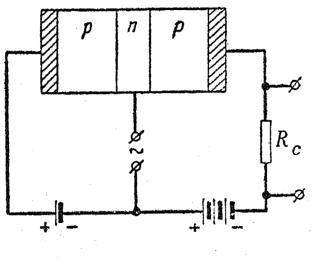

FIG. 2. *p-n-p* triode in a common emitter network

$$\beta = \frac{\Delta I_{eh}}{\Delta I_{eh}}$$

The losses in the base are caused by a partial recombination of holes with electrons. Obviously, to keep β near to unity it is necessary that $w \ll L_h$. The value of β can be calculated from the expression:

$$\beta = \frac{1}{\cosh\,(w/L_d\,)}$$

3. Collector efficiency a

The holes which have entered the collector region come under the influence of the accelerating field and can cause an avalanche process of hole increase. For the flat alloy triodes normally $a^* = 1$.

The current gain will be determined by the product of the three above-mentioned factors $a = \gamma\, \beta\, a^*$. We have neglected here possible losses in the outer network and the influence of the frequency on the amplifying properties of the triode. Therefore, a will be the current gain for low frequencies and for the short-circuited collector junction. The factor a is an important physical characteristic of a triode and does not depend on the method of connexion in the circuit. The current gain for real circuits will be different. The circuit in Fig. 1 is called the circuit with a common base. This circuit has a small input and a large output resistance. The current gain of this circuit is less than a. This is true only for a short-circuited collector junction, i.e. when $R_c = 0$, $K_i = a$. Two other methods of connecting a triode are possible. Fig. 2 shows a triode with a common emitter. This is characterized by large input and output resistances. Input and output voltages are of the opposite phase. This circuit gives the largest amplification. The factor K_i for $R_c = 0$ has the value

$$k\,\frac{a}{1-a}\,.$$

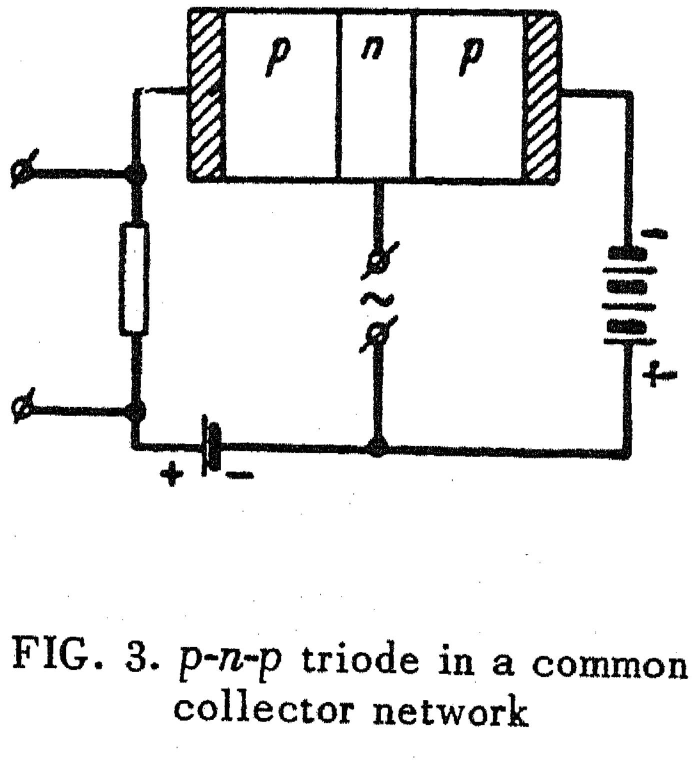

FIG. 3. p-n-p triode in a common collector network

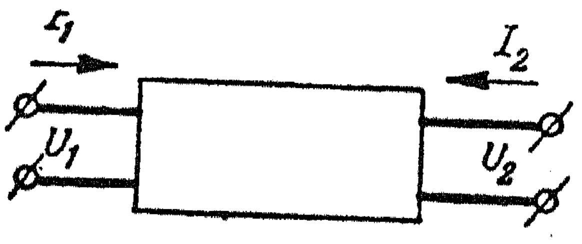

FIG. 4. Four-terminal network

Since normally $a > 0.9\ K_i$, is large, this circuit is mainly used for flat apparatus. In Fig. 3 we see a circuit with a common collector. It has high input and low output resistance. The current gain for $R_c = 0$ is

$$k_i = \frac{1}{1 - a}\ .$$

Omitting discussion of the processes occuring inside the triode we can consider it as an active four-terminal network, whose diagram is shown in Fig. 4. To describe the influence of such a four-terminal network on the external network it is necessary to know four quantities: input (U_1) and output (U_2) voltages, and input (I_1) and output (I_2) currents. Obviously, we can consider any two of these quantities as independent variables, and two other as dependent, which are determined by the independent variables and by the parameters of the four-terminal network.

We assume that $U_1 = f\,(I_1)$ and $U_2 = f\,(I_2)$. A change in the current by $\Delta\, I_1$ and $\Delta\, I_2$ will cause a change of voltage ΔU_1 and ΔU_2, hence

$$\Delta U_1 = \frac{\partial U_1}{\partial I_1}\,\Delta I_1 + \frac{\partial U_1}{\partial I_2}\,\Delta I_2; \tag{1}$$

$$\Delta U_2 = \frac{\partial U_2}{\partial I_1}\,\Delta I_1 + \frac{\partial U_2}{\partial I_2}\,\Delta I_2. \tag{1a}$$

If we assume that changes of currents and voltages are small in comparison with values U_1, U_2, I_1, I_2, and this is valid for low signal levels, then the assumption of the linear dependence of ΔU_1, ΔU_2 on ΔI_1, and ΔI_2 is justifiable; consequently

$$\frac{\partial U_1}{\partial I_1} = Z_{11};\quad \frac{\partial U_1}{\partial I_2} = Z_{12};\quad \frac{\partial U_2}{\partial I_1} = Z_{21};\quad \frac{\partial U_2}{\partial I_2} = Z_{22}.$$

Then equation (1) will be:

$$\Delta U_1 = Z_{11}\Delta I_1 + Z_{12}\Delta I_2; \tag{2}$$

$$\Delta U_2 = Z_{21}\Delta I_1 + \Delta Z_{22} I_2. \tag{2a}$$

These four resistances determine entirely the behaviour of the triode in a circuit. There is no difficulty in finding these resistances by direct measurement. Using the values of these resistances and solving the equations for the four-terminal network, we can determine the current and power gain of the triode in any circuit in which it may be connected.

To find the value Z_{11} it is necessary that I_2 should be equal to zero, i.e. it can be measured with the open circuit output. To determine Z_{12}, we measure ΔU_1 and ΔI_2 with the open-circuit input. In exactly the same way, having measured ΔU_2, ΔI_1, and ΔI_2 with the open-circuit input and short-circuited output, we can determine Z_{21} and Z_{22}. Therefore, this network is called a network of no-load operation, or briefly, a network of Z-parameters. Its disadvantage consists in using the short-circuited output. But usual conditions of operation are near to short-circuit conditions at the output, since the collector junction resistance is large in comparison with the load resistance. Moreover, at high frequencies, the collector capacitance becomes appreciable, and it is difficult to realize no-load conditions. It is more convenient to use a network of admittances, determined by the following equations of the four-terminal network.

$$\Delta I_1 = y_{11}\Delta U_1 + y_{22}\Delta U_2;$$
$$\Delta I_2 = y_{21}\Delta U_1 + y_{22}\Delta U_2.$$

To determine y parameters it is necessary to make ΔU_1 and ΔU_2 alternately equal to zero, i.e. to produce short-circuit conditions; this method being very convenient for high frequencies. This system of parameters is called the short-circuit system or the system of y parameters. Its disadvantage consists in using a short-circuit at the input, and this does not correspond to the actual conditions in the working of a triode.

Obviously, it would be convenient to choose such parameters in such a way as to measure them in conditions of the open-circuit input and short-circuited output. For this purpose, using the assumed linear relationship of currents and voltages, we estblish the following two equations of the four-terminal network.

$$\Delta U_1 = h_{11} I_1 + h_{12}\Delta U_2;$$
$$\Delta I_2 = h_{21} I_1 + h_{22}\Delta U_2,$$

where h_{11}, h_{12}, h_{21} and h_{22} are coefficients of proportionality. Such a system is very convenient since to determine the coefficients we have to produce conditions of open-circuit input $\Delta I_1 = 0$ and of short-circuited output $\Delta U_2 = 0$; and these conditions are similar to the conditions of the normal working of the triode. Moreover, these parameters have a quite definite physical meaning:

h_{11} is the input impedance with output short-circuit;
h_{12} is the voltage feedback ratio;
h_{21} is the current amplification with output short-circuit; and
h_{22} is the output admittance with input open-circuit.

The most widely used triode made by our industry for low power radio networks is the triode model P-6. Its construction is shown on Fig. 5. This triode is a *p-n-p* type amplifier; it is made by fusion of indium into a germanium lamina of dimensions 2.3 x 2.3 mm. The original germanium has resistance of 1 – 2 Ω cm and a diffusion length $\geq$ 0.4 mm.

This triode is made in five types. Limiting operation values of these triodes are given in Table 1, and their basic electrical characteristics in Table 2. In Table 2 electrical data are given for normal operation conditions in a network with a common base.

For calculation of the output cascade stage it is necessary to know the input and output triode characteristics.

TABLE 1. Limiting values of the triodes model P - 6 at $t = 20^\circ$C.

Parameters	P6A	P6B	P6C	P6D	P6E
Collector voltage with respect to the base $U_{c\ \max}$ with $I_e = 0$ (V)	−30	−30	−30	−30	−30
Collector voltage with respect to the emitter $U'_{c\ \max}$ (V)	−15	−20	−20	−15	−20
Reverse emitter voltage $U_{e\ \max}$ with $U_b = 0$ (V)	−30	−30	−30	−20	−30
Collector current I_c (mA)	50	50	50	50	50
Emitter current (with $U_e = 5$ V) (m A)	50	50	50	50	50
Junction temperature t_j (°C)	>100	>100	>100	>100	>100
Collector dissipation $P_{c\ \max}$ (m W)	150	150	150	150	150

TABLE 2. Fundamental electrical characteristics of the triode model P-6 for $t = 20 + 5^\circ$C in the common base network.

Parameter	P6A	P6B	P6C	P6D	P6E
Output admittance (with input open-circuited) h_{22} (MΩ)	1.0	0.7	0.7	0.7	0.7
Current amplification (with output short-circuited) h_{21}	0.92	0.93	0.965	0.98	0.97
Input insistance (with output short-circuited)h_{11} (Ω)	27	27	27	27	27
Voltage feedback ratio (input open-circuited) $h_{12} \times 10^{-4}$	0.4	2.0	2.0	3.0	2.0
Collector capacitance C_c(pF)	30	30	30	30	30
Collector reverse current I_{c_0} (μA)	5	3	3	3	3
Emitter reverse current I_{e_0} (μA)	5	3	3	3	3
Temperature rise R_t (°C/mW)	0.3	0.3	0.3	0.3	0.3

Fig. 6 shows average input characteristics of the triode model P6D for $U_c = -5$ V with indication of possible deviations from mean values, and Fig. 7 shows output characteristics for the same group of triodes.

TABLE 3. Fundamental electric characteristic of the flat germanium triode model P4.

Triode model	$f\alpha$ (kc/sec)	Power gain kp (dB)	Current gain (common emitter network)	Power given to the load in class P_{out} (W)	Collector "zero" current, for $U_c = 10$ V (mA)	Voltage drop between emitter and collector for $I_c = 2$A, $I_B = 300$ mA (V)	Limiting collector voltage (common emitter network) for $U_B = 0$ (V)	Limiting collector current (A)	Limiting collector dissipation with a heat dissipating device keeping the temperature of the triode frame not over 50°C (W)	Coefficient of non-linear distortion
P4A	100	20	>5	10	$\leqslant 0,5$	—	—50	5	$\geqslant 20$	0,15
P4B	100	23	8 . . . 20	10	$<0,4$	$<0,5$	—60	5	$\geqslant 25$	0,10
P4C	100	—	>10	10	$<0,4$	$<0,5$	—35	5	$\geqslant 25$	—
P4D	100	27	10 . . 20	10	$<0,4$	—	—50	5	$\geqslant 25$	0,10
P4E	100	30	>20	10	$<0,4$	—	—50	5	$\geqslant 25$	0,10

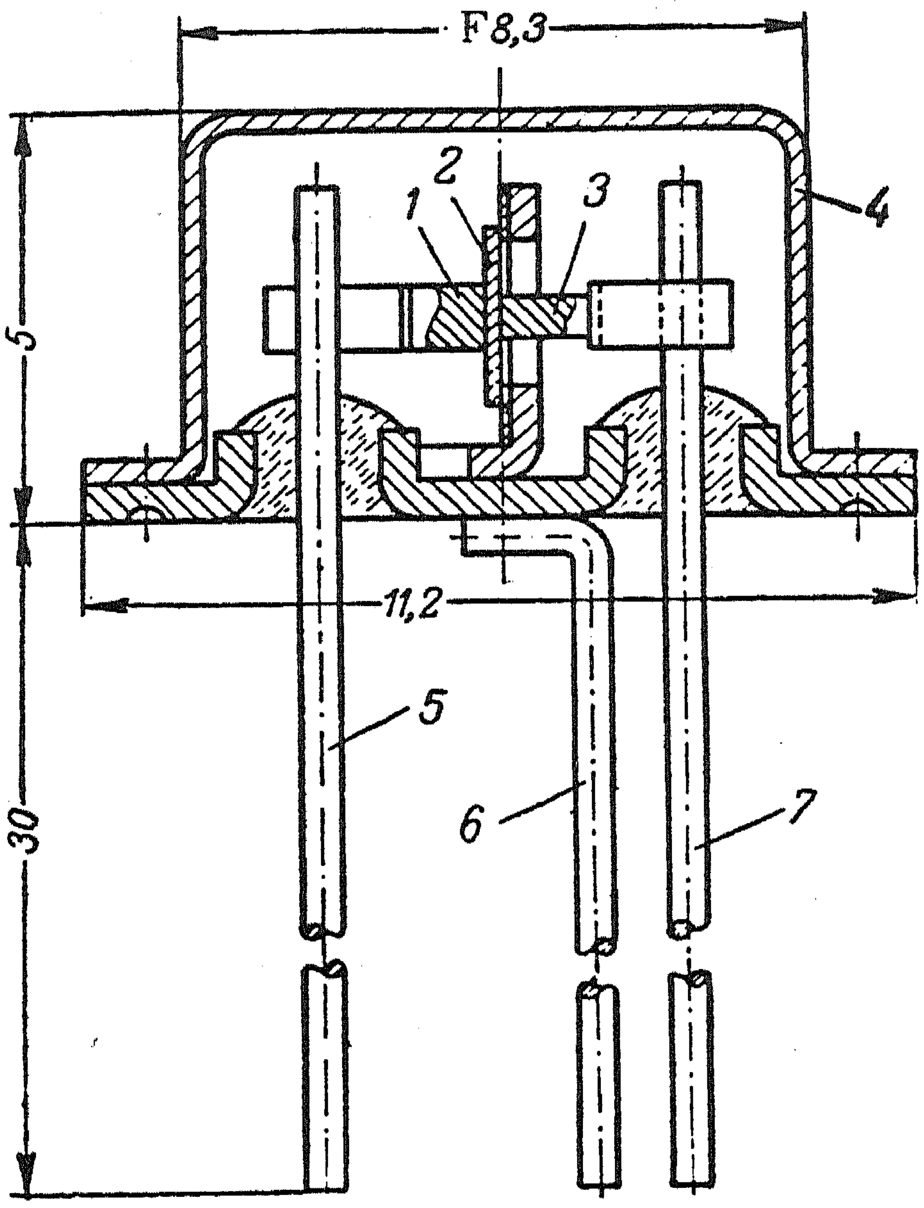

FIG. 5. Germanium triode, model P6.
1 – collector electrode;
2 – germanium crystal;
3 – emitter electrode;
4 – housing;
5 – collector;
6 – base;
7 – emitter

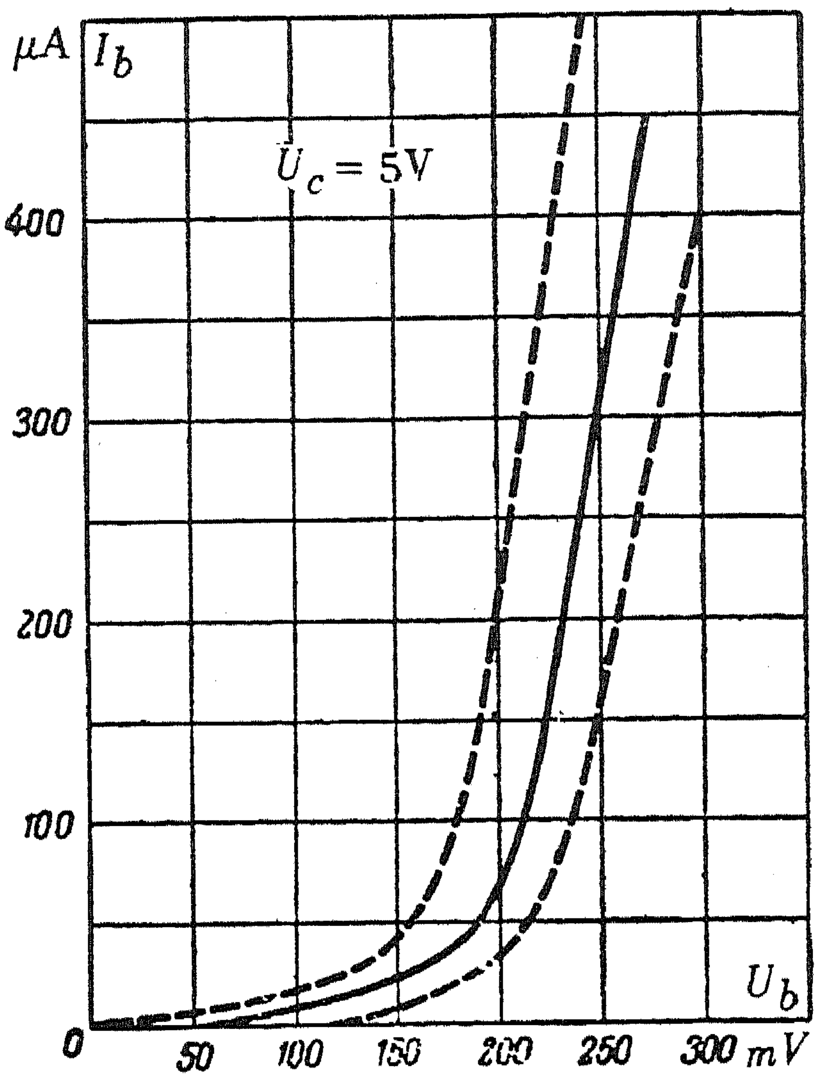

FIG. 6. Input characteristics of the P6G triode for U_c = – 5V in a common emitter network
———— – averaged parameters;
– – – minimum and maximum parameters.

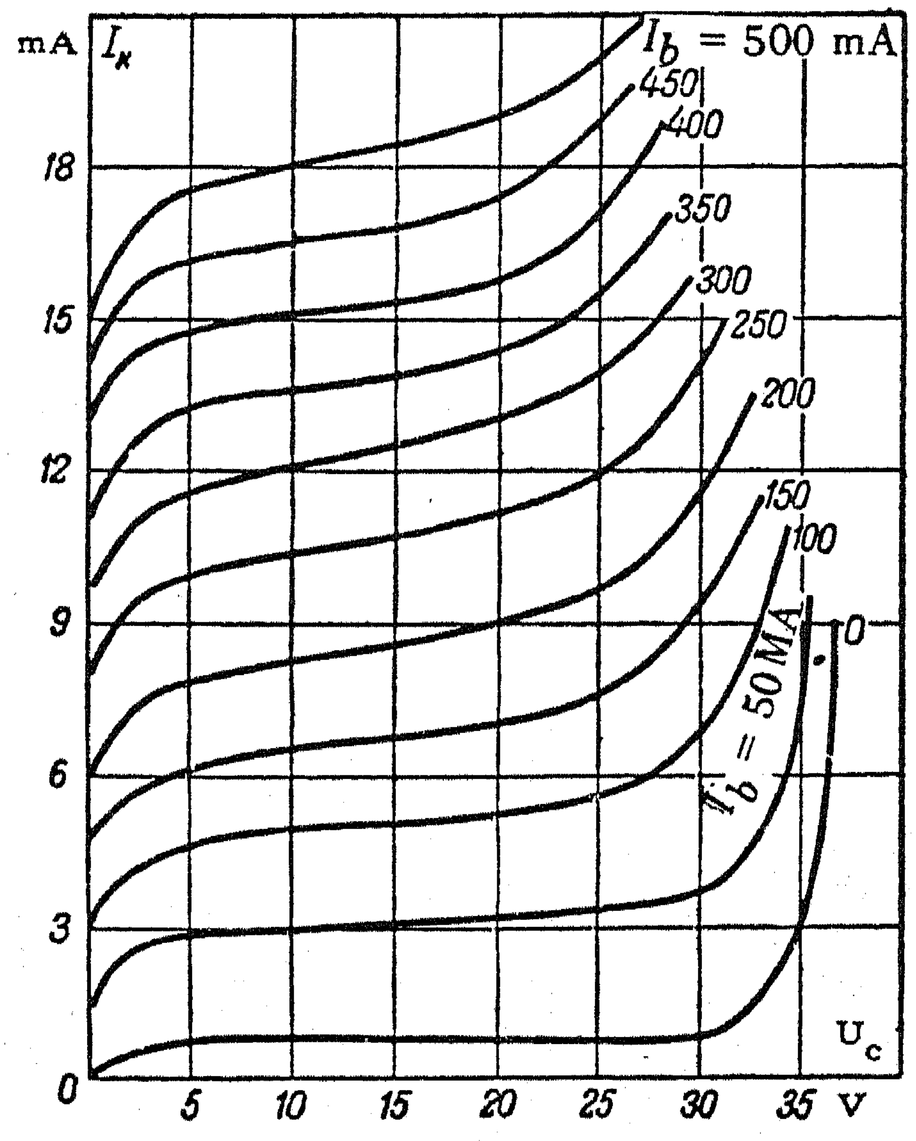

FIG. 7. Averaged input characteristics of the P6G triode in a common emitter network.

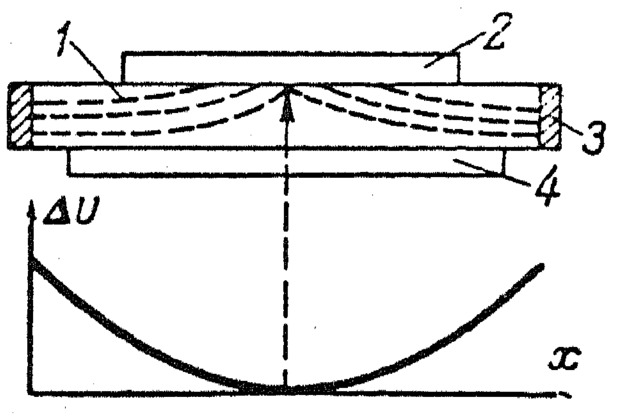

FIG. 8. Voltage drop caused by the electron current.
1 – lines of the electron current in the base;
2 – emitter;
3 – base contact;
4 – collector.

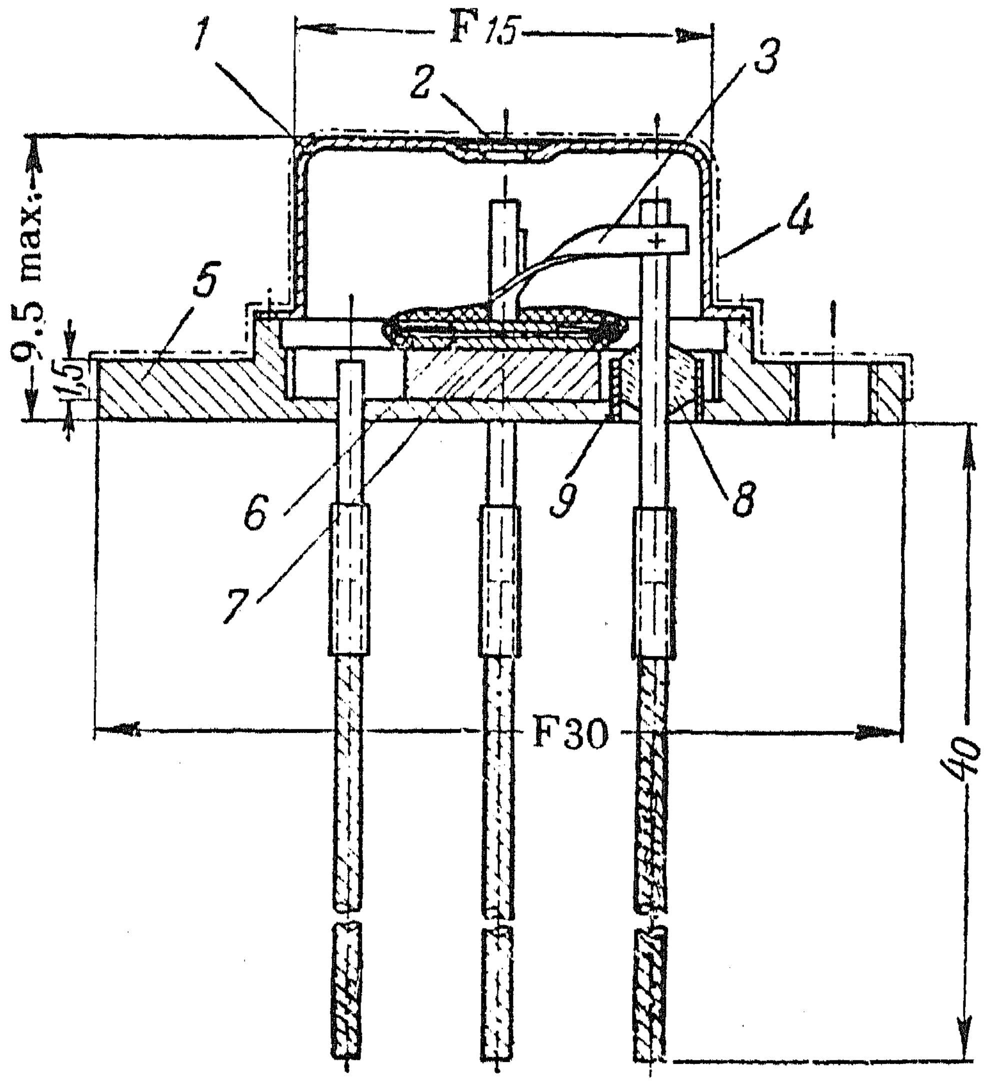

FIG. 9. Germanium triode model P-4
1 – housing;
2 – disc;
3 – lead;
4 – black paint;
5 – flange;
6 – junction;
7 – washer;
8 – insulator;
9 – tube.

Powerful semiconductor triodes

The increase in power of triodes plays an important role in widening the scope of the application of semiconductor instruments. This problem, however, meets with many serious limitations; because of this, it has yet not been possible to produce a triode of more than 100 W dissipation without forced cooling.

The main difficulty in making powerful triodes is non-uniform current distribution in the emitter. This can be explained thus: in the *p-n-p* triode base there is always, besides the hole current, flowing from the emitter and reaching the collector, an electron current as well, caused by recombination of holes in the base. This current flows in the direction from separate points of the base to the base contact and is parallel to the surface of the emitter. Since germanium has a sufficient resistance, this current creates an electric field in the base directed from the centre to the periphery. Lines of the electron current in the base and the drop in the voltage caused by the current are shown in Fig. 8. Under the influence of this field, holes leaving the emitter are pushed towards the periphery. In consequence, non-uniform emitter current distribution occurs. This phenomenon causes the lowering of the current gain in the triode.

The larger the diameters of the emitter and collector, the more important this becomes. Therefore, although increasing the power of the triode, we cannot at the same time considerably increase the electrode diameters for improving conditions of heat dissipation in the collector junction.

Using germanium with a longer life expectancy, and thus lowering the base current and bringing the emitter efficiency nearer to unity by subsituting special alloys for indium, we can reduce the value of the electron current and, consequently, reduce the non-uniformity in the emitter current distribution.

Industry produces powerful triodes of the P3 type with dissipation 3.5 W, of the P201 type with dissipation 10 W and of the P4 type with dissipation 25 W as well as other models.

Fig. 9 shows the construction of the P4 triode. Its fundamental electrical parameters are given in Table 3.

To increase the emitter efficiency, an alloy of indium with 1 per cent of gallium is used instead of indium. Since gallium has a coefficient of separation 100 times greater than indium, the addition of 1 per cent of indium reduces the resistance of *r*-germanium, formed after recrystallization, by one half. To reduce the recombination rate in the base, ordinary *n*-germanium is used with diffusion length not less than 1.2 mm.

With the elimination of factors producing non-uniform current distribution in the emitter, the production of the alloy triodes with dissipation up to 100 W is now possible.

Translated by S. Szymanski

COLLEGE OF ENGINEERING GUINDY
LIBRARY BOOK
No.

A STUDY OF THE SYNCHRONIZATION PROCESS IN COMPOUND EXCITED MOTORS *

V.L. INOSOV and V.E. KRUTIKOVA

(Received 7 February 1957)

In the processes of starting and synchronizing a synchronous motor, the major role is played by the damping cage, the design of which must be based on analysis of the motor synchronization process. The present paper gives the results of a study of the synchronization process in compound excited motors [1,2]; they may also be extended to other types of compound synchronous motor.

The motion of the rotor of a synchronous machine is described by the non-linear differential equation:

$$\frac{M}{\omega}\delta'' + \frac{D(\delta,\delta')}{\omega}\delta' + P_e(\delta,\delta') = P_0, \tag{1}$$

where

δ is the angle of lag of the rotor;

M is the constant of inertia of the rotor, in sec;

D is the damping coefficient in relative units, which is a function of the angle and its first differential;

P_e is the electrical torque of the machine (stator) in relative units, this depending on the angle and its differential;

P_0 is the load on the machine shaft;

ω is the angular speed of rotation of the machine.

A study of the synchronization process in a motor involves analysis of this equation in the range where the machine is slipping slightly; except for the method of numerical integration, this analysis can only be carried out by studying the trajectory of the motion in the phase-plane.

Two methods are known for carrying out such an investigation: the isocline method [3, 4] and the construction of separatrices [5, 6]. Both methods are notable in that they are comparatively very laborious. Thus, in the isocline method it is necessary to seek and plot the geometrical locations of points of equal slope on the integral curves, whereas the separatrix construction involves calculating successive intervals by the trajectory method, and therefore takes up a considerable amount of time.

---

* *Elektrichestvo* No. 2, 56-59, 1958 [Reprint Order No. EL 53].

In the present investigation, the co-ordinate grid method was used. The construction of integral curves by this method is carried out as follows. Writing $\delta' = d\delta/dt = y$, we find from equation (1) the tangent of the angle of slope of tangents to the trajectory of rotor motion on the phase-plane:-

$$\tan\alpha = \frac{d_y}{d\delta} = \frac{[P_0 - P_e(\delta, y)]\,\omega}{My} - \frac{D(\delta, y)}{M}. \qquad (2)$$

For the various points on the phase-plane lying at the corners of the co-ordinate grid (δ_i, y_i) the values of $\tan a_i$ are determined and plotted on the plane in the form of arrows (Fig. 1).

Approximate rotor-motion trajectories are constructed, in accordance with the slope of the arrows; the shape of the curves provides a qualitative solution to the problem; i.e., it establishes whether the motor will get into synchronism. Since the direction of slipping does not reverse between the moment of starting and that of reaching synchronism, it is sufficient to construct the trajectories in the lower half-plane only. The synchronization criterion for a motor is the reduction of rotor slip after one complete pole-pitch has been slipped (in the range of small degrees of slip); i.e. the reduction of the absolute value of y at the end of an interval $(\pi; -\pi)$ as compared with its value at the start of the interval.

Trajectories of rotor motion, constructed by this method and calculated by the successive interval method, using an electronic computer, agree reasonably well.

The completeness and carefulness of an analysis of the synchronization process are determined by the degree to which other factors influencing the damping coefficient and the electromagnetic torques P_e of the machine are taken into account. However, the attempt to take into account all the factors involved in the complicated synchronization process in compound excited motors in general would have no practical significance, because of the immensity of the task. Thus, for a start, calculations were made to elucidate the magnitude of the effects of various factors on the synchronization process, so as to decide which factors could be neglected. The conclusions reached were checked by experiment. As a result of the preliminary calculations and experimental work it was established that one could ignore the saturation of the machine and the presence of valves in the rotor circuit, since the test showed that in the compound excitation circuit the rotor current does not change direction during synchronization. The transient process on switching the motor on to the rectifier was also ignored. The effect of the remaining factors was accounted for as follows.

The relationship between the damping coefficient and the angle of rotor lag and slip was taken in accordance with the Zhdanov formula [7]:

$$D=U^2\left[\frac{x_d-x'_d}{x_d x'_d}\cdot\frac{T'_d}{1+(yT'_d)^2}\sin^2\delta+\right.$$
$$+\frac{x'_d-x''_d}{x'_d x''_d}\cdot\frac{T''_d}{1+(yT''_d)^2}\sin^2\delta+ \tag{3}$$
$$\left.+\frac{x-x''_q}{x_q x''_q}\cdot\frac{T''_q}{1+(yT''_q)^2}\cos^2\delta\right].$$

The electrical torque P_e of the machine was determined as the sum of three terms taking into account the reactive moment of the machine, the effect of currents induced in the rotor winding, and the synchronous moment (allowing for the active resistance of the stator) respectively; thus:

$$P_{e1}=U^2\frac{x_d-x_q}{x_d x_q}\sin 2\delta; \tag{4}$$

$$P_{e2}=-\frac{U^2}{2}\cdot\frac{x_d-x'_d}{x_d x'_d}\cdot\frac{(yT'_d)^2}{1+(yT'_d)^2}\sin 2\delta; \tag{5}$$

$$P_{e3}=\frac{E_d^2}{\sqrt{r^2+x_d^2}}\sin\alpha+\frac{E_d U}{\sqrt{r^2+x_d^2}}\sin(\delta-\alpha), \tag{6}$$

where $\alpha=90^\circ-\tan^{-1}\frac{x_d}{r}$.

The existence of a series component of excitation in the circuit of normally-adjusted compound excited motors, with and without regard to the angle of lag of the rotor in respect of the rotor current in relation to the damping cage was correspondingly taken into account by introducing the relationship between the e.m.f. E_d and the angle δ:

$$E_d=\frac{1}{2}[(1+n)+(1-n)\cos\delta]U; \tag{7}$$

$$E_d=\frac{1}{2}\left[(1+n)+(1-n)\frac{\cos(\varphi+\psi)}{\sqrt{1+(yT''_d)^2}}\right]U, \tag{8}$$

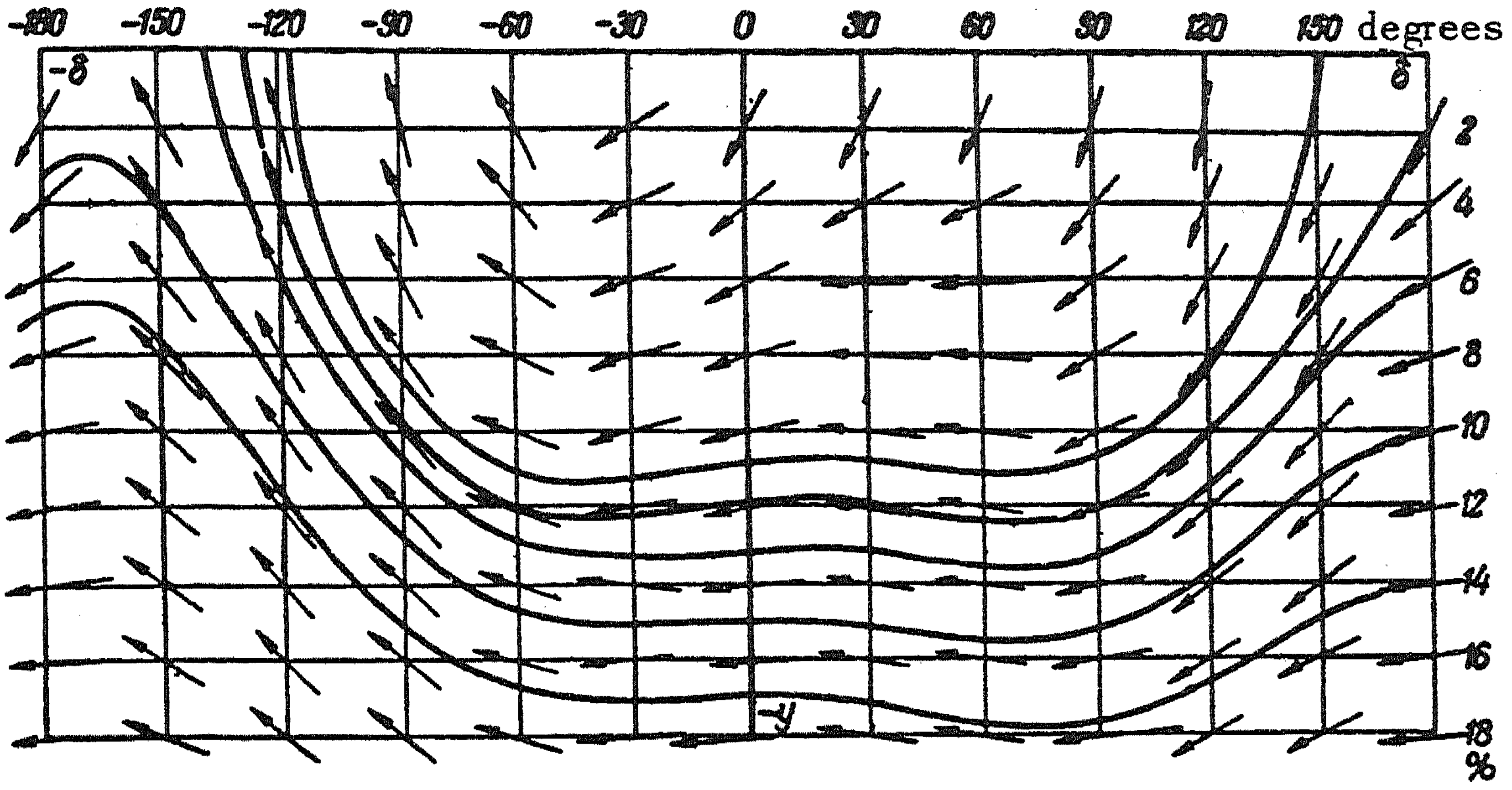

FIG. 1. Trajectories of rotor motion, calculated by the co-ordinate grid method for a motor of the following parameters:-
$x = 1.6$; $\kappa'_d = 0.312$; $\kappa_q = 0.95$; $M = 1.27$ sec; $T'_d = 0.08$ sec.

Where n – is the ratio of the growth of e.m.f. E_d to the series component of excitation, as angle δ varies from 0 to π:

$$\psi = \cos^{-1} \frac{1}{\sqrt{1+(yT''_d)^2}}.$$

The value of n is determined by the compounding coefficient K and the synchronous reactance x_d:

$$n = \frac{x_d + k}{x_d - k}.$$

From equations (3) to (8) it follows that the expression for tan α can be written as a sum of the form:

$$\tan\alpha = \Sigma F_1(y) F_2(\delta),$$

where F_2 (δ) are simple trigonometric functions.

Values of F (y), calculated for any y value whatever, remain invariant as angle δ varies; these calculations are thus not laborious and can be completed in a short time.

From a comparison of rotor motion trajectories calculated for a series of cases, it could be established that lag in the change of magnetic flux in the rotor, relative to the change of excitation current due to the present of compounding, had an adverse effect on the conditions of synchronization of the machine, since it is equivalent to negative damping. This deduction was confirmed by experimental

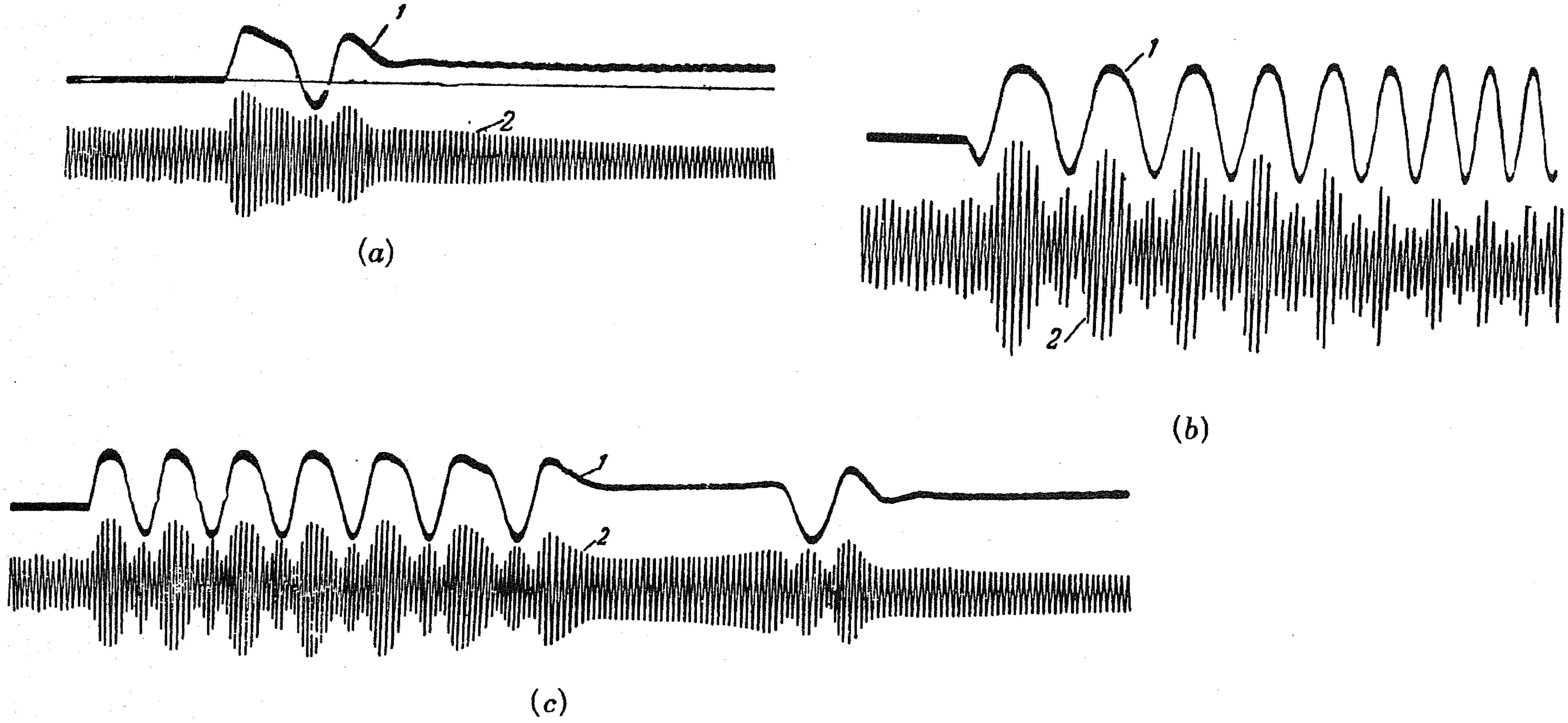

FIG. 2. Oscillograms of synchronization of type SG — 4.5 motor:
1 — rotor current; 2 — stator current.
Rotor current: (a) 6.0 A; (b) 7.0 A; (c) 8.1 A.

tests which showed that, in the presence of compounding, a machine which falls out of synchronism is very rapidly retarded almost to a standstill, whereas with constant excitation it either pulls itself back periodically into synchronism or rotates asynchronously with a small amount of slipping.

Synchronization conditions are also adversely affected by active resistance in the stator circuit, and if the latter is considerable, there is an optimum level of excitation for synchronization of the machine.

The existence of an optimum level of excitation is confirmed by the oscillographs shown in Fig. 2. The motor gets back into synchronism in the very first cycle of oscillation (Fig. 2a), at a certain value of excitation current. At a lower excitation current the motor does not get into synchronism. As the excitation current is increased the synchronization time is extended (Fig. 2b), and at a still higher excitation current, synchronization is not achieved (Fig. 2c).

The effect of the active stator resistance on the synchronization process of the machine and the optimum excitation level can also be established analytically. Let the excitation (non-compounded) of the machine operate in a stable asynchonous condition. In this case the sum of the mean values of electromagnetic torques acting on the rotor must equal the torque due to the shaft load. The mean value of the torque P_e is:-

$$P_{e.m}=\frac{E_d^2}{\sqrt{r^2+x_d^2}}\sin\alpha,$$

and the torque at the motor shaft is:

$$P_0=D_m s-\frac{E_d^2}{\sqrt{r^2+x_d^2}}\sin\alpha,$$

where s is the slipping in the machine:

$$\sqrt{r^2+x_d^2}=Z_{11}.$$

The critical slipping, at which the machine will synchronize itself, is found from the well known Edgerton formula [8]:

$$s_{cr}=\frac{245}{n_c}\sqrt{\frac{P_{\max}}{fGD^2}},$$

where n_c is the synchronous speed of the motor;
$P_{\max}=UE_d/x_d$ is the maximum motor power output;
GD^2 is the moment of gyration of the motor;

f is the frequency.

Substituting the value of critical slipping in the formula, we obtain the limiting power output for conditions of synchronization at the shaft of a synchronous motor (non-compounded), taking into account the effect of its active resitance:

$$P_{0\,nred}=\frac{245}{n}D_{mp}\sqrt{\frac{UE_d}{x_d fGD^2}}-\frac{E_d^2}{\sqrt{r^2+x_d^2}}\sin\alpha. \qquad (9)$$

Equating to zero the differential of this expression (with respect to E_d) and bearing in mind that $\sin a \approx r/x_d$ we find that the maximum load torque at which synchronization is still possible will be for the value of E_d equal to

$$E_d=\sqrt[3]{\left(\frac{245D_{mp}}{4n_cR}\right)^2\frac{Ux_d}{fGD^2}}$$

On the basis of the work carried out it must be concluded that compounded synchronous motors should be synchronized with the compounding switched out. This eliminates the "negative damping" effect and reduces the active resistance of the machine. If a compound excited motor is synchronized with the compounding in action (which simplifies the starting device), then, as the phase-plane studies and the experimental tests have shown, in this case, to determine the limiting load torque for synchronization, it is also possible to use the Edgerton formula to find the correct level of compounding, accepting references [1, 2] to the effect that

$$P_{\max}=\frac{U_2}{4a}-b,$$

where a and b are coefficients defining the loss ΔP in the motor, as a function in the motor, as a function of the current I, according to the formula $\Delta P = I^2 + b$.

This deduction has been checked experimentally and shows good agreement with experiments. Thus, a 3.6 kW motor, designed on the basis of an SG-4.5 generator, came into synchronism at 70 per cent nominal load. In this case the maximum load torque found from formula (9), at which the motor can still be synchronized, is 66 per cent of nominal. An 11.8 kW motor, designed on the basis of an MSA-72/4 generator, synchronized at 68 per cent of nominal loss, and the calculation from formula (9) gives the same value of the torque, namely 68 per cent.

Translated by E. Bishop

1. V.L. Inosov and V.E. Krutikova; A Synchronous compound excited motor, *Elektrichestvo*, No. 6 (1956).
2. V.L. Inosov; A synchronous compound excited motor and the theory of its operation, *Sborn. trud. inst. elektrotekh. Akad. Nauk SSSR*, 14 (1956).
3. A.A. Andronov and S.E. Khaikin; *Teoriia kolebanii (Theory of oscillation)*, United Scientific and Technical Press (1937).
4. K.M. Polivanov; *Fizicheskie osnovy elektrotekhniki (Physical principles of electrotechnology)* (1950).
5. V.L. Inosov and V.E. Krutikova; A study of the synchronization conditions of excited generators, brought asynchronously into circuit, *Sborn. trud. inst. elektrotekh. Akad. Nauk SSSR*, 13 (1956).
6. Dzh. Stoker; *Nelineinye Kolebaniia v mekhanicheskykh i elektricheskikh sistemakh (Non-linear oscillations in mechanical and electrical systems)* Izdatel'stvo inostrannoi lit., Moscow (1953).
7. P.S. Zhdanov; Synchronization of machines after disturbances of stability. *Elektrichestvo* No. 6 (1934).
8 H.E. Edgerton and P. Fourmarier; Synchronization of open-pole motors, *Elect. Engng.* (1932).

THE PERFORMANCE OF CURRENT-MEASURING TRANSFORMERS UNDER INCREASED POWER OUTPUT CONDITIONS *

V.S. BURTAKOV and M.I. GLAZOV
Moscow Power Institute

(Received 8 October 1957)

In the operation of protective relay circuits, at a variable actuating current, the current transformers operate with high load resistances under conditions which differ markedly from normal, since the circuit-breaker cut-out coils and the rapid-saturation transformers are usually connected to their secondary coils. The inductances in the current transformer cores under such conditions are not hundreds of gauss, as under normal conditions, but reach 15 to 25 kG. Thus, the current transformer cores are highly saturated and the magnetization current is sharply increased, resulting in a noticeable drop in the secondary current, i.e. in an increased error. This refers particularly to built-in current transformers with small transformation ratios. Reduction of the secondary current also results in a relative reduction of the power output of the transformer.

The power output of a current transformer depends on both the value of the current passing through the transformer and the value of the load resistance. For each current value a load resistance can be found which corresponds to maximum transformer power output. In particular, at currents of the order of the nominal rating, this maximum occurs at load resistances of the order of 1 Ω.

In cases when the cut-out coils of the circuit-breakers are connected in series with the relay (on the main cores of the current transformers), it is necessary, for calculation of the relay setting, to know the transformer errors when their power output is near maximum. These errors must also be known in the design of circuits with rapid-saturation current transformers, which are in the open circuit condition and thus have high resistances at the instant when the relay operates.

The present paper considers the stabilizing conditions of current transformer operation and the conclusions which are of value in the calculation of protective circuits with an operation time which is sufficient for attenuation of the transient process in the current transformer.

---

* *Elektrichestvo* No. 2, 59-61, 1958 [Reprint Order No. EL 54],

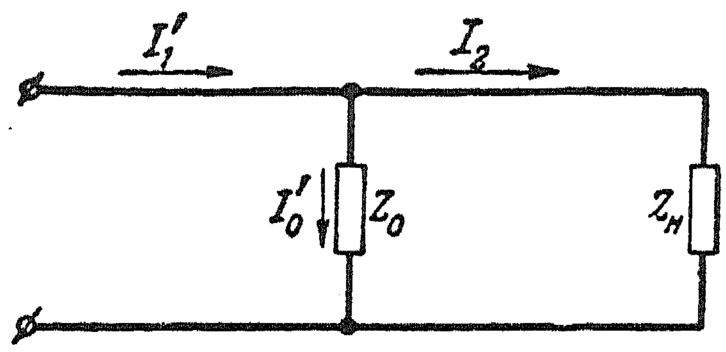

FIG. 1. Simplified equivalent circuit for current transformer.

A current transformer can be replaced by an equivalent non-linear resistance Z_0 (Fig.1), the value of which is determined so as to correspond to the dynamic magnetization curve. The source of supply to the current transformer can be regarded as a source of infinite power and the secondary winding resistance can be ignored, since in circuits on operative a.c. it is much smaller than the load resistance.

In the calculations, errors in the current transformer angle are usually ignored, since, as experiments show, with the normal inductive load on protective relay circuits this error is small. Curves of power output against load resistance are constructed for various values of primary current. From these results are found the maximum values of power output for the transformer, and the optimum load resistances and errors corresponding to these outputs.

If the magnetic flux in the transformer is sinusoidal, the transformer power output can be expressed mathematically by the following relationship:-

$$S = U_2 I_2 \equiv BH_2, \tag{1}$$

where $B \equiv U_2$ is the amplitude value of the inductance, found from the dynamic magnetization curve;

$H_2 = \frac{I_2 w_2}{l_m}$ is the partial secondary magnetic field intensity (w_2 is the number of turns in the secondary coil; L_m is the mean length of the magnetic path).

We denote the partial primary magnetic field intensity by the value

$$H_1 = \frac{I_1 w_1}{l_m},$$

where w is the number of turns in the primary winding of the current transformer.

Since
$$H_2 = H_1 - H_0, \tag{2}$$
we find that the power output S to the load is proportional to the shaded rectangular area in Fig. 2.

It can be seen from Fig. 2 that for a fixed value of primary intensity H_1, as the inductance increases, the power output of the transformer first increases and then falls, reaching zero at $H_0 = H_1$.

The maximum power output value is found from the condition:-

$$\frac{dS}{dH_0} = 0.$$

Taking (1) and (2) into account, we obtain

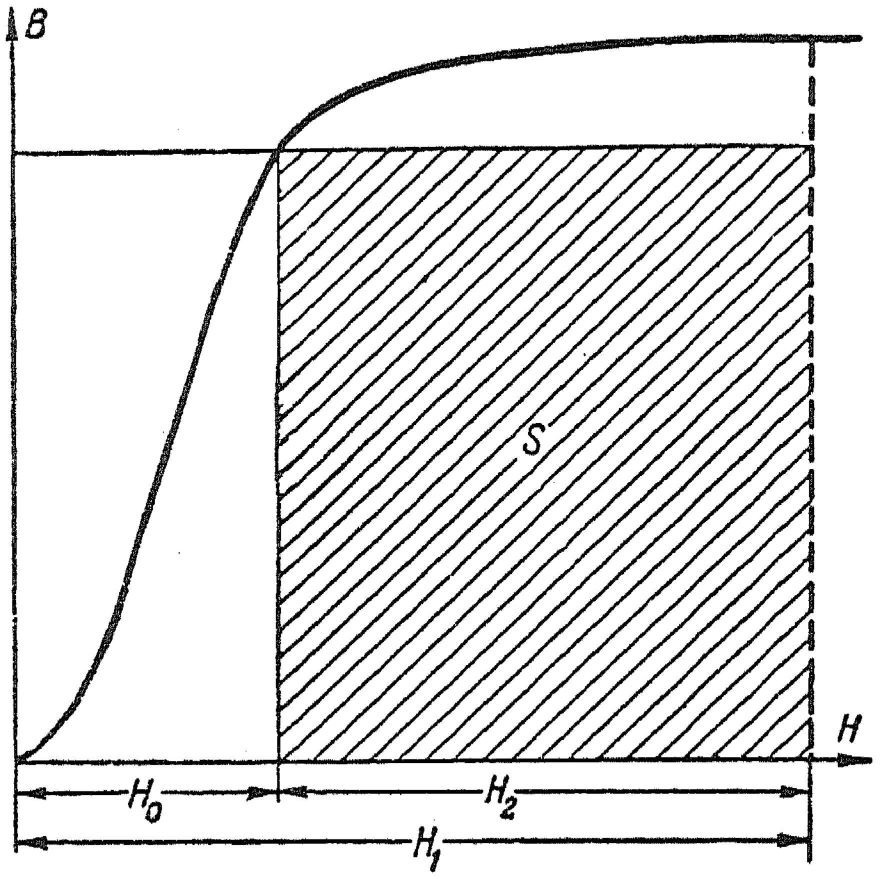

FIG. 2.

$$\frac{dB}{dH_0}(H_1 - H_0) - B = 0. \tag{3}$$

Introducing the following rotations:-

$\mu_{\partial} = \frac{dB}{dH_0}$ the differential magnetic permeability;

$\mu_{\text{н}} = \frac{B}{H_0}$ the nominal magnetic permeability,

we find the optimum value of intensity H_0 corresponding to maximum power output at a given value of H_1:

$$H_{\text{o.opt}} = \frac{1}{1+\frac{\mu_{H.\text{opt}}}{\mu_{\delta\ \text{opt}}}} H_1, \tag{4}$$

where $\mu_{H\ \text{opt}}$ and $\mu_{\delta\ \text{opt}}$ are the magnetic permeabilities

for $H_0 = H_{0\cdot\text{opt}}$

To construct this relationship (Fig. 3) it is necessary to postulate $H_{0\cdot\text{opt}}$ values, to find on the magnetization curve the corresponding values of $\mu_{H.\text{opt.}}$ and $\mu_{\delta\ \text{opt.}}$ and to calculate the value of H_1.

It can be shown that the optimum load resistance is proportional to the tangent of the angle of slope of the tangent to the magnetization curve at the point corresponding to maximum S. Actually, from equation (3), we can obtain:

$$\frac{dB}{dH_0} = \frac{B}{H_2} \equiv \frac{U_2}{I_2} = z_2. \tag{5}$$

The error of a current transformer at maximum power output can be found

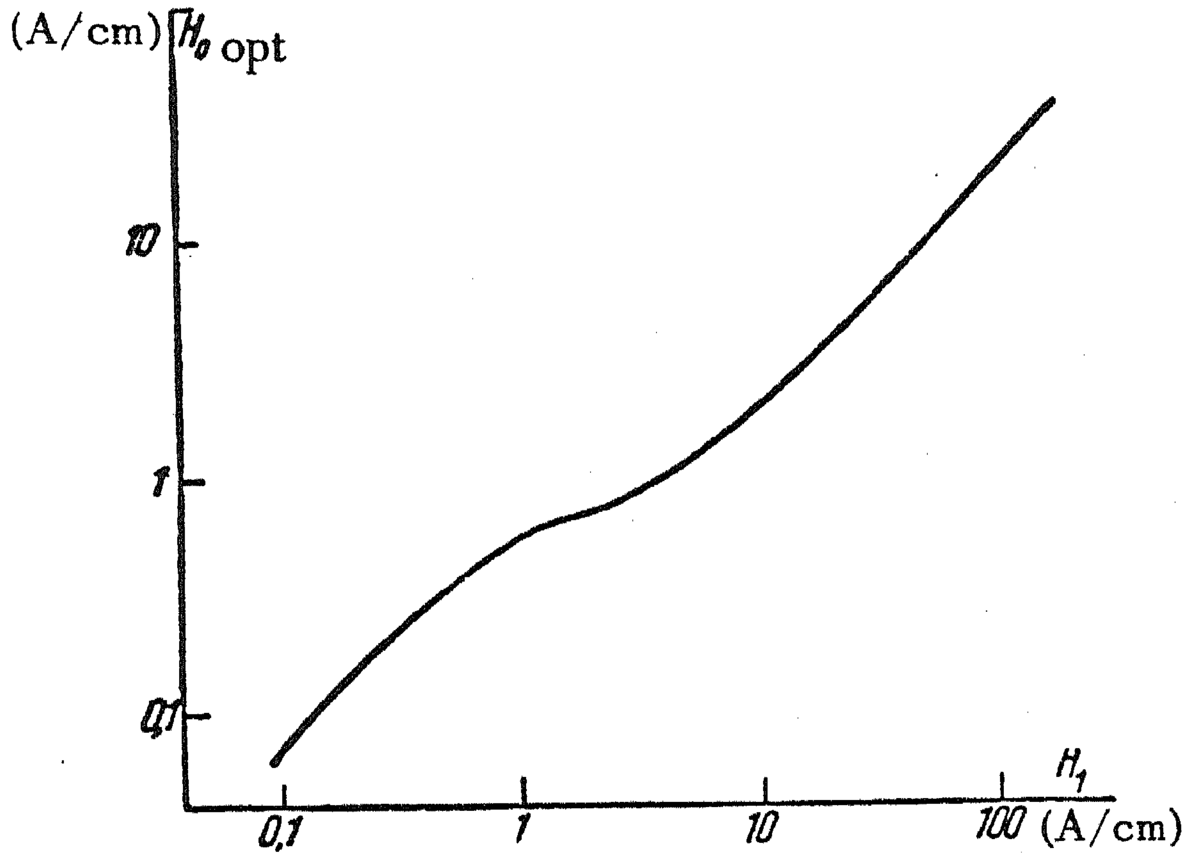

FIG. 3. Relationship between $H_{0.\mathrm{opt}}$ and H_1 for a type TPF-10 current transformer (core 0.5).

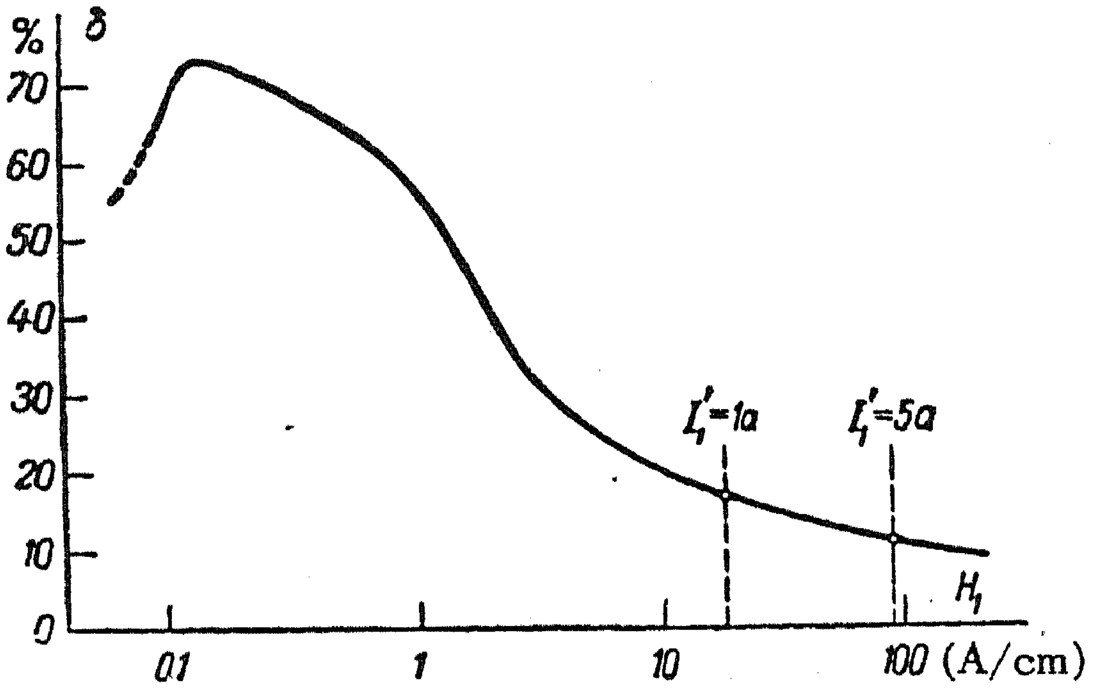

FIG. 4. Error of type TPF-10 current transformer (core 0.5), under maximum power output conditions.

from formula (4), taking into account the fact that the ratio of the currents shown is equal to the ratio of the corresponding intensities:-

$$\delta^0/_0 = \frac{100}{1+\frac{\mu_{H.\mathrm{opt}}}{\mu_{\delta\,\mathrm{opt}}}}.$$

The character of the relationships between $\mu_{H.\mathrm{opt.}}$, $\mu_{\delta\cdot\mathrm{opt}}$ and the intensity H_1 is determined by the relationship $\delta = f(H_1)$. In the initial part of the magnetization curve $\mu_{\delta\mathrm{opt.}}$ increases more rapidly than $\mu_{H.\mathrm{opt.}}$ and therefore as H_1 increases the transformer error increases (Fig. 4). The maximum error ($\delta = 60-70$ per cent) corresponds to the part of the magnetization curve which can be normally replaced by a parabola ($B = 10$ to 10^3G). When the field strength is increased further, $\mu_{\delta\mathrm{opt.}}$ increases more slowly than $\mu_{H.\mathrm{opt.}}$ and correspondingly δ starts to fall. Reduction of the error continues also after passing the $\mu_{\delta\mathrm{opt.}}$ and $\mu_{H\,\mathrm{opt.}}$ maxima, since $\mu_{\delta\mathrm{opt.}}$ falls more rapidly than $\mu_{H.\mathrm{opt.}}$ At high values of intensity the error increase again (not shown in Fig. 3), reaching 50 per cent in the limit.

Current transformers in protective relay circuits on operative a.c. operate within definite limits of inductance value. At currents near the nominal rating the inductances under maximum power output conditions have values of the order of 10^4G and the errors for various transformer designs are within the range of 20 to 30 per cent. At high currents, the errors under maximum power output conditions fall to 10 per cent. The inductances to which corresponds the subsequent increase in errors up to 50 per cent are considerably in excess of the inductance values at which current transformers operate.

Thus the previous opinion, regarding the high values (of the order of 50 per cent and more) of the errors of current transformers operating under maximum power output conditions, must be regarded as incorrect.

Translated by E. Bishop

A STUDY OF THE EFFECT OF NOZZLE PARAMETERS ON ARC EXTINGUISHING BY A COMPRESSED AIR JET *

R.A. MIKAELIAN

(Lenin All-Union Electro-technology Institute)

(Received 1 March 1957)

The present paper gives results obtained in an experimental investigation of arc-extinguishing nozzles of various designs made from insulating and conducting materials. In order to obtain a clearer picture of the characteristics of various arc-extinguishing jets, these investigations were carried out in a model arc-extinguishing chamber with a lateral blast.

The chamber contained 0.2 g of air compressed to 1.5 atm. Air from the chamber flowed through the nozzle for a period of 0.016 sec. The diameters of the fixed and moving arc-extinguishing contacts were 16 and 10 mm, respectively. The contacts were of copper. The value of the restoring voltage (effective value) at the opened circuit-breaker contacts was 6 kV. The frequency of self-oscillation in the short-circuit loop was 20,000 c/s.

It was established experimentally that the relationships obtained on the model between the nozzle parameters and the magnitude of the current which can be broken can be increased proportionately and thus extended to actual circuit-breakers.

Comparison of nozzles made from ceramic materials showed that "cardioride" nozzles were the most arc-resistant. During repeat experiments the working surface of this nozzle became gradually coated with a vitreous conducting mass. After approximately fifty breaks at a current of 400 A, the nozzle cracked and ceased extinguishing the arc. Nozzles made from other ceramic materials could only break the circuit for a smaller number of times.

Marble nozzles survived fourteen to sixteen breaks at a current of 400 A after which arc-extinguishing capacity was rapidly lost.

When nozzles were made of conducting materials it was found impossible to carry out more than six or seven breaks, after which the working surface of the nozzle built up, preventing the moving contact from passing into the nozzle any longer.

---

* *Elektrichestvo* No. 2, 61-63, 1958 [Reprint Order No. EL 55].

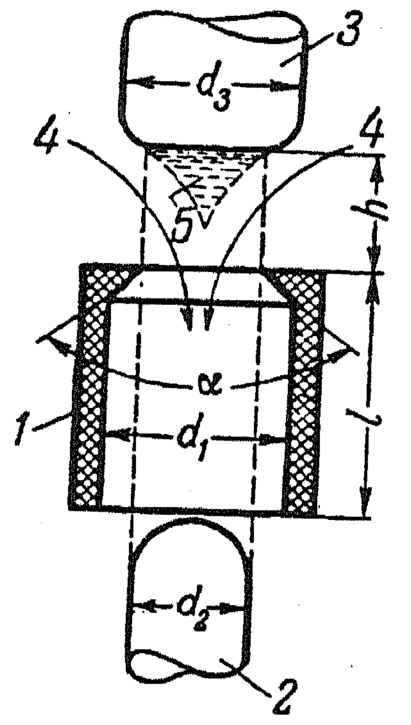

FIG. 1. Plexiglas nozzle of optimum arc-extinguishing capacity.

1. nozzle;
2. moving contact;
3. fixed contact;
4. direction of compressed air flow;
5. stagnant region.

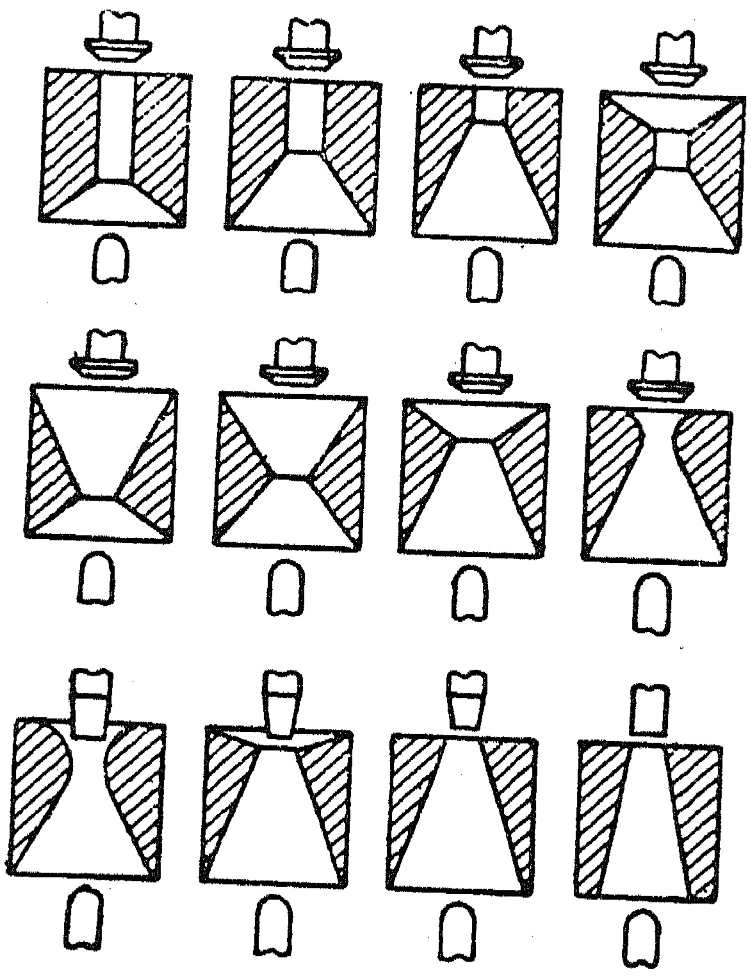

FIG. 2. Plexiglas nozzles, studied for arc-extinguishing capacity.

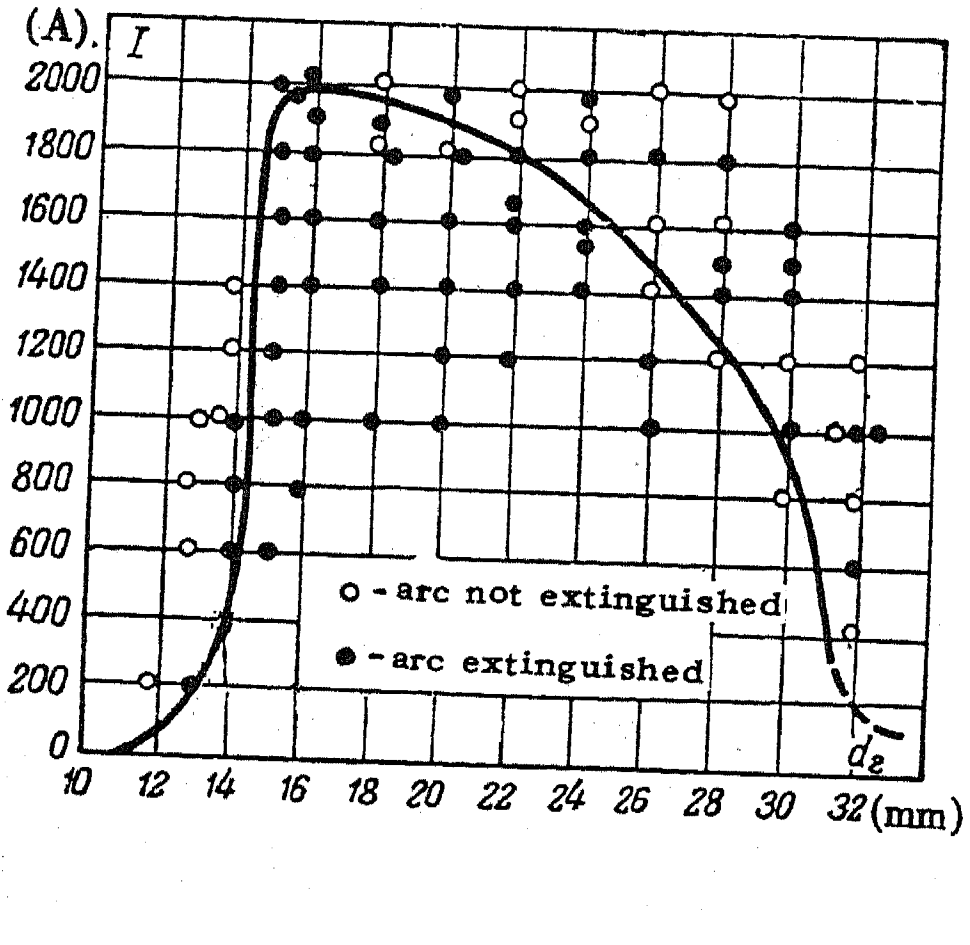

FIG. 3. Relationship between current which can be broken and internal diameter of cylindrical section of nozzle. (open circles – arc not extinguished) (black circles – arc extinguished)

Nozzles made from materials which evolve gases under the influence of the high arc temperature wore out after twenty to thirty breaks at a 400 A current, with a large amount of soot deposit.

Nozzles as shown in Fig. 1 were found to be very durable. A nozzle of this type made of plexiglass has a considerably greater arc-extinguishing capacity than other nozzles investigated (Fig. 2), which were made of more heat-resistant materials than plexiglass.

The basic parameters of nozzles (Fig. 1) are: the angle a of the conical funnel, the internal diameter d_1 of the cylindrical section of the nozzle funnel, the radius of curvature r of the nozzle edge and the position of the fixed contact above the nozzle. We shall consider each of these parameters individually.

It was established experimentally that the most successful arc extinction takes place in the case when at the very start of extinction the air flow is determined by the area of the nozzle opening and not by the area of the annular gap between the moving contact and the nozzle. To ensure this condition it is essential for the angle of the conical section of the nozzle to have the maximum possible value. In order to avoid mechanical breakdown of the tip the angle taken was $a = 120^\circ$. If nozzles are made from mechanically stronger material, this angle can be increased.

The internal diameter of the cylindrical section of the nozzle is selected in such a way that the area of the annular section between the moving contact and the inner nozzle wall is not less than that of the nozzle exit opening. This condition follows directly from the experimental curve shown in Fig. 3. The curve shows that the maximum value of the current which can be broken at a nozzle exit opening diameter of 10.5 mm is reached when the internal diameter of the cylindrical section of the nozzle is 16 mm. As this diameter is reduced, the arc-extinguishing capacity of the nozzle falls sharply. Increase of the internal diameter of the cylindrical section of the nozzle beyond 16 mm has comparatively little effect on the arc-extinguishing capacity.

The radius of curvature of the nozzle tip has a substantial influence on the magnitude of the current which can be broken. The results of tests with varying radii of curvature in the range from $r = 0$ to $r = 5$ mm, at a constant value of 16 mm for the internal diameter in the cylindrical portion of the nozzle, are shown in Fig. 4.

This relationship, showing that as the radius of curvature of the nozzle tip is reduced the arc-extinguishing capacity is improved, does not agree with the results of investigations by a number of other authors. In particular it has been shown that the breaking power of a nozzle which is good from a streamlining point of view and free from eddying is better than that of a nozzle with sharp edges [1].

It might be supposed that a nozzle with sharpened edges could not undergo any large number of breaks, since the edge sharpness will reduce the already low

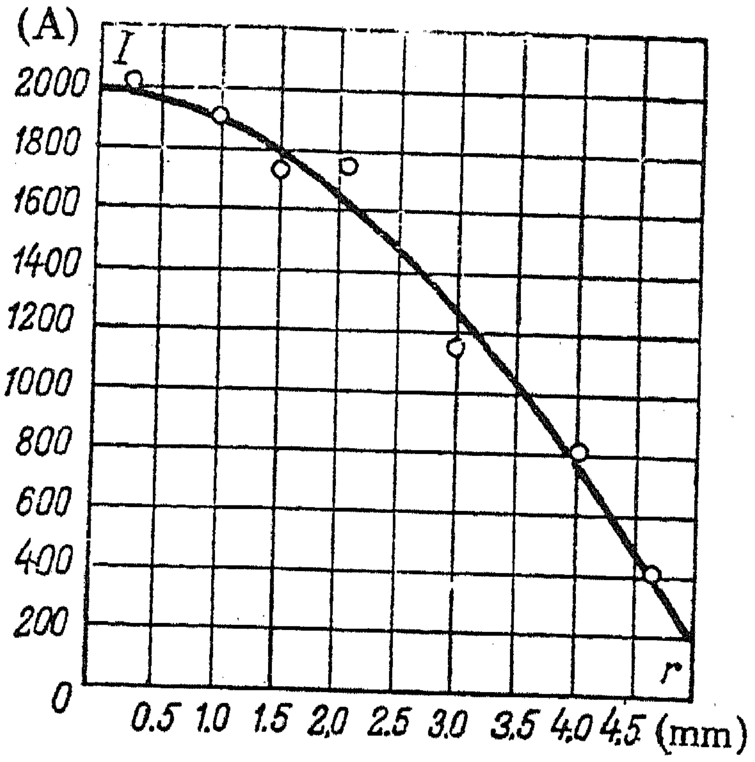

FIG. 4. Relationship between current which can be broken and radius of curvature of nozzle edge.

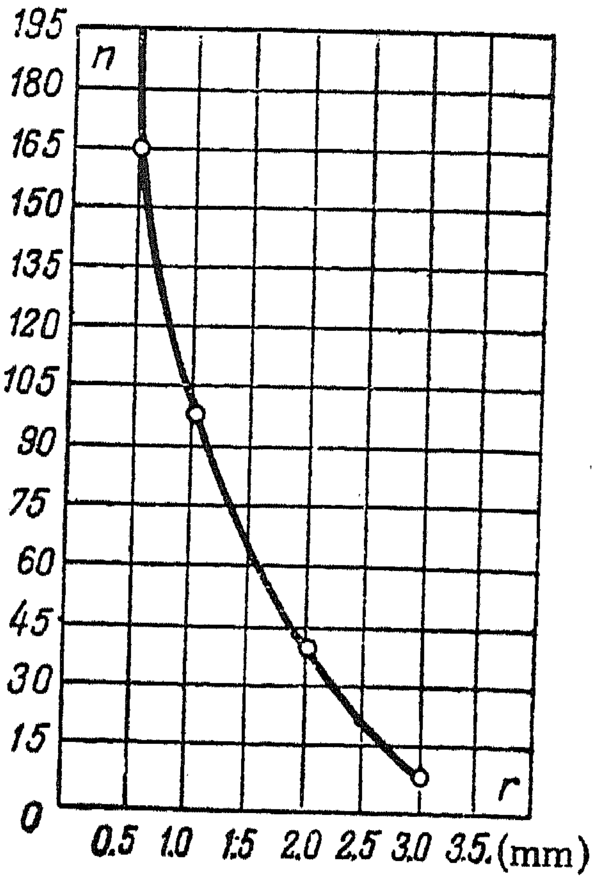

FIG. 5. Relationship between number of successful breaks at a current of 1 kA and radius of curvature of nozzle edge.

heat resistance of the nozzle material, (the decomposition temperature of plexiglass is about 150°C). However, experiments did not confirm this supposition, as Fig. 5 shows: as the radius of curvature of the edge is increased, the number of successful breaks is reduced.

The nozzle shown in Fig. 1 was able to break currents at short circuit values of the order of 4 kA (Fig. 6). The high arc resistance of a nozzle with sharp edges can be explained on the grounds of the formation of air eddies which, encircling the sharp edge, protect the latter from destruction by the incandescent arc gases. The positive effect of sharp nozzle edges on the magnitude of the current which can be broken may also be explained by the tearing from them of streams of cold air into the arc column which must substantially increase the intensity of the cooling effect.

On the basis of the results presented, it can be confirmed that improvement in the arc-extinguishing properties of nozzles made from insulating materials and extension of their service life can be obtained by using nozzles with sharp edges.

A relationship was also found by experiment, between the magnitude of the current which can be broken and the distance between the fixed contact and the nozzle. The maximum current-breaking value corresponds to the optimum distance $h_{\text{opt.}} = 2.7$ mm.

In this case the area of the nozzle exhaust opening $f_1 = \pi d_2^2/4$, and the area of the cylindrical surface $f_2 = \pi d_2 h$, through which the air enters the nozzle, are equal. Here, it is assumed that the area of the annular section $f_3 = (\pi/4).(d_1^2 - d_2^2)$ exceeds both these values.

If the distance between the fixed contact and the jet is below the optimum, then f_2 is the critical area. Since in this case $f_2 < f_1$, the air flow through the

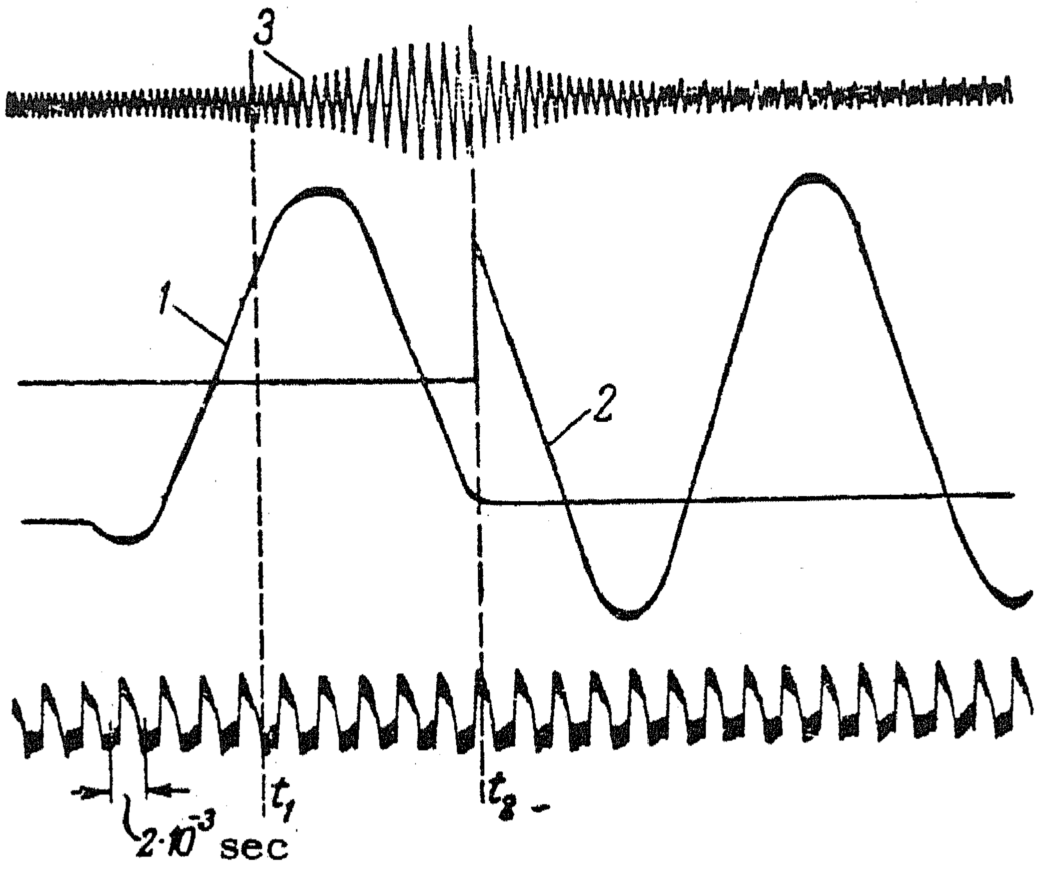

FIG. 6. Oscillagraph of current-breaking, using nozzle with sharp edges.
1. current ($I = 4.2$ kA);
2. voltage at circuit breaker contacts ($U = 6$ kV);
3. air pressure in chamber ($P_{max} = 1.4$ atm). 2 x 10^{-3} sec

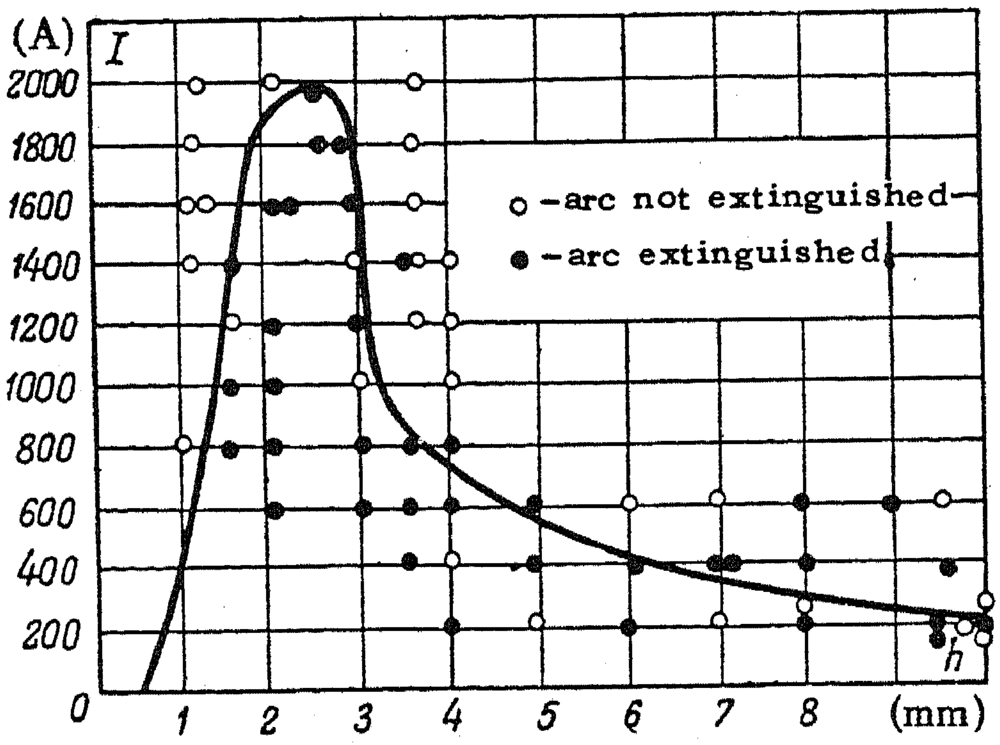

FIG. 7. Relationship between current which can be broken and distance between fixed contact and nozzle.

nozzle is reduced, lowering the value of current which can be broken (Fig. 7).

If the distance is increased beyond the optimum, f_1 becomes the critical area. This results in a fall in the radial component of the air stream velocity and so in a reduction in the penetration of cold air particles into the arc column. As a result, the arc is less intensely cooled. Moreover, in this case, there is a considerable increase in the "stagnant" region of incandescent gases (Fig. 1), which reduces the electric strength between the contacts.

This work was carried out under the direction of Prof. G.V. Butkevich, to whom the author extends his sincere thanks.

Translated by E. Bishop

REFERENCES

1. O. Mayr; *Hohe-leistungschalter ohne 01*, *ETZ*, No. 31, 759 (1934).

ELEKTRICHESTVO

Editor-in-Chief: N. G. Drozdov

Deputy Editor-in-Chief: I. A. Syromiatnikov

EDITORIAL BOARD

K. A. Andrianov, N. I. Borisenko, G. V. Butkevich, M. G. Chilikin, A. A. Glazunov, V. A. Golubtsova, E. G. Komar, M. P. Kostenko, L. R. Neiman, I. I. Petrov, V. I. Popkov, A. M. Fedoseev

---

IMPORTANT EDITORIAL NOTICE

To assist readers, reprints of any article appearing in *Electric Technology, U.S.S.R.*, can be obtained on application at a price of $2 (10s.) per reprint, to cover the overhead costs involved in production. The Reprint No. of each article (which appears on the foot of the first page of the article) must be quoted on every order. Orders should be accompanied by the correct remittance.

All orders for reprints of Russian articles should be addressed to The Administrative Secretary of the Pergamon Institute at either 122 East 55th Street, New York 22, or 4 and 5 Fitzroy Square, London W.1, whichever is more convenient.

Pergamon Press are also the publishers of the following journals:

Journal of Nuclear Energy (*including* The Soviet Journal of Atomic Energy *on behalf of Pergamon Institute, a non-profit-making foundation*)
Reactor Technology (*Journal of Nuclear Energy, Part B*)
Health Physics (*The Official Journal of the Health Physics Society*)
Journal of Inorganic and Nuclear Chemistry
Tetrahedron (*The International Journal of Organic Chemistry*)
Talanta (*An International Journal of Analytical Chemistry*)
International Journal of Applied Radiation and Isotopes
Biochemical Pharmacology
*Biophysics
*Journal of Microbiology, Epidemiology and Immunobiology
*Problems of Hematology and Blood Transfusion
*Problems of Virology
*Problems of Oncology
*Sechenov Physiological Journal of the U.S.S.R.
*Bulletin of the Academy of Sciences of the U.S.S.R.: Geophysics Series
*Radio Engineering
*Radio Engineering and Electronics
*Telecommunications
*The Physics of Metals and Metallography
*The Abstracts Journal of Metallurgy
*Applied Mathematics and Mechanics
Chemical Engineering Science
Journal of Atmospheric and Terrestrial Physics
Planetary and Space Physics
Geochimica et Cosmochimica Acta
Bulletin Géodésique
Annals of the International Geophysical Year
Spectrochimica Acta
Journal of the Mechanics and Physics of Solids
Acta Metallurgica (*for the Board of Governors of Acta Metallurgica*)
International Journal of the Physics and Chemistry of Solids
Deep-Sea Research
Journal of Neurochemistry
Journal of Psychosomatic Research
Journal of Insect Physiology
Journal of Air Pollution
International Abstracts of Biological Sciences (*for Biological and Medical Abstracts Ltd.*)
Rheology Abstracts
Vacuum
Operational Research Quarterly
Annals of Occupational Hygiene

*Translations of the Russian journals published on behalf of Pergamon Institute, a non-profit-making foundation.

Leaflets giving further details and subscription rates of each of these journals are available on request.

ELECTRIC TECHNOLOGY, U.S.S.R.

1958 VOLUME 4 DECEMBER

CONTENTS

PAGE

I. N. CHUPIATOV and V. F. BAIKO: Two-commutator rotary amplifier 1

N. A. MARKOV: The theory of the electrical circuit for the three-phase ore-reduction furnace 10

V. I. KLIUCHEV: The universal characteristics of the dynamic braking of asynchronous motors 18

A. S. MAIKOPAR and N. N. BELIAKOV: Arcing short-circuits on 400 kV transmission lines and methods of dealing with them 27

N. A. MELNIKOV, A. I. GERSHENGORN and A. N. SHERENTSIS: Earthwire earthing systems for long power-transmission lines 39

D. E. ARTEM'EV and S. S. SHUR: Experimental determination of parameters of electro-transmission: Kuibyshev Hydro-electric Power Station—Moscow 52

E. A. MEEROVICH and V. K. RED'KIN: Partial capacities (conductivities) of a system of electrodes and separate fluxes of the resultant field 70

F. F. SOKOLOV: The heat emission of rectifier stacks made of large selenium cells . . 78

A. N. ZEILIGER and B. P. NOVGORODTSEV: The use of 220 kV lines with split conductors 87

G. G. KOSTANIAN: Calculations of short-circuits in unbalanced phase transmission systems 97

D. P. MOROZOV, M. G. CHILIKIN, N. G. LYSENKOV and L. M. TVERDIN: A new circuit for high-speed pulse control in systems containing ionic converters 108

O. M. KOSTIUK and V. E. RYBINSKII: The controlled phase-type compound winding of synchronous generators with correlation as to voltage 118

A. A. MASLOV: Transistor amplifiers of the alloy type 132

V. L. INOSOV and V. E. KRUTIKOVA: A study of the synchronization process in compound excited motors 142

V. S. BURTAKOV and M. I. GLAZOV: The performance of current-measuring transformers under increased power output conditions 150

R. A. MIKAELIAN: A study of the effect of nozzle parameters on arc extinguishing by a compressed air jet 155

Made and printed in Great Britain by The Campfield Press, St. Albans